Glycolytic shunts are anaplerotic reactions for the Calvin-Benson-Bassham cycle

Dissertation
in fulfillment of the requirements for the degree “Dr. rer. nat.”
of the Faculty of Mathematics and Natural Sciences
at Kiel University

submitted by

Alexander Makowka

Kiel, 2019

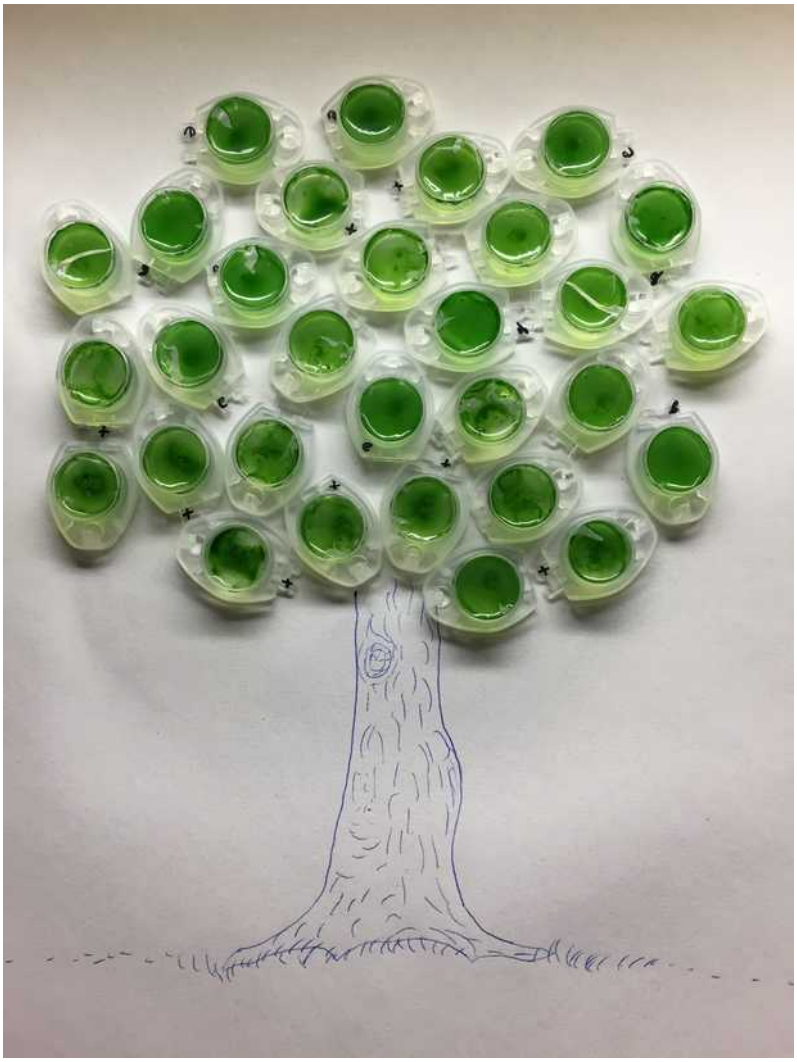

This dissertation was accomplished as part of the Young Research Group ‘Bioenergetics in Photoautotrophs’ headed by Dr. Kirstin Gutekunst.

First examiner: Prof. Dr. Rüdiger Schulz

Second examiner: PD Dr. Christoph Plieth

Day of oral examination: 21.10.2019

Acknowledgment

First and foremost, I want to thank Prof. Dr. Rüdiger Schulz, my doctor father, not only for letting me inside his lab, but also for his kindness and helpfulness. I am very grateful to have been a part of this group for the past several years.

I am also very grateful to PD Dr. Christoph Plieth for being my second examiner and for kindly aiding me during my enzyme activity measurements.

My great thanks is due to Dr. Kirstin Gutekunst, my supervisor. Without her, this work would have been impossible. I want to kindly thank her for giving me the opportunity to create this work, for giving me room to pursue my own ideas and to always guide them with respect, for her passion for science, which was able to motivate me even when all of my experiments went wrong and finally, and most importantly, for her empathy and caring,

Another special thanks is due to Dr. Lars Nichelmann. I want to thank him kindly not only for all of his ideas, which were essential for the CO_2 and qP measurements, but also for all of the aid he provided me during countless measurements. However, more than anything, I want to thank him for becoming a friend and for his talent to make me laugh and relax. He, more than anyone, made this a fun place to work.

I want to express my warm thanks to all the other people who collaborated with me or aided me during my experiments in the previous years. A special thanks goes to Katharina Spengler for helping me with my glycogen measurements, Marco Ebeling for his aid during the characterization of the pgi/ Δ*pgi* mutants, René Wollstadt for helping me during the characterization of the Δ*gap2* mutant and Dr. Marko Boehm for the work he did in the course of the GDH overexpression. I also want to thank Prof. Dr. Frank Sönnichsen from the department of Chemistry of the University of Kiel for doing the NMR measurements and Dr. Mohammad R. Hajirezaei for doing the LC-MS quantification of gluconate and KDPG. Furthermore I want to thank Prof. Dr. Martin Hagemann from the University of Rostock as well as Prof. Dr. Christoph Wittmann, Dr. Judith Becker and Dennis Schulze from the University of Saarbrücken for their collaborations.

I am furthermore very grateful to all the staff of the University of Kiel who worked on a daily basis in order to make my work possible. Among those are our technicians Claudia Marquardt and Katharina Spengler, our secretary Cornelia Herzog-Truxa as well as all the people from the administration, the maintenance, the workshop and the cleaning personal.

I also want to thank all former and present members of AG Schulz for making this a fun place to work. In particular, I want to thank Berit Bünger for her humor and all the great conversations we had, Katharina Spengler for her soothing way and her kindness and Dr. Yingying Wang for his happiness and for all the fun we had during our road-trip in the USA.

Last but not least, I want to kindly thank my parents, who always supported and encouraged me in my decisions and my girlfriend Robi for proofreading my dissertation and, more than anything, for endlessly providing emotional support during the past years.

Declaration of authorship

I herewith declare that the presented thesis is entirely my own work except where otherwise stated.

The thesis has not been submitted either partially or wholly as part of a doctoral degree to another examination body.

The thesis has been prepared subject to the Rules of Good Scientific Practice of the German Research Foundation.

Besides this, I declare that no academic degree has been revoked.

Alexander Makowka

Publications

Makowka, A., Hildebrandt, S., Schulze, D., Boehm, M., Wittmann, C., Gutekunst, K. (2019): The Entner-Doudoroff pathway branches off the oxidative pentose phosphate pathway in the cyanobacterium *Synechocystis sp.* PCC 6803 (under preparation)

Makowka, A., Nichelmann, L., Spengler, K., Forchhammer, K., Gutekunst, K. (2019): Glycolytic shunts replenish the Calvin-Benson cycle as anaplerotic reactions (Molecular Plant, under review)

Doello, S., Klotz, A., **Makowka, A.**, Gutekunst, K., Forchhammer, K. (2018): A Specific Glycogen Mobilization Strategy Enables Rapid Awakening of Dormant Cyanobacteria from Chlorosis. *Plant Physiology*; doi:10.1104/pp.18.00297

Chen, X., Schreiber, K., Appel, J., **Makowka, A**., Fähnrich, B., Roettger, M., Hajirezaei, M.R., Sönnichsen, F. D., Schönheit, P., Martin, W. F., Gutekunst, K. (2016): The Entner-Doudoroff pathway is an overlooked glycolytic route in cyanobacteria and plants. *Proceedings of the National Academy of Sciences*; doi: 10.1073/ 1521916113

Summary

Cyanobacteria have long been known to be capable of mixotrophic growth, by taking up organic molecules and metabolizing them during photoautotrophic conditions. Since cyanobacteria lack subcellular compartmentation, this implies that photoautotrophic carbon metabolism, as it is employed by the Calvin-Benson-Bassham (CBB) cycle, and chemoheterotrophic metabolism, as it is employed by glycolytic routes, can happen simultaneously in the same cellular compartment. A look at the underlying reactions reveals that the CBB cycle and glycolytic routes not only share a large margin of their reactions, but actually employ them in reverse directions. A simultaneous exhibition of both processes in the same cellular compartment would arguably result in severe futile cycling. Even though several metabolic flux analyses have been conducted in mixotrophically growing cyanobacteria, no conclusive explanation for this has been brought up yet. In this work, the hypothesis was put forward that three glycolytic shunts exist in order to funnel glucose that is taken up during mixotrophic growth conditions into the CBB cycle as anaplerotic reactions. These shunts, termed the ‘PGI shunt’, the ‘OPP shunt’ and the ‘ED shunt’, constitute the glucose-6-phosphate isomerase reaction, the two reactions of the oxidative part of the pentose phosphate pathway (glucose-6-phosphate dehydrogenase and 6-phosphogluconate dehydrogenase) and the Entner-Doudoroff pathway, respectively. The existence of the PGI and OPP shunt is in agreement to the flux data that has been published previously. In addition to that, experimental evidence for the existence of all three glycolytic shunts was brought up in this work.

The Entner-Doudoroff (ED) pathway has only recently been shown to occur in cyanobacteria and plants. In this work, a *Synechocystis* deletion strain of the key enzyme of the ED pathway, the KDPG aldolase, was physiologically characterized. The mutant displayed a phenotype during both autotrophic and mixotrophic growth conditions, which manifested itself in a reduced growth rate, a decreased CO_2 assimilation, an increased glycogen content and a reduced amount of photosynthetic pigments. Moreover, the mutant exhibited a reduced glycogen degradation rate during light and a delayed booting rate of the CBB cycle. Whether the phenotypes were due to a missing flux through the ED pathway/shunt or to secondary effects cannot be stated clearly. However, the results strongly suggest a key function of the ED pathway/shunt during light conditions.

Cyanobacteria have previously been shown to degrade glycogen during certain photoautotrophic growth conditions, for example after a transfer from high light to low light conditions. Degradation of glycogen during light results in a subcellular situation, which is very similar, if not identical, to mixotrophic growth conditions. In this work, it was shown that glycolytic shunts mediate the addition of glycogen-derived glucose to the CBB cycle. What is more, experimental evidence was brought forward that degradation of glycogen was able to improve restarting of the CBB cycle after a period of

darkness. This suggests, that cyanobacteria can tap their cellular glycogen pool upon demand in order to improve flux in the CBB cycle. The three glycolytic shunts thereby function as anaplerotic reactions. While various anaplerotic reactions have been described for the tricarboxylic acid cycle, hardly any information has been published on anaplerosis in the CBB cycle. This is surprising, considering that it is well known that anaplerotic reactions are essential to sustain autocatalysis of metabolic cycles. The results from this work show that the cyanobacterium *Synechocystis* employs three glycolytic shunts in order to provide an anaplerotic network around the CBB cycle. The three shunts not only vary in their entry points into the CBB cycle, but also in their ATP and NADPH yields. As a consequence, it can be assumed that glycolytic shunts can not only be employed to control metabolite stoichiometry in the CBB cycle, but also to influence the cellular ATP and NADPH pools and thus provide a tool to improve synchronization with the photosynthetic light reaction. Finally, it can be assumed that glycolytic shunts are not restricted to cyanobacterial carbon metabolism, but might be a general feature of the CBB cycle and thus also apply to plastidic metabolism in plants.

Zusammenfassung

Es ist seit langem bekannt, dass Cyanobakterien mixotroph wachsen können, indem sie organische Moleküle während photoautotrophem Wachstum aufnehmen und verstoffwechseln. Da Cyanobakterien intrazelluläre Kompartimentierung fehlt, bedeutet das, dass photoautotropher Stoffwechsel, wie er vom Calvin-Benson-Bassham (CBB) Zyklus ausgeführt wird, und chemoheterotropher Stoffwechsel, wie er von glykolytischen Wegen ausgeführt wird, gleichzeitig im gleichen Zellkompartiment ablaufen können. Ein Blick auf die zugrundeliegenden Reaktionen zeigt, dass der CBB Zyklus und die glykolytischen Wege sich nicht nur einen Großteil ihrer Reaktionen teilen, sondern darüber hinaus in unterschiedlicher Richtung ablaufen. Ein gleichzeitiges Ausführen von beiden Prozessen im gleichen Zellkompartiment würde in Leerlaufzyklen enden. Obwohl mehrere Fluxanalysen an mixotroph wachsenden Cyanobakterien durchgeführt wurden, wurde bisher keine plausible Erklärung für diesen Sachverhalt aufgebracht. Im Zuge dieser Arbeit wurde die Hypothese aufgestellt, dass drei glykolytische Shunts existieren, um Glukose, welche unter mixotrophen Bedingungen aufgenommen wurde, als anaplerotische Reaktionen in den CBB Zyklus einzuspeisen. Diese Shunts, welche “PGI Shunt”, “OPP Shunt” und “ED Shunt” benannt wurden, bestehen aus der Glukose-6-Phosphat Isomerase, den beiden Reaktionen des oxidativen Teils des Pentose Phosphat Wegs (Glukose-6-Phosphat Dehydrogenase und 6-Phosphoglukonat Dehydrogenase) beziehungsweise dem Entner-Doudoroff Weg. Die Existenz des PGI und OPP Shunts liegt im Einverständnis zu Fluxdaten, welche zuvor veröffentlicht wurden. Im Zuge dieser Doktorarbeit wurden zusätzliche experimentelle Beweise erbracht, welche die Existenz aller drei Shunts belegen.

Es wurde erst vor kurzem gezeigt, dass der Entner-Doudoroff (ED) Weg in Cyanobakterien und Pflanzen vorkommt. In dieser Arbeit wurde eine *Synechocystis* Deletionsmutante, in der das Schlüsselenzym des ED Wegs ausgeschaltet wurde, physiologisch charakterisiert. Die Mutante zeigte einen Phänotyp sowohl unter autotrophen als auch unter mixotrophen Bedingungen, welcher sich in Form einer reduzierten Wachstumsrate, eines erhöhten Glykogengehalts und einem reduzierten Gehalt an photosynthetischen Pigmenten äußerte. Des Weiteren zeigte die Mutante eine verlangsamte Glykogen Abbaurate während Lichtbedingungen sowie einen verlangsamt startenden CBB Zyklus. Ob der Phänotyp durch einen fehlenden Fluss durch den ED Weg/Shunt order durch sekundäre Effekte verursacht wurde, kann nicht mit Sicherheit gesagt werden. Eine Schlüsselfunktion des ED Wegs/Shunts während Lichtbedingungen kann jedoch angenommen werden.

Es konnte zuvor gezeigt werden, dass Cyanobakterien unter bestimmten photoautotrophen Bedingungen, zum Beispiel nach abnehmender Lichtstärke, Glykogen abbauen. Ein Glykogenabbau während des Lichts resultiert in einer zellulären Situation, welche der unter mixotrophen Bedingungen ähnelt, wenn nicht sogar identisch mit ihr ist. In dieser Doktorarbeit konnte gezeigt werden, dass glykolytische Shunts die Zufuhr von Glykogen-basierter Glukose in den CBB Zyklus vermitteln. Des

Weiteren wurde experimenteller Beweis erbracht, dass Zufuhr von Glukose einen Neustart des CBB Zyklus nach einer Dunkelperiode verbessern kann. Dies legt nahe, dass Cyanobakterien ihren Glykogenspeicher bei Bedarf anzapfen können um den Fluss im CBB Zyklus zu verbessern. Die drei glykolytischen Shunts fungieren dabei als anaplerotische Reaktionen. Während verschiedene anaplerotische Reaktionen für den Zitronensäurezyklus bekannt sind, gibt es kaum Informationen über Anaplerose im CBB Zyklus. Das ist erstaunlich, wenn man bedenkt, dass seit langem bekannt ist, dass anaplerotische Reaktionen essentiell sind, um die Autokatalyse eines Stoffwechselweges zu erhalten. Die Ergebnisse dieser Arbeit haben gezeigt, dass *Synechocystis* drei glykolytische Shunts betreibt, um ein anaplerotisches Netzwerk um den CBB Zyklus bereitzustellen. Die drei Shunts unterscheiden sich dabei nicht nur hinsichtlich ihrer Eintrittsorte in den CBB Zyklus, sondern auch in ihrer ATP und NADPH Ausbeute. Aus diesem Grund liegt die Annahme nahe, dass glykolytische Shunts nicht nur den Zweck erfüllen die Metabolit Stöchometrie im CBB Zyklus zu kontrollieren, sondern darüber hinaus auch die zellulären ATP und NADPH Pools beeinflussen können und somit ein Mittel darstellen, die Synchronisation mit der photosynthetischen Lichtreaktion zu verbessern. Zuletzt kann angenommen werden, dass glykolytische Shunts nicht auf cyanobakteriellen Stoffwechsel beschränkt sind, sondern auch auf plastidären Stoffwechsel in Pflanzen zutreffen.

Table of contents

1 Introduction

1.1 Cyanobacteria

Cyanobacteria are photosynthetic prokaryotes whose existence on planet Earth can be traced back to more than 3 billion years, which makes them one of Earth‘s earliest inhabitants (Schirrmeister *et al.,* 2015; Kulasooriya, 2011). The arguably most important achievement of cyanobacteria was the evolution of oxygenic photosynthesis, which caused the so-called great oxygenation event, a rapid increase of atmospheric oxygen from 0.00001 % to 10 % of the present level (Shih, 2015). The ability of oxygenic photosynthesis has proven such successful that it was transferred from endosymbiotic cyanobacteria to the plant lineage roughly 0.9 billion years ago (Shih & Matzke, 2013). Today, cyanobacteria still account for as much as 25 % of the planet‘s primary production (Knoot *et al.*, 2018). The most prominent cyanobacteria are the marine species *Synechococcus sp.* and *Prochlorococcus marinus*, the latter being one of the most abundant organisms on Earth (Partensky *et al.*, 1999). However, cyanobacteria are not limited to marine environments and are commonly found in freshwater or terrestric ecosystems, either free-living or in symbioses such as lichens (Whitton, 2012). Some extremophile cyanobacteria can find their homes even in Earth's most extreme environments such as desert soil (Belnap, 2003), hot springs (Strunecky *et al.*, 2019), salt lakes (Whitton, 2012) or antarctic rocks (De Los Ríos *et al.*, 2014) and were shown to even survive on the exterior of the International Space Station (Eitner & Augustin, 2017).

Another notable cyanobacterium is *Synechocystis,* a genus of unicellular non-diazotrophic freshwater cyanobacteria. The strain *Synechocystis sp.* PCC 6803 (hereafter *Synechocystis*) was isolated from a freshwater lake in California in 1968 and is one of the most extensively studied of all cyanobacteria (Stanier *et al.*, 1971; Ikeuchi & Tabata, 2001; Zerulla *et al.*, 2016). Its popularity as a model organism is due to its ease of genetic manipulation (Grigorieva & Shestakov, 1982) and metabolic flexibility by being able to grow photoautotrophically, chemoheterotrophically and mixotrophically (Anderson & McIntosh, 1991; Zavřel *et al.*, 2017). *Synechocystis* was the first cyanobacterium and the first phototrophic organism to be fully sequenced in 1996 (Kaneko *et al.*, 1996).

There are plenty of reasons to study cyanobacteria. These reasons range from their ecological relevance in almost every ecosystem, over their inherence as a model organism for oxygenic photosynthesis and plants in general to a variety of promising biotechnological applications, such as antibiotic or anti-inflammatory substances, bioplastic or biofuels such as alcohols, isoprenoids or even molecular hydrogen (Abed *et al.*, 2009). In current times, marked by a paradigm shift from fossil-derived towards renewable energy sources, biotechnological applications of cyanobacteria might play a key role in the initiation of a sustainable future.

1.2 Mixotrophy

1.2.1 General information

It is commonly practiced to classify organisms according to their exhibited trophic modes. The distinctions are typically made in regard to the utilized energy and carbon sources. Known bio-available energy sources are light (phototrophy) and redox reactions (chemotrophy) and carbon sources can be either of organic (heterotrophy) or inorganic (autotrophy) nature. While most organisms are limited to utilizing only one kind of energy and carbon source (most commonly phototrophy in combination with autotrophy and chemotrophy in combination with heterotrophy), some organisms are capable of using two energy and/or carbon sources simultaneously, which classifies them as being mixotrophic. Mixotrophy is usually employed facultatively as a mean to enhance growth. To current knowledge, there are three different groups of organisms that accomplish mixotrophic growth: The first group comprises some insects (obligate chemoheterotrophs) such as aphids or oriental hornets that can enhance their productivity by accomplishing additional phototrophic metabolism made possible by pigments that are integrated in their exoskeleton (Valmalette *et al.*, 2012; Plotkin *et al.*, 2010). The second group comprises many anoxygenic photosynthesizing bacteria (obligate photoheterotrophs) such as purple and green non-sulfur bacteria and heliobacteria that can enhance their growth by accomplishing additional chemotrophic or autotrophic metabolism (Eiler, 2006). As most of these organisms do not employ a functional Calvin-Benson-Bassham cycle (Eiler, 2006), autotrophy is accomplished by other CO_2 fixating mechanisms, for example the reductive tricarboxylic acid cycle (Buchanan, 1992). The third group of mixotrophic organisms comprises oxygenic photosynthesizers (obligate photoautotrophs) which include many cyanobacteria and plants that can utilize organic compounds and accomplish additional (chemo)heterotrophic metabolism to support their growth.

It is widely assumed that the prime goal for photoautotrophic organisms to become mixotrophic is to overcome nutrient shortage. Carnivorous plants, for example, tend to grow on nitrogen limiting soil and compensate the nitrogen-shortage by trapping and ingesting insects (Juniper *et al.*, 1989). The concomitantly taken up carbon is presumed to just be a byproduct. In a similar fashion, microalgae and marine cyanobacteria such as *Prochlorococcus* and *Synechococcus* take up organic compounds from their surrounding in times inorganic nutrients are scarce (Munoz-Marin *et al.*, 2013; Duhamel *et al.*, 2018). According to these authors, mixotrophy in photoautotrophs is rather an adaptation to low inorganic nutrient availability than a facultative pathway for carbon acquisition (Duhamel *et al.*, 2018). However, other studies showed that many cyanobacteria and microalgae can significantly increase their growth rates under mixotrophic conditions with glucose in comparison to photoautotrophic growth (Lopo *et al.*, 2012; Li *et al.*, 2014), thus indicating that the ecological relevance of mixotrophy in cyanobacteria might go beyond an improvement of nutrient acquisition.

Similarly, studies on plants in mycorrhizal communities have shown that plants can exploit the symbiotic relationship by extracting sugars from the fungus in times of low photosynthetic productivity (Selosse & Roy, 2009; Schmidt *et al*., 2013).

There is one important conceptual difference between mixotrophy in cyanobacteria and plants: Plants are capable of compartmentation. Compartmentation enables plants to spatially separate the photoautotrophic and chemoheterotrophic trophic modes by, for example, performing photoautotrophy in leaves and chemoheterotrophy in root cells. Even the unicellular green algae can compartmentize the processes intracellularly inside different cell organelles. Cyanobacteria, due to their prokaryotic nature, are unable to form cell compartments that are separated by a plasma membrane and thus can only execute photoautotrophy and chemoheterotrophy inside the same cellular compartment. It is therefore reasonable to differentiate between compartmented mixotrophy and uncompartmented mixotrophy. The focus of this dissertation will lie on the uncompartmented form of mixotrophy as it is accomplished by cyanobacteria. However, plants likely also exhibit uncompartmented mixotrophy, as will be shown in the following paragraph.

According to definition, the trophic mode of an organism is defined by its capability to utilize substrates or energy sources that are external (Madigan *et al.*, 1997). Utilization of internal storage compounds is usually disregarded in this context. Both cyanobacteria and plants build up carbon storage compounds (glycogen and starch, respectively) during the day and degrade them in the following night (Gründel *et al.*, 2012; Stitt & Zeeman, 2012). Although the underlying metabolism of carbohydrate degradation does not differ from those employed by chemoheterotrophic organisms, this growth capability is often forgotten. From here on I will refer to this growth mode as nighttime chemoheterotrophy. Interestingly, utilization of internal carbon storage has not only been shown to happen at nighttime but also during the day when photosynthesis is running in both cyanobacteria and plants. A net glycogen degradation during light conditions has been reported in cyanobacteria during awakening from dormancy (Doello *et al.*, 2018), after transfer from high CO_2 conditions to low CO_2 conditions (Eisenhut *et al.*, 2008) as well as after transfer from high light to low light conditions (Liu *et al.*, 2013; Ueda *et al.*, 2018). Similarly, net starch degradation during light has been shown in plants under various conditions, for example in diurnal-growth adapted leaves that were exposed to continuous illumination (Stitt & Heldt, 1981; Kruger *et al.*, 1983). In plants, plastidic starch granules are degraded either by β-amylase into maltose, which is then exported into the cytoplasm (Neuhaus & Schulte, 1996) or, alternatively, by an α-amylase into glucose phosphate (Asatsuma *et al.*, 2005; Sharkey & Weise, 2016). This creates a mixotrophic situation inside the chloroplast.

A similar situation might arise in the case of starch degradation in the endosperm of germinating plants. The starch-derived glucose is converted into sucrose and transported towards photosynthetically active sink tissues (Nomura *et al.*, 1969). While an import of starch-derived glucose into the chloroplast has not yet been shown, it is very possible, since chloroplasts are known to possess

transporters for diverse carbohydrates, such as glucose-6-phosphate, triosephosphates or phosphoenolpyruvate (Flügge *et al.*, 2011). Accordingly, studies by Quick *et al.* (1995) have shown that feeding of isolated chloroplasts with glucose-6-phosphate caused the induction of hexose-phosphate transporter activity. The observable import of glucose-6-phosphate into chloroplasts lead to an increased starch accumulation and a decreased CO_2 assimilation rate (Quick *et al.*, 1995).

Taken together, these results suggest that both cyanobacteria and plant cells exhibit mixotrophic metabolism during photoautotrophic growth conditions due to the degradation of storage compounds in photosynthetically active compartments.

1.2.2 Mixotrophy in cyanobacteria

Mixotrophy was first shown in cyanobacteria in glucose-tolerant strains of *Synechocystis* (Pelroy *et al.*, 1972). At the time of discovery, the authors described the observed growth mode as being photoheterotrophic and even much later many publications used the term photoheterotrophy to describe the simultaneous utilization of glucose, CO_2 and light in cyanobacteria (Cottrell & Kirchman, 2009). However, flux analyses with labeled ^{13}C have shown that CO_2 assimilation by the Calvin-Benson-Bassham cycle does not stop when glucose and light are supplied (Yang *et al.*, 2002; Nakajima *et al.*, 2014) and that the correct term for the underlying growth mode would thus have to be photoheteroautotrophy or photochemoheteroautotrophy which equals mixotrophy according to definition. Photoheterotrophic growth can only be approached artificially in cyanobacteria by application of inhibitors of the photosynthetic electron transport such as DCMU or atrazine (Nakajima *et al.*, 2014). However, even these inhibitors can not completely shut down CO_2 fixation but rather reduce it to a minimal level (Nakajima *et al.*, 2014). Next to *Synechocystis*, mixotrophy has been shown in various other cyanobacteria such as *Spirulina* (Chojnacka & Noworyta, 2004), *Prochlorococcus* (Munoz-Marin *et al.*, 2013; Moore, 2013) and *Synechococcus* (Yelton *et al.*, 2016). While the marine cyanobacteria *Prochlorococcus* and *Synechococcus* were shown to take up a variety of organic compounds such as glucose, diverse amino acids, peptides, phosphonates, dimethylsulfoniopropionate and even nucleotides (Munoz-Marin *et al.*, 2013; Duhamel *et al.*, 2018; Duhamel *et al.*, 2012; Michelou *et al.*, 2007), *Synechocystis* was only shown to take up glucose and amino acids during mixotrophic conditions (Pelroy *et al.*, 1972; Labarre *et al.*, 1987).

Growth rates during mixotrophic growth of *Synechocystis* on glucose are generally higher than during photoautotrophic growth under comparable cultivation conditions (Lopo *et al.*, 2012). Interestingly, mixotrophic growth yields are often even higher than the sum of photoautotrophic and chemoheterotrophic growth yields, as has been shown in the cyanobacteria *Synechocystis* (Chen *et al.*, 2016), *Spirulina* (Chojnacka & Noworyta, 2004), *Nostoc* (Yu *et al.*, 2008) but also in the microalga

Chlorella vulgaris (Liang *et al.*, 2009). This indicates that (uncompartmented) mixotrophy is more than a simple addition of photoautotrophic and chemoheterotrophic metabolism but rather a different and synergistic metabolism. The development of a synergistic growth model of uncompartmented mixotrophic growth will be a central point of this dissertation. In order to understand mixotrophic growth an understanding of the carbon metabolism during photoautotrophic and chemoheterotrophic growth is necessary. An overview will be provided in the following two chapters.

1.3 Chemoheterotrophic metabolism

Chemoheterotrophic growth is the default growth mode of all animals and of the majority of bacteria. However, obligate photoautotrophs (cyanobacteria and plants) are also capable of chemoheterotrophic growth, as they degrade internal carbon compounds such as glycogen or starch at nighttime. This nighttime chemoheterotrophy is usually distinguished from real chemoheterotrophic growth since no utilization of external substrates is taking place. However, the underlying metabolistic mechanisms during nighttime chemoheterotrophy and real chemoheterotrophy are largely the same. Some cyanobacteria and plants are also capable of taking up organic compounds from their surroundings during darkness (Francisco *et al.*, 2014; Schmidt *et al.*, 2013), although growth rates during chemoheterotrophic growth of obligate photoautotrophic organisms are usually smaller than during photoautotrophic growth (Lopo *et al.*, 2012). Glucose tolerant strains of the cyanobacterium *Synechocystis* can grow chemoheterotrophically on glucose but, for reasons still unknown, require a daily pulse of blue (or white) light to induce uptake and catabolism of glucose (Anderson & McIntosh, 1991). The following paragraph will describe the fundamental processes of chemoheterotrophic metabolism using glucose and oxygen as substrates.

Generally speaking, both the heterotrophic and the chemotrophic component need to be accomplished to enable growth. The heterotrophic component is accomplished by converting glucose into all kinds of carbon compounds (cellular building blocks) that are required for growth. The chemotrophic component is accomplished by extracting energy that is bound in the reduction grade of the carbon atoms of glucose. This is usually done by transferring the high energy electrons from glucose onto NAD(P) and further onto oxygen, while harvesting the concomitantly released energy by creating energy-rich phosphoanhydride bonds in form of ATP. In order to fulfill both the heterotrophic and chemotrophic components, a metabolic network has evolved which shows remarkably little variations between different domains of life, given the evolutionary time-span on the one hand and possibilities of chemical reactions on the other (Gottschalk, 2012). This metabolic network has been categorized into metabolic pathways, functional units of enzyme-catalyzed reactions. These metabolic pathways require gaplessly connected reactions that share a thermodynamically feasible flux direction (Bar-Even

et al., 2012 a). The most important metabolic pathways involved in chemoheterotrophic metabolism are glycolytic routes, the tricarboxylic acid (TCA) cycle and the respiratory electron transport chain. Glycolytic routes refer to the metabolic pathways that conduct the conversion of C6 sugars (usually glucose) to pyruvate. The three most common glycolytic routes are the Embden-Meyerhof-Parnas (EMP) pathway (fig. 1, red), the oxidative pentose phosphate (OPP) pathway (fig. 1, blue) and the Entner-Doudoroff (ED) pathway (fig. 1, green) (Schlegel, 2007). All three pathways have some reactions in common (fig. 1, black), such as the initial phosphorylation step catalyzed by hexokinase or the part between glyceraldehyde-3-phosphate and pyruvate (hereafter: lower glycolysis). Even though traditionally not belonging to the glycolytic routes, the enzymes of glycogen and starch degradation are closely connected. Degradation of these storage compounds is usually accomplished by a subsequent activity of glycogen/starch phosphorylase and phosphoglucomutase (fig. 1) (Gründel *et al*., 2012). The product glucose-6-phosphate can then enter one of the three glycolytic pathways.

In cyanobacteria, all three of the mentioned glycolytic routes (EMP, OPP and ED pathway) are present (Chen *et al.*, 2016). A potential fourth glycolytic pathway, the phosphoketolase pathway, has recently been shown in the cyanobacteria *Synechocystis* (Knoop *et al.*, 2013; Xiong *et al.*, 2015), *Anabaena* (Moriyama *et al.*, 2015) and *Cyanothece* (Alagesan *et al.*, 2013). However, this pathway does not describe the conversion of glucose to pyruvate but rather a conversion of phospho-ketoses (sedoheptulose-7-phosphate, fructose-6-phosphate or xylulose-5-phosphate) into acetyl-phosphate. Elucidation of the relevance and the physiological function of this pathway in cyanobacteria will not be topic of this dissertation.

1.3.1 Oxidative pentose phosphate pathway

It has been shown in various studies that the oxidative pentose phosphate (OPP) pathway is by far the most important glycolytic route during chemoheterotrophic growth in cyanobacteria (Yang *et al.*, 2002; Ueda *et al.*, 2018). Flux analyses with ^{13}C have shown that more than 90 % of the imported glucose are directed through the first reactions of the OPP pathway in *Synechocystis* (Yang *et al.*, 2002). A deletion of the OPP specific enzyme 6-phosphogluconate dehydrogenase (GND) was furthermore shown to prevent growth during chemoheterotrophic conditions with glucose (Wan *et al.*, 2017). Three reasons are postulated to cause this essential role of the OPP pathway under chemoheterotrophic conditions: First, it is by far the most efficient pathway for NADPH generation. Second, it is the only pathway to generate the biosynthesis precursors ribose-5-phosphate and erythrose-4-phosphate. Third, the majority of its required enzymes are already present in the Calvin-Benson-Bassham cycle (chapter 1.5) and thus do not need to be extra synthesized (Kruger & von Schaewen, 2003). In plants, the OPP pathway does usually operate both in plastids and the cytosol (Kruger & von Schaewen, 2003). From a general perspective, the OPP pathway can operate in two

variations: cyclic or non-cyclic in combination with the EMP pathway. In the cyclic variation, fructose-6-phosphate that is generated by the transaldolase and transketolase reactions is converted to glucose-6-phosphate by glucose-6-phosphate isomerase (PGI) and re-entering the OPP pathway. The other product, glyceraldehyde-3-phosphate, is further processed to pyruvate in lower glycolysis. In the non-cyclic variation, fructose-6-phosphate is further catabolized by reactions of the EMP pathway and lower glycolysis (Schlegel, 2007). The stoichiometries for both variations are shown below.

OPP cyclic: 1 Glucose → 3 CO_2 + 1 Pyruvate + 1 ATP + 6 NADPH + 1 NADH
OPP non-cyclic: 1 Glucose → 1 CO_2 + 1.67 Pyruvate + 1.67 ATP + 2 NADPH + 1.67 NADH

1.3.2 Embden-Meyerhof-Parnas pathway

The Embden-Meyerhof-Parnas (EMP) pathway, also called glycolysis, was the first metabolic pathway to ever be discovered in the 1930s (Kresge *et al.*, 2005). Its significance in cyanobacteria is still under debate. While Pelroy *et al.* could not detect activity of phosphofructokinase (PFK), the key enzyme of the EMP pathway, in *Synechocystis* (Pelroy *et al.*, 1972), it was later shown that two gene copies of this enzyme exist and that they are active in *Synechocystis* (Knowles & Plaxton, 2003). A metabolic flux analysis with ^{13}C labeled glucose could detect a significant flux (60 %) through PFK under chemoheterotrophic growth conditions (Yang *et al.*, 2002). However, the actual flux through the EMP pathway was considered to be much lower (only ~6 %), as could be deducted from the flux through glucose-6-phosphate isomerase (PGI) (Yang *et al.*, 2002). This indicates that the majority of flux through PFK is due to a non-cyclic OPP pathway rather than the EMP pathway. The EMP pathway is the most efficient glycolytic route, having an ATP yield of 2 for the conversion of 1 glucose to 2 pyruvate (stoichiometries shown below). This makes it especially valuable for fermentative processes (Bar-Even *et al.*, 2012 a).

EMP: 1 Glucose → 2 Pyruvate + 2 ATP + 2 NADH

1.3.3 Entner-Doudoroff pathway

The Entner-Doudoroff (ED) pathway is typically considered as an alternative route to the EMP pathway since it has a similar stoichiometry (shown below). The conceptual difference between the two pathways is that in the ED pathway the oxidation of an aldehyde to a carboxylic acid (glucose-6-phosphate to 6-phosphogluconate) is not coupled to a substrate phosphorylation with inorganic phosphate, while in the EMP pathway it is (glyceraldehyde-3-phosphate to 1,3-bisphosphoglycerate). This leads to an overall lower ATP yield of the ED pathway on the one hand, but a higher metabolic

driving force due the higher amount of dissipated energy (ΔG_r‘) on the other. The higher metabolic driving force implies a higher turnover number per given amount of enzyme or, in other words, a lower amount of required enzyme to achieve a given turnover (Bar-Even *et al.*, 2012 a). For many organisms, the choice between ED and EMP pathway is thus a trade-off between energetic efficiency and enzymatic resource cost (Flamholz *et al.*, 2013). This makes the ED pathway a preferable choice in aerobic organisms that do not rely on the energy output of glycolytic routes and a less preferable choice in organisms that employ fermentative growth (Flamholz *et al.*, 2013). There are several variations to the classical scheme of the ED pathway that is depicted in fig. 1. Bacteria that can facultatively feed on gluconate, such as *E. coli*, have been shown to employ an inducible ED pathway that is only expressed in case gluconate is present (Peekhaus & Conway, 1998). An additional gluconate kinase is expressed to provide downstream connection with the ED pathway. Interestingly, *E. coli* also possesses a quinone-dependent glucose dehydrogenase which, together with gluconate kinase, provides a full bypass to the classical way as it is accomplished by hexokinase and glucose-6-phosphate dehydrogenase (Conway, 1992). Another variation of the ED pathway is employed in hyperthermophilic archaea which possess a non-phosphorylating ED pathway (Selig *et al.*, 1997). This pathway skips the phosphorylation step and thus works with gluconate and 2-keto-3-deoxygluconate instead of 6-phosphogluconate and 2-keto-3-deoxy-6-phosphogluconate. Contrary to the long-established belief that the ED pathway is exclusively present in prokaryotes, recent studies have reported that the ED pathway is also present in plants. These studies have shown activity of the key enzyme of the ED pathway, the KDPG aldolase, in barley as well as the cyanobacterium *Synechocystis* (Chen *et al.*, 2016). Blast genome analyses of the KDPG aldolase revealed a widespread presence in both cyanobacteria and plants and furthermore suggest an endosymbiotic gene transfer of the ED pathway from cyanobacteria to the plant lineage (Fabris *et al.*, 2012; Chen *et al.*, 2016). Physiologic analyses of a KDPG aldolase deletion mutant of *Synechocystis* revealed a crucial function of the ED pathway under mixotrophic conditions and presumably no function under chemoheterotrophic growth conditions. A growth impairment during diurnal photoautotrophic growth conditions could furthermore be shown. The authors also suggested the presence of a glucose dehydrogenase/gluconate kinase bypass, similar as it was reported in *E. coli*.

ED: 1 Glucose → 2 Pyruvate + 1 ATP + 1 NADPH + 1 NADH

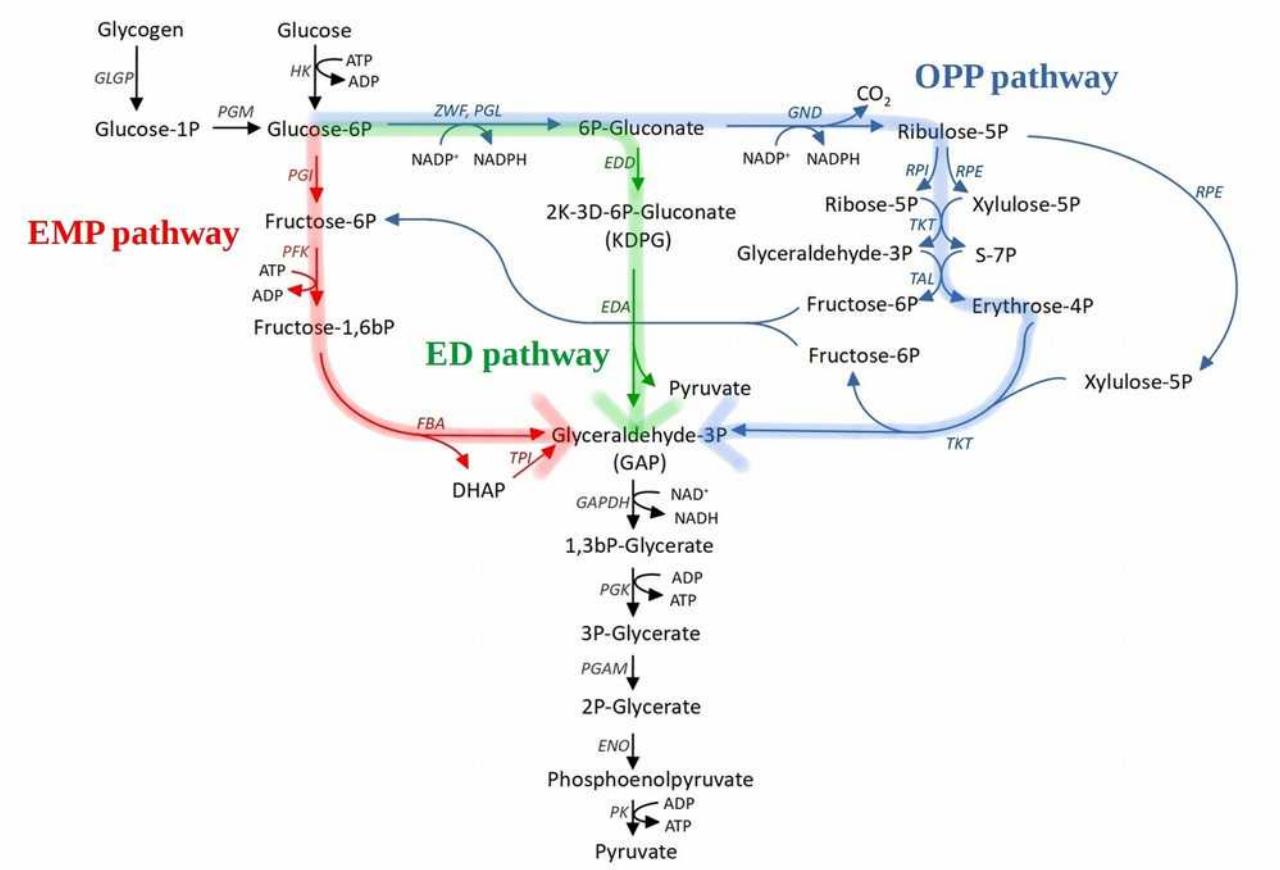

Figure 1: Glycolytic routes in cyanobacteria. Shown is an overlap map of the three most common glycolytic routes: oxidative pentose phosphate pathway (blue), Embden-Meyerhof-Parnas pathway (red) and Entner-Doudoroff pathway (green). Fat translucent arrows indicate glycolytic flux direction. Stoichiometries were not considered.

1.3.4 Tricarboxylic acid cycle

For a long time, the tricarboxylic acid (TCA) cycle, often also called citric acid cycle or krebs cycle, was believed to be incomplete in cyanobacteria due to the lack of a 2-oxoglutarate dehydrogenase. However, recent studies have reported the existence of functional bypasses to this enzyme in cyanobacteria, thereby enabling a complete TCA cycle (fig. 2, red and blue) (Knoop *et al.*, 2010; Zhang & Bryant, 2011). Flux analyses with ^{13}C have shown that both under photoautotrophic and chemoheterotrophic conditions, the dominant flux direction in the TCA cycle is still non-cyclic in *Synechocystis* (fig. 2, black) (Knoop *et al.*, 2013; Wan *et al.*, 2017). The observable flux represents the main function of the TCA cycle in cyanobacteria, which is the distribution of carbon to various precursor molecules for the formation of cellular building blocks (Knoop *et al.*, 2010). The most notable precursors are 2-oxoglutarate and oxaloacetate, both required for amino acid syntheses (Schlegel, 2007). The second inherent role of the TCA cycle is the complete oxidation of acetyl-CoA to CO_2 and the concomitant generation of reducing equivalents. This function is generally considered as the pivotal point for aerobic chemoheterotrophic growth. However, due to the incomplete TCA flux in cyanobacteria, NAD(P)H generation by the TCA cycle is presumably of minor importance during chemoheterotrophic growth of cyanobacteria. This is consistent with the previously mentioned finding that cyanobacteria generate their majority of reducing equivalents in the dark by the OPP pathway (Yang *et al.*, 2002).

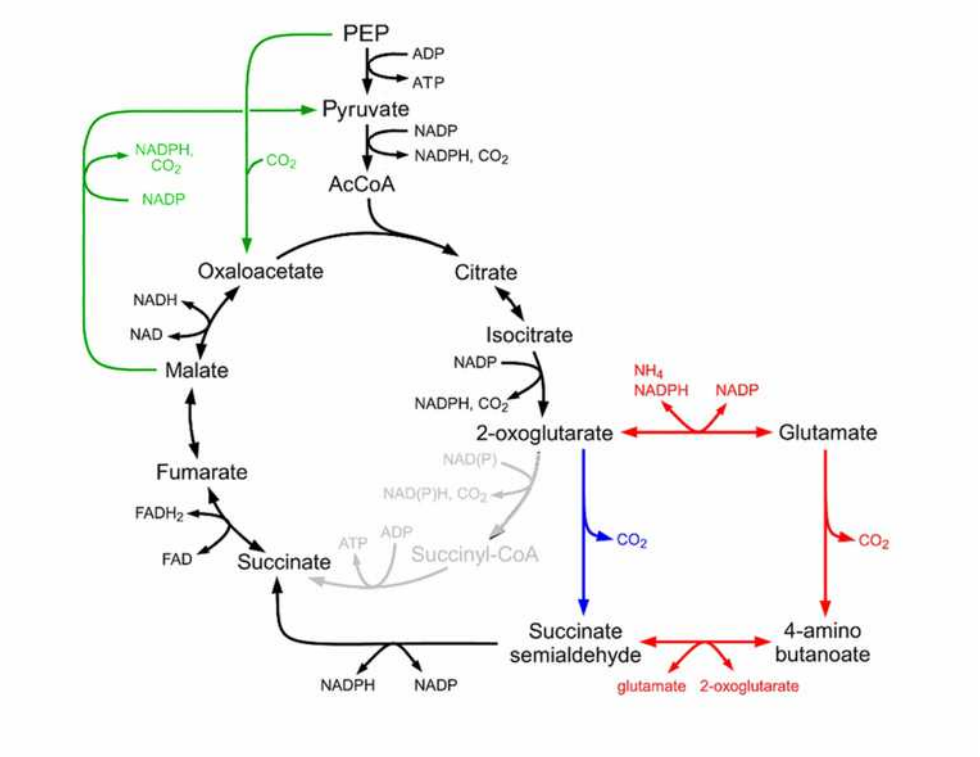

Figure 2: Tricarboxylic acid (TCA) cycle in cyanobacteria (modified from Knoop *et al.*, 2013). Shown are the classic variant of the TCA cycle with 2-oxoglutarate dehydrogenase (gray) and two variations of a complete TCA cycle in cyanobacteria (blue and red). Furthermore shown are the phosphoenolpyruvate carboxylase and the malic enzyme (green).

1.3.5 Oxidative phosphorylation

Oxidative phosphorylation, often also called respiration or respiratory electron transport, is the process in which cells couple the oxidation of cellular compounds to the generation of a proton gradient which is used chemiosmotically for the phosphorylation of ADP. The ATP that is generated in this process is the main energy source during aerobic chemoheterotrophic growth (Schlegel, 2007). Cyanobacteria perform oxidative phosphorylation both in their thylakoid and cytoplasmic membrane (Vermaas, 2001). Since the thylakoid membrane is also venue of the photosynthetic electron transport, an intersection between the respiratory and photosynthetic electron transport chain is given. The consequences of an intersected electron transport during light will be outlined in the following chapter (chapter 1.4). Figure 3 shows the respiratory electron transport chain as it is accomplished in cyanobacteria under chemoheterotrophic conditions, according to current knowledge. The contribution of different electron donors is still under debate. Recent studies have shown that not NADPH but reduced ferredoxin acts as an electron donor for the respiratory complex NDH-1 (Schuller *et al.*, 2019) and that NADPH can thus not transfer electrons directly into the respiratory electron chain. While NADPH can theoretically transfer electrons to ferredoxin via the ferredoxin-NADPH reductase (FNR), this process is thermodynamically unfavored due to the more negative redox potential of ferredoxin (Carrillo & Ceccarelli, 2003). The diaphorase subunit of the bidirectional hydrogenase is postulated to fulfill a similar role as the FNR (Gutekunst, 2018). However, the contribution of these processes under physiological conditions is unclear. Another potential electron flux is from NADPH to its unphosphorylated counterpart NAD^+ via the thylakoid-membrane-bound transhydrogenase (Kämäräinen *et al.*, 2017). It is assumed that NADH can funnel its electrons into the respiratory chain via NDH-2 (Peltier *et al.*, 2016) (not shown in fig. 3). However, contrary to its pivotal role during the oxidative phosphorylation in many organisms, NADH is believed to only play a minor role as an electron donor for oxidative phosphorylation in cyanobacteria (Vermaas, 2001). It is considered that succinate is the major electron donor during chemoheterotrophic conditions and that NDH-1 predominantly plays a role during fine tuning of photosynthesis (Cooley *et al.*, 2000; Vermaas, 2001; Nogales *et al.*, 2012; Mullineaux, 2014).

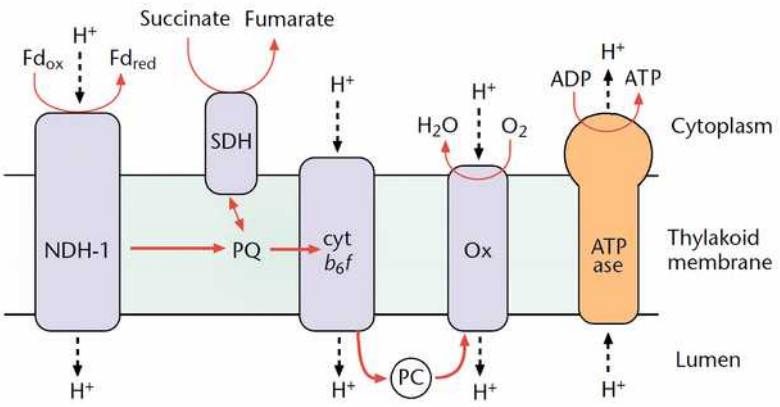

Figure 3: Respiratory electron transport in cyanobacteria (modified from Vermaas, 2001).

1.4 Photoautotrophic metabolism

Photoautotrophic metabolism, as accomplished by oxygenic photosynthesizers, consists of the following two fundamental concepts: 1. conversion of light energy into chemically bound energy in form of ATP (phototrophic component), 2. transfer of electrons from water to $NADP^+$ which is used to fixate inorganic carbon (autotrophic component). Rather than using a trophic distinction, oxygenic photosynthesis is usually segmented into the underlying metabolic pathways, which are the photosynthetic electron transport chain (PETC) on the one hand and the Calvin-Benson-Bassham (CBB) cycle on the other. The two pathways are tightly connected by the cellular NADPH and ATP pools. Synchronization of NADPH and ATP supply and demand is one of the key challenges of photoautotrophic metabolism (Nogales *et al.*, 2012).

1.4.1 Photosynthetic electron transport chain

The photosynthetic electron transport chains (PETC) of cyanobacteria and plants are essentially identical (Vermaas, 2001). The driving force of the PETC is light. Photons that are absorbed by photosynthetic pigments inside the two thylakoid-membrane-bound photosystems (PSI and PSII) cause electron excitations and oxidations within those pigments. In case of PSII, the electrons of the photo-oxidized pigments are transferred onto the membrane-bound electron carrier plastoquinone (PQ) (fig. 4). Almost simultaneously, the pigments become re-reduced by electrons deriving from water (water splitting). PQ further transports the electrons to the cytochrome b6f complex where they are transferred to PSI by the luminal electron carrier plastocyanin (PQ). In cyanobacteria, this transport can also be accomplished by cytochrome c6, which normally functions as an electron carrier during oxidative phosphorylation. The photo-oxidized pigments of PSI transfer their electrons further onto ferredoxin and eventually to $NADP^+$ (Schlegel, 2007). Reduced $NADP^+$ can be used for CO_2 fixation in the CBB cycle. In parallel to the generation of NADPH, the photosynthetic electron transport enables the conversion of light energy into chemically bound energy in form of ATP (phototrophic component). The underlying principle is the same as during oxidative phosphorylation, namely the generation of a proton gradient which is used chemiosmotically for phosphorylation of ADP by an ATP synthase.

One of the major differences is that in cyanobacteria the PETC is intersected with the respiratory electron transport (fig 4). This intersection, being mainly due to the fact that cyanobacteria use the same mobile electron carriers (PQ and PC/Cyt c) in both processes, enables some interesting electron fluxes. For instance, electrons from non-photosynthetically-derived ferredoxin or succinate can enter the PQ pool and be further processed in photosynthetic electron transport (Mullineaux, 2014). This phenomenon, similar to the cyclic electron transport around PSI, where photosynthetically derived ferredoxin is re-entering the PQ pool (Nogales *et al.*, 2012), causes additional protons to be pumped

across the membrane and thus effectively increases the cellular ATP/NADPH ratio. This funneling of non-photosynthetically-derived electrons is considered to be the reason why cyanobacteria maintain a high PSI/PSII ratio (around 5 in *Synechocystis*) (Shen *et al.*, 1993). Another unconventional electron flux that is made possible by an intersecting electron transport is the transfer of photosynthetically-derived electrons from PC/Cyt c to the cytochrome oxidase and further on to oxygen (Mullineaux, 2014). This phenomenon, similar to the Mehler reaction where electrons are transferred from NADPH onto oxygen, is an effective tool to dissipate electrons and thereby increases the cellular ATP/NADPH ratio. Other alternative electron acceptors that cause a similar effect are nitrate or protons (hydrogenase-reaction) (Nogales *et al.*, 2012).

The second major alteration between the photosynthetic electron transport of cyanobacteria and plants is the structure and composition of their light harvesting complexes. While the light harvesting complexes of plants are embedded in the thylakoid membrane and comprise chlorophylls and carotenoids as photosynthetic pigments (Cheng & Fleming, 2009), the light harvesting complexes of cyanobacteria, the so-called phycobilisomes, are multiproteincomplexes that sit on top of the photosystems (usually PS II) and contain only phycocyanin and allophycocyanin as photosynthetic pigments (Grossman *et al.*, 1993). It has been shown that the phycobilisomes can move between the two photosystems (state transitions), which is presumed to help fine-tuning of photosynthesis during changing light conditions (Mullineaux & Emlyn-Jones, 2004). Studies have furthermore shown the presence of a non-photosynthetic quenching mechanism inside phycobilisomes which is accomplished by an orange carotenoid protein (Wilson *et al.*, 2006). Thermal energy dissipation by this protein can help to protect the pigments from photodamage.

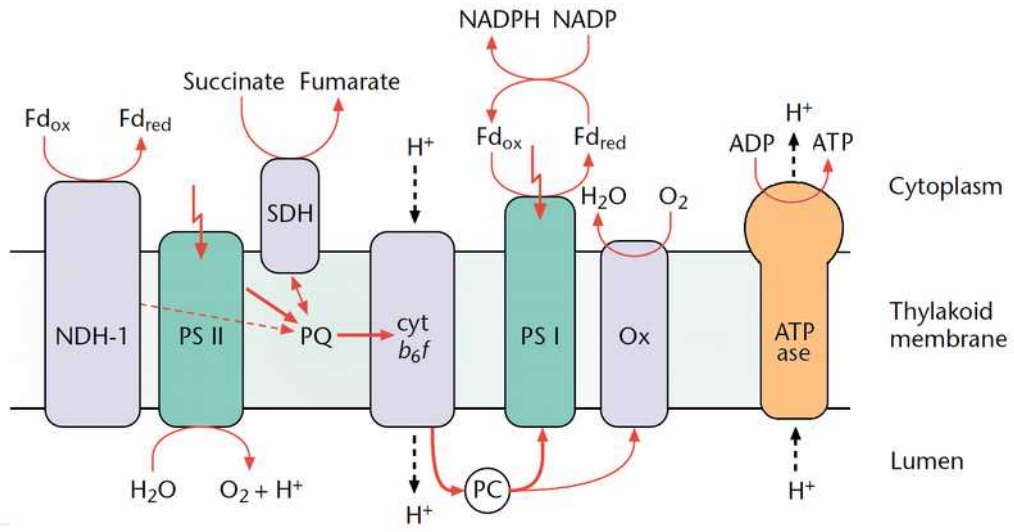

Figure 4: Photosynthetic electron transport chain in cyanobacteria (modified from Vermaas, 2001).

1.4.2 Calvin-Benson-Bassham cycle and glycogen synthesis

The Calvin-Benson-Bassham (CBB) cycle, also called reductive pentose phosphate pathway (Bar-Even *et al.*, 2012 c), is the major CO_2 fixating mechanism in oxidative photosynthesizers. From a thermodynamic perspective, fixation of inorganic CO_2 always requires the accomplishment of two unfavorable reactions, namely the creation of a new carbon-carbon bond and the reduction of a carboxyl group to an aldehyde (Bar-Even *et al.*, 2012 b). These unfavorable reactions are enabled by investment of ATP, which is generated in the process of the photosynthetic electron transport chain (chapter 1.4.1). However, among CO_2 fixation pathways, the CBB cycle is the only one that invests ATP for other than the two mentioned reaction types (Bar-Even *et al.*, 2012 c), presumably, to increase its overall metabolic driving force. The CBB cycle (fig. 5) is commonly subdivided into three phases: 1. the CO_2 fixation phase, 2. the reduction phase and 3. the regeneration phase.

The CO_2 fixation reaction is accomplished by ribulose-1,5-bisphosphate carboxylase/oxygenase (RubisCO or RBC). In cyanobacteria, RubisCO is located together with a carbonic anhydrase within subcellular micro-compartments, the so-called carboxysomes (Price *et al.*, 2007). It has been shown that carbonic anhydrase activity can increase the CO_2+HCO_{3^-} concentration inside the carboxysomes to as high as 40 mM (Price *et al.*, 2007). This carbon concentrating mechanism (CCM) enables higher turnover rates of RubisCO as well as a reduced oxygenation reaction in comparison to C3 plants, which do not employ CCM (Price *et al.*, 2007). Similar as in plants, cyanobacteria possess photorespiratory pathways to dispose of or recycle phosphoglycolate, the toxic product of the oxygenation reaction of RubisCO (Eisenhut *et al.*, 2008). It could be shown that photorespiration can be induced as an ATP dissipating mechanism and thus provide another tool to help synchronization with the CBB cycle (Nogales *et al.*, 2012).

The second phase of the CBB cycle is characterized by the reduction of the carboxylation product 3-phosphoglycerate to glyceraldehyde-3-phosphate. This thermodynamically unfavorable reduction of an carboxyl group to an aldehyde is made possible by coupling it to ATP hydrolysis. The reaction is accomplished in two steps: first, 3-phosphoglycerate is phosphorylated by ATP via phosphoglycerate kinase (PGK) and then 1,3-bisphosphoglycerate is reduced to glyceraldehyde-3-phosphate by utilizing the energy from the phosphoester bond hydrolysis. In cyanobacteria, this reaction is catalyzed by glyceraldehyde-3-phosphate dehydrogenase 2, a NADH/NADPH unspecific isoform to the NADH specific enzyme present in lower glycolysis (Koksharova *et al.*, 1998). The GAPDH2 reaction is considered to be the main electron sink of NADPH from the photosynthetic electron transport (Nogales *et al.*, 2012).

The third phase of the CBB cycle, the regeneration phase, fulfills two important functions: First, it regenerates the CO_2 fixation substrate ribulose-1,5-bisphosphate and thereby ensures autocatalysis of the CBB cycle. Second, it constitutes a carbon network that comprises precursor molecules for the

formation of cellular building blocks. These precursor molecules are either directly present in the CBB cycle or accessible via connections with other metabolic pathways such as lower glycolysis and the TCA cycle. A closer look at the underlying reactions of the regenerative part of the CBB cycle reveals that all involved enzymes are also present in glycolytic routes where they accomplish the respective reactions in reverse direction.

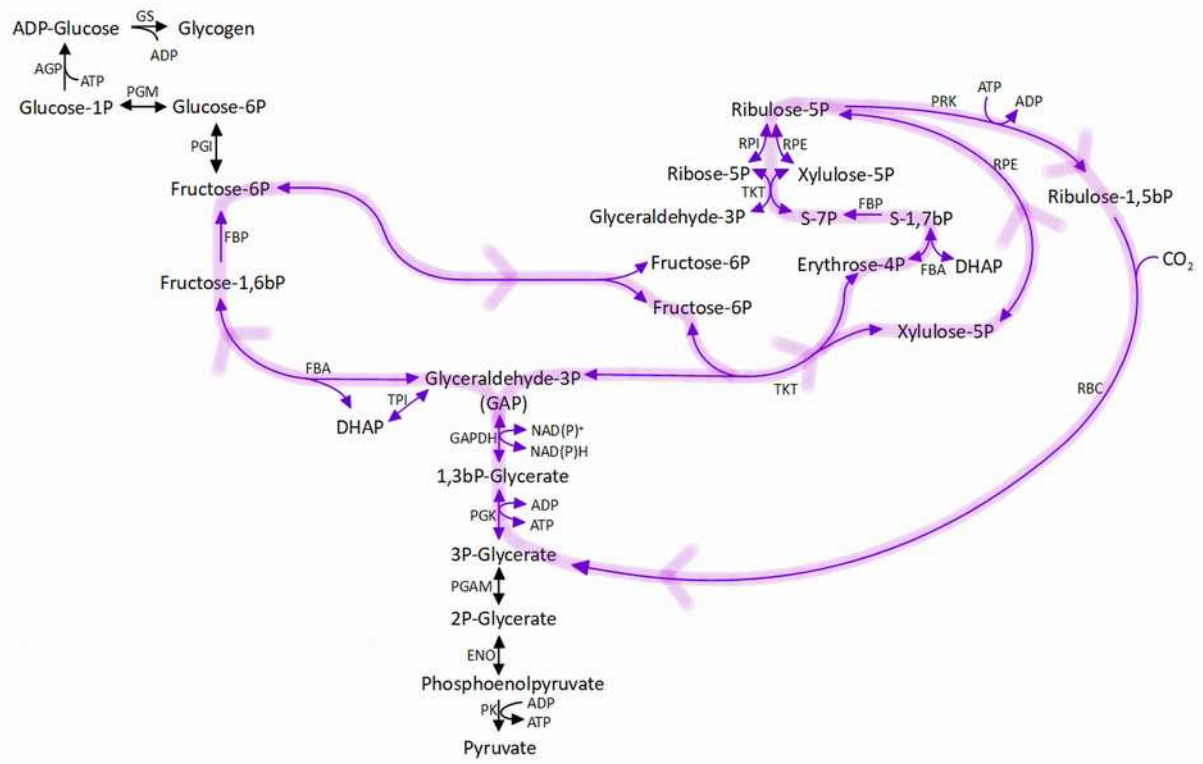

Figure 5: The Calvin-Benson-Bassham cycle. Shown is the Calvin-Benson-Bassham cycle (purple) together with reactions for the synthesis of glycogen and lower glycolysis (black). Two-headed arrows indicate bidirectionality under physiological conditions (according to Flamholz *et al*., 2012). In case of the GAPDH reaction, anabolic and catabolic fluxes are distributed between two isoforms. Flow direction of the Calvin-Benson-Bassham cycle is indicated by fat translucent arrows. Stoichiometries were not considered.

The CBB cycle is tightly coupled to glycogen metabolism. For glycogen synthesis, the CBB cycle intermediate fructose-6-phosphate is first isomerized to glucose-1-phosphate via glucose-6-phosphate isomerase (PGI) and phosphoglucomutase (PGM), then additionally activated by coupling to an ADP molecule and finally transferred onto a pre-existing glycogen chain by forming an α-1,4 glycosidic bond. The glycogen chain can be further branched by insertion of α-1,6 glycosidic bonds by the branching enzyme (Gründel *et al.*, 2012). To current knowledge, glycogen is considered to fulfill two functions in cyanobacteria: 1. to provide a carbon reserve compound for nighttime chemoheterotrophic metabolism as well as starvation conditions and 2. to provide a metabolic buffer during overflow metabolism (Gründel *et al.*, 2012). Glycogen synthesis is primarily regulated by ADP-glucose

pyrophosphorylase (AGP) activity, which is activated by the CBB cycle intermediate 3-phosphoglycerate and thioredoxin and inhibited by orthophosphate (Cano *et al*., 2018).

Both cyanobacteria and plants inactivate the CBB cycle in the dark by a redox-mediated switch. According to current knowledge, the small redox-sensitive protein CP12 forms a complex with phosphoribulokinase (PRK) and glyceraldehyde-3-phosphate dehydrogenase (GAPDH2) of the CBB cycle, which leads to an inactivation of the two enzymes (Wedel & Soll, 1998; López-Calcagno *et al.*, 2014). While this association is known to be thioredoxin-mediated in plants, no interaction between thioredoxins and CP12 formation could be shown in cyanobacteria yet (Tamoi *et al.*, 2005). However, a dependency of complex formation on oxidized $NADP^+$ seems very likely (Tamoi *et al.*, 2005).

1.5 Mixotrophic carbon flux

A comparison of the growth rates of various cyanobacteria during photoautotrophic, chemoheterotrophic and mixotrophic growth conditions indicated that (uncompartmented) mixotrophy is more than a simple addition of photoautotrophic and chemoheterotrophic metabolism but rather a different and synergistic metabolism (chapter 1.2.2). A look at the underlying metabolic pathways of photoautotrophic and chemoheterotrophic metabolism revealed a mutual metabolistic network with many enzymes that are involved in both processes. Especially the CBB cycle and the glycolytic routes essentially have the same enzymatic machinery (chapter 1.3 and 1.4). This chapter will take a look at the current knowledge of the carbon flux under mixotrophic conditions in cyanobacteria in order to elucidate uncompartmented mixotrophic carbon metabolism.

Various flux analyses in the cyanobacterium *Synechocystis* have shown a net flux through the oxidative part of the PP pathway under mixotrophic conditions (You *et al.*, 2014; Nakajima *et al.*, 2014; Ueda *et al.*, 2018). The authors concluded that a cyclic OPP pathway is operating, fulfilling the function of NADPH production to support photosynthesis during low light. However, the same flux analyses have also shown that the CBB cycle is active under these conditions. How these two pathways, that share a large margin of their reactions, can operate simultaneously in reverse directions was not stated. In a similar fashion, the observable net flux through glucose-6-phosphate isomerase (PGI) towards fructose-6-phosphate formation has been attributed to a flux through the EMP pathway (Ueda *et al.*, 2018). The fact that many reactions of the EMP pathway are also present in the CBB cycle in reverse direction was not discussed.

Theoretically, there are two possibilities for a simultaneous operation of the CBB cycle and glycolytic routes: 1. spatial separation of the CBB cycle and glycolytic routes or 2. no spatial separation and thus a free exchange between the metabolite pools of the CBB cycle and glycolytic routes. Since

cyanobacteria lack subcellular compartmentation, both the CBB cycle and glycolytic routes operate in the cytoplasm. The only way to achieve metabolic isolation between those pathways would be substrate channeling. Substrate channeling describes the process where subsequent enzymes of a metabolic pathway interact such that intermediate diffusion into the bulk solvent (cytoplasm) is prevented or, at least, reduced (Sweetlove & Fernie, 2018). It has been postulated that the main advantage of such an interaction is to obtain the ability to regulate metabolic flux at branch points (Sweetlove & Fernie, 2018). Enzyme complexes that are capable of substrate channeling, so-called metabolons, have, among others, been reported for enzymes of the TCA cycle (Zhang *et al.*, 2017) as well as for enzymes of the cytosolic EMP pathway (Graham *et al.*, 2007) and OPP pathway (Debnam *et al.*, 1997) in plants (Fernie *et al.*, 2018). However, substrate channeling has neither been reported in cyanobacteria nor in chloroplasts so far. The metabolon required to achieve a metabolic isolation between the OPP pathway and the CBB cycle would have to include at least five enzymes, namely ribose-5-phosphate isomerase (RPI), ribose-5-phosphate epimerase (RPE), transketolase (TKT), transaldolase (TAL) and glucose-6-phosphate isomerase (PGI). In case of the EMP pathway, again five enzymes would have to combine: phosphofructokinase (PFK), fructose-1,6-bisphosphate aldolase (FBA), triosephosphate isomerase (TPI), glyceraldehyde-3-phosphate dehydrogenase 1 (GAPDH1) and phosphoglycerate kinase (PGK). Seven of the mentioned enzymes, namely RPI, RPE, TKT, PGI, FBA, TPI and PGK fulfill a role both in the CBB cycle and in one of the glycolytic routes, and what is more, they do not possess isoforms. This implies, that, in order to form metabolons, these enzymes would have to partition into two populations: one population catalyzing the CBB cycle reaction, while the other population is catalyzing the glycolytic reaction in metabolic separation. Whether cyanobacteria and plants perform a spatial separation of glycolytic routes and the CBB cycle in form of substrate channeling is an interesting question that should be addressed in future studies. However, according to current knowledge, a situation without spatial separation is to be assumed. The following chapter will suggest a model of cyanobacterial metabolism, where a free exchange of intermediates between the CBB cycle and glycolytic routes is assumed.

2 Hypothesis development

2.1 Three glycolytic shunts: PGI shunt, ED shunt and OPP shunt

In order to illustrate the overlap between glycolytic routes and the CBB cycle, a schematic overlay picture has been constructed (fig. 6 A). Flow direction of the CBB cycle is indicated by violet shading. It is apparent that many reactions of the OPP pathway as well as the EMP pathway are identical with reactions of the regenerative part of the CBB cycle (fig. 6 A, orange boxes). All of the shared reactions have a $\Delta G_r'$ close to zero (calculated according to Flamholz *et al.*, 2012). Net flux direction of these reactions will be determined by substrate and product concentrations, which are in turn determined by the activity of more exergonic adjacent reactions. When the CBB cycle is operating, high amounts of 3-phosphoglycerate are formed due to the irreversible activity of PRK and RubisCO. This will shift many of the shared reversible reactions into an anabolic direction. Metabolic flux analyses in *Synechocystis* have confirmed that even under low light mixotrophic conditions, all shared reactions show a net flux in anabolic (CBB cycle) direction. When glucose utilization is taking place via the oxidative part of the PP pathway (ZWF, PGL and GND), as observed during light, ribulose-5-phosphate is formed. Since there is a net flux of the non-oxidative part of the PP pathway in anabolic direction (CBB cycle direction), as has been measured by You *et al.* (2014), Nakajima *et al.* (2014) and Ueda *et al.* (2018), ribulose-5-phosphate has to flow into the CBB cycle via PRK to solve the flux equation. Thus, the oxidative part of the PP pathway functions as an anaplerotic reaction for the CBB cycle. This metabolic path will from now on be referred to as ‘OPP shunt’. Glucose utilization via the PGI reaction, as has been observed under higher light intensities, was attributed by the authors as a flux through the EMP pathway (Yang *et al.*, 2002; Ueda *et al.*, 2018). However, under the same conditions the FBA and FBP reactions showed a net flux in anabolic direction (towards glucose formation). In order to solve this flux equation, the PGI-derived fructose-6-phosphate will, according to the here presented model, not proceed the EMP flux via PFK, but rather enter the CBB cycle as an anaplerotic reaction (fig. 6 B). This metabolic path will be referred to as ‘PGI shunt’. The Entner-Doudoroff pathway has not been subject to flux analyses yet. However, due to the strong growth phenotype of the KDPG aldolase mutant Δ*eda* under mixotrophic conditions (Chen *et al*., 2016), a metabolic function under these conditions is likely. I suggest that the first two reactions of the ED pathway, namely EDD and EDA, also represent an anaplerotic reaction for the CBB cycle. This metabolic path will from now on be referred to as ‘ED shunt’. The three hypothetical shunts alongside the CBB cycle are illustrated in figure 6 B or on the last page of this document.

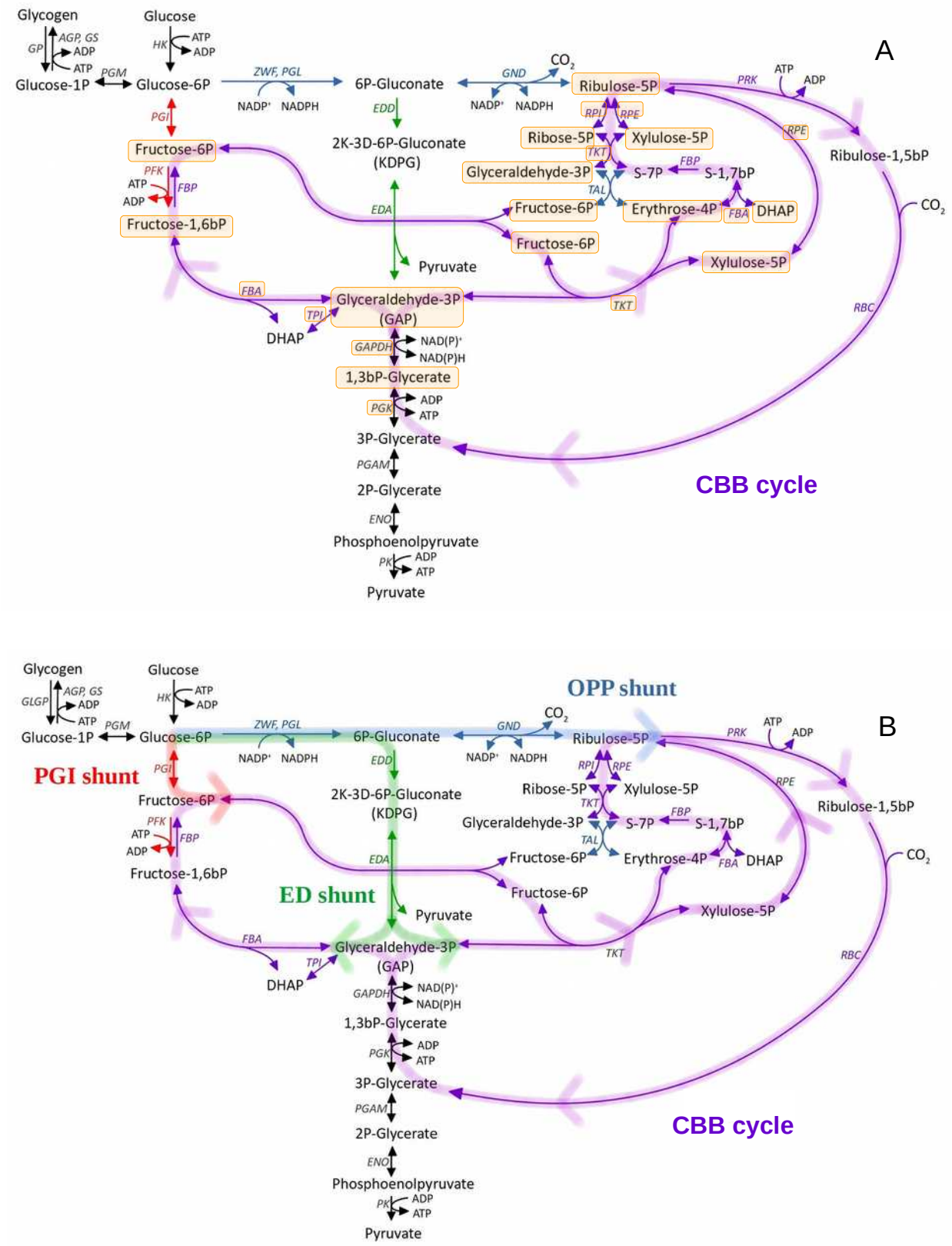

Figure 6: Three glycolytic shunts. Shown are two schematic overlay pictures of the CBB cycle and glycolytic routes in cyanobacteria. Enzymes and intermediates that are shared between the CBB cycle and glycolytic routes are marked with orange boxes (A). The second picture (B) shows the three hypothesized glycolytic shunts next to the CBB cycle: the PGI shunt (red), the OPP shunt (blue) and the ED shunt (green). Two-headed arrows indicate bidirectionality under physiological conditions (according to Flamholz *et al*., 2012). In case of the GAPDH reaction, anabolic and catabolic fluxes are distributed between two isoforms. Expected overall flow direction is indicated by fat translucent arrows. Stoichiometries were not considered.

Glycolytic shunts should not be restricted to mixotrophic growth conditions. As has been mentioned earlier, a mixotrophic situation can also occur intracellularly when glycogen is degraded during photoautotrophic growth conditions. Glycogen breakdown during light has been reported in cyanobacteria under several conditions, such as during awakening from dormancy (Doello *et al.*, 2018), after transfer from high CO_2 conditions to low CO_2 conditions (Eisenhut *et al.*, 2008) as well as after transfer from high light to low light conditions (Liu *et al.*, 2013; Ueda *et al.*, 2018). Glycogen phosphorylase and phosphoglucomutase generate glucose-6-phosphate, which, according to the model presented here, can be funneled into the CBB cycle via the three glycolytic shunts: OPP shunt, PGI shunt and ED shunt (fig. 7 B). This situation is very similar to the mixotrophic situation. Glycolytic shunts can also play a role without a net degradation of glycogen. In this scenario, glucose-6-phosphate, which is the substrate of all three glycolytic shunts, needs to be generated by a flux out of the CBB cycle via glucose-6-phosphate isomerase (PGI). However, since PGI can only have one net flux direction, usage of the PGI shunt under this condition is not possible. The OPP and ED shunt, on the other hand, can operate during these conditions (fig. 7 C).

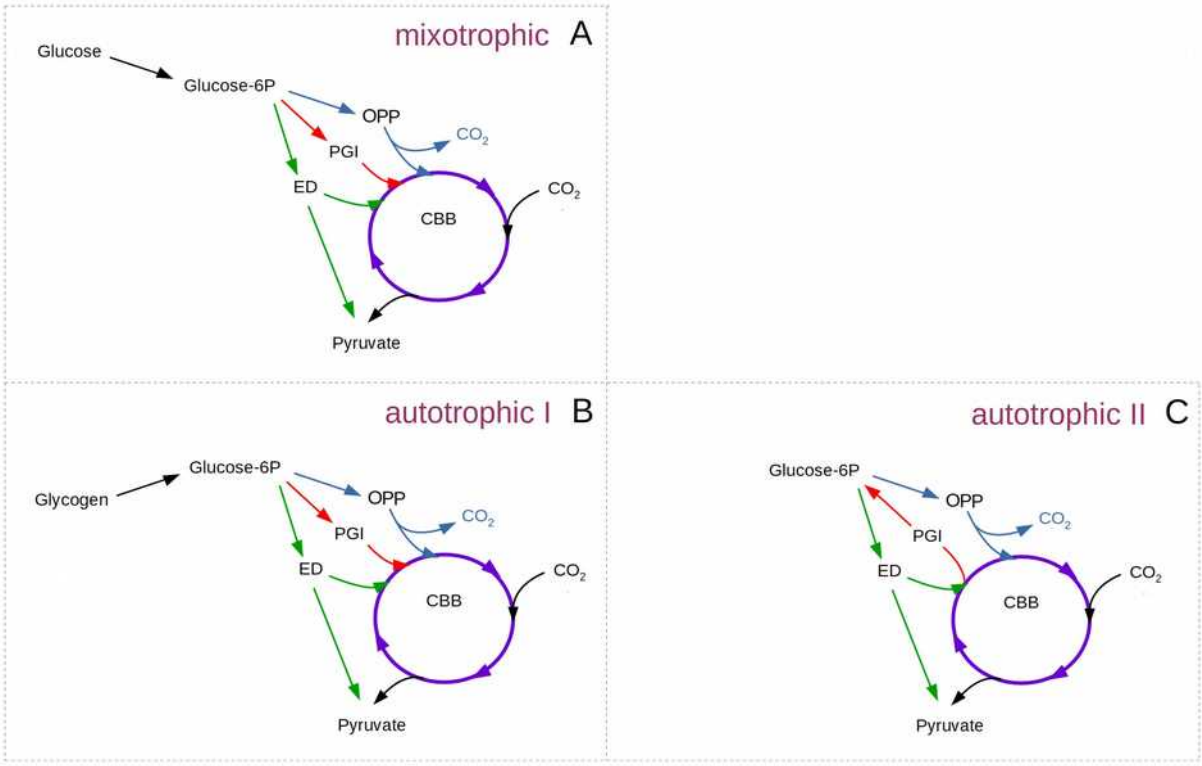

Figure 7: Schematic illustration of the CBB cycle with the three hypothetical glycolytic shunts under mixotrophic and photoautotrophic conditions. Shown is one scenario of glycolytic shunt utilization under mixotrophic conditions (A) as well as two scenarios under photoautotrophic conditions, either during a net glycogen degradation (B) or during a flux out of the CBB cycle via PGI (C).

2.2 Advantages of employing three glycolytic shunts

In an experiment where a functional CBB cycle was heterologously expressed in *E. coli*, it was shown that optimal CBB flux requires a strict regulation of reactions branching off the CBB cycle (Antonovsky *et al.*, 2016). If too much carbon leaves the CBB cycle via biomass producing reactions, for example for ribose production, autocatalysis of the cycle will be impaired since not enough carbon is regenerated for follow-up reactions. Thus, having three anaplerotic reactions with different entry points into the CBB cycle might increase metabolic flexibility and autocatalysis of the CBB cycle. Not only the balance of intermediates, but also of cofactors like ATP and NADPH, is essential for an optimal CBB cycle flux. In fact, synchronizing the ATP and NADPH demand of the CBB cycle with the outputs of the photosynthetic electron transport chain is one of the greatest challenges of photoautotrophic organisms (Nogales *et al.*, 2012). Usually, this synchronization process is accomplished by altering the output of the light reaction. However, the underlying mechanisms are rather slow. During quickly changing environmental conditions, it might be beneficial to have additional faster response mechanisms. The usage of different shunts could provide such a mechanism.

2.3 Hypothesis formulation

Taking these thoughts together, the following hypothesis can be formulated: The three glycolytic shunts PGI shunt, OPP shunt and ED shunt are anaplerotic reactions for the CBB cycle. They constitute an entrance for either glucose that is taken up during mixotrophic conditions or for glycogen-derived glucose during photoautotrophic conditions into the central carbon metabolism. The ED and OPP shunt can also occur during photoautotrophic conditions without a degradation of glycogen, thereby providing bypass reactions to the classical regenerative phase of the CBB cycle. These anaplerotic reactions can stabilize flux in the CBB cycle during changing environmental conditions by refilling the cycle with intermediates or by influencing ATP and NADPH ratios and thereby improving synchronization with the photosynthetic electron transport.

3 Aim of this dissertation

(1) Characterization of the physiological role of the Entner-Doudoroff pathway in the cyanobacterium *Synechocystis sp.* PCC 6803.

(2) Experimental confirmation of the glycolytic shunt hypothesis under mixotrophic conditions and photoautotrophic conditions.

(3) Development of a new model for the central carbon metabolism of cyanobacteria and plants.

4 Material & Methods

4.1 Material

4.1.1 Chemicals

All chemicals were purchased in analytical quality from Becton Dickinson (Heidelberg, Germany), Merck (Darmstadt, Germany), Roth (Karlsruhe, Germany) or Sigma Aldrich (Steinheim, Germany). Water for preparation of solutions and buffers was ultrapurified by a water purification device (Purelab Chorus 1, Elga Labwater, Celle, Germany).

4.1.2 Enzymes

Enzyme	Activity	Supplier (location)
Amyloglucosidase (from *Aspergillus niger*)	70 U/mg	Sigma Aldrich (Steinheim, Germany)
Hexokinase/Glucose-6-phosphate dehydrogenase solution (from *yeast*)	340 U/mL HK 170 U/mL G6PDH	Roche (Mannheim, Germany)
6-phosphogluconate dehydrogenase (from *E. coli*)	50 U/mL	Megazyme (Wicklow, Ireland)
Gluconate kinase (from *E. coli*)	400 U/mL	Megazyme (Wicklow, Ireland)
Glucose dehydrogenase (from *Pseudomonas sp*.)	200 U/mg	Sigma Aldrich (Steinheim, Germany)
Phosphoglucoisomerase (from *yeast*)	2 mg/mL	Boehringer (Mannheim, Germany)
DreamTaq DNA polymerase	5 U/µL	Thermo Fisher Scientific (Waltham, USA)
Pfu DNA polymerase	2.5 U/µL	Thermo Fisher Scientific (Waltham, USA)
EcoRI	10 U/µL	Thermo Fisher Scientific (Waltham, USA)
HindIII	10 U/µL	Thermo Fisher Scientific (Waltham, USA)
XhoI	10 U/µL	Thermo Fisher Scientific (Waltham, USA)

4.1.3 Oligonucleotides

Oligonucleotides (primers) are short DNA fragments (usually 16-20 bp) that bind specifically to single stranded DNA in a polymerase chain reaction (chapter 4.2.2) and thereby define the amplified region. All oligonucleotides that were used during this dissertation are shown below. All oligonucleotides were designed manually and were ordered from Sigma Aldrich (Steinheim, Germany). Oligonucleotides were categorized into 3 blocks: 1. primers for generation of knock-out constructs, 2. primers for generation of overexpression constructs and 3. sequencing primers.

Primer name	Primer sequence (5‘ to 3‘)	Annealing temperature
Pgi-out1	TTAACCACACACTGTCGCCAAA	58 °C
Pgi-in1	TCAATAATATCGAATTCCTGCAG-GCCAATCTTGATAACGTTGCCA	58 °C
Pgi-in2	AGCGAGGTGCCGCCATCAAGCTT-CCAGTGGCGGAGTTAAGACAGA	58 °C
Pgi-out2	TTGGTGTCAACGGGGGAATCGT	58 °C
Gap2out1	GTTAACGTCTACAATCACCTGCCGG	58 °C
Gap2in1	ATCAGAGATTTTGAGACACAACGTGG-GTTCGTCTTGCCCTCTCTGTTTTAGC	58 °C
Gap2in2	CTTTCTGGCTGGATGATGGGGCGAT-GTGGACTTGGCTGAAATTGTGGCTA	58 °C
Gap2out2	CCATAACCCTGAAAGCATTTCTGTG	58 °C
Psm2-Pcpc-for	CATGAAGCGGTGAGTTTAGC-ACCTGTAGAGAAGAGTCCCTGAA	58 °C
Pcpc-R-Gdh	GTTTTTCCAGTTAATTCCAT-TGAATTAATCTCCTACTTGACTTTATG	58 °C
Gdh-F	ATGGAATTAACTGGAAAAAC	54 °C
Gdh-R-Trbc	CCGACAATCCAAACACCGGT-CTAAAACTTCAAATATTCTGCTCC	54 °C
Trbc-F	ACCGGTGTTTGGATTGTCGG	58 °C
Trbc-psm2-rev	CCTCATCCTGTCTCTTGATCC-GCTGTCGAAGTTGAACATCAG	58 °C
M13 forward	AGGGTTTTCCCAGTCACGACGTT	
M13 reverse	GAGCGGATAACAATTTCACACAGG	
Psm2_for	GACCCAGTTAATGGCAAACA	
Psm2-4.16-rev	GAATAGCCTCTCCACCCAAG	

4.1.4 Plasmids

Plasmid	Target organism	Supplier/reference
TOPO pCR 2.1	*E. coli*	Thermo Fisher Scientific (Waltheim, USA)
pSM2	*Synechocystis*	Zhou *et al.*, 2014

4.1.5 Bacterial strains

Synechocystis sp. PCC 6803 (glucose tolerant)

single deletion strains

Strain	Deleted genes	Gene number	AB	Ref.
Δ*eda*	KDPG-Aldolase	sll0107	Gm	Chen *et al.*, 2016
Δ*zwf*	Glucose-6-phosphate dehydrogenase	slr1843	Cm	Chen *et al*., 2016
Δ*gnd*	6-Phosphogluconate dehydrogenase	sll0329	Em	Chen *et al*., 2016
Δ*pfk*	Phosphofructokinase 1 and 2	sll1196 & sll0745	Km, Sp	Chen *et al.*, 2016
pgi/Δ*pgi*	Glucose-6-phosphate isomerase	slr1349	Cm	this thesis
Δ*gap2*	Glyceraldehyde-3-phosphate dehydrogenase	sll1342	Km	this thesis
Δ*glgP*	Glycogen phosphorylase 1 and 2	sll1356 & slr1367	Km, Sp	Nichelmann, 2019, unpublished

multi deletion strains

Strain	Ref.
Δ*eda*Δ*pfk*	Chen *et al*., 2016
Δ*eda*Δ*zwf*	Gutekunst, 2017, unpublished
Δ*eda*Δ*gnd*	Schreiber, 2016
Δ*eda*Δ*pfk*Δ*zwf*Δ*gnd*	Chen *et al*., 2016
Δ*pfk*Δ*zwf*	Chen *et al*., 2016
Δ*pfk*Δ*zwf*Δ*gnd*	Chen *et al*., 2016
pgi/Δ*pgi*Δ*eda*	this thesis
pgi/Δ*pgi*Δ*gnd*	this thesis
pgi/Δ*pgi*Δ*eda*Δ*gnd*	this thesis

overexpression strains

Strain	Overexpressed genes	Gene number	AB	Ref.
$PcPc_{560}$gdh1 in pSM2	Glucose dehydrogenase 1 (putative)	sll1709	Km	this thesis

Escherichia coli

Strain	Reference
One Shot TOP10	Thermo Fisher Scientific (Waltheim, USA)
BL21 (DE3)	Thermo Fisher Scientific (Waltheim, USA)

4.1.6 Cultivation media

BG11 medium (Stanier *et al.*, 1971) was used for cultivation of *Synechocystis* and LB medium for cultivation of *E. coli*. Both media were prepared in water and autoclaved for at least 20 min before usage. In case of liquid media, $FeNH_4$ citrate (for BG11), antibiotics (optionally) and glucose (optionally) were added after autoclaving.

BG11 medium

Ingredient	Concentration
$NaNO_3$	17.6 mM
N-Tris(hydroxymethyl)methyl-2-aminoethane sulfonic acid (TES)	5 mM
$MgSO_4$	0.304 mM
$CaCl_2$	0.245 mM
Na_2CO_3	0.189 mM
K_2HPO_4	0.175 mM
H_3BO_3	46.3 µM
Citric acid	31.2 µM
$FeNH_4$ citrate	22.8 µM
$MnCl_2$	9.1 µM
Na_2EDTA	2.79 µM
Na_2MoO_4	1.61 µM
$ZnSO_4$	0.77 µM
CuSO4	0.32 µM
$Co(NO_3)_2$	0.17 µM

Supplement	Concentration
Bacto Agar	15 g/L
$Na_2S_2O_3$ (for agar plates)	1 mM
Kanamycin	50 mg/L
Spectinomycin	20 mg/L
Chloramphenicol	20 mg/L
Erythromycin	25 mg/L
Gentamycin	5 mg/L

LB medium

Ingredient	Concentration
yeast extract	5 g/L
tryptone	10 g/L
NaCl	10 g/L

Supplement	Concentration
Bacto Agar	15 g/L
Ampicillin	100 mg/L
Kanamycin	50 mg/L

4.2 Molecular biological methods

4.2.1 Genomic DNA isolation of *Synechocystis*

Genomic DNA was extracted from *Synechocystis* according to the phenol-chloroform method (from Chomczynski & Sacchi, 1987). An OD volume of 20-30 OD*mL culture was pelleted (5 min, 9000 g, 4 °C) and resuspended in 1 mL fresh BG11 medium. The resuspendate was transferred to a centrifugation cup and again centrifuged (5 min, 9000 g, 4 °C). The pellet was then resuspended in 100 µL TE buffer (10 mM Tris and 1 mM EDTA, pH 7.4) and afterwards lysated by addition of 2 µL 10 % (w/v) SDS, 100 µL phenol-chloroform-isoamylalcohol solution (25:24:1) (v/v/v) (4 °C), 100 µL glassbeads (0.17-0.18 mm diameter; Sartorius, Göttingen) followed by 3 min of vortexing. The lysate was then centrifuged (2 min, 10000 *g*, RT), which resulted in the emergence of three phases. The uppermost phase, containing the nucleic acids, was transferred to a new centrifugation cup. For further purification of the nucleic acid phase, 100 µL phenol-chloroform-isoamylalcohol solution (25:24:1) (v/v/v) (4 °C) were added and the solution was again centrifuged (2 min, 10000 g, RT). The uppermost phase was again transferred to a new centrifugation cup, this time mixed with 100 µL chloroform-isoamylalcohol solution (24:1) (v/v) (RT) and again centrifuged (2 min, 10000 *g*, RT). This process was repeated twice. The resulting supernatant was then transferred to a new centrifugation cup and 3 M sodium acetate (pH 5), according to 10 % of the supernatant volume, were added and the cup mixed by inverting it. Afterwards, absolute ethanol (-20 °C) was added according to 250 % of the supernatant volume. Samples were then incubated at -20 °C for 2 h and afterwards DNA was precipitated by centrifugation (15 min, 13000 *g*, -9 °C). The supernatant was discarded and the pellet washed by addition of 1 mL 70 % (v/v) ethanol (-20 °C) followed by another centrifugation step (5 min, 13000 *g*, RT). The supernatant was discarded and the pellet dried in a SpeedVac vacuum concentrator (Keutz, Reiskirchen, Germany) for 5-10 min. Finally, the dried pellet was dissolved in 20 µL TE buffer and DNA concentration determined photometrically with the help of a NanoDrop 2000 (ThermoFisher Scientific, Waltham, USA).

4.2.2 Polymerase Chain Reaction

The Polymerase chain reaction (PCR) is an *in vitro* method that allows a specific amplification of DNA sections (Mullis *et al.*, 1986). The PCR reaction can be divided into three functional steps: 1. denaturation of a double stranded DNA template, 2. annealing of the forward and reverse primer (chapter 4.1.3) on two complementary single stranded DNA strands, 3. attachment of a DNA polymerase to each primer and strand elongation in 5‘ to 3‘ direction. Repetition of these steps led to an exponential amplification of the DNA section that is flanked by the two primers. In this dissertation, two different DNA polymerase were used: the Dream Taq DNA polymerase and the Pfu DNA polymerase (both from Thermo Fisher Scientific, Waltham, USA). Due to its 3‘ to 5‘ exonuclease activity (proof-reading), the Pfu polymerase was used for amplification of fragments for the generation of overexpression constructs. Dream Taq DNA polymerase was used for amplification of fragments for the generation of deletion mutants. PCR reactions were prepared according to table 1 and performed inside a PTC-200 gradient thermocycler (MJ Research, Watertown, USA) using the protocol shown in table 2. The annealing temperature was dependent on the primer properties and are listed next to each primer in chapter 4.1.3.

Table 1: reagents of a PCR reaction

Reagent	stock conc.	end conc.	Volume
Dream Taq buffer or Pfu buffer	10 x	1x	5 µL
dNTP mix	2 mM each dNTP	0.2 mM each dNTP	5 µL
forward primer	5 µM	0.5 µM	5 µL
reverse primer	5 µM	0.5 µM	5 µL
template DNA	2 ng/µL	0.2 ng/µL	5 µL
Dream Taq DNA Pol. or Pfu DNA Pol.	5 U/µL 2.5 U/µL	0.04 U/µL 0.02 U/µL	0.4 µL
water	-	-	24.6 µL
total	-	-	50 µL

Table 2: PCR reaction protocol

Step	Temperature	Duration	
Initial Denaturation	95 °C	1 min	
Denaturation	95 °C	30 s	35 x
Annealing	chapter 4.1.3	30 s	
Extension	72 °C	0.5 - 1 kb/min	
Final Extension	72 °C	10 min	

4.2.3 Fusion PCR

The fusion PCR is a modified polymerase chain reaction protocol that can be used to assemble multiple DNA fragments in a desired orientation. The fusion PCR generally consists of three seperated PCR reactions: 1. amplifcation of the to-be-assembled DNA fragments via PCR with primers that contain 5‘ overhangs with complementary parts to the ends of the neighbouring fragments, 2. the acual fusion PCR where the to-be-assembled fragments are denaturated and aligned via annealing of their complementary ends, 3. the reamplification PCR, where succesfully aligned fragments are amplified using the forward primer of the first and the reverse primer of the last fragment. The amplification of fragments (1st PCR) was performed according to the general PCR protocol (chapter 4.2.2). PCR products were gel purified (chapter 4.2.5) before being used in the next reaction. Table 3 shows the reagents of a fusion PCR (2nd PCR). The template fragments were used in concentrations relative to their size in an end concentration of 2 ng/µL * (bp fragment/ total bp all fagments) of each fragment. Fusion PCRs were performed in a PTC-200 gradient thermocycler (MJ Research, Watertown, USA) using the same protocol as the normal PCR (chapter 4.2.2, tab. 2). For the reamplification PCR (3rd PCR), the fusion PCR product (template) was diluted 1:1000. The protocol of the reamplification PCR was otherwise consistent with the normal PCR protocol.

Table 3: reagents of the fusion PCR

Reagent	stock conc.	end conc.	Volume
Dream Taq buffer	10 x	1x	5 µL
dNTP mix	2 mM each dNTP	0.2 mM each dNTP	5 µL
DNA fragments	10 * (bp fragment/bp total) ng/µL each fragment	2 * (bp fragment/bp total) ng/µL each fragment	10 µL
Dream Taq DNA Pol.	5 U/µL	0.04 U/µL	0.4 µL
water	-	-	29.6 µL
total	-	-	50 µL

4.2.4 Isothermal DNA assembly

Isothermal DNA assembly describes a category of *in vitro* processes that enable the assembly of multiple DNA fragments. The most prominent isothermal DNA assembly is the Gibson assembly (Gibson *et al.,* 2009). In this dissertation, the NEBuilder Hifi DNA Assembly Cloning Kit was used (New England Biolabs, Frankfurt am Main). Similar as has been described for the fusion PCR (chapter 4.2.3), the to-be-assembled fragments require complementary sections (15-80 bp) at their end regions. The assembly is accomplished by the combined activity of three enzymes, namely an exonuclease, a DNA polymerase and a DNA ligase. First, the exonulcease creates single-stranded 3‘ overhangs which enable complementary parts to anneal. The DNA polymerase then fills in gaps within each annealed fragment. Finally, the DNA ligase seals nicks in the assembled DNA. Contrary to the fusion PCR, DNA assembly can be used to assemble inserts into a vector. DNA assemblies were performed according to the recommendation from the supplier (New England Biolabs, Frankfurt am Main, Germany) with a vector to insert ratio of 1:1. The desired fragments were amplified via PCR and gel purified (chapter 4.2.5). The vector (pSM2) was linearized by restriction digest and also gel purified. The reaction was then prepared according to table 4 and incubated at 50 °C for 60 min.

Table 4: reagents of a NEBuilder Hifi DNA asembly

Reagent	stock conc.	end conc.	Volume
NEBuilder master mix	2 x	1 x	10 µL
inserts		0.032 pmol each	< 10 µL
vector (pSM2)		5 ng/µL (0.032 pmol)	< 10 µL
water	-	-	< 10 µL
total	-	-	20 µL

4.2.5 Agarose-gelelectrophoresis and gel purification

The agarose-gelelectrophoresis allows a seperation of DNA molecules by size. In an applied electrical field, DNA molecules experience a force that causes them to move through an agarose matrix towards a positively charged anode. The pores of the agarose gel cause a retardation of passing DNA molecules that is proportional to their respective size. Thus, the larger the DNA molecules, the shorter their travel distance at a given time. In order to achieve a calibratation of travel distance with DNA size, a DNA ladder with known fragment sizes is applied alongside the DNA samples. In this dissertation, the GeneRuler 1 kb DNA ladder (Thermo Fisher Scientific, Waltham, USA) was used. Agarose-gelelectrophoreses were accomplished for two purposes: Preperatively as a measure to purify DNA fragments or analytically for mere size determination. Preparative gels were carried out in volumes of 60 µL, of which 50 µL were constituted by sample DNA (either from PCR or restriction digest) and 10 µL by 5x loading dye (tab. 5). For analytical gels, 2.5 µL sample DNA (in case of PCR product) or 10 µL (in case of restriction digest) were mixed with 3 µL 5x loading dye and filled up to 15 µL with water. Samples were then loaded into a previously prepared agarose gel (tab. 5), which was inserted into a gel chamber (Biometra, Göttingen, Germany) filled with TBE buffer (tab. 5) and run at 140 V for 20 to 40 min. Afterwards, gels were transferred into a gel documentation system (TF 20 M Vilber Lourmat, Torcy, France; Alpha Imager 2200, Biozym, Hess. Oldendorf, Germany) where DNA fragments were visualized by illumination with UV light with a wavelength of 312 nm. Visualization was made possible by ethidium bromide, a DNA-intercalating dye that emits orange light (590 nm) upon UV light absorption. In case of prepeartive gels, only weak intensities of UV light (70 %) were used and DNA fragments of interest were cut out using a scalpel.

DNA was purified from agarose cut-outs with help of a Nucleospin DNA purification kit (Macherey-Nagel, Düren, Germany). The protocol that is listed in the following is consistent with the recommendations from the supplier and all listed buffers and columns were included in the kit. In the first step, the gel cut-out was dissolved in NTP buffer (200 µL per 100 mg of gel) by incubation for approximately 5 min at 50 °C. The resulting solution was then loaded onto a Nucleospin gel clean-up column and centrifuged for 30 s at 11000 *g* at RT to bind the DNA molecules to the silica membrane of the column. In order to remove unwanted carry-over substances, the column was washed by adding 700 µL washing buffer NT3 and centrifugating for 30 s at 11000 g. This process was repeated twice. Afterwards, the column was once more centrifuged (30 s, 11000 *g*) in order to completely remove remaining liquids. For elution of DNA, the column was put into a new microcentrifuge tube, 20 µL preheated elution buffer NE were added and incubated for 5 min at 70 °C. Then, the column was centrifuged for 1 min at 11000 *g* at RT. In order to improve elution efficiency, another 20 µL elution buffer were added and the centrifugation repeated. DNA concentration of the eluate was determined photometrically with the help of a NanoDrop 2000 (ThermoFisher Scientific, Waltham, USA).

Table 5: substances and buffers of an agarose-gelelectrophoresis

Substance/buffer	Ingredients
agarose gel	0.8 % (w/v) agarose, 0.001 % (w/v) ethidium bromide in 1x TBE buffer
5 x loading dye	50 % (v/v) glycerine, 50 % (v/v) 1x TBE, 0.2 mg/ml bromphenol blue
1 x TBE buffer	10.8 g/l Tris, 5.5 g/l boric acid, 0.93 g/l $Na_2EDTA^* 2 H_2O$

4.2.6 Restriction digestion

A restriction digestion allows the *in vitro* cleavage of DNA molecules at specific recognition sites using restriction endonucleases. In this dissertation, restriction disgests were done either for cloning purposes (preparative digestion) or to verify succesful construction of plasmid DNA (analytical digestion). Preparative restriction digests were carried out in volumes of 50 µL comprising of 30 µL sample DNA, 2 µL restriction enzyme, 5 µL enzyme specific digestion buffer and 13 µL water. Analytical restriction digests were carried out in a total volume of 10 µL, comprising 3 µL sample DNA (plasmid), 0.5 µL restriction enzyme, 1 µL ezyme specific digestion buffer and 5.5 µL water. Reactions were carried out at 37 °C for 30 min in case of analytical digests or up to 2 h in case of preparative digests. Table 6 shows all restrictions enzymes and their respective buffers that were used in this dissertation.

Table 6: restriction enzymes and their respective reaction buffers that were used in this dissertation

Enzyme	Reaction buffer
EcoRI	buffer EcoRI (Thermo Fisher Scientific, Waltheim, USA)
HindIII	buffer R (Thermo Fisher Scientific, Waltheim, USA)
XhoI	buffer R (Thermo Fisher Scientific, Waltheim, USA)

4.2.7 Ligation into the TOPO vector

In vitro ligations allow the covalent linkage of DNA fragments, usually with the help of a DNA ligase. For the ligation of inserts into the TOPO vector, however, no DNA ligase was needed since the vector had topoisomerases attached to its 3‘ ends, which could perform ligation of the insert into the vector. One requirement for the ligation of inserts into the TOPO vector was that inserts had a 3‘ adenosine overhang, which could be achieved by using inserts that have been amplified with a taq polymerase. TOPO ligation was performed according to the TOPO TA cloning protocol (Thermo Fisher Scientific, Waltheim, USA), however in a 50 % reduced volume. 2 µL PCR product were mixed with 1 µL salt solution (Thermo Fisher Scientific, Waltheim, USA), 0.5 µL TOPO vector (Thermo Fisher Scientific, Waltheim, USA) and 0.5 µL water. The reaction was then carried out at RT for 5 min.

4.2.8 Transformation of *E. coli*

Transformation is the name of the process in which bacteria take up and utilize exogenous DNA, usually in form of a plasmid. The ability to take up exogenous DNA is defined as competence. Though competence occurs naturally in some bacteria (like *Synechocystis*), it needs to be induced in the laboratory for most bacteria (including *E. coli*), for example in form of a heat shock (chemical competence) (Sambrook & Russell, 2001). *E. coli* transformations were performed either with the chemically competent TOP10 strain (in case of TOPO vector) or the also chemically competent BL21 (DE3) strain (in case of pSM2 vector). For transformations of TOP10 cells, cells were thawed on ice and 2 µL of the TOPO cloning reaction were added. Cells were incubated on ice for 5 min and afterwards heat-shocked at 42 °C for 30 s in order to induce uptake of exogenous DNA. After the heat shock, cells were transfered back to ice and 250 µL SOC medium (Thermo Fisher Scientific, Waltheim, USA) was added. Cells were then shaken at 80 rpm and 37 °C for 1 h in a shaking incubator (4400 Innova Incubator Shaker; New Brunswick Scientific, Nurtingen, Germany). Afterwards, 100 µL were added to a pre-warmed LB agar plate containing ampicillin (100 mg/L) and incubated overnight at 37 °C.

4.2.9 Plasmid preparation

Plasmid preparation describes the procedure of extracting and purifying plasmid DNA from bacteria. Prior to the plasmid preparation, colonies were picked from the transformation spread-out (chapter 4.2.8) or alternatively 50 µL of a glycerine culture were taken and mixed with 2.5 mL fresh LB medium containing the respective antiobiotics and incubated overnight in a shaking incubator at 80 rpm and 37 °C. On the following day, plasmid DNA was isolated with help of a NucleoSpin plasmid purification kit (Macherey-Nagel, Düren, Germany). The protocol that is listed in the following is consistent with the recommendations from the supplier and all listed buffers and columns were included in the kit. First, 2 mL of the overnight cultures were centrifuged for 30 s at 11000 *g*. The supernatant was discarded and the pellet resuspended in 250 µL resuspension buffer A1. Afterwards, 250 µL lysis buffer A2 were added, tubes inverted for 6-8 times and incubated for 5 min at RT. Then, 300 µL neutralization buffer A3 were added and tubes again inverted for 6-8 times. Samples were then centrifuged for 5 min at 11000 *g* to precipitate cell debris. The emerging supernatant was loaded onto a Nucelospin plasmid column and centrifuged for 30 s at 11000 *g* at RT to bind the DNA molecules to the silica membrane of the column. In order to remove unwanted carry-over substances, the column was subsequently washed with 500 µL washing buffer AW (preheated to 50 °C) and 600 µL washing buffer A4, each time centrifugating for 30 s at 11000 *g* and discarding the flow through. Afterwards, the column was once more centrifuged (2 min, 11000 *g*) in order to completely remove remaining liquids. For elution of DNA, the column was put into a new microcentrifuge tube, 20 µL preheated

elution buffer AE were added and incubated for 5 min at 70 °C. Then, the column was centrifuged for 1 min at 11000 *g* at RT. In order to improve elution efficiency, another 20 µL elution buffer were added and the centrifugation repeated. DNA concentration of the eluate was determined photometrically with the help of a NanoDrop 2000 (Thermo Fisher Scientific, Waltheim, USA).

4.2.10 Transformation of *Synechocystis* and segregation of mutants

Since *Synechocystis* is naturally competent, no induction of competence was necessary. An OD volume of 50-100 OD*mL of an exponentially growing culture (two days after inoculation in Kniese tube) was pelleted by centrifugation (10 min, 8000 *g*) and resuspended in 600 µL BG11 medium. 300 µL of this suspension were mixed with 6-18 µg plasmid (transformation sample) and incubated for 5 h in darkness. Then, 90 µL of this suspension were added onto a nitrocellulose filter that was placed on top of a BG11 agar plate and distributed with a Drigalski spatula. After three days of cultivation, the nitrocellulose filter was transferred onto new agar plates containing the respective antibiotics of the plasmid to segregate for successful transformants. The agar plates were passaged every 2-3 weeks at least 6 times.

4.2.11 DNA sequencing

The sequencing (reaction) allows the in-vitro determination of the nucelotide sequence of a DNA molecule. Sequencing was performed according to the chain-termination method (Sanger *et al.*, 1977) by the Zentrum für Molekulare Biowissenschaften (ZMB) in Kiel. For the sequencing reaction, 3 µL plasmid (100 ng/µL) were mixed with 1 µL sequencing primer (chapter 4.1.3).

4.3 Physiological methods

4.3.1 Cultivation of strains

Synechocystis was cultivated in three different ways: 1. on agar plates, 2. in 50 mL Erlenmeyer flasks and 3. in Kniese tubes (manufactured by Eydam, Kiel, Germany). Cultivation on agar plates (1.5 % (w/v) Bacto Agar in BG11 medium) was used as storage of strains in between experiments or during segregation of mutants. Cells on agar plates were passaged every 2-3 weeks. Knock-out and overexpression strains were grown on agar plates containing antibiotics (see chapter 4.1.5 and 4.1.6). All agar plates were kept in a climate chamber at 28 °C, 60 % humidity and 50 µE m^{-2} s^{-1} of white light. Three to five days prior to an experiment, cells were scraped from agar plates and inoculated in liquid BG11 medium to form a batch preculture. Precultures were cultivated according to the type of follow-up experiment, thus either in Erlenmeyer flasks (in case of nitrate resuscitation experiments) or in Kniese tubes (for all other experiments). Erlenmeyer flasks were kept in a climate chamber at 28 °C, 60 % humidity and 50 µE m^{-2} s^{-1} of white light while shaking on a shaker (Shaker 3020, GFL, Burgwedel) at 100 rpm. Kniese tubes were placed in a photobioreactor (manufactured by Willi Hilke, Uslar, Germany), receiving 50 µE m^{-2} s^{-1} white light while being moderately bubbled with ambient air. The photobioreactors were kept in a clima chamber at 28 °C and 60 % humidity.

4.3.2 Growth rate analysis

In order to simplify comparison of growth curves of different experiments, a novel growth curve evaluation method was developed in this dissertation. It is common practice to describe bacterial growth behavior in form of growth rates (Novick, 1955). These growth rates usually rely on the assumption of an exponentially growing culture. While (most of the times) chemoheterotrophic bacteria can be brought to exponential growth quite easily, this is very difficult to accomplish for photoautotrophically growing cyanobacteria since an equal distribution of their growth substrates, namely light and CO_2, is very difficult to achieve due to self shading effects of the culture and limitations in bubbling technology. The resulting photoautotrophic growth curve can often be better described by a polynomial function of second degree (ax^2+bx+c). However, such a function has three parameters (a, b and c), which makes a comparable evaluation difficult. A novel growth curve evaluation method has been developed in this dissertation. The procedure will be explained by reference to an example experiment (fig. 8). The general idea was to approximate growth curves by creating several small linear regressions ($ax+b$) of three consecutive datapoints (so-called triplets) (fig. 8 A). This was done for the two investigated deletion strains and a *Synechocystis* WT that was cultivated in parallel (tab. 7). The slopes (a) of the linear functions of the deletion mutant triplets were divided by the slopes of the respective WT triplets. This resulted in a mutant/WT slope ratio for each triplet (tab. 8). These mutant/WT slope ratios were averaged and the resulting mean slope ratio can be

interpreted as the growth rate of the respective mutant in comparison to WT (fig. 8 B). As can be deduced from the here presented method, it is essential to always cultivate an identically-treated WT in parallel to the deletion mutants of interest. What is more, in order for the method to give reliable results, the WT, to which a mutant‘s growth behavior is compared, needs to be in a similar growth stage as the mutant. If, for example, the mutant exhibits a lag phase or the WT is already approaching the stationary phase while the mutant is still growing at maximum rates, the method will not give viable results.

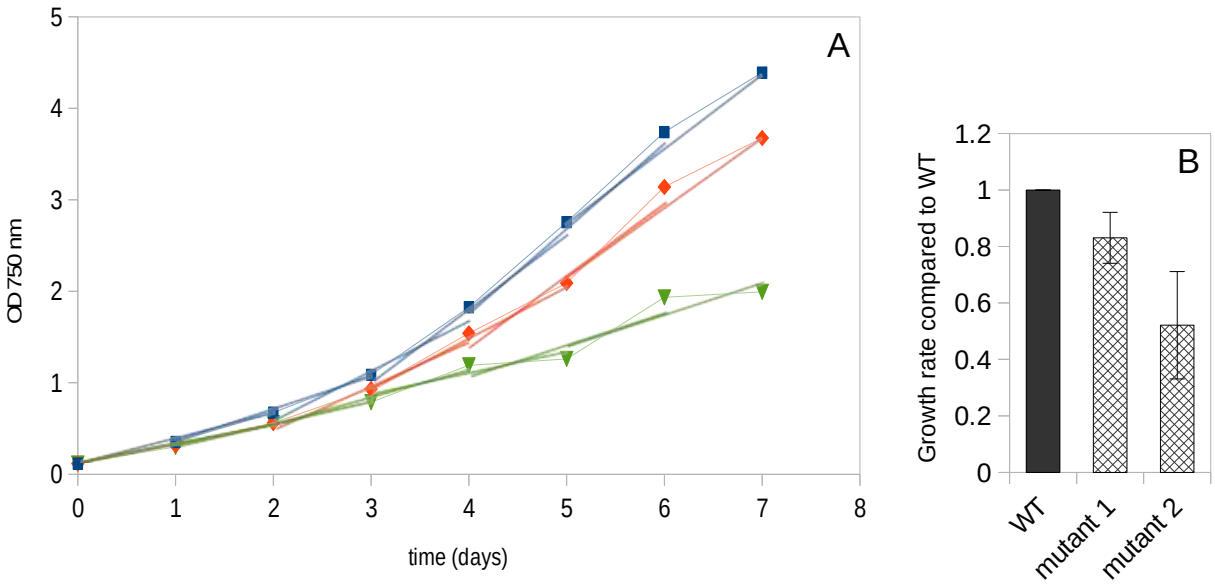

Figure 8: The ‚triplet regression‘ method. (A): Linear regressions were calculated for every consecutive three datapoints (triplets) of three fictional growth curves of WT (blue) and two mutants (orange and green) and are shown as fat transparent lines. (B): The resulting growth rates in comparison to WT. Shown are the mean triplet slopes of WT (=1) and the two mutants from table 8. Error bars represent standard deviation of triplets.

Table 7: Triplet slopes. Shown are the slopes of the six triplets from figure 8.

triplet	1	2	3	4	5	6
day	0-2	1-3	2-4	3-5	4-6	5-7
WT	0.28	0.37	0.58	0.83	0.96	0.82
mutant 1	0.22	0.31	0.49	0.58	0.80	0.79
mutant 2	0.22	0.24	0.32	0.24	0.37	0.37

Table 8: Triplet slopes relative to WT. The six triplet slopes of the two mutants from table 7 have been divided by the respective triplet slopes of WT. The mean value of all relative triplet slopes can be considered as the relative growth rate in comparison to WT.

triplet	1	2	3	4	5	6		mean	SD
mutant 1/WT	0.80	0.84	0.85	0.69	0.84	0.97		0.83	0.09
mutant 2/WT	0.79	0.67	0.55	0.28	0.39	0.45		0.52	0.19

4.3.3 Normalization of physiological parameters on OD volume

To simplify comparison of results from different experiments, a normalization parameter was used. The normalization parameter of choice was OD volume, which is the product of culture density (OD) and volume (mL). It could be shown by a colleague that OD volume correlates well with biomass but not with cell number. One OD*mL corresponds to 0.1894 mg cell dry weight (Jens Appel, unpublished). Optical densities were measured at 750 nm in a double-beam spectrophotometer (Uvikon 810, Kontron, Augsburg, Germany).

4.3.4 Measurement of chlorophyll *a* and phycocyanin contents

Intracellular chlorophyll *a* contents were measured either as absolute values or relatively in form of absorbance ratios. An absolute quantification was accomplished according to Lichtenthaler (Lichtenthaler, 1987). For this, an OD volume of 0.2-2 OD*mL sample culture was pelleted by centrifugation (5 min, 10000 *g*, RT). Pellets were then resuspended in 1 mL absolute methanol and shaken in an overhead shaker at around 50 rpm for 15 min to extract chlorophyll. Afterwards, cell debris was precipitated by centrifugation (5 min, 10000 *g*, RT) and the supernatant transferred to glass cuvettes. Absorption at 666 nm was measured and chlorophyll *a* concentration calculated by using the following equation: absorbance (666 nm)/0.0809 = chlorophyll *a* (µg/mL). Chlorophyll *a* concentrations (µg/mL) were then converted to cellular chlorophyll *a* contents (µg/OD*mL) by multiplying it with the precipitated volume (in this case 1 mL) and dividing it by the respective OD volume. As a second method, chlorophyll *a* contents were measured relatively in form of absorbance ratios. For this, an absorbance spectrum between 400 and 800 nm of 1 mL culture of an OD of 0.1–0.3 was taken by a double-beam spectrophotometer (UV-2501PC; Shimadzu, Kyoto, Japan). Relative chlorophyll *a* contents were then estimated by the following formula: (absorbance (685 nm) – absorbance (750 nm)) / absorbance (750 nm). Phycocyanin contents were also measured relatively in form of absorbance ratios. For this, an absorbance spectrum between 400 and 800 nm of 1 mL culture of an OD of 0.1–0.3 was recorded by a double-beam spectrophotometer (UV-2501PC; Shimadzu, Kyoto, Japan). Relative phycocyanin contents were then estimated by the following formula: (absorbance (618 nm) – absorbance (750 nm)) / absorbance (750 nm).

4.3.5 Measurement of CO_2 assimilation rates

CO_2 assimilation/respiration rates of *Synechocystis* were measured with the portable gas exchange system GFS-3000 from Walz (Effeltrich, Germany) (fig. 9 A). Since the device was plant-oriented and not suitable for liquid cultures, a novel protocol was designed to adjust the system to cyanobacteria. The basic idea was to mimic plant leaves by attaching cyanobacterial cultures onto agar plates that could be inserted into the measuring device. For this, lids were cut off 5 mL centrifugation cups (Eppendorf, Hamburg, Germany) and filled with 400 µL carbonate-free BG11 medium supplemented with 1.5 % (w/v) agar prior to the actual experiment. For sampling, an OD volume of 4 to 12 OD*mL sample culture was pelleted by centrifugation (5 min, 8000 *g*, RT) and resuspended in 200 µL carbonate-free BG11 medium. From this suspension, OD was measured and the volume was transferred equally onto two previously prepared agar-filled lids. The loaded lids were then put in front of a fan for 20 to 30 minutes to let excess medium evaporate and let the cells attach to the agar (fig. 9 B). Afterwards, the lids were stored in a plastic box that was inlayed with wet tissue and covered by a glass plate to provide a humid atmosphere. During drying and storage, cells were continuously illuminated by 50 µE m^{-2} s^{-1} light emitted by a fluorescence lamp (F17T8/Tl741, Philips, Hamburg, Germany). For the actual measurement, two replicate lids were put simultaneously inside the standard measuring head of the GFS-3000 device, where CO_2 assimilation/respiration rates were measured under varying light intensities. All other parameters were kept constant during all measurements: Flow rate was set to 750 µmol/s, CO_2 concentration to 550 ppm, relative humidity to 60 % and temperature to 28 °C. The light source was red light coming from an LED array module 3055 from Walz (Effeltrich, Germany). Each light intensity was measured for 1 min while measurement points were taken every 5 seconds. The assimilation rate (A) of each measurement point was calculated by the GFS software and was displayed as µmol CO_2 * m^{-2} * s^{-1}, which is its commonly used unit when measuring plant leaves. However, for the cyanobacterial system a calibration on biomass was preferred, which was accomplished by multiplying the value with the surface area of the agar plates, which was 3 cm^2 (2 x 1.5 cm^2), and then dividing it by the OD volume to finally yield pmol CO_2 / (S * OD * mL). Results from all cohesive measurement points were averaged and blank corrected. As a blank, cell-free agar-filled lids were measured. Figure 9 C shows typical light curves of *Synechocystis* WT as well as cell-free blanks. It can be seen that blanks conducted a small CO_2 assimilation of usually 0.01 – 0.05 µmol / (m^2 * s), most likely caused by a diffusion of atmospheric CO_2 into agar. This interpretation is supported by preliminary results (data not shown), which indicated that the CO_2 assimilation rates of blanks correlated with the difference between ambient CO_2 concentration and the concentration inside the measuring head. Measurement of the biomass dependency of the CO_2 signal furthermore showed that the optimal OD volume on the agar lids seemed to be between 4 and 12 OD*mL (fig. 9 D). OD volumes lower than 4 led to higher error bars, most likely due to the previously mentioned agar-diffusion effects and the resolution limit of the GFS device. At OD volumes higher

than 12, the signal seemed to decline slowly. This effect was most likely due to either light or CO_2 shading effects.

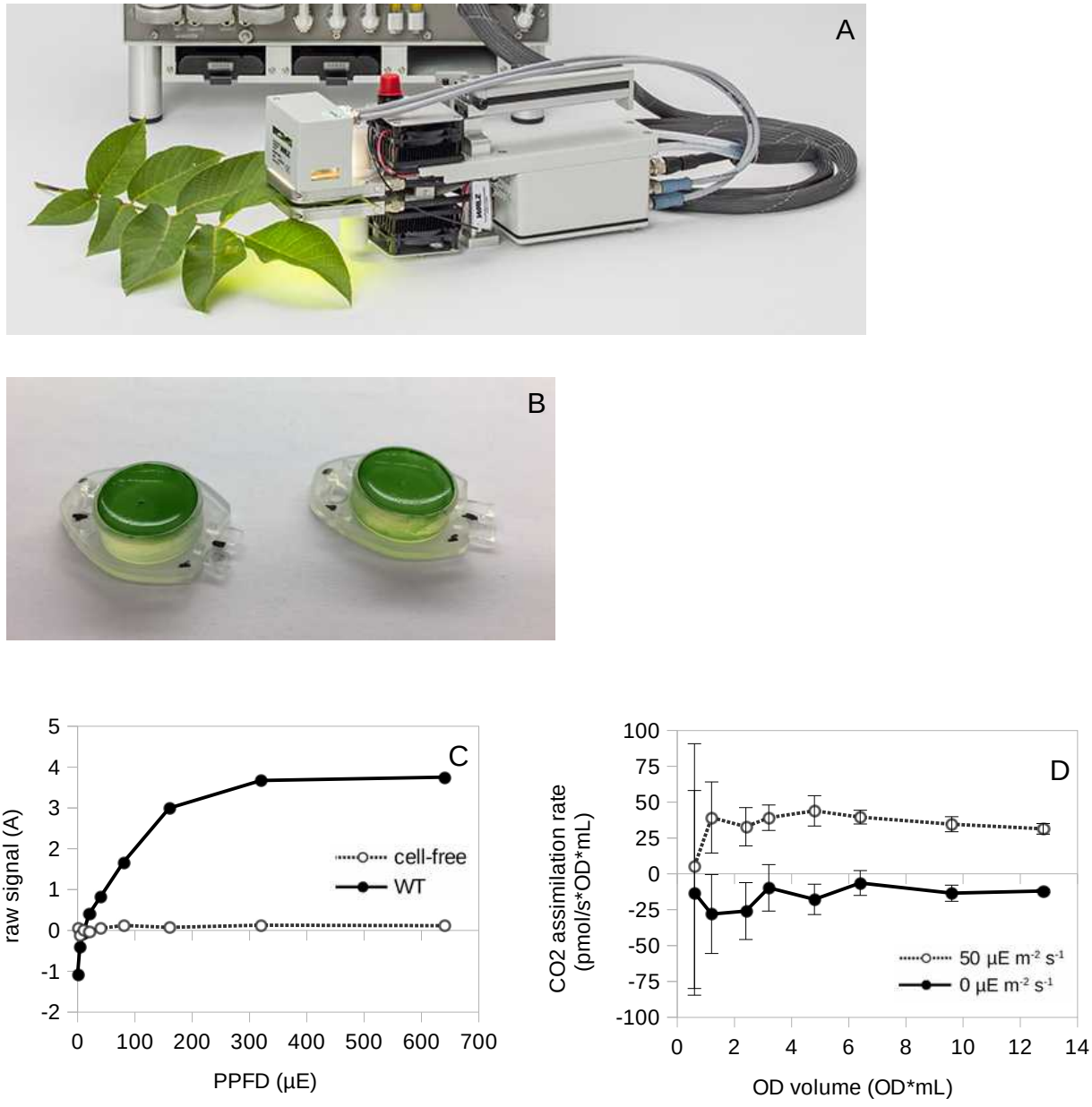

Figure 9: Measurement of CO_2 assimilation in cyanobacteria. Image A shows a GFS-3000 gas exchange system from Walz (Effeltrich, Germany) with a standard measuring head for measuring plant leaves (image taken from www.walz.com). Image B shows *Synechocystis* attached to custom-made agar-filled lids. Chart C shows typical CO_2 assimilation light curves of *Synechocystis* WT and a cell-free negative control. The ordinate shows raw signal (µmol $CO_2/(m_2*s)$), also called *A*, as given out by the GFS device. Chart D shows the dependency of the amount of biomass (in form of OD volume) that has been loaded onto the agar lids on the CO_2 assimilation rate. Error bars represent standard deviation between measurement points.

4.3.6 Enzyme activity measurements

Enzyme activity was measured in crude cells extracts. For the generation of crude cell extracts of *Synechocystis*, an OD volume of 30-50 OD*mL sample culture was pelleted by centrifugation (5 min, 9000 *g*, 4 °C) and the pellet resuspended in 0.5 mL 100 mM Tris buffer (pH 7.6). The resuspendate was then transferred to centrifugation cups with screwed lids (max 500 µL/cup) and glass beads (0.17-0.18 mm diameter; Sartorius, Göttingen, Germany) were added so that 1-2 mm liquid remained above the dispersion. Samples were then vortexed for 10 min in a cold room (4 °C). Afterwards, the glass beads were pelleted by centrifugation in two consecutive centrifugation steps (1 min, 1000 *g*, 4 °C and 10 min, 1600 *g*, 4 °C). The supernatant was transferred to new centrifugation cups in between centrifugations. In order to precipitate cell debris, the supernatant was centrifuged (15 min, 18000 *g*, 4 °C) one more time. The supernatant constituted the final cell extract and was measured for its protein concentration (chapter 4.3.7) and kept on ice until further enzyme activity measurements.

Enzyme activity was measured photometrically in form of NADP(H) turnover. NAD(P)H has a distinctive absorption peak at 340 nm which makes it photometrically quantifiable. If the investigated enzymatic reaction did not lead to a NADP(H) turnover itself, it was coupled to one or two following reactions that caused NADP(H) turnover. Table 9 shows all tested enzymes with their coupled follow-up reactions. 20-50 µL cell extract were used for each measurement. All reactions were carried out in 90-100 mM Tris buffer (pH 7.4). Reactions were started by addition of substrate and kinetics monitored with a double-beam spectrophotometer (Uvikon 810, Kontron, Augsburg, Germany) for 5-10 minutes.

Table 9: All tested enzymes with their coupled reactions and needed reagents

Tested enzyme	Coupled reactions	Substrates, cofactors and enzymes
GDH	-	20 mM glucose, 5 mM $NAD(P)^+$, 10 mM $MgCl_2$
GDH	GK, 6PGDH	20 mM glucose, 5 mM DMB or DQ, 10 mM $MgCl_2$, 5 mM ATP, 5 mM $NADP^+$, 0.02 U GK, 0.005 U 6PGDH
PGI	G6PDH	20 mM F6P, 10 mM $MgCl_2$, 5 mM $NADP^+$, 0.085 U G6PDH

4.3.7 Protein quantification

Protein concentrations were determined according to Bradford (1976). The test constitutes two steps: 1. an unspecific binding of the dye Coomassie Blue to cationic and unpolar side chains of the protein sample with a resulting absorption shift of Coomassie Blue from 465 nm to 595 nm and 2. a photometric quantification of bound Coomassie Blue at 595 nm and calculation of protein content with help of a standard curve. In the first step, 1 µL protein sample (cell extract) was mixed in triplicates with 799 µL water. Then, a bovine serum albumin (BSA) standard curve was prepared by diluting a 100 µg/mL BSA stock solution in 200 mM potassium phosphate buffer (pH 7.8) to yield 2, 5, 10, 15 and 20 µg/mL BSA standards in an end volume of 800 µL. 200 µL Bradford reagent (tab. 10) was then added to all standards and samples followed by an incubation at RT for 10 min. Finally, absorption at 595 nm was measured for all samples and standards and sample protein concentration was calculated by using the standard curve.

Table 10: Bradford reagent recipe

Bradford reagent	100 mg/L Coomassie Serva Blue G-250 (Bio-Rad, Munich, Germany), 5 % (v/v) ethanol, 8.5 % (v/v) H_3PO_4

4.3.8 Glycogen quantification

Intracellular glycogen contents of *Synechocystis* were determined according to Gründel *et al.* (2012). Their protocol was modified and established in the working group during this dissertation. In general, the protocol consists of six steps: 1. precipitation of cells, 2. cell lysis, 3. precipitation of glycogen, 4. washing of glycogen pellet, 5. digestion of glycogen to glucose and 6. enzymatic quantification of released glucose (see chapter 4.3.9). First, an OD volume of 2-10 OD*mL sample was pelleted by centrifugation (5 min, 9000 *g*, 4 °C). The pellet was then resuspended in 300 µL 30 % (w/v) KOH and incubated at 95 °C for 2 h to accomplish cell lysis. After that, 900 µL absolute ethanol were added and the samples were incubated at -20 °C over night. On the next day, samples were centrifuged (10 min, 10000 g, 4 °C) to precipitate glycogen. Pellets were then washed with 1 mL absolute and 1 mL 70 % (v/v) ethanol subsequently (5 min, 10000 *g*, 4°C) and afterwards dried in a heat block at 50 °C for 10 to 20 min. The dried pellets were solved in 200 µL (if photoautotrophic culture) or 500 µL (if mixotrophic or chemoheterotrophic culture) 100 mM sodium acetate buffer (pH 4.5) containing 1.5 mg/mL amyloglucosidase and incubated at 60 °C for 90 min. After that, samples were centrifuged (10 min, 10000 *g*, RT) and 50 µL of supernatant transferred to a new cup. Glucose was then quantified as will be described in the following chapter (chapter 4.3.9). The resulting glucose concentration (mM) was converted into glycogen mass (µg) by multiplying it with the lysate volume (200 µL for photoautotrophic or 500 µL for mixotrophic cultures) and the molar mass ratio of glycogen to glucose (162.16/180.16). Finally, glycogen mass was converted into specific cellular glycogen content (µg/OD*mL) by dividing it by the respective OD volume. Figure 10 demonstrates test viability by showing correlation between OD volume and glycogen contents of photoautotrophically cultivated *Synechocystis* WT.

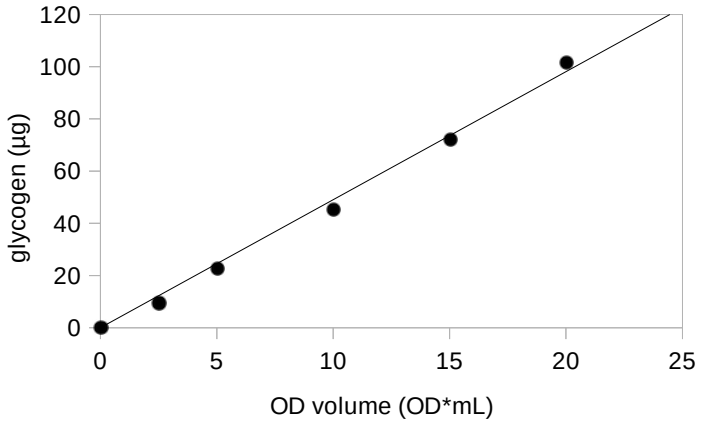

Figure 10: Dependency of measured glycogen mass on applied cyanobacterial biomass. Shown are measured glycogen masses in dependency of applied OD volumes (as a measure of biomass) of *Synechocystis* WT that has been cultivated photoautotrophically.

4.3.9 Glucose quantification

Glucose concentrations were determined according to Gründel *et al.* (2012). Their protocol was modified and established in the working group during this dissertation. The rational behind this test is an enzymatic conversion of sample glucose to 6-phosphogluconate, which goes hand in hand with equimolar formation of NADPH, which in turn could be quantified by a photometer by making use of its distinctive absorption peak at 340 nm. Glucose quantification was achieved for two different applications: 1. to measure glucose concentration in the cultivation medium of chemoheterotrophically, mixotrophically or fermentatively grown cells or 2. to measure the glucose amount that has been released during the glycogen quantification assay (see chapter 4.3.8). For quantification of medium glucose concentrations, 1 mL culture was pelleted by centrifugation (5 min, 10000 *g*, RT) and 50 µL of supernatant were transferred to a new cup. If medium glucose concentration was expected to exceed 5 mM, samples were diluted. In case of measurement of glycogen-derived glucose samples, 50 µL of the final solution mentioned in chapter 4.3.8 was used. Regardless of the origin of samples, 50 µL glucose standards with the following concentrations were prepared: 0 mM, 0.625 mM, 1.25 mM, 2.5 mM and 5 mM. Furthermore, a 'NADP buffer' (recipe shown in tab. 11) was prepared. 940 µL 'NADP buffer' were added to all samples and standards, which were then transferred to acryl-cuvettes and absorption at 340 nm was measured in a double-beam spectrophotometer (Uvikon 810, Kontron, Augsburg, Germany) (baseline absorption). After that, 10 µL 'enzyme sol.'(tab. 11) were added to all samples and standards. Samples and standards were then incubated at 37 °C for 60 min to ensure complete enzymatic conversion of glucose to 6-phosphogluconate. Finally, absorption at 340 nm was measured again (endpoint absorption). The baseline absorption values of all samples and standards was subtracted from the respective endpoint absorption values to yield Δabsorption. Δabsorption values of standards were used to create a glucose standard curve, which was used to convert Δabsorption values of samples into glucose concentrations.

Table 11: Recipes of 'NADP buffer' and 'enzyme sol' as needed for the glucose quantification test. Shown are the stock solution concentration (second column), the end concentration in the reaction (third column), the dilution factor (fourth column) and the end volume in the reaction (fifth column) of all ingredients of the glucose quantification test, namely: sample/standard, $NADP^+$, ATP, $MgCl_2$, hexokinase/glucose-6-phosphate dehydrogenase solution and Tris-HCl buffer (pH 7.4). The end volumes in the reaction were divided into 'NADPH buffer' and 'enzyme sol' and the respective volumes are shown in the two rightmost columns.

Reagent	stock conc.	end conc.	dil. factor	end vol.	NADP buffer vol.	enzyme sol. vol.
Sample/standard	< 5 mM	< 0.25 mM	20	50 µL	-	-
$NADP^+$	150 mM	2 mM	75	13.33 µL	13.33 µL	-
ATP	150 mM	2 mM	75	13.33 µL	13.33 µL	-
$MgCl_2$	300 mM	3 mM	100	10 µL	10 µL	-
HK/ G6PDH	340 U/mL 170 U/mL	0.17 U 0.085 U	2000	0.5 µL	-	0.5 µL
Tris-HCl (pH 7.4)	100 mM	91.3 mM	1.1	912.83 µL	903.33 µL	9.5 µL
total				1000 µL	940 µL	10 µL

4.3.10 6-Phosphogluconate quantification

A novel 6-phosphogluconate quantification test was designed and established in the working group in the course of this dissertation. The rational behind this test is an enzymatic conversion of sample 6-phosphogluconate to ribulose-5-phosphate and CO_2 which goes hand in hand with equimolar formation of NADPH, which could be quantified by using a photometer. However, while the test was reliable under conditions where an accumulation of 6-phosphogluconate is occurring, WT levels of 6-phosphogluconate seemed to be below the detection limit (fig. 11 A). For quantification of intracellular 6-phosphogluconate concentration, an OD volume of 5 to 50 OD*mL cell culture was pelleted by centrifugation (5 min, 9000 *g*, 4 °C). Cell lysis was achieved by solving the pellet in 1 mL 0.2 M HCl, followed by a 15 min incubation at 95 °C. The lysates were centrifuged (10 min, 18000 *g*, 4°C) and the supernatants transferred to new cups where they were neutralized by addition of 1 mL 1 M Tris/HCl buffer (pH 8.0). Samples were then split into two (each sub-pool 900 µL), one half being referred to as ‘positive’ and one as ‘control’. All ‘positive’ and ‘control’ samples were then supplied with 90 µL of an 11.11 mM $NADP^+$ solution. Then, 10 µL of a 5 U/mL 6-phosphogluconate dehydrogenase solution were added to all ‘positive’ samples and 10 µL of water to all ‘control’ samples. All samples were then incubated at 37 °C for 30 min and the absorption at 340 nm was measured using a double-beam spectrophotometer (Uvikon 810, Kontron, Augsburg, Germany). The ‘control’ absorption value was subtracted from the ‘positive’ absorption value to yield Δabsorption. 6-phosphogluconate standards were prepared (0 mM, 0.05 mM, 0.1 mM, 0.2 mM, 0.4 mM and 0.8 mM) and measured in the same way as samples. Δabsorption values of standards were used to create a standard curve, which was then used to convert sample Δabsorption values into 6-phosphogluconate concentrations. The resulting 6-phosphogluconate concentration (mM) was converted into specific cellular 6-phosphogluconate content (µg/OD*mL) by multiplying it with the molar mass and dividing it by the respective OD volume. Figure 11 B demonstrates test viability by showing correlation between OD volume and cellular 6-phosphogluconate contents of a *Synechocystis* mutant that accumulates 6-phosphogluconate (Δ*eda*Δ*gnd*).

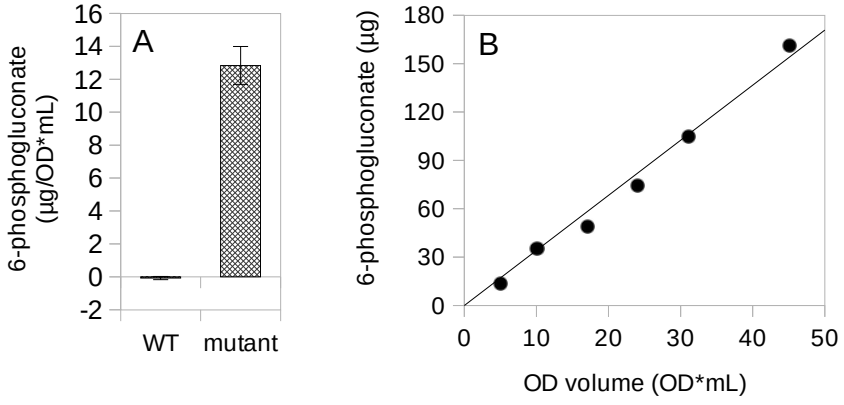

Figure 11: 6-phosphogluconate quantification. Chart A shows mean 6-phosphogluconate levels of *Synechocystis* WT and a mutant that accumulates 6-phosphogluconate (Δ*eda*Δ*gnd*) and chart B shows measured 6-phosphogluconate contents of the same mutant in dependency on applied OD volumes (as a measure of biomass).

4.3.11 Measurement of photochemical quenching (qP)

Photochemical quenching was measured by using a pulse amplitude modulation (PAM) fluorometer. In this dissertation, qP values were measured as a mean to identify the flux of the CBB cycle. For determination of qP values, 2 ml of an photoautotrophically growing *Synechocystis* culture were transferred to a centrifugation cup and illuminated with 50 µE m^{-2} s^{-1} PPFD LED white light for at least 30 min. Cells were then pelleted by centrifugation (10 min, 8000 *g*, RT). Since centrifugation was accomplished in the dark, this step was also meant to initiate dark metabolism and thereby shut down the CBB cycle. After centrifugation, the supernatant was discarded and the pellet resuspended in a modified BG11 medium, which was nitrate-free but contained 5 mM sodium dithionite, until an OD of 20 was reached. These modifications were meant to remove nitrate and oxygen as CBB-cycle-competing electron acceptors. Samples were then submitted to PAM measurements with a PAM-2500 from Walz (Effeltrich, Germany). Prior to the actual measurement, 10 µE m^{-2} s^{-1} PPFD blue LED-light were applied for 20 seconds in order to oxidize the PQ pool and induce state transition of antennae to PSII. If ground fluorescence was roughly 400 mV, qP measurements with a fluorescence induction curve were accomplished according to the following protocol: 1. determination of F_v/F_m after 4 seconds, 2. waiting for 40 seconds, 3. switching on actinic light with PPFD of 35 µE m^{-2} s^{-1} provided by internal red LED, 4. saturation pulses in 30 second interval for 5 min, 5. switching off actinic light, 6. F_0' determination at the end with far red light according to the measuring routine of the PAM-2500.

4.4 Experimental hierarchy and statistical data analysis

The following experimental hierarchy was used:

experiment > experimental repetitions (*n*) > biological replicates (3) > technical replicates (1-4)

Each experiment that was accomplished in this dissertation consisted of a number of experimental repetitions which were executed independently from different cell passages. The number of experimental repetitions is represented by the letter *n*. While for most experiments *n* was between 3 and 5, for some experiments (for example growth rate analyses) *n* reached numbers of up to 20. Each experimental repetition consisted of three biological replicates (if not otherwise stated). These biological replicates stem from different precultures but ultimately from the same agar plate passage. For some experiments with a high data scattering due to technical reasons (for example CO_2 assimilation measurements), several technical replicates were accomplished for each biological replicate. However, for most experiments only one technical replicate was used. The results that will be presented in the following results chapter showed either one representative experimental repetition (in case of curves) or mean values from all experimental repetitions (in case of bar charts). Sometimes values are shown inside the bars, which represent the number of experimental repetitions (*n*). Error bars represent standard deviations. In order to check for statistical significance of differences, unpaired Student's t-tests were performed using mean values, standard deviations and *n* from all experimental repetitions of an experiment. This test was preferable to other tests since only two datasets were compared in all cases (either mutant with WT or photoautotrophic with mixotrophic result). In order to indicate the statistical significance of results, *p*-values are shown.

5 Results

5.1 Construction of deletion and overexpression strains

5.1.1 Glyceraldehyde-3-phosphate dehydrogenase deletion mutants (Δ*gap2*)

In order to obtain a method to disrupt flux in the CBB cycle, the gene for the CBB cycle isoform of the glyceraldehyde-3-phosphate dehydrogenase (GAPDH2) was knocked out in *Synechocystis*. This was accomplished by replacing the *gap2* gene (sll1342) of WT with a kanamycin resistance cassette. In the first step, two 200-300 bp long DNA fragments, one up- and one downstream of the *gap2* gene, were amplified by PCR using the ‘gap2out1’ and ‘gap2in1’ primers as well as the ‘gap2in2’ and ‘gap2out2’ primers. The ‘gap2in1’ and ‘gap2in2’ primers had non-homologuous 5‘ overhangs that introduced novel sequences into the fragments in order to make their ends complementary to the ends of the kanamycin resistance cassette. The two fragments were then connected to the kanamycin resistance cassette by a fusion PCR. The resulting PCR product was gel purified and cloned inside the TOPO pCR2.1 vector. The vector was transformed into *E. coli* and segregated on agar plates containing kanamycin. Afterwards, the vector was isolated and its sequence verified by a restriction digest with EcoRI as well as by Sanger sequencing using the M13 sequencing primers. The vector was then transformed into *Synechocystis* WT and segregation was accomplished by cultivation on kanamycin containing agar plates (supplied with 10 mM glucose). Success of segregation was confirmed via PCR and gelelectrophoresis, by showing that no GAP2 could be amplified from genomic DNA of the Δ*gap2* mutant (data not shown). It was furthermore attempted to create a double deletion strain, where both GAPDH2 and the KDPG aldolase (EDA) are knocked out. For this, the vector containing the GAP2 deletion construct was also transformed into an KDPG aldolase knock-out mutant (Δ*eda*). However, segregation was unsuccessful due to the inability of Δ*gap2*Δ*eda* to survive. Transformation was attempted four times.

5.1.2 Glucose-6-phosphate isomerase deletion mutants (Δ*pgi/pgi*)

In order to obtain a method to investigate the role of the PGI shunt, knock-out of the glucose-6-phosphate isomerase (PGI) was attempted. For this, two 200-300 bp long DNA fragments, one up- and one downstream of the glucose-6-phosphate isomerase gene (*pgi*, slr1349), were amplified by PCR using the ‘pgi-out1’ and ‘pgi-in1’ primers as well as the ‘pgi-in2’ and ‘pgi-out2’ primers. The ‘pgi-in1’ and ‘pgi-in2’ primers had non-homologuous 5‘ overhangs that introduced novel sequences into the fragments in order to make their ends complementary to the ends of a chloramphenicol resistance cassette. The two fragments were then connected to the chloramphenicol resistance cassette by a

fusion PCR. The resulting PCR product was gel purified and cloned inside the TOPO pCR2.1 vector. The vector was transformed into *E. coli* and segregated on agar plates containing kanamycin. Afterwards, the vector was isolated and its sequence verified by restriction digest with EcoRI as well as Sanger sequencing using the M13 sequencing primers. The vector was then transformed into *Synechocystis* WT, a KDPG aldolase knock-out mutant (Δ*eda*), a 6-phosphogluconate dehydrogenase knock-out mutant (Δ*gnd*) and a KDPG aldolase + 6-phosphogluconate dehydrogenase double knock-out mutant (Δ*eda*Δ*gnd*) in order to create Δ*pgi*, Δ*pgi*Δ*eda*, Δ*pgi*Δ*gnd* and Δ*pgi*Δ*eda*Δ*gnd*. Segregation of mutants was then attempted on agar plates containing chloramphenicol and the respective antibiotics for the other deletions. Testing of segregation success via amplification of *pgi* gene copies showed that all strains remained *pgi* gene copies and that segregation was thus incomplete (data not shown). As a consequence, the resulting strains were named *pgi*/Δ*pgi*, *pgi*/Δ*pgi*Δ*eda*, *pgi*/Δ*pgi*Δ*gnd* and *pgi*/Δ*pgi*Δ*eda*Δ*gnd*.

5.1.3 Putative glucose dehydrogenase overexpression strain (gdh1:oe)

In order to test for the existence of a glucose dehydrogenase in *Synechocystis*, a putative glucose dehydrogenase gene (*gdh1*, sll1709) was overexpressed homologously in *Synechocystis* using the method from Zhou *et al.* (2014). For this, the *gdh1* gene as well as the promoter of cyanophycin (*pcpc560*) and the terminator of the large RubisCO subunit (*trbc*) were amplified via PCR from *Synechocystis* WT. Simultaneously, the expression vector pSM2 was linearized by restriction digestion with XhoI. The PCR products and the digested vector were gel purified and ligated via isothermal DNA assembly, such that the *pcpc* promoter was in front of *gdh1* and the *trbc* terminator behind *gdh1*. The vector was transformed into *E. coli* and segregated on kanamycin containing agar plates. Afterwards, the vector was isolated and its sequence verified by restriction digest with HindIII and Sanger sequencing using the ‘psm2_for’ and ‘psm2-4.16-rev’ sequencing primers. The vector was then transformed into *Synechocystis* WT and segregated on agar plates containing kanamycin. The resulting strain $PcPc_{560}$gdh1 in pSM2 will from here on be referred to as gdh1:oe.

5.2 Fermentative growth analysis

It has been reported that *Synechocystis* does not exhibit growth under fermentative conditions (anaerobic, in darkness, in presence of glucose) (Stal & Moezelaar, 1997). In order to test whether *Synechocystis* is metabolically active during fermentative conditions, a modified growth protocol was established. This protocol consisted of two phases: 1. the fermentative phase, during which cells were cultivated in absence of air bubbling and light (except for 10 minutes per day, similar as in LAHG growth (Anderson & McIntosh, 1991) but in presence of 5 mM glucose, 2. the recovery phase, during

which light and air bubbling was switched back on to enable cells to recover into mixotrophic metabolism.

The fermentative growth behavior of WT as well as the glycolytic deletion strains Δ*eda* (KDPG aldolase), Δ*pfk* (phosphofructokinase), Δ*zwf* (glucose-6-phosphate dehydrogenase) and Δ*gnd* (6-phosphogluconate dehydrogenase) was measured according to the protocol described above. While none of the measured strains was able to grow during the fermentative phase (fig. 12 A; day 0-7), nearly all strains were capable of recovery (fig. 12 A; day 7-15). However, the two strains where the OPP pathway was knocked out (Δ*zwf* and Δ*gnd*) showed either a strongly delayed or no recovery at all. The phosphofructokinase deletion mutant Δ*pfk* showed a slightly impaired growth during the recovery phase compared to WT. Recovery of the Entner-Doudoroff pathway deletion mutant (Δ*eda*) was also slightly impaired in comparison to WT. However, considering that Δ*eda* is known to show a growth phenotype during mixotrophic growth (Chen *et al.*, 2016), the effect can most likely not be attributed to the fermentative treatment. Taken together, these results indicate that the OPP pathway, and potentially also the EMP pathway, are functional under fermentative conditions. To further elucidate cellular metabolism during the fermentative phase, glucose uptake was determined by measurement of medium glucose concentration (fig. 12 B). The measurement showed that no significant amount of glucose was taken up during the fermentative phase by any of the measured strains. However, due to the low OD of the cultures, a small uptake of glucose might have happened but was not seen due to the detection limit of the glucose quantification method. During the recovery phase, glucose concentration declined in a similar rate as the OD increased.

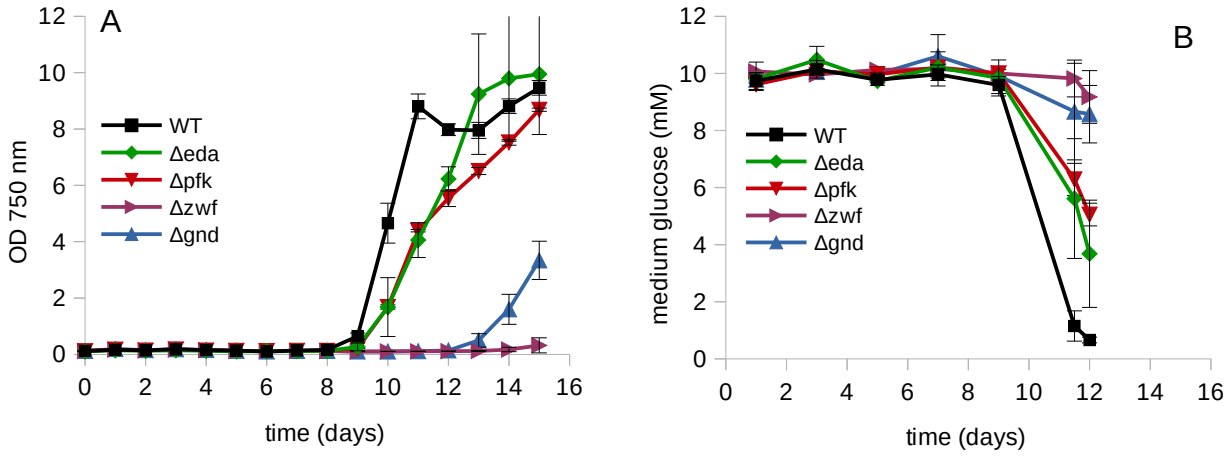

Figure 12: Fermentative experiments. Shown is a fermentative growth curve of WT, Δ*eda*, Δ*pfk*, Δ*zwf* and Δ*gnd* (A) and the respective medium glucose concentration The fermentative experiment consisted of two phases: the fermentative phase in absence of light and air supply (day 0-7) and the recovery phase with light and air bubbling (>day7). Shown are representative results from three experimental repetitions.

In order to simplify comparison of the growth behavior of the glycolytic deletion mutants under different growth conditions, an overview panel was made (fig. 13). Shown are representative growth curves of WT, Δ*eda*, Δ*pfk*, Δ*zwf* and Δ*gnd* under photoautotrophic, mixotrophic, chemoheterotrophic (LAHG) as well as fermentative growth conditions. As has been published earlier (Chen *et al.*, 2016), Δ*eda* showed an impaired growth under mixotrophic conditions and slightly also under photoautotrophic conditions but not under chemoheterotrophic conditions. Under chemoheterotrophic conditions, Δ*zwf* and Δ*gnd*, both of which have a deleted OPP pathway, were unable to grow, thus demonstrating the essential role of the OPP pathway under this condition. The Δ*pfk* deletion mutant that can not employ the EMP pathway does not show a growth phenotype during photoautotrophic and mixotrophic condition but a small growth impairment during chemoheterotrophic conditions thus proposing a function of the EMP pathway under this condition.

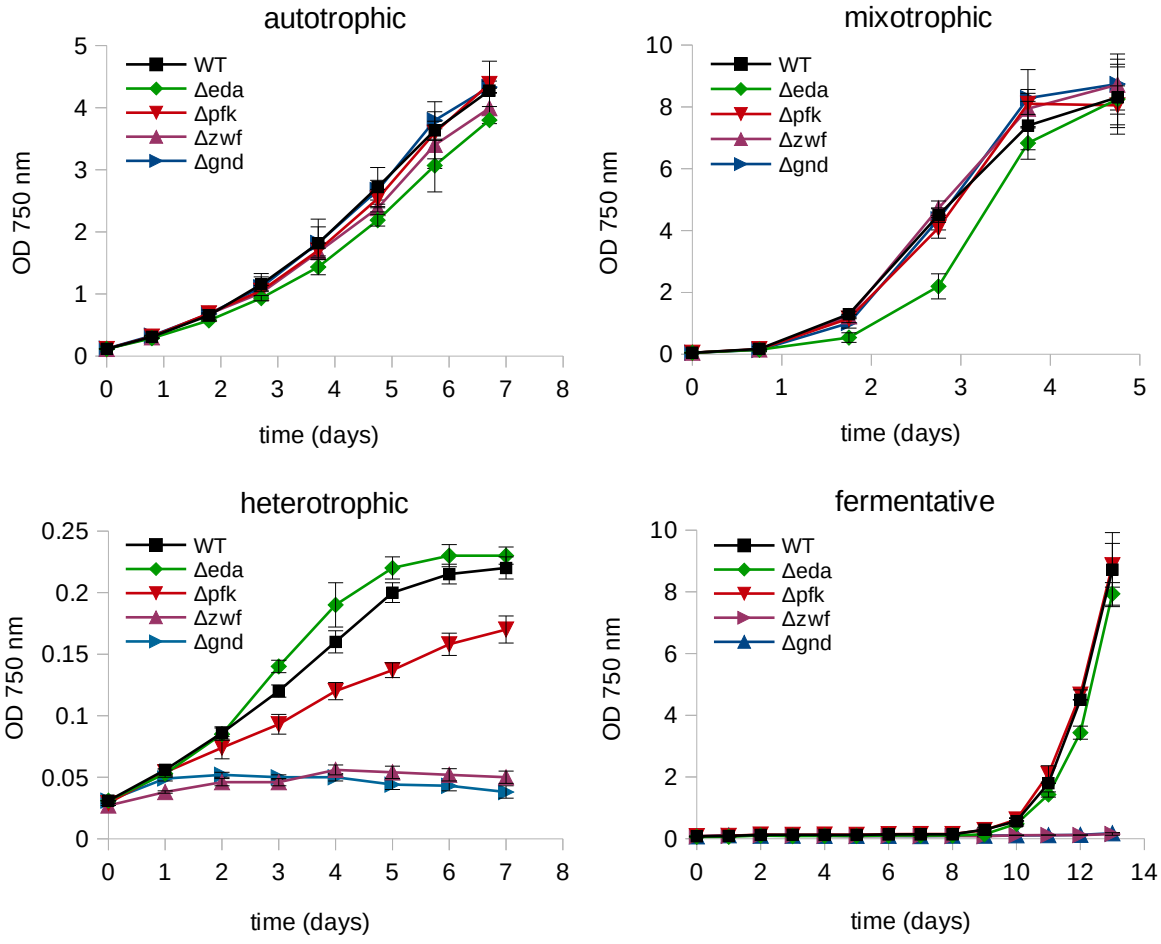

Figure 13: Growth behavior of various glycolytic deletion mutants under photoautotrophic, mixotrophic, chemoheterotrophic (LAHG) and fermentative growth conditions. Shown are representative growth curves of WT, Δ*eda*, Δ*pfk*, Δ*zwf* and Δ*gnd* from at least three experimental replicates. Error bars represent standard deviation from three biological replicates (parallel cultures).

5.3 Testing the existence of a glucose dehydrogenase/gluconate kinase bypass

At the start of this dissertation, it was unclear whether *Synechocystis* employs a glucose dehydrogenase (GDH)/gluconate kinase (GK) bypass, similar as it has been observed in *E. coli*. Previous results with putative glucose dehydrogenase deletion mutants (Δ*gdh1* and Δ*gdh2*) indicated the presence of such a bypass. A functional GDH/GK bypass can provide explanatory power for a couple of growth phenotypes of glycolytic deletion mutants of *Synechocystis*, such as the difference in growth behavior of Δ*eda* and Δ*zwf* under mixotrophic conditions (Chen *et al.*, 2016). In order to test for the existence of a GDH/GK bypass in *Synechocystis*, two approaches were used: 1. analysis of glucose dehydrogenase (GDH) and gluconate kinase (GLK) activity in cell extracts, 2. metabolite quantification of gluconate, KDPG and 6-phosphogluconate in cell extracts.

The first piece of evidence came from the investigation of metabolite concentrations. Concentrations of gluconate and KDPG, which are intermediates of the GDH/GK bypass and the ED pathway, respectively, were determined in crude cell extracts of mixotrophically grown WT as well as a glucose-6-phosphate dehydrogenase/phosphofructokinase double deletion strain (*ΔpfkΔzwf)* by IC-ESI-MSMS (measurement done by Dr. Mohammad R. Hajirezaei, Gatersleben, Germany). The results showed the presence of gluconate in WT (fig. 14 E; published in Chen *et al.*, 2016). What is more, significant amounts of KDPG were detectable in a mutant where glucose-6-phosphate dehydrogenase (G6PDH) was knocked out (*ΔpfkΔzwf*). Both observations spoke in favor of an operative GDH/GK bypass.

In further experiments, glucose dehydrogenase (GDH) activity was measured in crude extracts of WT, a glucose-6-phosphate dehydrogenase (G6PDH) deletion mutant (Δ*zwf*) as well as a GDH overexpression mutant (gdh1:oe) that has been constructed in the course of this dissertation. All strains were cultivated either under photoautotrophic or mixotrophic conditions. The enzyme test was based on a direct photometric quantification of NADPH that has been generated by GDH. The results showed no significant amount of GDH activity in any of the tested strains (fig. 14 A). In a second experiment, the GDH reaction was enzymatically coupled to the gluconate kinase (GK) and 6-phosphogluconate dehydrogenase (G6PDH) reactions. This enabled a testing of different electron acceptors that are not photometrically quantifiable themselves. In total, NAD^+ and $NADP^+$ as well as the two quinones 2,3-dimethoxy-5-methyl-1,4-benzoquinone (DMB) and duroquinone (DQ) were tested. For this experiment, only crude extract of the Δ*zwf* strain was used, as presence of G6PDH would have falsified the test by causing a reduction of $NADP^+$ due to oxidation of glucose-6-phosphate. The results showed no GDH activity with any tested electron acceptor (fig. 14 B). In a similar fashion, gluconate kinase activity was measured in crude extracts of *Synechocystis* WT and Δ*zwf* that have been cultivated either under photoautotrophic or mixotrophic conditions (fig. 14 C). The GK reaction was coupled to the G6PDH reaction to enable quantification in form of $NADP^+$ reduction. Again, no GK activity was detectable under any testing condition.

The last piece of evidence comes from quantification studies of the metabolite 6-phosphogluconate (6PG). The double deletion mutant Δ*eda*Δ*gnd* was shown to accumulate 6PG both under photoautotrophic and mixotrophic conditions (fig. 14 D). Contrarily, no accumulation occurred in the quadruple deletion mutant Δ*eda*Δ*gnd*Δ*pfk*Δ*zwf* (fig. 14 D). It can thus be concluded that an additional knock-out of G6PDH (Δ*zwf*), as it is accomplished in the Δ*eda*Δ*gnd*Δ*pfk*Δ*zwf* mutant, prevents accumulation of 6PG. This suggests that G6PDH is the only metabolic reaction to generate 6PG both under photoautotrophic and mixotrophic conditions and further neglects the hypothetical existence of a GDH/GK bypass.

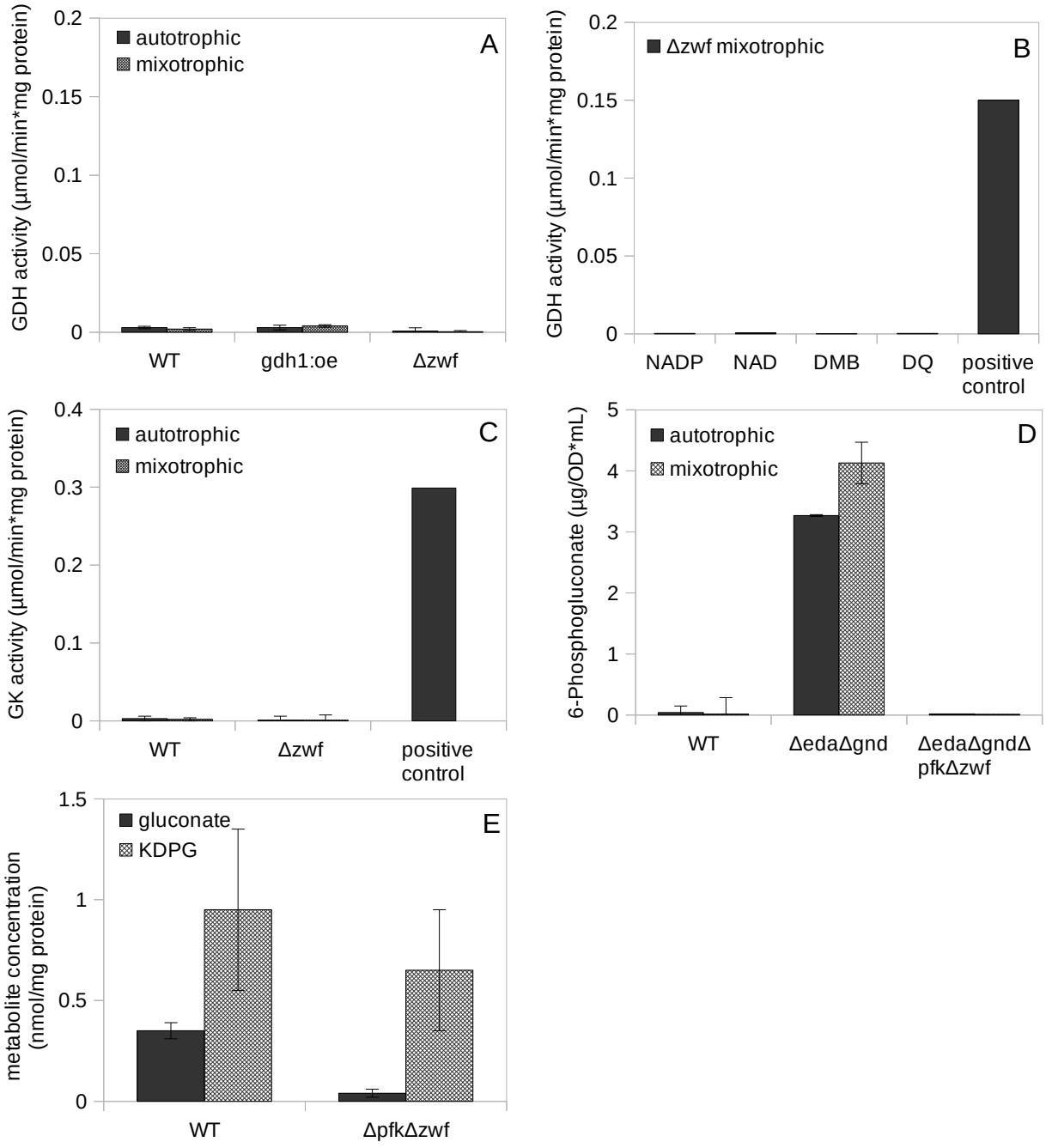

Figure 14: Testing the existence of a GDH/GK bypass by enzyme activity and metabolite concentration measurements. Glucose dehydrogenase (GDH) activity was measured in crude extracts of *Synechocystis* via a direct (A) or coupled (B) enzyme test. In case of the direct test (A), crude extracts from WT, a G6PDH deletion mutant (Δ*zwf*) or a GDH overexpression mutant (GDH1:oe), that were cultivated either under photoautotrophic or mixotrophic conditions, were measured in the presence of glucose and $NADP^+$. In case of the coupled test (B), only Δ*zwf* mixotrophic crude extract was measured but different cofactors were supplied: $NADP^+$, NAD^+, 2,3-dimethoxy-5-methyl-1,4-benzoquinone (DMB) or duroquinone (DQ). The GDH reaction was coupled to the gluconate kinase (GK) and the 6-phosphogluconate dehydrogenase (6PGDH) reaction. Glucose, $NADP^+$, GK, ATP, $MgCl_2$ and 6PGDH were supplied. For the positive control, (bought) GDH was added. GK activity was measured in crude extracts of *Synechocystis* via a coupled enzyme test (C). For this, crude extracts of WT and a G6PDH deletion mutant (Δ*zwf*), that were cultivated either under photoautotrophic or mixotrophic conditions, were measured. The GK reaction was coupled to the 6PGDH reaction. Gluconate, ATP, $MgCl_2$, $NADP^+$ and 6PGDH were supplied. For the positive control, (bought) GK was added. Chart D shows enzymatically-determined 6-phosphogluconate contents of *Synechocystis* WT and the Δ*eda*Δgnd and Δ*eda*Δ*gnd*Δ*pfk*Δ*zwf* deletion mutants that were cultivated under photoautotrophic or mixotrophic conditions. Chart E shows gluconate and KDPG concentrations of WT and Δ*pfk*Δ*zwf* crude extracts that were measured by IC-ESI-MSMS (measurement done by Dr. Mohammad R. Hajirezaei, Gatersleben, Germany).Error bars represent standard deviation from three technical replicates in case of chart A and C, three biological replicates in case of chart E and three experimental replicates in case of chart D.

5.4 Physiological characterization of the ED pathway knock-out mutant Δ*eda*

5.4.1 Photoautotrophic growth conditions

Physiology of the ED pathway knock-out mutant Δ*eda* was characterized under photoautotrophic growth conditions with continuous illumination. Several physiological parameters such as growth behavior, cellular glycogen content, CO_2 assimilation properties as well as photosynthetic pigment composition were determined in exponentially growing cultures. Figure 15 A shows a typical growth curve of Δ*eda* and WT under photoautotrophic conditions. All photoautotrophic growth curves of Δ*eda* that were accomplished in this dissertation were analyzed according to the 'triplet regression model' (chapter 4.3.2), which gives out growth rates in comparison to WT. The calculated growth rates are presented as mean data in figure 15 B. The results showed a relative growth rate of Δ*eda* of 0.82 or, in other words, a growth impairment of 18 % in comparison to WT ($p = 0.002$). In order to test whether the Δ*eda* growth phenotype remained constant during the course of this dissertation, the relative growth rates of Δ*eda* were plotted against the respective experimental dates (fig. 15 C). The results showed no correlation between relative growth rate and date of experiment ($p = 0.428$). In a similar approach, growth rates were plotted against the inoculation OD in order to test for an influence of culture density on the growth phenotype (fig. 15 D). Again, no correlation was observable ($p = 0.418$). Investigation of cellular glycogen contents showed a strongly increased (+145 %; $p < 0.001$) glycogen content of Δ*eda* in comparison to WT (fig. 15 E). Just as it has been done for growth rates, glycogen contents were plotted against the respective experimental dates (fig. 15 F). The results showed no correlation of either WT or Δ*eda* glycogen contents with the date of experiment ($p = 0.720$ and 0.334, respectively). CO_2 assimilation rates were determined inside a gas exchange chamber at 50 µE m^{-2} s^{-1} and directly afterwards at 0 µE m^{-2} s^{-1}. While CO_2 assimilation at 0 µE m^{-2} s^{-1} can be interpreted as respiration, CO_2 assimilation at 50 µE m^{-2} s^{-1} has to be interpreted more cautiously since it does not reflect the real CO_2 fixation but rather the apparent CO_2 fixation which is the sum of all CO_2 fixating and decarboxylating reactions. The results showed a slightly decreased CO_2 assimilation rate at both 50 µE m^{-2} s^{-1} and 0 µE m^{-2} s^{-1} of Δ*eda* in comparison to WT (fig. 15 G). The two most important photosynthetic pigments in cyanobacteria, chlorophyll *a* and phycocyanin, were quantified photometrically in WT and Δ*eda*. Quantification was not done in form of absolute values but rather as relative ratios, using a pigment specific wavelength (685 nm for chlorophyll *a* and 618 nm for phycocyanin) as dividend and a cell number specific wavelength (750 nm) as divisor. The results showed reduced contents of both chlorophyll *a* (-24 %; $p < 0.001$) and phycocyanin (-19 %; $p < 0.001$) in Δ*eda* in comparison to WT (fig. 15 H). In another experiment, light dependence of the Δ*eda* growth phenotype was investigated. For this, Δ*eda* and WT were cultivated at three different light intensities (25 µE m^{-2} s^{-1}, 60 µE m^{-2} s^{-1} and 250 µE m^{-2} s^{-1}) and relative growth rates of Δ*eda* in comparison to WT were calculated. The results showed the lowest relative growth rate of Δ*eda* at low light and thus indicated a negative correlation between growth impairment and light intensity (fig. 16).

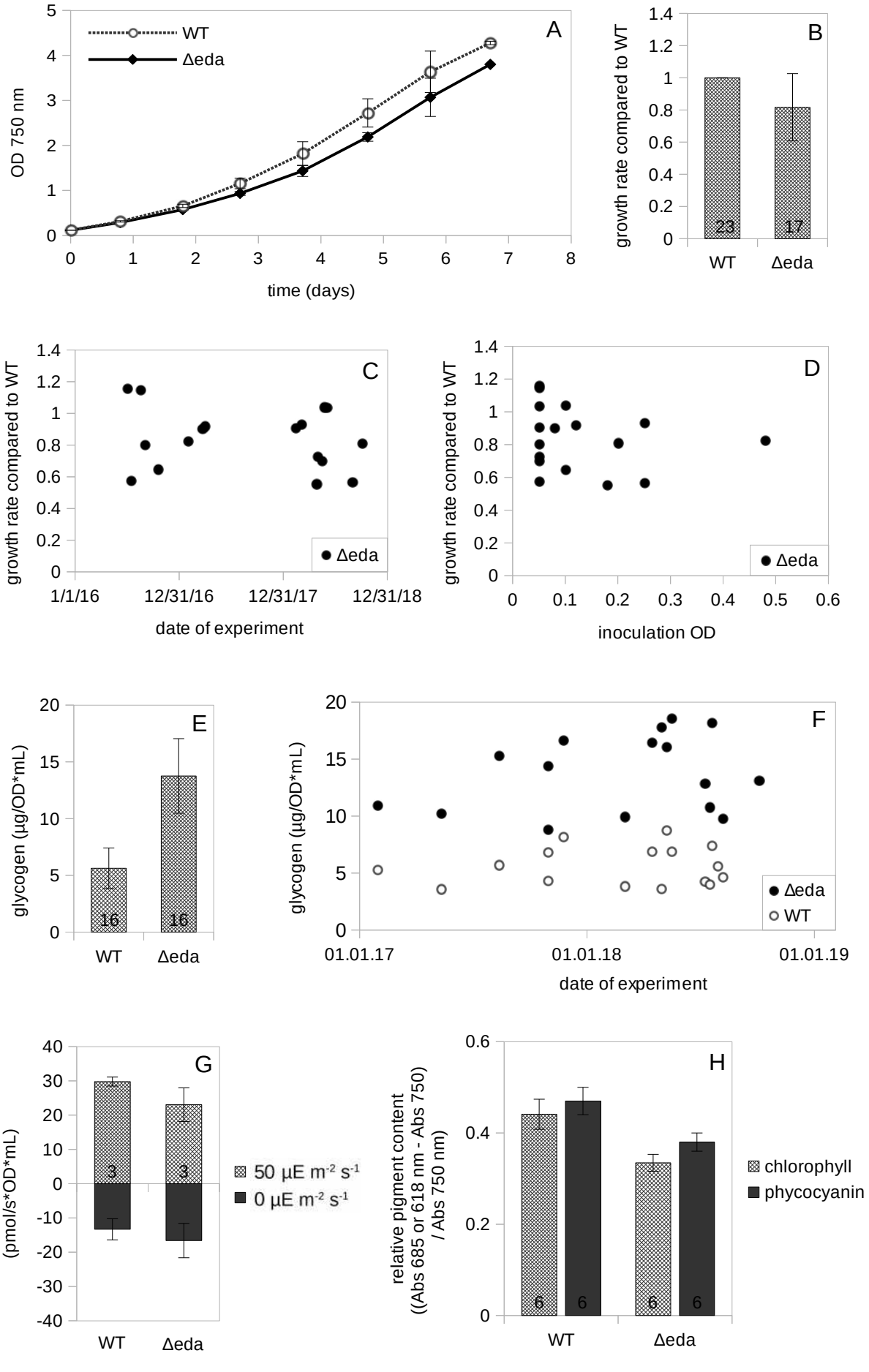
A
WT
Δeda
OD 750 nm
time (days)
B
growth rate compared to WT
23
17
WT
Δeda
C
growth rate compared to WT
Δeda
1/1/16
12/31/16
12/31/17
12/31/18
date of experiment
D
growth rate compared to WT
Δeda
inoculation OD
E
glycogen (µg/OD*mL)
16
16
WT
Δeda
F
glycogen (µg/OD*mL)
Δeda
WT
01.01.17
01.01.18
01.01.19
date of experiment
G
CO2 assimilation rate (pmol/s*OD*mL)
3
3
50 µE m-2 s-1
0 µE m-2 s-1
WT
Δeda
H
relative pigment content ((Abs 685 or 618 nm - Abs 750) / Abs 750 nm)
6
6
6
6
chlorophyll
phycocyanin
WT
Δeda

Figure 15: Various physiological parameters of WT and Δ*eda* under photoautotrophic growth conditions. Chart A shows a typical photoautotrophic growth curve of WT and Δ*eda*. All growth curves that have been accomplished in this dissertation were analyzed according to the 'triplet regression model' (chapter 4.3.2) and calculated mean growth rates in comparison to WT are shown in chart B. The calculated growth rates of Δ*eda* were plotted against date (C) and inoculation OD (D) of the respective experiments. Glycogen, CO_2 assimilation and pigment data were collected during the exponential growth phase. Chart E shows mean cellular glycogen contents and chart F shows glycogen contents plotted against date of the respective experiments. CO_2 assimilation rates were measured at 50 µE m^{-2} s^{-1} PPFD and directly afterwards during darkness (0 µE m^{-2} s^{-1}) and are shown as mean results in chart G. Relative amounts of chlorophyll *a* and phycocyanin were determined photometrically and are shown as absorbance ratios (685 nm – 750 nm) / 750 nm in case of chlorophyll and (618 nm – 750 nm) / 750 nm for phycocyanin) in chart H. Values inside bars represent number of experimental repetitions (*n*).

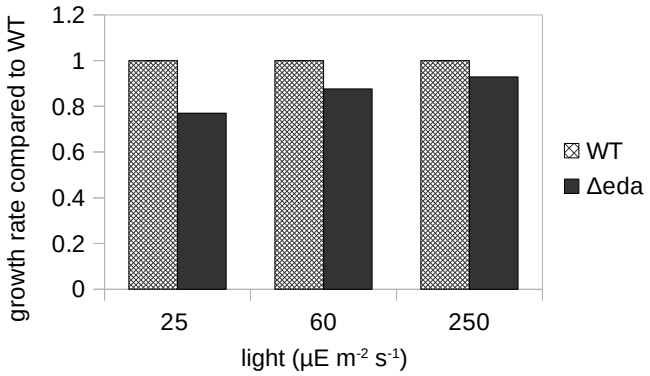

Figure 16: Light dependence of the Δ*eda* growth phenotype. WT and Δ*eda* were cultivated photoautotrophically at either 25 µE m^{-2} s^{-1}, 60 µE m^{-2} s^{-1} or 250 µE m^{-2} s^{-1} PPFD and relative growth rates of Δ*eda* in comparison to WT were calculated. Shown are mean results from two experimental repetitions.

5.4.2 Transition from photoautotrophic to mixotrophic growth

In this experiment, the adaptation phase of *Synechocystis* WT and the ED pathway knock-out mutant Δ*eda* to mixotrophic growth conditions was characterized. For this, cells that were adapted to photoautotrophic conditions were transferred into new medium containing 10 mM glucose. Then, various physiological parameters such as growth behavior, cellular glycogen content, glucose uptake and CO_2 assimilation rate were monitored over a time course of three days. The experiment was repeated four times and the results from one representative experiment are presented in figure 17. The results showed an impaired growth rate of Δ*eda* (fig. 17 A), as has also been observed in previous studies (Chen *et al.*, 2016). The growth impairment was rather small compared to previous results, which, however, might have been due to the relatively high inoculation OD of 0.5, as will be shown in the following chapter (chapter 5.4.3). Cellular glycogen contents increased rapidly during the first hours upon addition of glucose both in WT and Δ*eda* (fig. 17 B). However, the glycogen production rate during the first 8 hours did not differ between WT and Δ*eda*, as is demonstrated in figure 18 F. Maximum glycogen contents, on the other hand, were higher in the Δ*eda* mutant (fig. 17 B). Since glycogen production rates did not differ, it can be concluded that the difference of the maximum glycogen contents was due to an extended period of glycogen production in Δ*eda*. After reaching their maximum, glycogen contents of both WT and Δ*eda* often fluctuated and increased further at around 50 hours (fig. 17 B). These observations were presumably caused by culture density effects. Measurements of medium glucose concentration showed that both WT and Δ*eda* did not take up significant amounts of glucose during the first 8 hours upon glucose addition and afterwards took up glucose in a manner that was proportional to their respective OD (fig. 17 C). Specific glucose uptake rates (µg/OD*mL) were slightly higher in WT than in Δ*eda*. As another physiological parameter, CO_2 assimilation rates were measured at 50 µE m^{-2} s^{-1} and (directly afterwards) at 0 µE m^{-2} s^{-1} (fig. 17 D+E). The results show that CO_2 assimilation rates at both 50 µE m^{-2} s^{-1} and 0 µE m^{-2} s^{-1} decreased in WT and Δ*eda* in the first 24 hours upon addition of glucose, thus indicating that CO_2 fixation via the CBB cycle was restrained and/or respiration activated. In some experimental replicates, CO_2 assimilation at 50 µE m^{-2} s^{-1} increased again after 24 to 48 hours even though medium glucose was not used up yet. When this happened, the effect was usually stronger in WT than in Δ*eda* (fig. 17 D). In a different experimental replicate, chlorophyll contents were measured. The results showed that chlorophyll contents decreased both in WT and Δ*eda* upon addition of glucose and reached their minimum after around 24 hours (fig. 17 H). WT chlorophyll levels were constantly higher than Δ*eda* chlorophyll levels. The increase that happened at 96 hours was most likely due to a complete consumption of medium glucose and the resulting readaptation back to autotrophy (fig. 18).

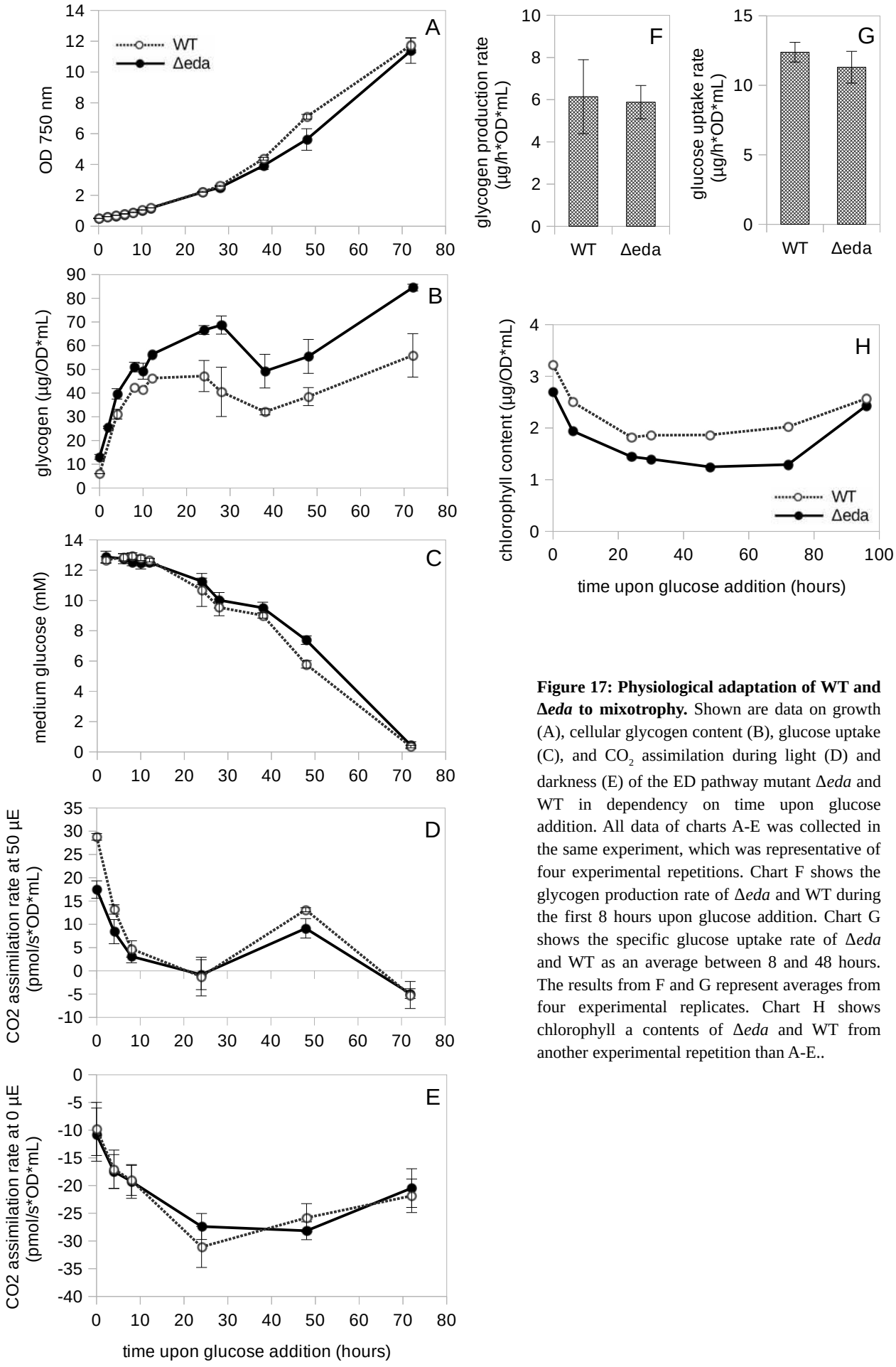

Figure 17: Physiological adaptation of WT and Δ*eda* to mixotrophy. Shown are data on growth (A), cellular glycogen content (B), glucose uptake (C), and CO_2 assimilation during light (D) and darkness (E) of the ED pathway mutant Δ*eda* and WT in dependency on time upon glucose addition. All data of charts A-E was collected in the same experiment, which was representative of four experimental repetitions. Chart F shows the glycogen production rate of Δ*eda* and WT during the first 8 hours upon glucose addition. Chart G shows the specific glucose uptake rate of Δ*eda* and WT as an average between 8 and 48 hours. The results from F and G represent averages from four experimental replicates. Chart H shows chlorophyll a contents of Δ*eda* and WT from another experimental repetition than A-E..

The accumulated amount of carbon that was taken up in WT and Δ*eda* during the experiment shown in figure 18 A-E was calculated and plotted against time. Additionally, the accumulated amount of carbon that was stored as glycogen was calculated and also included. The resulting plots showed the overall carbon allocation in WT and Δ*eda* during the early phase of mixotrophy (fig. 18 A+B). It can be seen that the majority of acquired carbon stems from glucose and only 10-20 % of cellular carbon were derived from CO_2 assimilation. What is more, glycogen accounted for as much as 25 % of all cellular carbon in WT and for up to 40 % in Δ*eda*. In order to test whether the carbon bound in glycogen affects the culture OD, additional plots were generated: In the first plot, the sum of all carbon that was taken up (glucose + CO_2) was plotted against time and in the second plot the carbon that was stored as glycogen was subtracted from the carbon that was taken up (glucose + CO_2 -glycogen) and also plotted against time (fig. 18 C+D). The results showed that the plot without a subtraction of glycogen (fig. 18 C) resembled the actual culture OD (fig. 18 A) much closer than the plot that included a subtraction of glycogen (fig. 18 D). In order to mathematically test this observation, the two datasets were plotted against the respective culture OD (fig. 18 E+F) and linear regressions were performed for both plots. It can be seen that in the plot without a subtraction of glycogen, WT and Δ*eda* had roughly the same correlation coefficient with OD (fig. 18 E) but in the one that included a subtraction of glycogen they had not (fig. 18 F). Another regression was made between all datapoints (WT + Δ*eda*) and the OD for both scenarios, which resulted in a regression coefficient of 7.815 in case glycogen was included (fig. 18 E) and 5.367 if not (fig. 18 F). These values, which corresponded to the amount of carbon (µmol) per OD were then converted to mass of carbon (µg) per OD by multiplication with the molecular weight of carbon. Using the calibration factor between OD and cellular dry weight (1 OD = 189.4 µg dry weight; supplied by Dr. Jens Appel) the relative amount of carbon in cellular dry weight was calculated. The results were 49.5 % in case glycogen was not subtracted and 34 % if glycogen was subtracted. It could previously be shown that the carbon content of (dry) biomass almost always lies between 45 and 50 % (Schlesinger & Bernhardt, 2013). This analysis demonstrates that the cellular glycogen pools influence the measured OD.

The relative contribution of glycogen to biomass can be calculated. For this, the average cellular glycogen contents per OD volume (WT: 5.62 µg/OD*mL under photoautotrophic and 50.17 µg/OD*mL under mixotrophic conditions; Δ*eda*: 13.75 µg/OD*mL under photoautotrophic and 65.67 µg/OD*mL under mixotrophic conditions; data from chapter 5.4.1 and 5.4.3) were converted to amount of carbon per OD volume (µmol C/OD*mL) and divided by the total amount of carbon per OD volume (7.815 µmol C/OD*mL). The resulting contribution of glycogen to biomass (in terms of carbon) was on average 23.7 % in WT and 31.3 % in Δ*eda* under mixotrophic conditions and 2.3 % in WT and 6.2 % in Δ*eda* under photoautotrophic conditions.

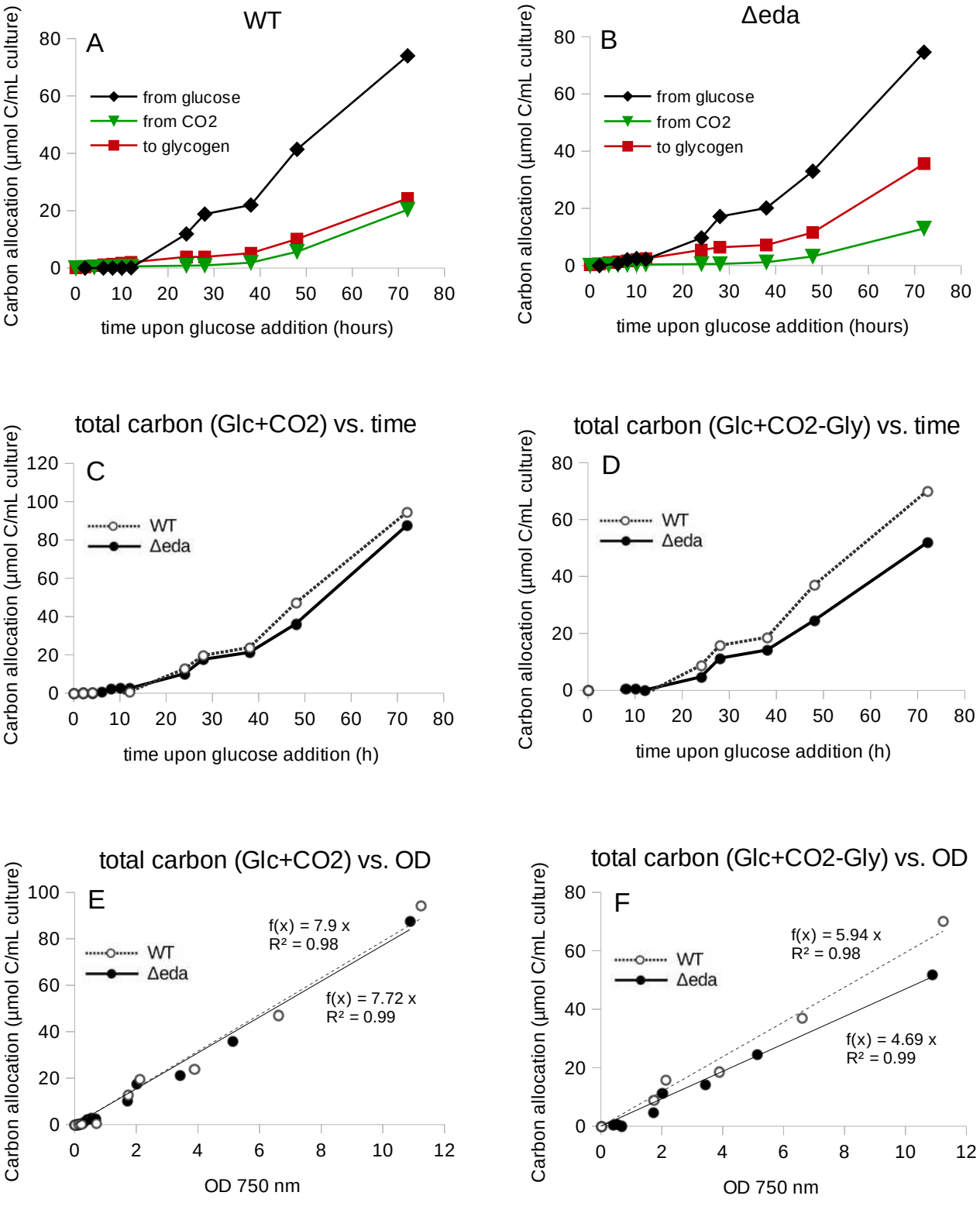

Figure 18: Carbon allocation in WT and Δ*eda* during mixotrophic adaptation. Chart A and B show the carbon allocation in WT and Δ*eda* during one representative experiment from fig. 18 A-E. Shown is the accumulated amount of carbon (µmol carbon/mL culture) that was taken up either from glucose or CO_2 as well as the accumulated amount of carbon that was stored as glycogen. Chart C+E show the amount of carbon that was taken up (sum of glucose and CO_2 uptake) plotted against time (C) and OD (E). In chart D+F, the carbon allocation in form of glycogen was subtracted from the amount of carbon that was taken up and plotted against time (D) and OD (F).

On basis of the just presented experiments, a scheme for the physiological adaptation during the first days of mixotrophy was created (fig. 19). The scheme consists of three functional phases: the first phase of mixotrophic adaptation is characterized by the absence of glucose uptake and usually lasts around 8 hours. Glycogen contents and respiration rates increase while photosynthesis and chlorophyll *a* contents decrease. The second phase of mixotrophic adaptation is marked by a further increase of respiration and a decrease of chlorophyll contents as well as CBB cycle CO_2 fixation and it lasts around 16 hours. A potential third phase begins approximately one day after glucose addition in case CO_2 fixation increases again. This phase seems to last for 0-24 hours.

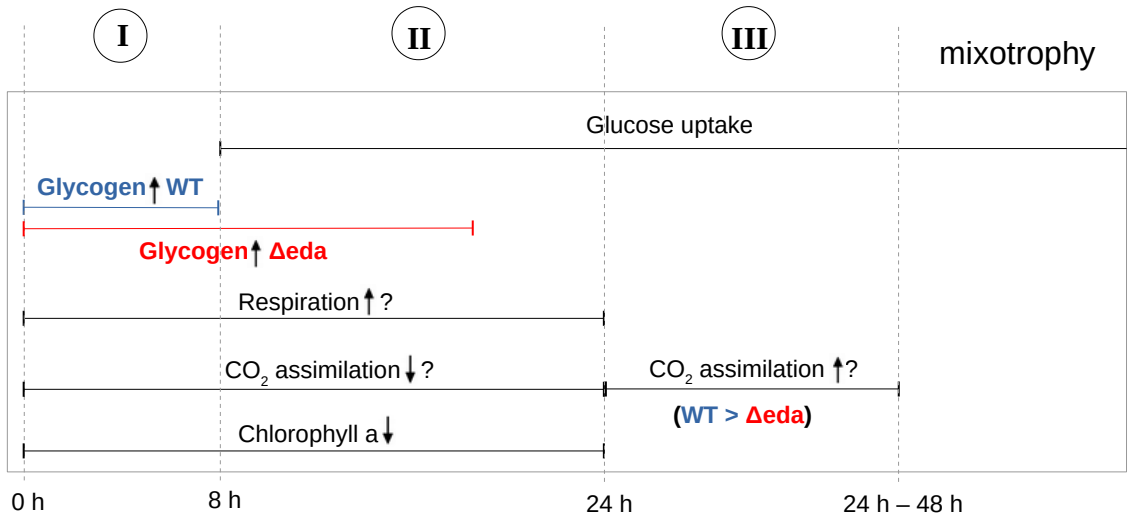

Figure 19: Schematic illustration of physiological processes during mixotrophic adaptation of *Synechocystis*. Shown are three hypothetical phases during mixotrophic adaptation of *Synechocystis* WT and the ED pathway knock-out mutant Δ*eda*. The first phase is characterized by an absence of glucose uptake and an increase of cellular glycogen contents (0-8 h). Respiration increases and CBB cycle fixation and chlorophyll *a* content decrease during the first and second phase (0-24 h). In some experimental replicates CBB cycle fixation increased again which marks the third phase (24-48 h).

5.4.3 Mixotrophic growth conditions

Similar as has been done under photoautotrophic conditions, the following physiological parameters of Δ*eda* and WT were measured under mixotrophic growth conditions with continuous illumination: growth behavior, cellular glycogen content, CO_2 assimilation rate as well as chlorophyll *a* and phycocyanin contents. Measurements were performed 48 hours post glucose addition to avoid the adaptation phase. Figure 20 A shows a typical growth curve of Δ*eda* and WT under mixotrophic conditions. Average mixotrophic growth rates of Δ*eda* in comparison to WT were calculated and are presented in figure 20 B. The results showed a strong growth impairment (-38 %; $p < 0.001$) of Δ*eda* in comparison to WT. In order to test whether the Δ*eda* growth phenotype remained constant during the course of this dissertation, the relative growth rates of Δ*eda* were plotted against the respective experimental dates (fig. 20 C). No correlation between growth rate phenotype and date of experiment was observable ($p = 0.473$), thus indicating that the phenotype of Δ*eda* remained constant. In a similar approach, growth rates were plotted against inoculation OD in order to test for an influence of culture density on growth phenotype (fig. 20 D). The results indicated a positive correlation between inoculation OD and growth rate of Δ*eda*, or in other words, a negative correlation between inoculation OD and growth phenotype severity. The negative effect of high inoculation ODs on the growth phenotype is most likely explainable by the resulting shorter exponential growth phase. Investigation of cellular glycogen contents showed an increased (+30 %; $p = 0.014$) cellular glycogen content of Δ*eda* in comparison to WT under mixotrophic conditions (fig. 20 E). Just as has been done for the growth phenotype, glycogen contents of WT and Δ*eda* were plotted against the respective date of measurement in order to test whether the phenotype changed during the course of this dissertation. The results showed no correlation between glycogen content and date of measurement for both WT and Δ*eda* ($p = 0.777$ and 0.865, respectively) (fig. 20 F). As another physiological parameter, CO_2 assimilation rates were measured. Figure 20 G shows mean net CO_2 assimilation values at 50 µE m^{-2} s^{-1} and 0 µE m^{-2} s^{-1} PPFD of mixotrophically cultivated Δ*eda* and WT. It can be seen that Δ*eda* showed a slightly decreased CO_2 assimilation rate at 50 µE m^{-2} s^{-1} and an increased CO_2 assimilation rate at 0 µE m^{-2} s^{-1}, thus indicating a reduced respiration. However, these results have to be interpreted cautiously as they do not allow do discriminate between CO_2 fixation and respiration. Cellular contents of the photosynthetic pigments chlorophyll *a* and phycocyanin were determined photometrically in WT and Δ*eda* that have been cultivated mixotrophically. Quantification was not done in absolute values but rather relatively in form of absorbance ratios, using a pigment specific wavelength (685 nm for chlorophyll *a* and 618 nm for phycocyanin) as dividend and a cell number specific wavelength (750 nm) as divisor. The results revealed decreased contents of both chlorophyll *a* (-25 %; $p = 0.004$) and phycocyanin (-13 %; $p = 0.04$) in Δ*eda* in comparison to WT (fig. 20 H). In another experiment, CO_2 dependence of the Δ*eda* growth phenotype was investigated. For this, Δ*eda* and WT were cultivated at three different air bubbling intensities (~20 %, 100 % and ~400 % of normal bubbling) and relative

growth rates of Δ*eda* in comparison to WT were calculated (fig. 21). The results indicated no correlation between CO_2 availability and growth phenotype of Δ*eda*.

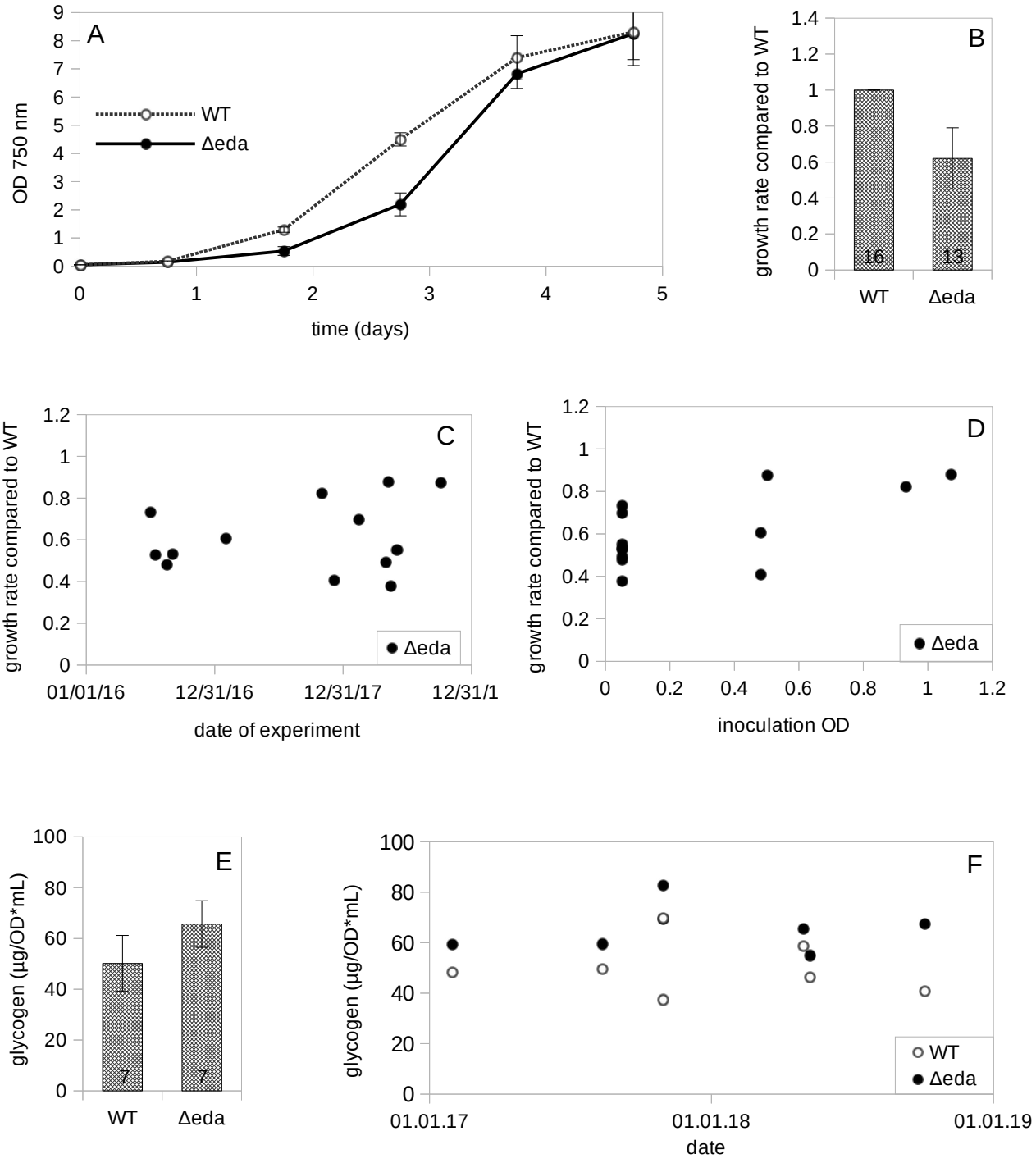

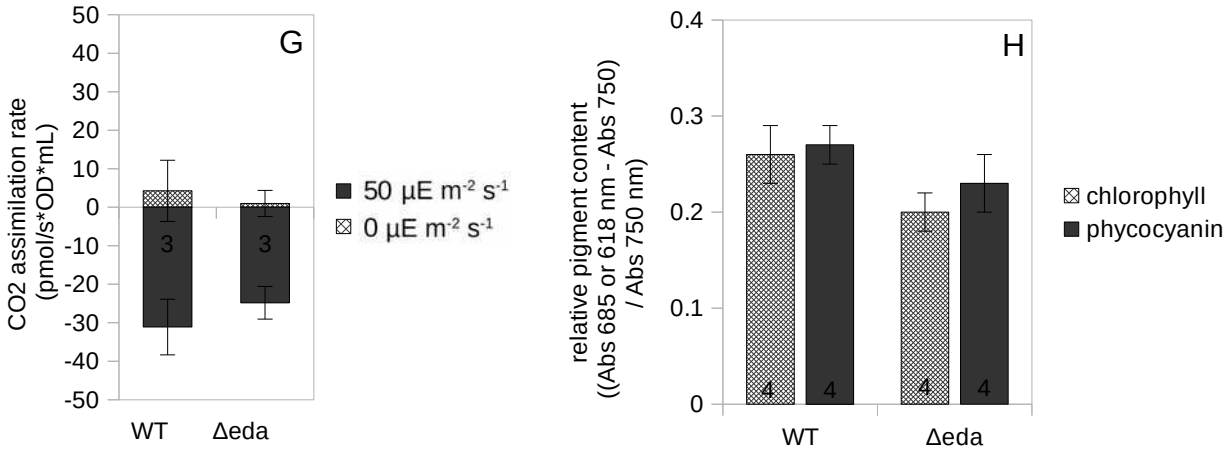

Figure 20: Various physiological parameters of WT and Δ*eda* under mixotrophic growth conditions. Chart A shows a typical mixotrophic growth curve of WT and Δ*eda*. All growth curves that have been accomplished in this dissertation were analyzed according to the 'triplet regression model' (chapter 4.3.2) and calculated mean growth rates in comparison to WT are shown in chart B. The calculated growth rates were plotted against date (C) and inoculation OD (D) of the respective experiments. Glycogen, CO_2 assimilation and pigment data were collected during the exponential growth phase, 48 hours upon glucose addition. Chart E shows mean cellular glycogen contents and chart F glycogen contents plotted against date of the respective experiments. CO_2 assimilation rates were measured at 50 µE m^{-2} s^{-1} PPFD and directly afterwards during darkness (0 µE m^{-2} s^{-1}) and are shown as mean results in chart G. Relative amounts of chlorophyll *a* and phycocyanin were determined photometrically and are shown as absorbance ratios ((685 nm - 750 nm) / 750 nm in case of chlorophyll *a* and (618 nm - 750 nm) / 750 nm for phycocyanin) in chart H. Values inside bars represent number of experimental repetitions (*n*).

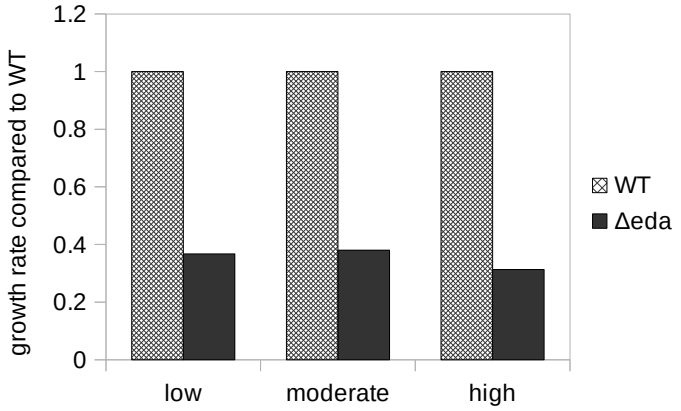

Figure 21: CO_2 dependence of the Δeda growth phenotype. WT and Δ*eda* were cultivated mixotrophically at three different air bubbling intensities and relative growth rates of Δ*eda* in comparison to WT were calculated. The bubbling rate at 'moderate' constituted the normal bubbling rate, 'low' was approximately 20 % of normal bubbling and 'high' approximately 400 %. Shown are the results from one experimental repetition.

5.4.4 Mixotrophic vs. photoautotrophic growth conditions

The previous chapters have shown that *Synechocystis* reacts to mixotrophic growth conditions by adapting various physiological parameters, such as cellular glycogen content, CO_2 assimilation rates and pigment composition. For a better visualization of these adaptations, data on various physiological parameters that was obtained in WT under mixotrophic conditions (chapter 5.4.3) was put into relation with data on the same parameters under photoautotrophic conditions (chapter 5.4.1). This was accomplished by dividing the mixotrophic values by the respective photoautotrophic values. The resulting ratios represent the relative change of each parameter between the photoautotrophic and mixotrophic growth condition. Figure 22 A shows ratios for growth behavior, cellular glycogen contents, CO_2 assimilation at 0 µE m^{-2} s^{-1} (respiration), CO_2 assimilation range (value 50 µE m^{-2} s^{-1} minus value 0 µE m^{-2} s^{-1}) as well as chlorophyll *a* and phycocyanin content in WT. It can be seen that glycogen showed the strongest difference (+790 %; $p < 0.001$), followed by growth rate (+420 %; $p < 0.001$), respiration rate (+145 %; $p = 0.096$), phycocyanin content (-43 %; $p < 0.001$), chlorophyll *a* content (-41 %; $p < 0.001$) and CO_2 range (-22 %; $p = 0.390$).

In a similar data analysis, the intensity of the Δ*eda* phenotype was calculated by putting physiological data on Δ*eda* into relation with the respective data on WT. Figure 22 B shows Δ*eda*/WT ratios for growth behavior, cellular glycogen content, CO_2 assimilation at 0 µE m^{-2} s^{-1} (respiration), CO_2 assimilation range (value 50 µE m^{-2} s^{-1} minus value 0 µE m^{-2} s^{-1}) as well as chlorophyll *a* and phycocyanin contents under photoautotrophic and mixotrophic conditions. The results showed the strongest phenotype of Δ*eda* in form of glycogen content under photoautotrophic conditions (+145 %; $p < 0.001$), followed by growth rate under mixotrophic conditions (-38 %; $p < 0.001$), glycogen content under mixotrophic conditions (+31 %; $p = 0.018$), chlorophyll contents under mixotrophic (-25 %; $p = 0.004$) and photoautotrophic (-24 %; $p < 0.001$) conditions, respiration rates under photoautotrophic (+23 %; $p = 0.093$) and mixotrophic (-19 %; $p = 0.065$) conditions, phycocyanin content under photoautotrophic conditions (-19 %; $p < 0.001$), CO_2 range under mixotrophic conditions (-18 %; $p = 0.166$), growth rate under photoautotrophic conditions (-16 %; $p = 0.002$), phycocyanin content under mixotrophic conditions (-13 %; $p = 0.04$) as well as CO_2 range under photoautotrophic conditions (-9 %; $p = 0.434$).

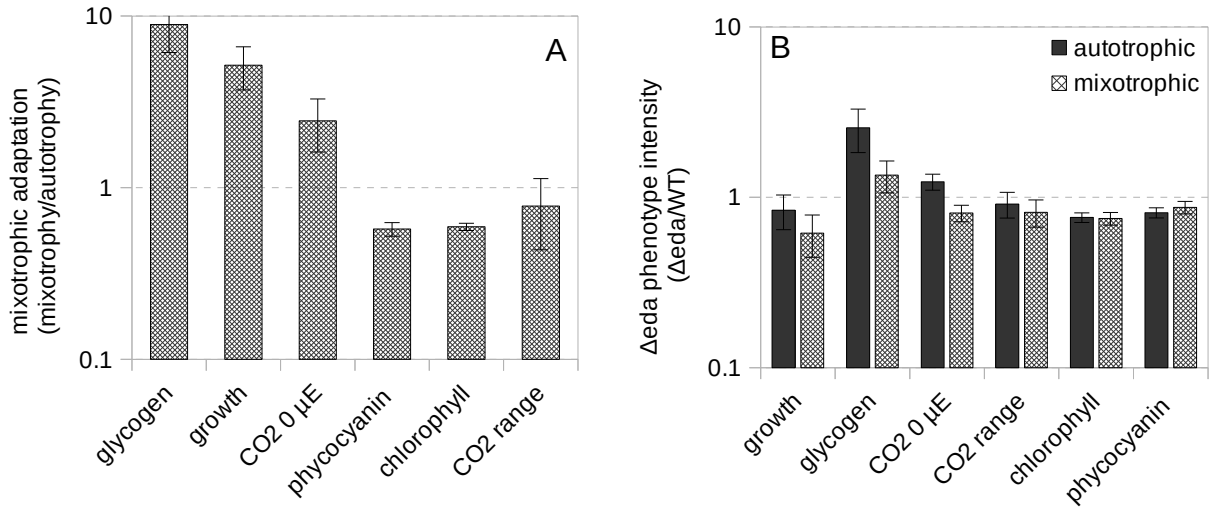

Figure 22: Mixotrophic adaptation of WT and phenotype intensity of Δ*eda*. Physiological parameters that have been measured in the previous chapters were used to create two new charts to visualize on the one hand the physiological adaptations under mixotrophic conditions in comparison to photoautotrophic conditions (A) and on the other hand the phenotype intensity of Δ*eda* under photoautotrophic and mixotrophic conditions (B). The first was accomplished by dividing the obtained mixotrophic values from WT of growth, cellular glycogen content, CO_2 assimilation at 0 µE m^{-2} s^{-1}, CO_2 assimilation range (value 50 µE m^{-2} s^{-1} minus value 0 µE m^{-2} s^{-1}) as well as chlorophyll *a* and phycocyanin content by the respective photoautotrophic values (A). Intensity of the Δ*eda* phenotype was calculated by dividing the obtained values from Δ*eda* by the respective values from WT, once under photoautotrophic and once under mixotrophic conditions (B). Shown are mean results from several experimental repetitions.

5.4.5 *Δeda* growth phenotype under continuous mixotrophic growth conditions

In order to test whether the growth phenotype of the ED pathway deletion mutant Δ*eda* that is observable under mixotrophic conditions is due to an adaptation problem, a prolonged growth experiment was performed. Δ*eda* was inoculated in BG11 medium containing 10 mM glucose at an OD 0.05 and growth was monitored as usual. However, before reaching the stationary phase, the culture was diluted back to an OD of 0.05 with new medium containing glucose (fig. 23 A). This process was repeated twice. The results show that Δ*eda* had an impaired growth after each inoculation under mixotrophic conditions (fig. 23 A). Thus, it can be concluded that the mixotrophic growth phenotype of Δ*eda* is not due to an adaptation problem to mixotrophy. However, the cells might still have encountered other adaptation processes since the culture density was constantly changing during the experiment. Figure 23 B shows the effect of the culture density on the cellular chlorophyll *a* content. It can be seen that chlorophyll *a* contents positively correlate with culture density (OD): after each inoculation, the cellular chlorophyll *a* content drops to increase again with rising culture density. In summary it can be said, therefore, that the mixotrophic growth phenotype of Δ*eda* is not due to an adaptation to mixotrophy but culture density effects can not be excluded.

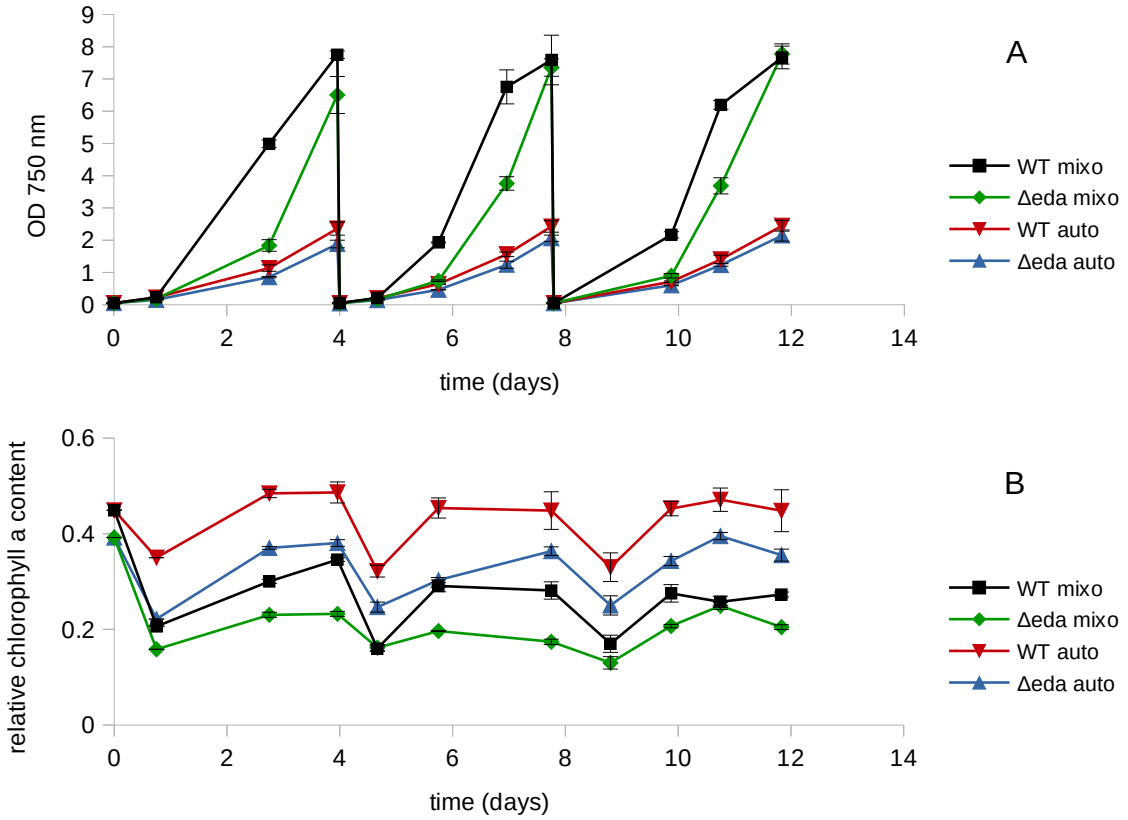

Figure 23: Continuous mixotrophic growth curve of Δ*eda* and respective chlorophyll *a* contents. The ED pathway deletion mutant Δ*eda* was inoculated with an OD of 0.05 in BG11 medium with 10 mM glucose (mixotrophic) or without glucose (photoautotrophic). On day 4 and 8 the cultures were diluted back to an OD of 0.05 with new BG11 medium containing 5 mM glucose in case of mixotrophic conditions. An exemplary growth curve of four experimental repetitions is shown in chart A. Chart B shows relative chlorophyll *a* contents, which were calculated by subtracting photometrically measured absorbance at 750 nm from absorbance at 685 nm and then dividing it by absorbance at 750 nm (OD).

5.5 Determination of mixotrophic carbon flux by NMR spectroscopy

In this experiment, nuclear magnetic resonance (NMR) spectroscopy was used to accomplish a qualitative flux analysis of mixotrophic carbon metabolism in *Synechocystis*. This allows a comparison between flux data gained by other groups with the strain and cultivation conditions that were used in this work. What is more, this constitutes the first reported flux analysis to measure flux through the Entner-Doudoroff (ED) shunt/pathway. *Synechocystis* was cultivated mixotrophically in presence of either ^{13}C1 or ^{13}C3 labeled glucose and medium samples were taken. Afterwards, the medium samples were measured by ^{1}H-NMR spectroscopy and the labeling pattern of acetate that has been excreted during mixotrophic cultivation was determined. Since the labeling pattern of acetate depends on the metabolic reactions that have been undertaken for its formation, this constitutes a reliable method to qualitatively measure metabolic fluxes. The expected labeling patterns of acetate in regard to usage of different metabolic pathways have been deduced from the structural schemes in fig. S1-S18 (appendix) and are summarized in table 12. Rows 1-4 show the expected labeling patterns of acetate after usage of the three glycolytic shunts that have been introduced in the previous chapter. One open question that has not been addressed so far is whether transaldolase (TAL) is active under mixotrophic (and photoautotrophic) conditions. TAL, which is known to play an essential role for the OPP pathway under chemoheterotrophic conditions, might help distributing fructose-6-phosphate that is generated during usage of the PGI shunt into the CBB cycle. As illustrated in table 12, an operation of TAL can be identified at the labeling pattern of acetate when ^{13}C3 glucose has been supplied (tab. 12, comparison of row 1 and 2). The table furthermore shows the expected labeling patterns of acetate for scenarios, when the three glycolytic routes (EMP, ED and OPP) are used without involvement of the CBB cycle (tab. 14, rows 5-8). The OPP pathway can either operate in a cyclic way (tab. 12, row 7) or a non-cyclic way with involvement of the EMP enzymes PFK and FBA (tab. 12, row 8). Another thing to be aware of is that decarboxylating enzymes, such as 6PGDH in the OPP shunt or several enzymes of the TCA cycle, can cause the release of labeled $^{13}CO_2$, which could potentially be refixated by RubisCO. Fig S17 (appendix) and table 12 show that such a refixation of $^{13}CO_2$ will result in a complete labeling of acetate both when ^{13}C1 and ^{13}C3 glucose has been supplied (tab. 12, row 9).

From a methodical point of view, labeling of acetate causes isotopic shifts in the ^{1}H-NMR spectra that can be distinguished as shown in figure 24. Generally speaking, the C2 labeling of acetate causes the satellite peaks (at 1.8 and 2.06 ppm) to be narrow and high, while a double labeling at C1 and C2 leads to broader and flatter peaks. Table 13 shows the ^{1}H-NMR spectra of acetate samples from mixotrophically grown WT as well as from the glycolytic deletion mutants Δ*eda*, Δ*pfk*, Δ*pfk*Δ*zwf* and Δ*pfk*Δ*zwf*Δ*gnd* that have been cultivated with either ^{13}C1 or ^{13}C3 labeled glucose. A look at the WT spectra reveals that ^{13}C1 labeled glucose causes the appearance of two sharp satellite peaks at around 1.8 and 2.06 ppm, which indicate that acetate is labeled at C2. Usage of ^{13}C3 glucose on the other hand, yields broader and flatter satellite peaks, which indicate a double labeling of acetate. All deletion

strains show the same labeling pattern as the WT: ^{13}C1 glucose yields a C2 label and ^{13}C3 glucose a C1 and C2 label on acetate. A comparison of the observed labeling pattern (tab. 12, lower half) with the expected labeling patterns for the usage of various shunts and pathways (tab. 12, upper half) reveals the PGI shunt as the responsible metabolic pathway. While theoretically, the observed labeling pattern could also have been generated by the usage of a combination of different pathways, such as CBB + PGI shunt w/o TAL + ED shunt, this can be excluded since all deletion mutants yielded the same labeling pattern as the WT. Another observation that can be made from the NMR spectra is that the satellite peaks of C2 labeled acetate were more prominent in the strains where phosphofructokinase is deleted (Δ*pfk*) than in the WT. This could indicate that a deletion of Δ*pfk* increases the flux through the PGI shunt, due to accumulation and redirection of fructose-6-phosphate. However, since the method does not produce quantitative results, these interpretations have to be done cautiously. An effect due to refixation of labeled $^{13}CO_2$ can furthermore be neglected, since acetate showed no labeling at the C1 atom when cells were cultured with ^{13}C1 glucose.

Table 12: Expected and observed labeling pattern of acetate during mixotrophic cultivation of *Synechocystis* with either ^{13}C1 or ^{13}C3 labeled glucose. The table shows the expected labeling patterns of acetate for different mixotrophic carbon flux scenarios: Usage of the three glycolytic shunts (row 1-4), the three glycolytic routes without involvement of the CBB cycle (row 5-8) and refixation of previously decarboxylated $^{13}CO_2$ (see fig. S1-18 (appendix)). The second table shows the observable acetate labeling patterns of all measured strains (WT, Δ*eda*, Δ*pfk*, Δ*pfk*Δ*zwf* and Δ*pfk*Δ*zwf*Δ*gnd*) after ^{13}C1 and ^{13}C3 glucose cultivation.

expected	^{13}C1 Glucose		^{13}C3 Glucose	
Acetate label pos.	C1	C2	C1	C2
CBB + PGI shunt		■	■	■
CBB + PGI shunt w/o TAL		■	■	
CBB + ED shunt				■
CBB + OPP shunt			■	
EMP pathway		■		
ED pathway				■
OPP pathway				
OPP pathway + PFK/FBA			■	■
CBB refixation of $^{13}CO_2$	■	■	■	■

observed	^{13}C1 Glucose		^{13}C3 Glucose	
Acetate label pos.	C1	C2	C1	C2
all measured strains		■	■	■

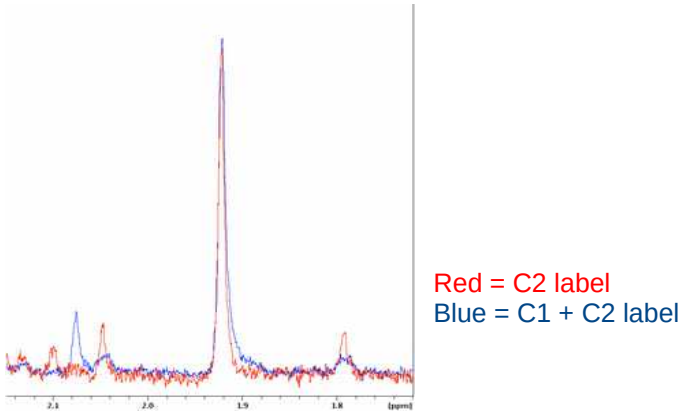

Figure 24: 1H-NMR spectrum of acetate, either labeled at the C2 atom (red) or at both C atoms (blue). Sample was taken from *Synechocystis* WT.

Table 13: ^{1}H-NMR spectra of acetate samples from WT and several deletion strains. WT and several deletion strains (Δ*eda*, Δ*pfk*, Δ*pfk*Δ*zwf* and Δ*pfk*Δ*zwf*Δ*gnd*) were cultivated in the presence of either ^{13}C1 or ^{13}C3 labeled glucose and acetate samples were taken from the supernatant. Acetate labeling was determined by 1H-NMR. The acetate spectra from figure 27 served as interpretation reference. The deduced labeling positions of acetate are listed in the third and fifth column ('acetate label pos.').

strain	^{1}H NMR spectrum for ^{13}C1-Glucose	Acetate label pos.	^{1}H NMR spectrum for ^{13}C3-Glucose	Acetate label pos.
WT (control)		no		no
WT		C2		C1+C2
Δ*eda*		C2		C1+C2
Δ*pfk*		C2		C1+C2
Δ*pfk*Δ*zwf*		C2		C1+C2
Δ*pfk*Δ*zwf*Δ*gnd*		C2		C1+C2
	2.0 1.5 [ppm]		2.0 1.5 [ppm]	

5.6 Characterization of various single and double glycolytic deletion mutants

5.6.1 Characterization of *pgi*/Δ*pgi*

In order to obtain a method to investigate the role of the PGI shunt, characterization of various merodiploid glucose-6-phosphate isomerase single and multi knock-out mutants (*pgi*/Δ*pgi*) was done. Growth rate measurements of *pgi*/Δ*pgi*, *pgi*/Δ*pgi*Δ*eda*, *pgi*/Δ*pgi*Δ*gnd* and *pgi*/Δ*pgi*Δ*eda*Δ*gnd* showed that none of the strains exhibited a significant growth impairment in comparison to WT (fig. 25 A) under photoautotrophic growth conditions. In order to test whether PGI activity was reduced in the merodiploid strains, PGI activity was measured in crude cell extracts of exponentially photoautotrophically growing cells. With the exception of *pgi*/Δ*pgi*Δ*eda*Δ*gnd*, all of the *pgi*Δ*pgi* mutation strains remained WT levels of PGI activity (fig. 25 B). Since there is no secondary isoform of PGI in *Synechocystis*, these results show that the remaining gene copies of PGI in the merodiploid mutant suffice to generate WT levels of PGI activity. Due to the inability of the PGI mutant to fully segregate, an indispensable role for PGI can be assumed.

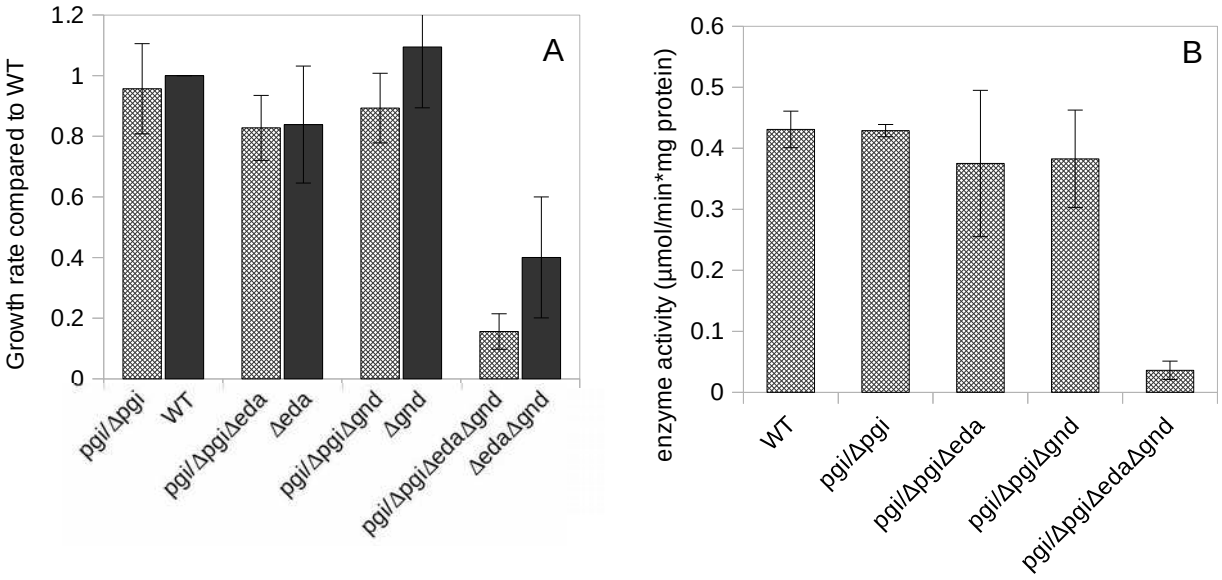

Figure 25: Growth behavior and glucose-6-phosphate isomerase activity of diverse glucose-6-phosphate isomerase (PGI) deletion mutants. Shown are the relative growth velocities of the *pgi*/Δ*pgi* single knock-out and diverse multi knock-out mutants in relation to WT under photoautotrophic conditions(A). In order to visualize the effect of PGI mutation, the PGI knock-out conditions have been paired with non-knock-out conditions. Chart B shows measured PGI activities of WT, the single PGI knock-out mutant (*pgi*/Δ*pgi*) and diverse multi knock-out mutants that have been cultivated under photoautotrophic conditions. Shown are mean data from three experimental repetitions.

5.6.2 Growth analysis of Δ*gap2*

The CBB cycle isoform of the glyceraldehyde-3-phosphate dehydrogenase (GAPDH2; sll1342) was knocked out in *Synechocystis*. This enzyme is part of the regenerative part of the CBB cycle. Investigation of the Δ*gap2* deletion mutant was accomplished in order to obtain information regarding the hypothesis that glycolytic shunts can (partially) take over regeneration of ribulose-5-phosphate during mixotrophic growth. Growth behavior of the Δ*gap2* deletion mutant was investigated under photoautotrophic, mixotrophic and chemoheterotrophic (LAHG) growth conditions. The results showed that Δ*gap2* was unable to grow under photoautotrophic conditions (fig. 26 A). Under mixotrophic conditions, Δ*gap2* was able to grow but showed an impaired (-56 %; p = 0.040) growth rate in comparison to WT (fig. 26 A). Additionally, the stationary phase seemed to be reached at lower culture densities than in WT. Growth analyses under chemoheterotrophic conditions revealed an increased (+141 %; p = 0.012) growth rate of Δ*gap2* in comparison to WT (fig. 26 A).

A further analysis of the growth phenotypes revealed that Δ*gap2* was able to grow faster under mixotrophic conditions than WT under photoautotrophic conditions (+153 %; p = 0.075) and Δ*gap2* under chemoheterotrophic conditions (+5700 %; p = 0.021) (fig. 26 B). This shows that addition of glucose can (partially) rescue the Δ*gap2* mutant during light. Since the mixotrophic growth rate of Δ*gap2* is much faster than the chemoheterotrophic growth rate, it can be deduced that the observable growth is not due to chemoheterotrophic metabolism. It can, however, not be excluded that heterotrophic metabolism was accomplished in combination with phototrophic metabolism, resulting in a photoheterotrophic metabolism, similar as it can be induced by addition of inhibitors of the photosynthetic electron chain, like DCMU or atrazine (Nakajima *et al.*, 2014). Further experiments, for example in form of measurements of CO_2 assimilation rates, would need to be conducted to show that the observable growth mode was indeed mixotrophic.

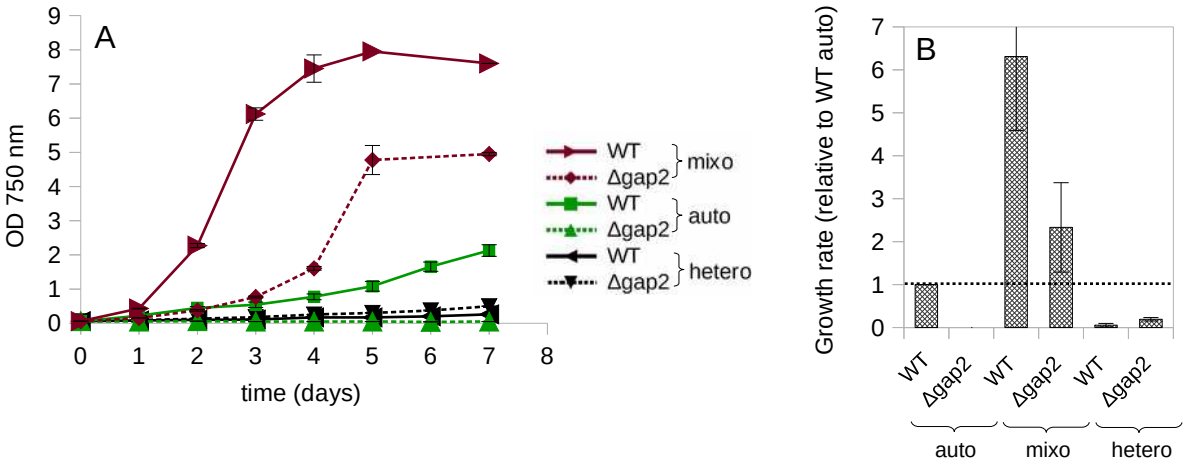

Figure 26: Growth behavior of a glyceraldehyde-3-phosphate dehydrogenase (GAPDH2) deletion mutant. Shown is a representative growth curve of the Δ*gap2* knock-out mutant and WT under photoautotrophic, mixotrophic and chemoheterotrophic (LAHG) conditions (A). Mean growth rates relative to WT under photoautotrophic conditions from three experimental repetitions are shown in the right chart (B).

5.6.3 Growth analysis of Δ*pfk*, Δ*zwf*, Δ*gnd*, Δ*eda*Δ*pfk*, Δ*eda*Δ*zwf* and Δ*eda*Δ*gnd*

Growth behavior of the glycolytic deletion mutants Δ*pfk* (phosphofructokinase), Δ*zwf* (glucose-6-phosphate dehydrogenase), Δ*gnd* (6-phosphogluconate dehydrogenase) as well as the double mutants Δ*eda*Δ*pfk*, Δ*eda*Δ*zwf* and Δ*eda*Δ*gnd* of *Synechocystis* was analyzed under photoautotrophic and mixotrophic growth conditions. Data from all growth curves that have been obtained in the course of this dissertation was evaluated according to the 'triplet regression' method (chapter 4.3.2) and are expressed as growth rates compared to WT in figure 27. The photoautotrophic results showed an impaired growth behavior of all mutants where the ED pathway has been knocked out: Δ*eda* (-18 %; $p = 0.002$), Δ*eda*Δ*pfk* (-37 %; $p = 0.023$), Δ*eda*Δ*zwf* (-42 %; $p < 0.001$) and Δ*eda*Δ*gnd* (-60 %; $p < 0.001$) compared to WT (fig. 27). A comparison between the four ED pathway knock-out mutants revealed that Δ*eda*Δ*zwf* and Δ*eda*Δ*gnd* were both growing worse than Δ*eda* (-30 %; $p = 0.015$ and -51 %; $p < 0.001$, respectively) and Δ*eda*Δ*gnd* was furthermore growing worse than Δ*eda*Δ*zwf* (-30 %; $p = 0.084$). The single deletion mutant Δ*zwf* also seemed to have an impaired growth rate compared to WT (-18 %; $p = 0.163$), however, the result remains uncertain due to the small sample size of growth data on Δ*zwf* (n=5). No difference in growth behavior could be shown for Δ*pfk* and Δ*gnd* in comparison to WT. Under mixotrophic growth conditions only Δ*eda* and Δ*eda*Δ*gnd* were analyzed. While Δ*eda* showed an impaired growth (-38 %; $p < 0.001$), Δ*eda*Δ*gnd* did not grow at all under mixotrophic conditions (fig. 27). The three ED pathway double mutants Δ*eda*Δ*pfk*, Δ*eda*Δ*zwf* and Δ*eda*Δ*gnd* were furthermore analyzed for their growth phenotype stability, similar as has been done for Δ*eda* in chapter 5.4. For this, growth rates were plotted against the respective date of experiment (fig. 28). The results showed a positive correlation between growth rates and experimental date in all three investigated mutants under photoautotrophic conditions (Δ*eda*Δ*pfk* ($p = 0.003$), Δ*eda*Δ*zwf* ($p < 0.001$) and Δ*eda*Δ*gnd* ($p < 0.001$)), thereby demonstrating that the severeness of the growth phenotypes became smaller in the course of this dissertation. This was possibly due to physiological adaptation processes.

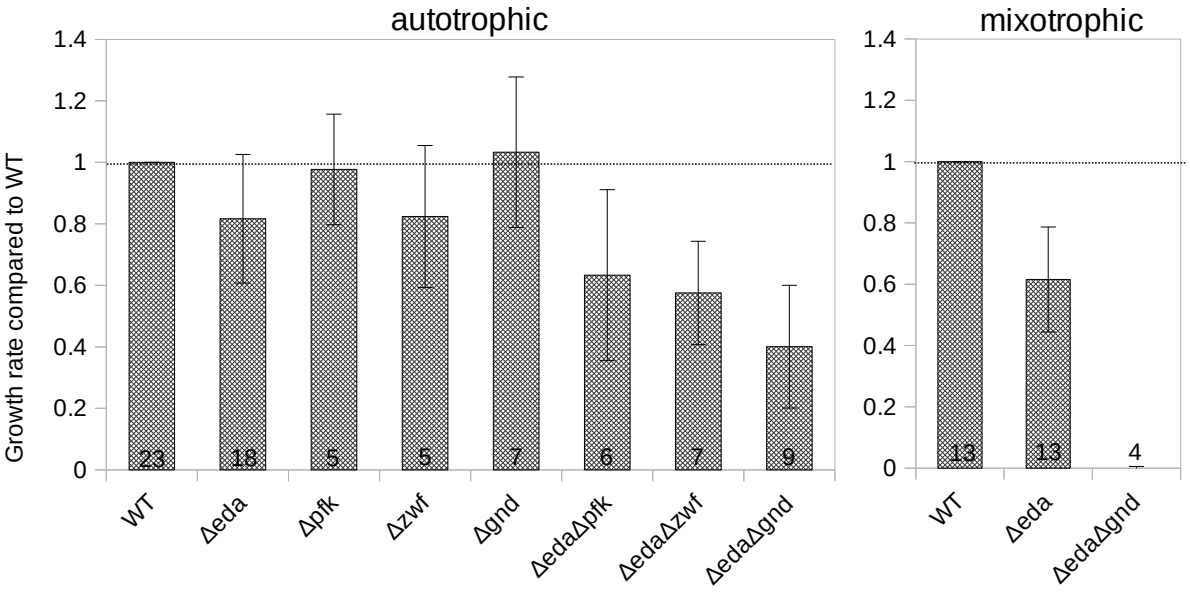

Figure 27: Growth behavior of various glycolytic deletion mutants under photoautotrophic and mixotrophic conditions. Shown are the mean growth rates in comparison to WT of the glycolytic deletion mutants Δ*eda*, Δ*pfk*, Δ*zwf*, Δ*gnd*, Δ*eda*Δ*pfk*, Δ*eda*Δ*zwf* and Δ*eda*Δ*gnd* under photoautotrophic (left chart) as well as Δ*eda* and Δ*eda*Δ*gnd* under mixotrophic (right chart) growth conditions. Values inside bars represent number of experimental repetitions (*n*).

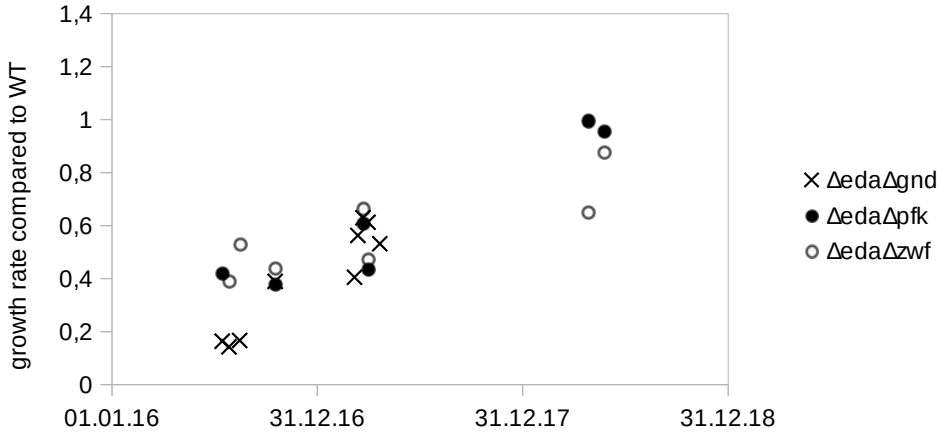

Figure 28: Growth phenotype evolution of ED pathway double deletion mutants. Shown are the relative growth rates of the three ED pathway double deletion mutants Δ*eda*Δ*gnd*, Δ*eda*Δ*pfk* and Δ*eda*Δ*zwf* plotted against date under photoautotrophic growth conditions. Each dot represents one experiment.

5.6.4 Δ*eda*Δ*gnd* and 6-phosphogluconate (6PG)

It has been shown during the investigation of the existence of a GDH/GK bypass (chapter 5.3) that the metabolite 6-phosphogluconate (6PG) accumulated in the Δ*eda*Δ*gnd* deletion mutant. A measurement of cellular 6PG contents of the glycolytic deletion mutants Δ*eda*, Δ*pfk*, Δ*zwf*, Δ*gnd*, Δ*eda*Δ*pfk*, Δ*eda*Δ*zwf* and Δ*eda*Δ*gnd* under photoautotrophic growth conditions revealed that Δ*eda*Δ*gnd* was the only one of all measured mutants that accumulated 6PG (fig. 29 B). It has also been shown that an additional knock-out of Δ*pfk* and Δ*zwf* in the Δ*eda*Δ*gnd* mutant, as accomplished in the Δ*eda*Δ*gnd*Δ*pfk*Δ*zwf* mutant, prevented 6PG accumulation (fig. 29 D). What is more, Δ*eda*Δ*gnd*Δ*pfk*Δ*zwf* seemed to grow better than Δ*eda*Δ*gnd* under photoautotrophic and especially under mixotrophic conditions (fig. 29 C). Thus, additional deletion of Δzwf and Δ*pfk* seemed to rescue the Δ*eda*Δ*gnd* mutant (to a certain degree). A likely conclusion is that 6PG accumulation was responsible for the growth impairment of Δ*eda*Δ*gnd*. Without G6PDH (ZWF), no 6PG can accumulate in the Δ*eda*Δ*gnd* mutant. This could also provide an explanation for the inferior growth of Δ*eda*Δ*gnd* compared to Δ*eda*Δ*zwf*. In another experiment, relative growth velocities as well as 6PG contents of Δ*eda*Δ*gnd*, that has been cultivated photoautotrophically under varying CO_2 supply, were measured (fig. 29 E+F). The results showed that Δ*eda*Δ*gnd* had no growth impairment under low CO_2 conditions but was unable to increase its growth at high CO_2 concentrations. The cellular 6PG concentration in Δ*eda*Δ*gnd* seemed to be rather constant (3.5-4.5 µg/OD*mL) under all measured conditions. Taking these results together, an inhibitory effect of 6PG on CO_2 fixation seems likely.

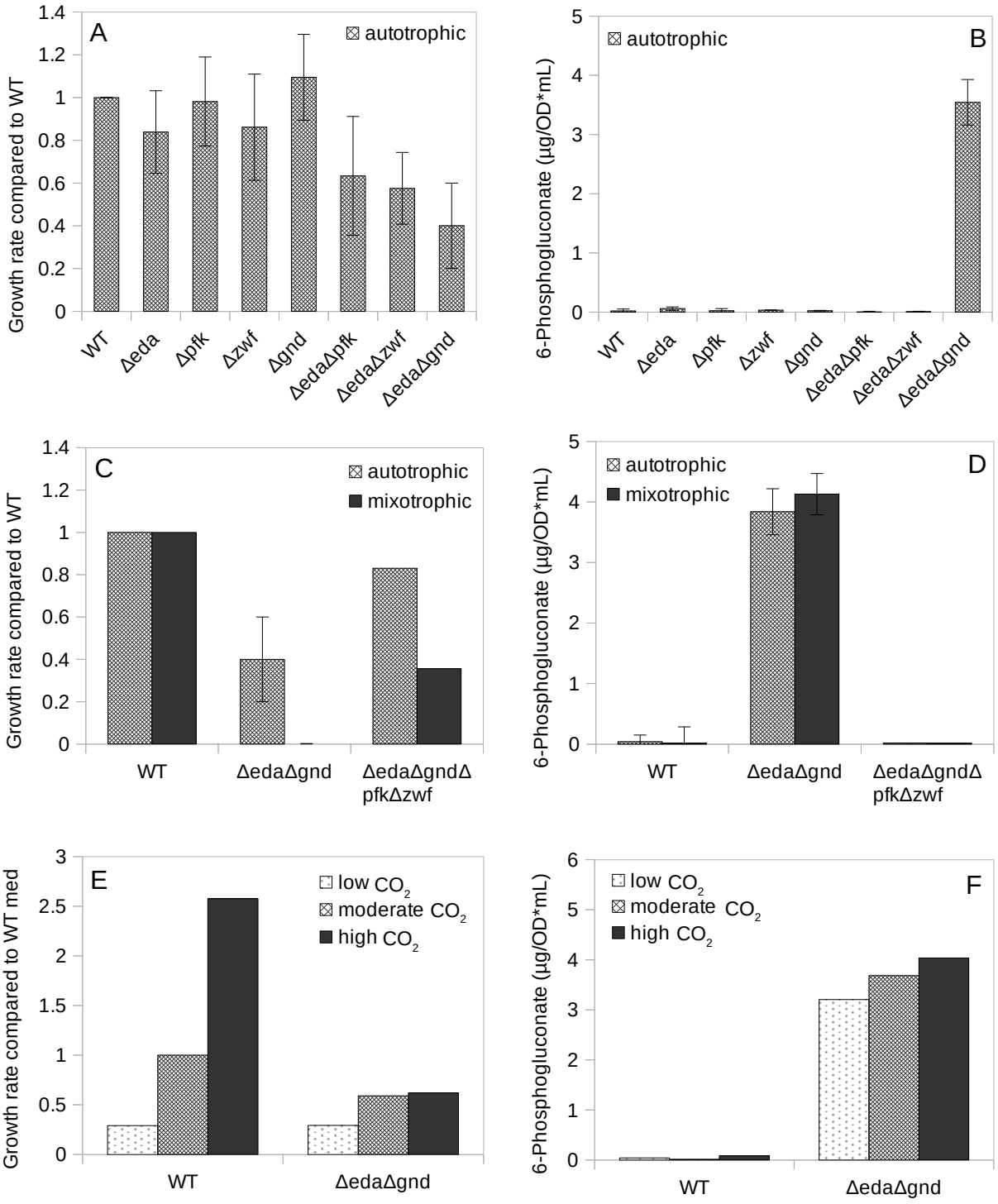

Figure 29: Growth behavior and 6-phosphogluconate contents of Δ*eda*Δ*gnd* and other glycolytic deletion mutants. Shown are relative growth velocities (A) and cellular 6-phosphogluconate contents (B) of WT, Δ*eda*, Δ*pfk*, Δ*zwf*, Δ*gnd*, Δ*eda*Δ*pfk*, Δ*eda*Δ*zwf* and Δ*eda*Δ*gnd* under photoautotrophic conditions. Furthermore, relative growth velocities as well as cellular 6-phosphogluconate contents of Δ*eda*Δ*gnd* and Δ*eda*Δ*gnd*Δ*pfk*Δ*zwf* were compared under photoautotrophic and mixotrophic conditions (C+D). The bottom charts show the relative growth velocities of WT and Δ*eda*Δ*gnd* that were cultivated under photoautotrophic conditions with varying CO_2 supply and the respective cellular 6-phosphogluconate contents (E+F). Shown are mean data from at least three experimental repetitions.

5.6.5 CO_2 assimilation

The glycolytic deletion mutants Δ*eda*, Δ*pfk*, Δ*zwf*, Δ*gnd*, Δ*eda*Δ*pfk*, Δ*eda*Δ*zwf* and Δ*eda*Δ*gnd* as well as WT were analyzed for their CO_2 assimilation capabilities. The strains were cultivated either under photoautotrophic or mixotrophic conditions and during the exponential growth phase cell samples were taken, transferred onto custom-made agar plates and put inside a gas exchange chamber where CO_2 assimilation rates were measured in dependence on light intensity expressed as PPFD. It is important to be aware that the measured CO_2 assimilation does not reflect the real CO_2 fixation but rather the apparent CO_2 fixation which is the sum of all CO_2 fixating and decarboxylating reactions. Figures 30 A+B show two light curves of the strains WT, Δ*eda*, Δ*eda*Δ*pfk*, Δ*eda*Δ*zwf* and Δ*eda*Δ*gnd* that have been cultivated either under photoautotrophic (A) or mixotrophic (B) conditions. The light protocol ranged from 5 µE m^{-2} s^{-1} to 700 µE m^{-2} s^{-1}. Figure 30 C furthermore shows a mixotrophic light curve with a light protocol ranging from 0 µE m^{-2} s^{-1} to 50 µE m^{-2} s^{-1} and back to 0 µE m^{-2} s^{-1}. The results showed that the Δ*eda*Δ*gnd* mutant has a strongly reduced CO_2 assimilation rate under medium to high light intensities (>50 µE m^{-2} s^{-1}) under photoautotrophic (fig. 30 A), and even more so under mixotrophic (fig. 30 B) conditions compared to WT and all other mutants. These results fit well with the growth behavior of Δ*eda*Δ*gnd*. The CO_2 assimilation rates of all mutants where the OPP shunt/pathway is knocked out (Δ*eda*Δ*zwf*, Δ*eda*Δ*gnd*, Δ*zwf* and Δ*gnd*) showed no negative CO_2 assimilation (respiration) during low light and darkness under mixotrophic conditions (fig. 30 B+C), thus indicating that the OPP shunt is operating during low light conditions. Other observable phenotypes of CO_2 assimilation were less prominent: Δ*eda* showed a tendency to have a slightly higher CO_2 assimilation than WT under medium to high light photoautotrophic conditions (fig. 30 A) and a slightly less negative CO_2 assimilation under low light mixotrophic conditions (fig. 30 B). The Δ*eda*Δ*pfk* mutant showed a similar curve as Δ*eda* both under photoautotrophic and mixotrophic conditions but with a slightly reduced CO_2 assimilation under medium light intensities (fig. 30 A+B). Δ*eda*Δ*zwf* showed a slightly reduced CO_2 assimilation under medium and high light intensities when grown under photoautotrophic conditions (fig. 30 A). Δ*pfk* showed a slightly decreased CO_2 assimilation under all light intensities when grown under mixotrophic conditions (fig. 30 C).

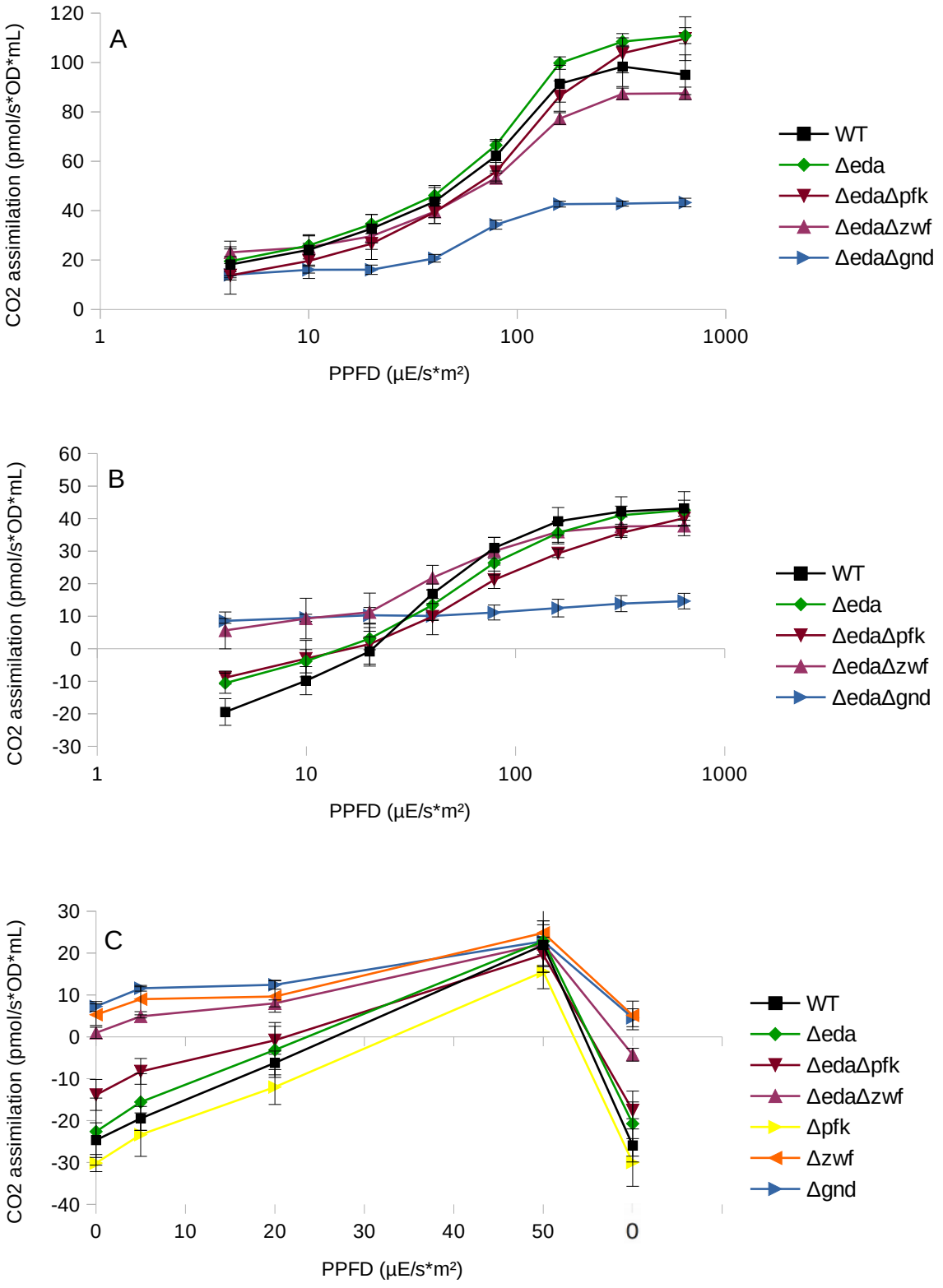

Figure 30: CO_2 assimilation rates of various glycolytic deletion mutants grown under photoautotrophic and mixotrophic conditions. CO_2 assimilation rates were measured in dependence on light intensity expressed as PPFD (photosynthetically active photon flux density) in the strains WT, Δ*eda*, Δ*eda*Δ*pfk*, Δ*eda*Δ*zwf* and Δ*eda*Δ*gnd* grown under photoautotrophic (A) or mixotrophic (B+C) conditions. Values from two experimental repetitions were averaged.

5.6.6 Cellular glycogen contents

Cellular glycogen contents of the glycolytic deletion mutants Δ*eda*, Δ*pfk*, Δ*gnd* and Δ*zwf* as well as WT were determined under photoautotrophic and mixotrophic growth conditions. The results showed no significant difference between glycogen contents of Δ*pfk*, Δ*gnd*, Δ*zwf* and WT under photoautotrophic conditions (fig. 31). Only Δ*eda* showed an increased glycogen content (+145 %; $p < 0.001$), which has already been analyzed in more detail in chapter 5.4.

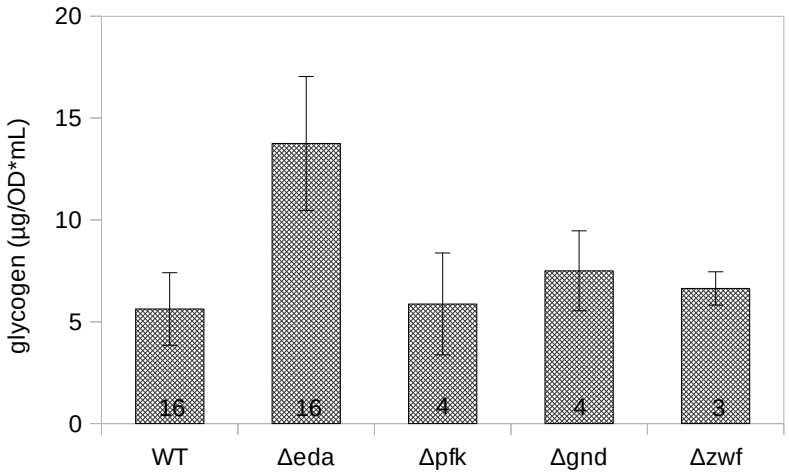

Figure 31: Cellular glycogen contents of various glycolytic deletion mutants under photoautotrophic growth conditions. Shown are the mean cellular glycogen contents of WT, Δ*eda*, Δ*pfk*, Δ*gnd* and Δ*zwf* under photoautotrophic conditions. Values inside bars represent number of experimental repetitions (*n*).

5.7 Discontinuous growth analysis

5.7.1 Transfer from mixotrophic to photoautotrophic growth conditions

Measurements of glycogen contents during mixotrophic conditions revealed that *Synechocystis* cultures start to degrade glycogen when medium glucose is fully consumed (chapter 5.4.2). This constitutes another situation where glycogen is degraded during photoautotrophic growth conditions. In order to see the influence of the ED pathway on glycogen degradation during these conditions, WT and Δ*eda* were precultivated under mixotrophic growth conditions for 48 hours and afterwards transferred to new BG11 medium without glucose to be further cultivated under photoautotrophic conditions. In parallel to the mixotrophically adapted preculture (pre_m), a photoautotrophically adapted preculture (pre_a) was used as a control. Growth behavior and cellular glycogen contents were monitored over the first 24 hours upon medium exchange. Figure 32 A shows cellular glycogen contents plotted against time. The results showed a degradation of glycogen in the mixotrophically precultivated cultures during the first 12 hours upon medium exchange. Glycogen degradation rates were calculated and are shown either as absolute values (µg/h*OD*mL) (fig. 32 B) or as relative values in comparison to WT (fig. 32 C). The results showed a mean glycogen degradation rate of 3.34 µg/h*OD*mL in WT and 2.54 µg/h*OD*mL in Δ*eda*. The relative impairment of Δ*eda* was 29 % (p = 0.071). Figures 32 D+E show typical growth behavior of WT and Δ*eda* upon transition from mixotrophic to photoautotrophic growth conditions. Mean OD 750 gains during the first 12 hours were calculated and are shown in figure 32 C. It can be seen that the way of precultivation did not have a significant effect on growth behavior for both WT and Δ*eda*. Cultures that were precultivated under photoautotrophic conditions even showed a slightly increased growth rate during the first 12 hours upon medium exchange.

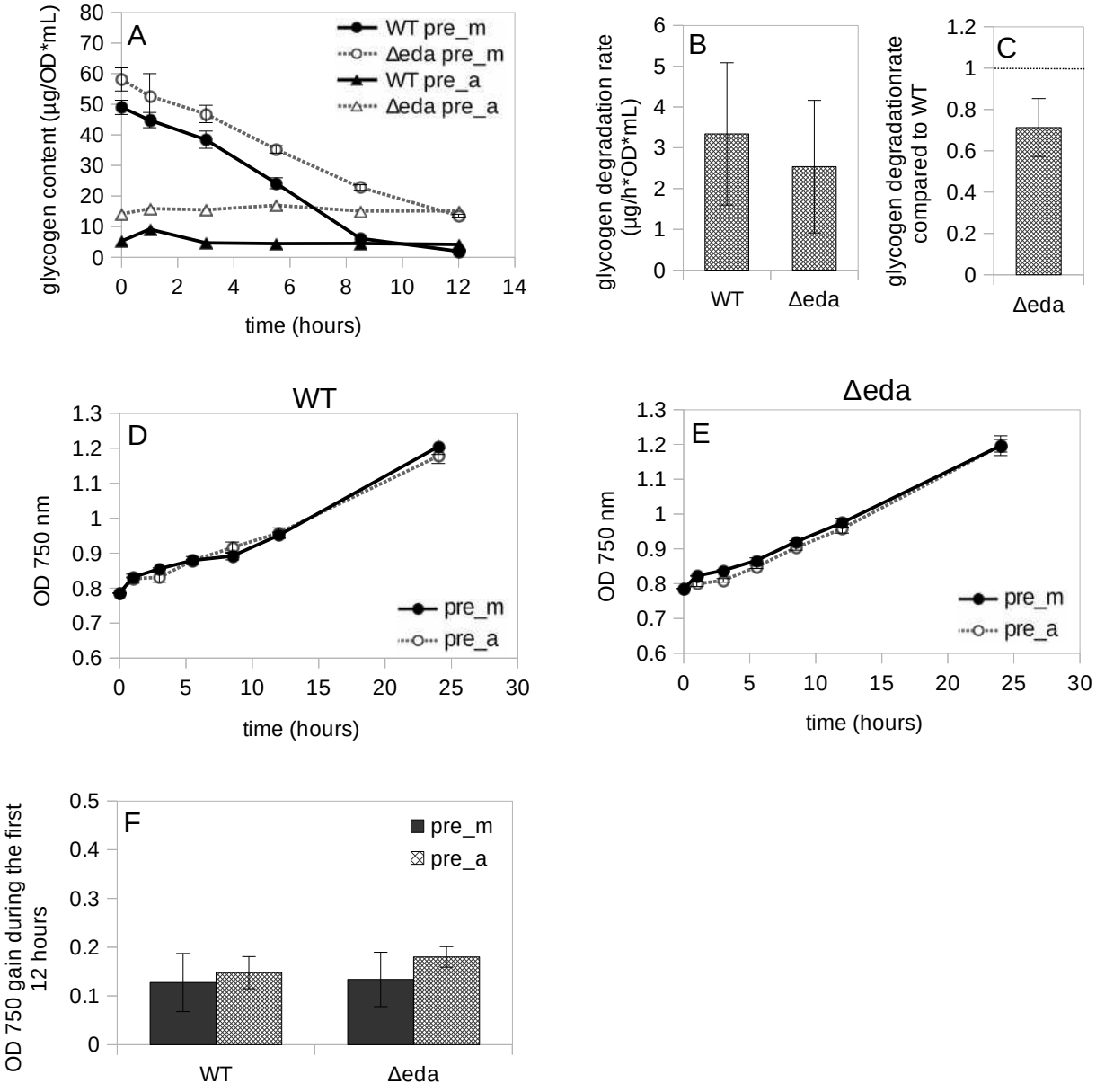

Figure 32: Growth behavior and glycogen content of WT and Δ*eda* after transfer from mixotrophic to photoautotrophic growth conditions. WT and Δ*eda* cultures were precultivated under mixotrophic conditions for 48 hours and afterwards transferred to new BG11 medium without glucose (photoautotrophic conditions). In parallel to the mixotrophically adapted preculture (pre_m), an photoautotrophically adapted preculture (pre_a) was used as a control. Growth behavior and cellular glycogen contents were monitored over the first 24 hours upon medium exchange. Charts A, D and E show glycogen contents and growth behavior of a representative experimental repetition. Mean cellular glycogen degradation rates were calculated from three experimental repetitions and are shown as absolute values (µg/h*OD*mL) in chart B or as relative values in comparison to WT in chart C. Chart F shows the average OD increase during the first 12 hours upon medium exchange from three experimental repetitions.

5.7.2 Transfer from mixotrophic to photoautotrophic and chemoheterotrophic growth conditions

The results from the previous chapter showed that Δ*eda* has an impaired glycogen degradation rate after transfer from mixotrophic to photoautotrophic conditions, thus supporting the hypothesis that the ED shunt is important for glucose metabolism during light. In order to test for a role of the ED pathway during glycogen degradation in the dark, a similar experiment was carried out where mixotrophically precultivated cultures were transferred to chemoheterotrophic conditions. This time, Δ*pfk*, Δ*zwf* and Δ*gnd* were included to see the role of the other two glycolytic pathways, namely the EMP and OPP pathway, during glycogen degradation in the dark. WT, Δ*eda*, Δ*pfk*, Δ*zwf* and Δ*gnd* cultures were precultivated under mixotrophic conditions for 48 hours and afterwards transferred to new medium without glucose to be cultivated either in light (photoautotrophic) or darkness (chemoheterotrophic). Cellular glycogen contents and growth behavior were then monitored for 24 hours. Figures 33 A-E show representative cellular glycogen contents plotted against time and figures 34 F+G show mean glycogen degradation rates either as absolute values (µg/h*OD*mL) or as relative values in comparison to WT. The calculated mean glycogen degradation rate of WT during light (4.75 µg/h*OD*mL) was higher than in the previous experiment. A comparison between glycogen degradation rates of WT during light and darkness showed no significant difference between the two cultivation conditions (fig. 33 A+F). However, while the glycogen degradation curve during darkness had an exponential shape, the curve during light cultivation showed a more sigmoidal shape, characterized by a lag phase in the beginning and higher maximum rates in the mid section. Such a sigmoidal glycogen degradation curve during light was also observable in the other strains (fig. 33 B-E). A comparison between the glycogen degradation rates of the different measured strains revealed an impaired degradation rate during light in Δ*eda* (-59 %; $p < 0.001$) and during darkness in Δ*eda* (-35 %; $p = 0.010$), Δ*gnd* (-89 %; $p < 0.001$) and Δ*zwf* (-92 %). Δ*pfk* showed no impairment either during light or darkness (fig. 34 F). In order to visualize the relative impairment between light and dark cultivation, glycogen degradation rates during light were divided by glycogen degradation rates during darkness. The results showed a significantly decreased light/dark glycogen degradation rate ratio of Δ*eda* (-32 %; $p = 0.002$) in comparison to WT (fig. 33 G). The OPP pathway deletion mutants Δ*gnd* and Δ*zwf* on the other hand exhibited increased light/dark glycogen degradation rate ratios (+860 %; $p = 0.008$ and +1060 %, respectively). These results confirm the hypothesized role of the ED pathway during glycogen degradation in the light as well as the importance of the OPP pathway for glycogen degradation during darkness. Figure 33 H shows the growth behavior of a representative WT culture during the first 24 hours upon medium exchange. It can be seen that while presence of light caused growth, absence of light led to a decline of culture density. In a more detailed analysis, the net OD change of all strains during the first 8.5 hours was calculated and the results are presented in figure 33 I in case of light cultivated cultures and in figure 33 J in case of darkness cultivated cultures. The results showed that all measured strains exhibited a similar level of growth at light and that WT, Δ*eda* and Δ*pfk* showed a significant decline of culture density in darkness. The two OPP pathway deletion

mutants Δ*gnd* and Δ*zwf* showed only a small decline of culture density at darkness. The decline was 75 % smaller than in WT (p = 0.015). These results suggest that glycogen degradation leads to a decline of OD and that the parameter OD is thus presumably partially dependent on the cellular glycogen content.

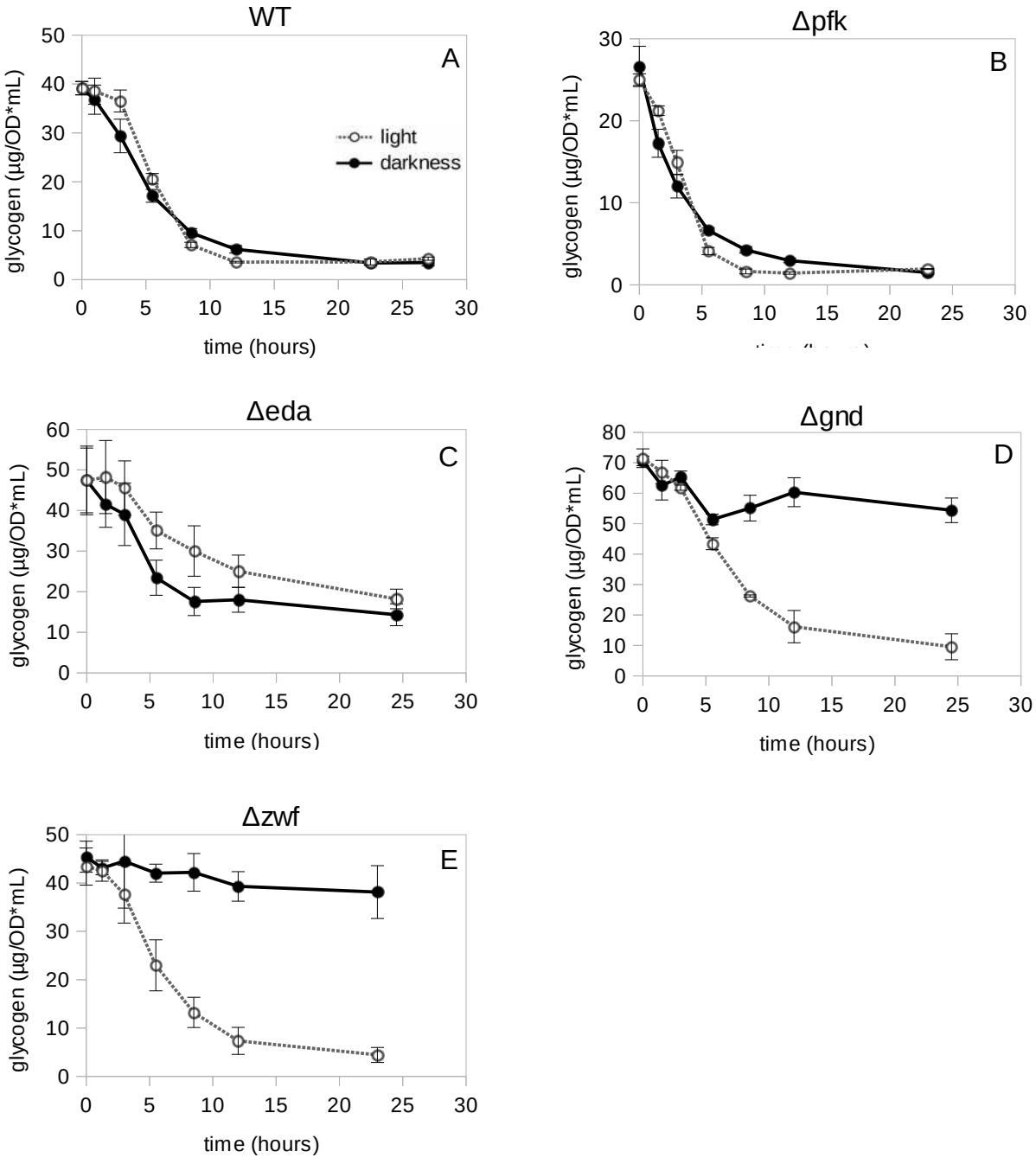

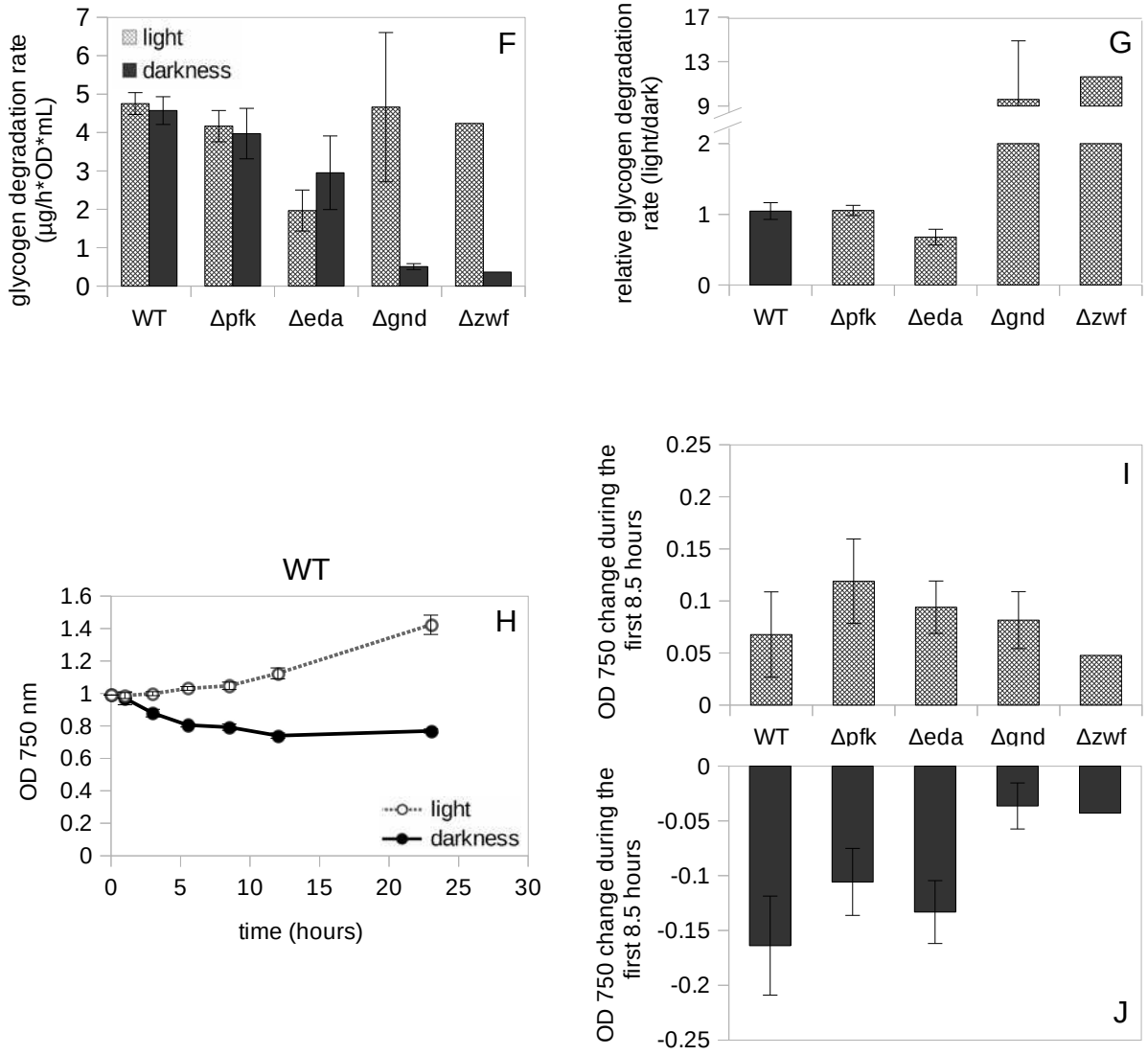

Figure 33: Glycogen contents and growth behavior of various glycolytic deletion mutants after transfer from mixotrophic to photoautotrophic or chemoheterotrophic growth conditions. WT, Δ*pfk*, Δ*eda*, Δ*gnd* and Δ*zwf* were precultivated under mixotrophic conditions for 48 hours and afterwards transferred to new BG11 medium without glucose and cultivated either in presence or absence of light. Growth behavior and cellular glycogen contents were monitored over the first 24 hours upon medium exchange. Charts A-E show glycogen contents of representative experimental repetitions. Mean cellular glycogen degradation rates were calculated from three experimental repetitions and are shown as absolute values (µg/h*OD*mL) in chart F or as relative values as ratios of light values/darkness values in chart G. Chart H shows the OD 750 of a representative WT culture after medium exchange during both light or darkness growth conditions. Mean changes in OD during the first 8.5 hours upon medium exchange were calculated for all strains and are shown for both growth conditions: light (I) and darkness (J) (*n*=3).

5.7.3 Resuscitation after nitrogen starvation

Another situation where glycogen is degraded during light in cyanobacteria is after awakening from dormancy. Klotz *et al.*, 2016 have shown that nitrogen starved *Synechocystis* builds up a glycogen reserve before bleaching and entering a metabolically inactive dormancy state after depletion of a nitrogen source. When nitrogen is resupplied, glycogen is degraded until normal photoautotrophic growth is fully resumed. WT and Δ*eda* cultures were precultivated for several weeks in absence of a nitrogen source to induce dormancy. Then, nitrate was resupplied and CO_2 assimilation rates, growth behavior and cellular glycogen contents were monitored for 48 hours. The results showed that CO_2 assimilation rates resumed to photoautotrophic levels within the first 48 h upon nitrogen resupply (fig. 34 A; published in Doello *et al.*, 2018). The increase was slightly slower in Δ*eda* in comparison to WT. Maximum cellular glycogen contents during nitrogen starvation were higher in Δ*eda* than in WT as can be seen at the 0 h value in figure 34 C. Upon resupply of nitrate, glycogen contents dropped almost linearly in both WT and Δ*eda* during the 48 hour measurement window (fig. 34 C). The results showed that glycogen degradation and CO_2 assimilation happened simultaneously (fig. 34 A+C, between 10 h and 48 h) which represents a mixotrophic metabolism within the cells. Glycogen degradation rates were calculated between 0 and 48 h. The results showed a decreased (-34 %; p = 0.060) glycogen degradation rate in Δ*eda* in comparison to WT (fig. 34 D+E). Figure 34 B shows the growth behavior during the resuscitation phase. A slightly delayed growth resumption of Δ*eda* in comparison to WT was observable.

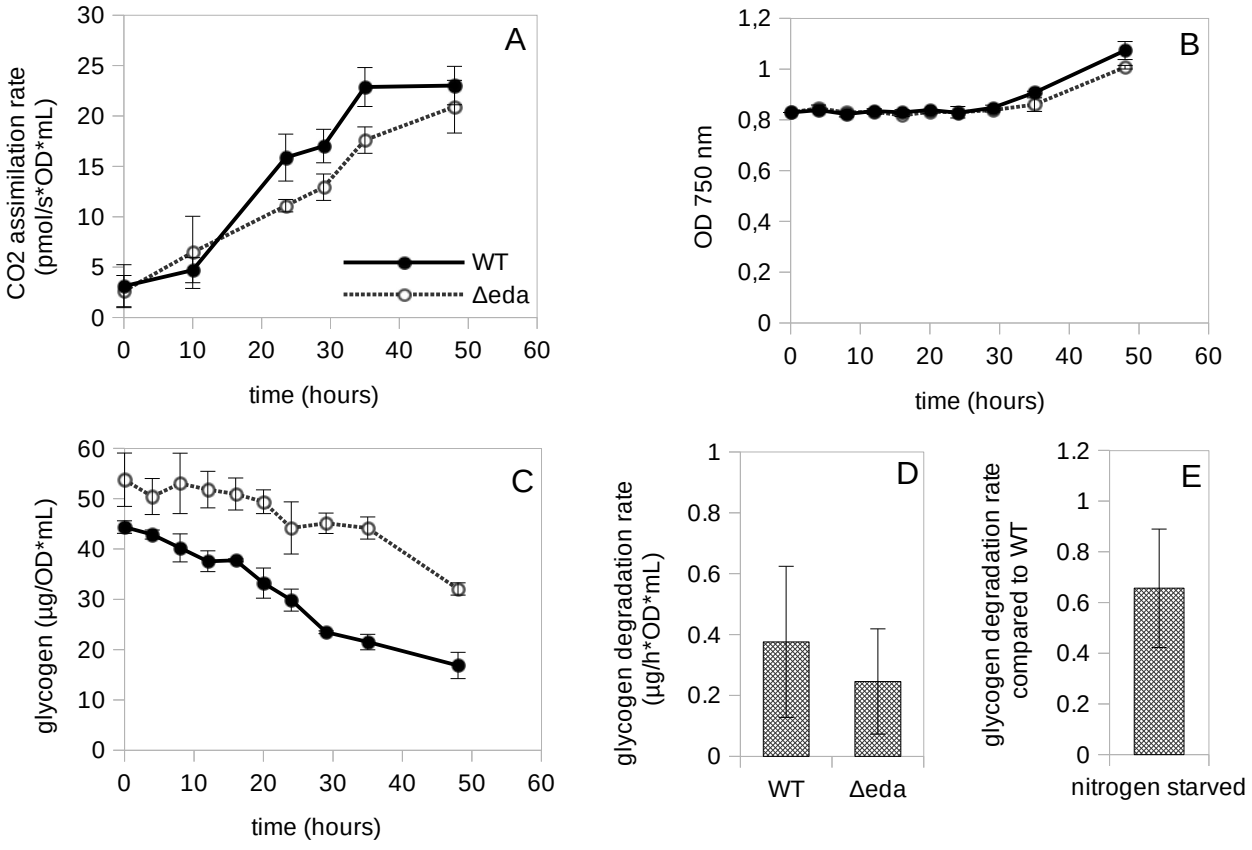

Figure 34: Growth behavior, CO_2 assimilation and cellular glycogen content of WT and Δ*eda* upon resupply of nitrate to nitrate-starved cultures. WT and Δ*eda* cultures were precultivated for 3-4 weeks in absence of a nitrogen source to induce dormancy. After resupply of nitrate, growth behavior, CO_2 assimilation rates and cellular glycogen contents were monitored for 48 hours. Charts A-C show the results of a representative experiment. Charts D and E show calculated mean glycogen degradation rates from four experimental repetitions, either as absolute values (µg/h*OD*mL) or as relative values in comparison to WT.

5.8 Photochemical quenching (qP) measurements after darkness/light shift

In order to test the hypothesis that glycolytic shunts help to refill intermediates of the CBB cycle, an experiment was carried out where the booting rate of the CBB cycle after a shift from darkness to light was measured. The CBB cycle rate was measured indirectly via photochemical quenching (qP), which is a measure for the proportion of open reaction centers at PSII. A qP value of 1 means that all reaction centers are open and that no electron jam in the PQ pool is occurring. Since the CBB cycle is the main sink of photosynthetically derived electrons, a correlation between the qP value and the CBB cycle flux can be assumed. To further improve the correlation, the CBB-cycle-competing electron acceptors nitrate and oxygen were removed by transferring cultures to nitrate-free medium and a subsequent gasing with liquid nitrogen. To shut down CBB cycle activity, cultures were put into darkness for 10 minutes. Afterwards, light was switched back on and qP value progression was measured over a course of 5 minutes. Measurement of WT showed that the qP signal dropped around 0.2 qP units upon illumination and recovers back to a value of 1 in the following 1-2 minutes (fig. 35 A). A control condition, where the CBB inhibitor glycolaldehyde was added, showed that inhibition of the CBB cycle prevented the qP value to recover after the initial drop (fig. 35 A) and thus confirms that the CBB cycle is the only available electron acceptor. Measurements of the glycolytic deletion mutants Δ*eda*, Δ*gnd, Δzwf* revealed a stronger initial qP drop (around 0.4 qP units) and also a delayed recovery compared to WT (fig. 35 B+C), thus confirming the hypothesis that rebooting of the CBB is delayed in absence of glycolytic shunts. The phosphofructokinase mutant Δ*pfk* exhibited an unaltered qP value progression in comparison to WT, thus showing that the EMP pathway was not essential for a restart of the CBB cycle. Measurement of a glycogen phosphorylase deletion mutant (Δ*glgP*, both isoforms are deleted, mutant supplied by Dr. Lars Nichelmann) that is incapable of glycogen degradation showed en even more impaired qP recovery than Δ*eda*, Δ*gnd* and *Δzwf* (fig. 35 D). This further shows that glycogen degradation is necessary for restarting of the CBB cycle upon darkness.

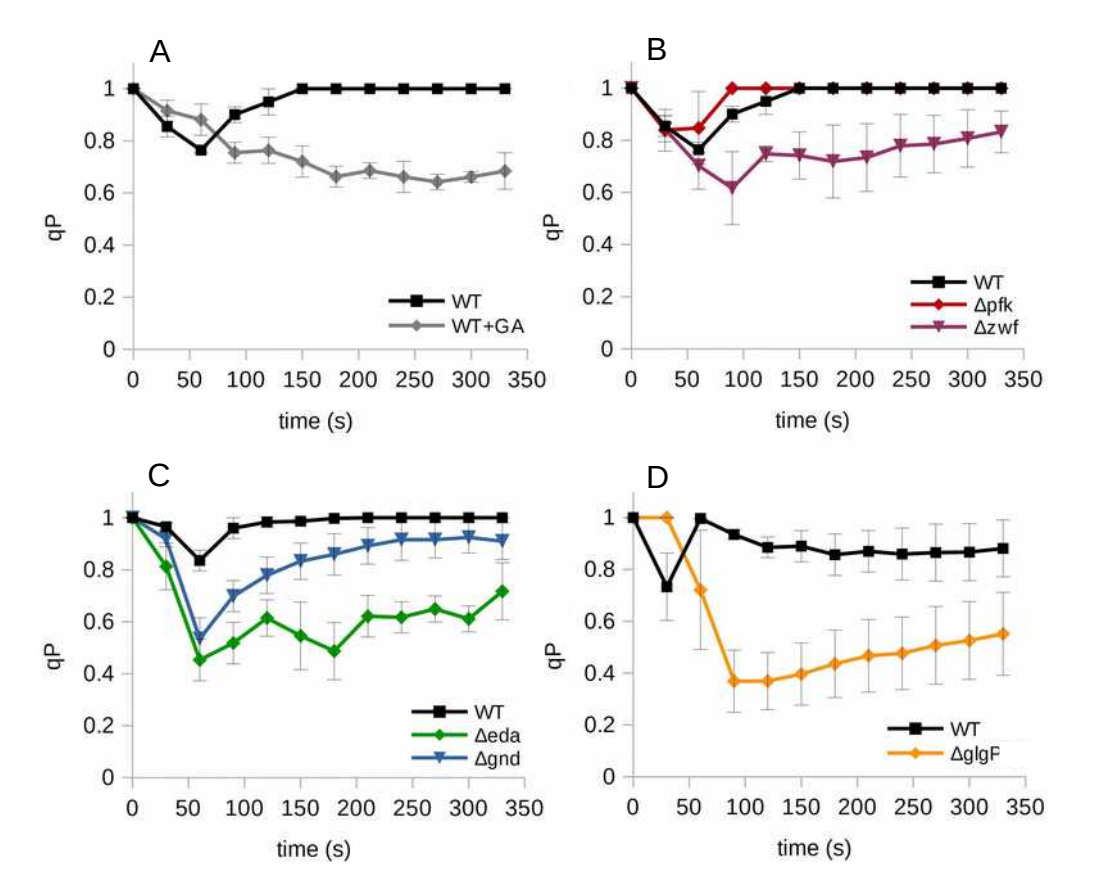

Figure 35: Photochemical quenching (qP) measurements after darkness/light shift in WT and diverse deletion mutants. Cultures were incubated in darkness for 10 min. Then, light was switched on and photochemical quenching (qP) value progression measured for 330 seconds with a PAM fluorometer. Chart A shows WT with and without 5 mM of the CBB cycle inhibitor glycolaldehyde (GA). Chart B-D show the deletion mutants Δ*pfk*, Δ*zwf*, Δ*eda*, Δ*gnd* and Δ*glgP* (deletion of both isoforms) next to WT. Shown are representative results from at least three experimental repetitions.

5.9 Calculation of ATP and NADPH stoichiometries during glycolytic shunt usage

In order to demonstrate that the usage of different shunts can alter the ATP and NADPH demand of the CBB cycle, ATP and NADPH yields of different mixotrophic scenarios of the CBB cycle with one (or several) glycolytic shunts, were calculated (fig. 36 and tab. 14). Calculations were based on the assumption that pyruvate is the sole organic end product in order to simplify comparison with the ED shunt. The second assumption that was made, is a CO_2 assimilation (by RubisCO) to glucose utilization ratio of 3:1, which is a realistic value during exponential mixotrophic growth (Yang *et al.*, 2002; You *et al.*, 2014; Nakajima *et al.*, 2014).

The results demonstrate that funneling of glucose-6-phosphate into the CBB cycle has a strong influence on the overall pyruvate, ATP and NADPH outcome. Fixation of 3 CO_2 via the CBB cycle alone requires 5 NADPH, 7 ATP and yields 1 molecule of pyruvate (Fig. 36 A). If additional glucose-6-phosphate enters the CB cycle via the PGI shunt, the overall pyruvate as well as NADPH yields are increased by 2 and the ATP yield is increased by 4 for each molecule glucose-6-phosphate (fig. 36 B+C, tab. 14 II). Usage of the ED shunt leads to the same pyruvate and NADPH yield as the PGI shunt but results in a lower ATP yield (only 2 compared to 4) per flux (tab. 14 II). Thus, usage of the ED shunt can be considered an ATP dissipating mechanism in comparison to the PGI shunt. Two molecules ATP are dissipated for each glucose-6-phosphate that enters the CBB cycle via the ED shunt instead of the PGI shunt (tab. 14 III). The OPP shunt is conceptually different from the other two shunts, due to the fact that it causes a decarboxylation, which changes the overall carbon stoichiometry (fig. 36 D). This does not only manifest itself in a lower pyruvate yield (only 1.67 pyruvate per molecule G6P) but also leads to a higher NADPH yield (3.67 NADPH per molecule G6P) (tab. 14 II). This can be explained by the fact that during a decarboxylation process, the decarboxylated carbon atom does not take the electrons from the carbon-carbon bond with it, which causes a reduction of the remaining carbon atom, which in turn enables additional NADPH reduction. The ATP yield of the OPP shunt is 3.33 per flux, which classifies the OPP shunt as another ATP dissipating mechanism when compared to the PGI shunt (tab. 14 II). However, the ATP dissipation (0.67 dissipated ATP per OPP flux instead of PGI flux) is not as high as it is for the ED shunt (2 dissipated ATP per ED flux instead of PGI flux) (tab. 14 III). An interesting possibility that has to be taken into account when regarding the yields of the OPP flux, is a refixation of the decarboxylated CO_2 (fig. 36 E). Such a refixation would lead to an increased flux in the CBB cycle (in the scenarios from fig. 36 the flux is now 4 instead of 3). Since the carbon stoichiometry is now the same as for the other shunts, the NADPH and pyruvate yields are also the same, that is 2 per OPP shunt flux (tab. 14 II). The increased CBB flux increases the overall ATP demand by 2.33 ATP per refixated CO_2, which makes this condition the one with the highest ATP dissipating capability (3 dissipated ATP per OPP flux (with refixation of lost CO_2) instead of PGI flux (tab. 14 III)).

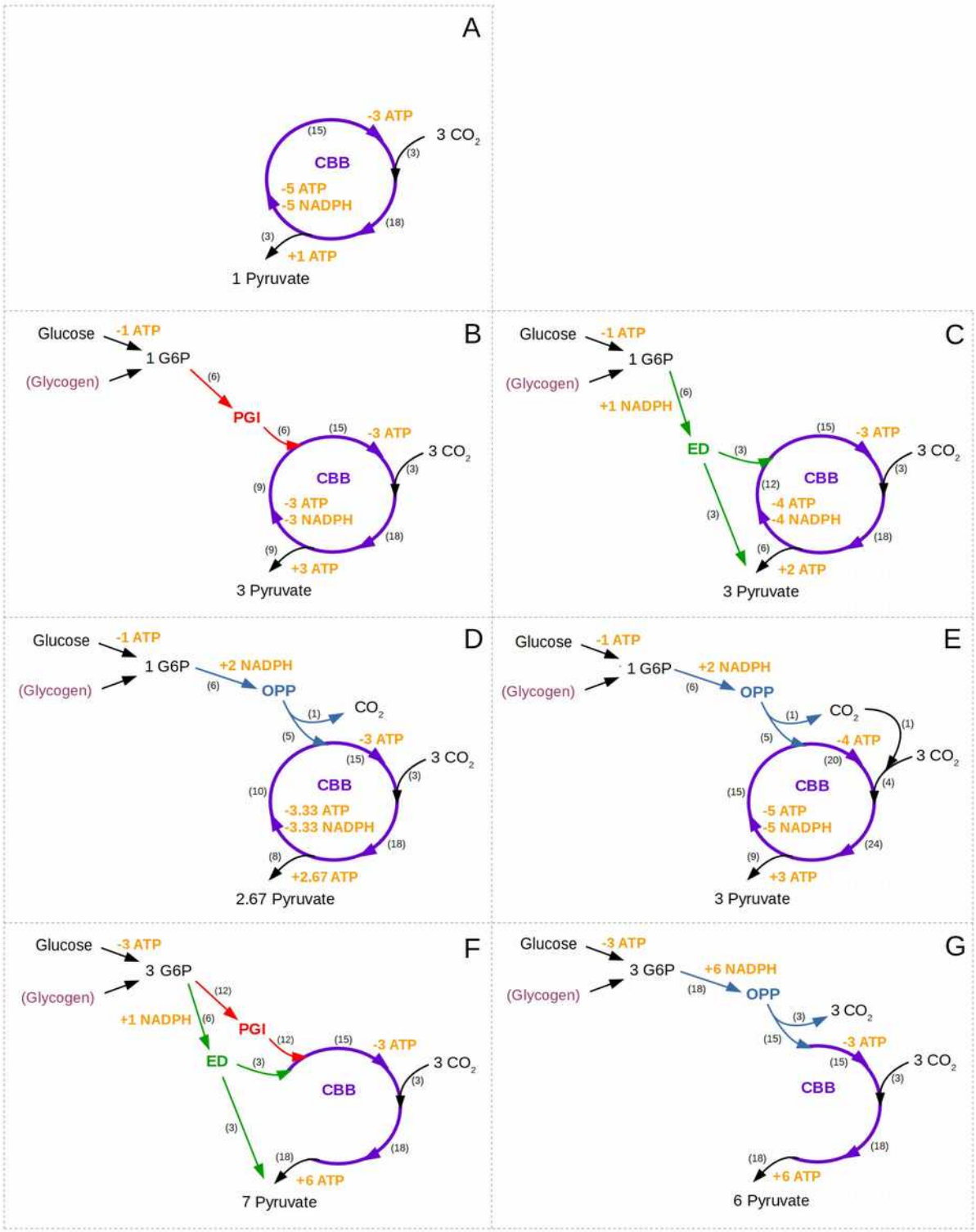

Figure 36: ATP, NADPH and pyruvate yields of different scenarios of the CBB cycle with adjacent glycolytic shunts under mixotrophic and photoautotrophic conditions. (A) CBB cycle without shunt flux, (B) CBB cycle plus PGI shunt, (C) CBB cycle plus ED shunt, (D) CBB cycle plus OPP shunt without and (E) with refixation of decarboxylated CO_2. Scenarios F and G show a complete regeneration of Ru5P either by a combination of (F) PGI and ED shunt or (G) by the OPP shunt alone. Calculations were based on the assumption that pyruvate is the sole organic end product. Numbers in brackets represent amount of carbon.

Table 14: ATP, NADPH and pyruvate yields of different scenarios of the CBB cycle with adjacent glycolytic shunts under mixotrophic and photoautotrophic conditions. Shown are the cumulative pyruvate, ATP and NADPH yields of the scenarios from fig. 37 (I), the pyruvate, ATP and NADPH yields per flux through either RubisCO (RBC), the PGI shunt, the ED shunt, the OPP shunt or the OPP shunt with a refixation of the lost CO_2 (II), as well as the pyruvate, ATP and NADPH yields of the ED shunt, OPP shunt or the OPP shunt with refixation per flux in comparison to the PGI shunt (III). Red numbers in brackets show values in case of glycogen-derived glucose.

I

		flux				yield		
	scenario	RBC	PGI	ED	OPP	pyruvate	ATP	NADPH
A	CBB	3	0	0	0	+1	-7	-5
B	CBB + PGI shunt	3	1	0	0	+3	-4 (-3)	-3
C	CBB + ED shunt	3	0	1	0	+3	-6 (-5)	-3
D	CBB + OPP shunt	3	0	0	1	+2.67	-4.67 (-3.67)	-1.33
E	CBB + OPP shunt comp.	4	0	0	1	+3	-7 (-6)	-3
F	CBB + PGI/ED shunt	3	2	1	0	+7	0 (+3)	+1
G	CBB + 3*OPP shunt	3	0	0	3	+6	0 (+3)	+6

II

	pyruvate /flux	ATP /flux	NADPH /flux
RBC	+0.33	-2.33	-1.67
PGI	+2	+3 (+4)	+2
ED	+2	+1 (+2)	+2
OPP	+1.67	+2.33 (+3.33)	+3.67
OPPc (OPP + RBC)	+2	+0 (+1)	+2

III

	pyruvate /flux	ATP /flux	NADPH /flux
ED	0	-2	0
OPP	-0.33	-0.67	+1.67
OPPc	0	-3	0

The last two scenarios from figure 36 assume a complete regeneration of ribulose-5-phosphate via glycolytic shunts, which means an absence of flux through phosphoglycerate kinase and glyceraldehyde-3-phosphate dehydrogenase. There are two possibilities for this: 1. a combined activity of the PGI and the ED shunt (fig. 37 F), which results in two molecules of fructose-6-phosphate and one molecule of glyceraldehyde-3-phosphate that can enter the regenerative part of the CBB cycle via transketolase and transaldolase or 2. the OPP shunt alone (fig. 37 G), which results in 3 molecules of ribulose-5-phosphate. These situations are unlikely to occur during continuous mixotrophic growth conditions since they imply a glucose utilization to CO_2 assimilation ratio of 1, which exceeds common mixotrophic values by far. However, during quickly changing environmental conditions, for example after a shading period, which reduces the CBB cycle flux, these situations should definitely be possible.

The presented calculations were done according to mixotrophic situations that assume an uptake and phosphorylation of glucose (as illustrated in fig. 36 A). In case of glycogen-derived glucose-6-phosphate (as illustrated in fig. 36 C) no ATP has to be invested in phosphorylation, since the glycogen-degradation product is already phosphorylated. The calculations for this situation have to be adapted by increasing the ATP yield by 1 (tab. 14 I, red numbers in brackets). However, the pyruvate, ATP and NADPH yields per shunt flux relative to PGI shunt flux (tab. 14 III) remain unchanged.

Similar as has been done for the mixotrophic situation and the photoautotrophic situation with a net glycogen degradation, ATP and NADPH yields for various photoautotrophic scenarios without a net glycogen degradation but a flux out of the CBB cycle via PGI were calculated (fig. 37 and tab. 15 I). The results again show the ATP dissipating capabilities of the ED and the OPP shunt: 2 molecules of ATP are dissipated per flux through the ED shunt, 0.67 molecules of ATP per flux through the OPP shunt and 3 molecules of ATP per flux through the OPP shunt when the decarboxylated CO_2 is refixated (tab. 15 II). These calculations are the same as for the previous situation when the ED and OPP shunt yields were put in relation to the PGI shunt yield (tab. 14 C).

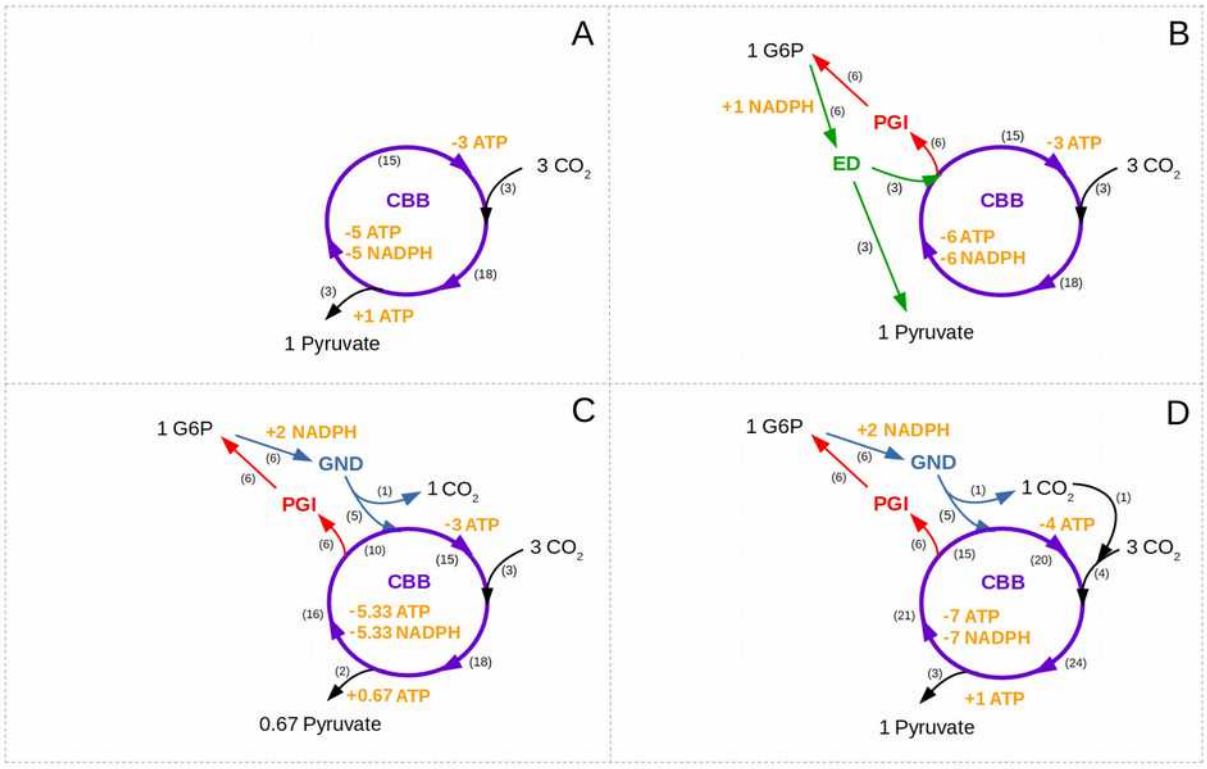

Figure 37: ATP, NADPH and pyruvate yields of different scenarios of the CBB cycle with adjacent glycolytic shunts under photoautotrophic conditions. (A) CBB cycle without shunt flux, (B) CBB cycle plus ED shunt, (C) CBB cycle plus OPP shunt without and (D) with refixation of decarboxylated CO_2. Numbers in brackets represent amount of carbon.

Table 15: ATP, NADPH and pyruvate yields of different scenarios of the CBB cycle with adjacent glycolytic shunts under photoautotrophic conditions. Shown are the cumulative pyruvate, ATP and NADPH yields of the scenarios from fig. 38 (I) as well as the pyruvate, ATP and NADPH yields per flux through either RubisCO (RBC), the PGI shunt, the ED shunt, the OPP shunt or the OPP shunt with a refixation of the lost CO_2 (II),

I

		flux			yield		
	scenario	RBC	ED	OPP	pyruvate	ATP	NADPH
A	CBB	3	0	0	+1	-7	-5
B	CBB + ED shunt	3	1	0	+1	-9	-5
C	CBB + OPP shunt	3	0	1	+0.67	-7.67	-3.33
D	CBB + OPP shunt comp	4	0	1	+1	-10	-5

II

flux	pyruvate /flux	ATP /flux	NADPH /flux
RBC	+0.33	-2.33	-1.67
ED	0	-2	0
OPP	-0.33	-0.67	+1.67
OPPc	0	-3	0

In summary it can be said that usage of glycolytic shunts can alter the ATP and NADPH outcome of the CBB cycle both under mixotrophic and photoautotrophic conditions. The ED shunt can be used for dissipation of ATP (-2 ATP per flux) and the OPP shunt for generation of NADPH (+1.67 NADPH per flux). Compensation of the CO_2 loss of the OPP shunt by an additional CO_2 fixation via RubisCO nullifies the NADPH gain but increases the ATP dissipation to be the highest among the shunts (-3 ATP per flux).

6 Discussion

6.1 Glucose dehydrogenase/gluconate kinase bypass

One open question at the beginning of this dissertation was whether the Entner-Doudoroff pathway in *Synechocystis* includes a functional glucose dehydrogenase (GDH)/ gluconate kinase (GK) bypass or if it branches off the oxidative pentose phosphate pathway as illustrated in figure 38.

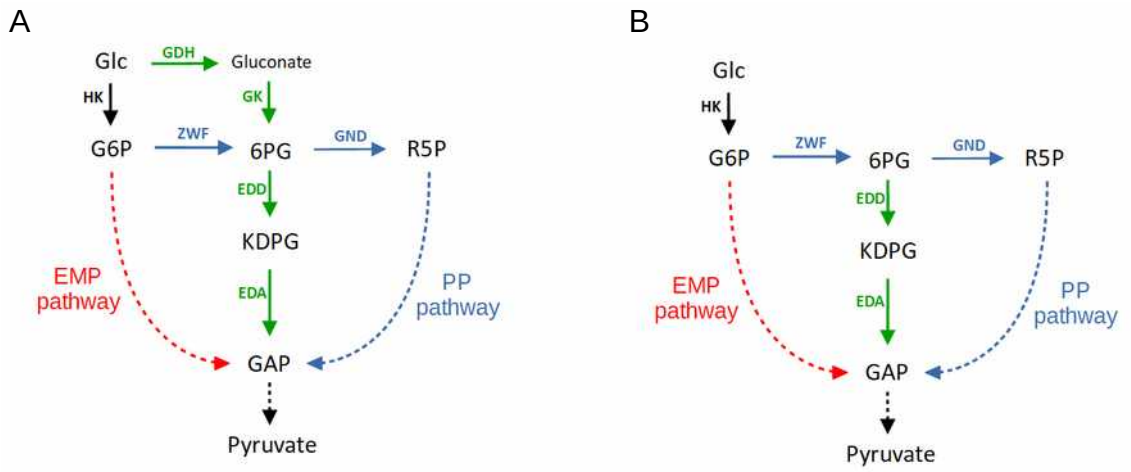

Figure 38: Glucose dehydrogenase (GDH)/gluconate kinase (GK) bypass. Shown is a simplified scheme of the central carbon metabolism in *Synechocystis* with a GDH/GK bypass (A) as well as without a GDH/GK bypass (B).

Both scenarios are common in nature. From a biochemical perspective, the main distinction between the two scenarios is the order in which phosphorylation and oxidation take place. Since unphosphorylated glucose can diffuse through the plasma membrane, it is arguably beneficial to accomplish phosphorylation prior to oxidation. Accordingly, many organisms that employ either an Entner-Doudoroff or an oxidative pentose phosphate pathway use hexokinase (or a phosphotransferase system) and glucose-6-phosphate dehydrogenase rather than a glucose dehydrogenase and gluconate kinase bypass. So why are there organisms that employ a glucose dehydrogenase / gluconate kinase bypass? A quick survey through literature reveals that glucose dehydrogenases are common in hyperthermoacidophilic archaea that employ a non- or semi-phosphorylating Entner-Doudoroff pathway (Selig *et al.*, 1997). These organisms have evolved a metabolism that skips generation of various phosphorylated intermediates. Due to different architectures of their plasma membranes and cell walls, loss of those compounds via diffusion into the exterior might be less likely than in bacteria or eukaryotic cells. What is more, it can be speculated that phosphorylated intermediates are more prone to spontaneous degradation at high temperatures or otherwise severe conditions that are faced by those hyperthermoacidophilic archaea. Other organisms that employ an Entner-Doudoroff pathway with a functional glucose dehydrogenase / gluconate kinase bypass are phosphate solubilizing bacteria such as *Pseudomonas* (Conway, 1992). These bacteria possess periplasmic glucose dehydrogenases,

which generate gluconate in the periplasm using membrane-bound quinones as redox mediators. Part of the generated gluconate willingly diffuses through the outer membrane into the exterior where it solubilizes phosphate containing minerals. The remaining gluconate is being imported through the plasma membrane and phosphorylated by a gluconate kinase to further enter the Entner-Doudoroff pathway (according to the scheme in fig. 38 A). Such a periplasmic glucose dehydrogenase has also been reported in some enterobacteria that possess an inducible Entner-Doudoroff pathway, for example *E. coli* (Peekhaus & Conway, 1998). It has been suggested that this enzyme is expressed to mediate periplasmic glucose oxidation in case extracellular glucose and quinones are present, which is a situation that is anticipated in phosphate-limited aquatic environments (Peekhaus & Conway, 1998). Except for archaea, NADP-dependent glucose dehydrogenases seem to be very scarce in nature. While such enzymes have been reported in *Gluconobacter* and *Acetobacter* species, its functionality under physiological conditions could not yet be shown (Pronk *et al.*, 1989; Attwood *et al.*, 1991). Interestingly, NADP-dependent glucose dehydrogenases have also been reported in cyanobacteria, more specifically, in the cyanobacterium *Nostoc* (Pulich & van Baalen, 1973). It has been suggested that this enzyme mediates glucose oxidation under chemoheterotrophic conditions, where phosphorylating power in form of ATP is scarce. According to the authors, the generated gluconate is not further metabolized, which would make NADPH the only relevant outcome of this reaction (Pulich & van Baalen, 1973). However, no further research on cyanobacterial glucose dehydrogenases has been published thereafter. A genome analysis of the cyanobacterium *Synechocystis* recently revealed the presence of two putative glucose dehydrogenases: sll1709 and slr1608. (Chen *et al.*, 2016). Due to its rossman fold, sll1709 was predicted to be NADP-dependent while slr1608, on the other hand, was predicted to be periplasmic and most likely quinone-dependent. Deletion of both genes caused a growth impairment under mixotrophic and chemoheterotrophic conditions (Chen *et al.*, 2016; Hildebrandt, own group, unpublished) which led to the conclusion that the enzyme might be important for glucose metabolism.

In the course of this dissertation, glucose dehydrogenase (GDH) and gluconate kinase (GK) activities were measured in crude cell extracts of *Synechocystis*. The results showed no GDH activity neither under photoautotrophic nor under mixotrophic conditions in extracts of WT, a glucose-6-phosphate dehydrogenase (G6PDH) deletion mutant (Δ*zwf*) as well as a GDH1 (sll1709) overexpression mutant when the electron acceptor $NADP^+$ was used (fig. 14 A). In a second study, different electron acceptors were used, namely NAD^+ as well as the quinones 2,3-dimethoxy-5-methyl-1,4-benzoquinone (DMB) and duroquinone (DQ). No GDH activity was detectable under any condition (fig. 14 B). However, a periplasmic quinone dependent GDH could potentially have been lost during the cell extract generation. Thus, according to these results, such an activity can not be excluded.

Activity of the second enzyme of the proposed GDH/GK bypass, namely gluconate kinase (GK), has also not been detectable in cell extracts (fig. 14 C). However, this result was less surprising since no

candidate gluconate kinase has been found in the genome of *Synechocystis* and, what is more, no gluconate kinase activity could be shown in any cyanobacterium yet.

In another analysis, the metabolites gluconate and KDPG were quantified in crude cell extracts of WT and a G6PDH deletion mutant (Δ*zwf*) (fig. 14 E). The presence of gluconate in WT and of KDPG in Δ*zwf* lead to the conclusion that a GDH/GK bypass might be operating (Chen *et al.*, 2016). However, an activity of the KDPG aldolase (EDA) in reverse direction could generate KDPG without involvement of either G6PDH or GDH. The ΔG_r' value of EDA under physiological conditions at 1 mM substrate and product concentrations is annotated as -4 kJ/mol, which implies a reversible reaction (Flamholz *et al.*, 2012). A quantification of KDPG in an Δ*eda*Δ*zwf* double deletion mutant in future studies would be necessary to prove this hypothesis. The occurrence of gluconate in WT is harder to explain without involvement of a GDH. One possible explanation could be a non-enzymatic degradation of 6-phosphogluconate during the metabolite quantification protocol. While an instability of 6-phosphogluconate has not been reported yet, another phosphorylated metabolite, namely fructose-1,6-bisphosphate, was shown to spontaneously dephosphorylate under conditions of high temperature and pH (Myung *et al*., 2010).

Another piece of evidence comes from quantification studies of the metabolite 6-phosphogluconate. It was shown that the observable 6-phosphogluconate accumulation in the Δ*eda*Δ*gnd* double deletion mutant could be prevented by additional deletion of Δ*zwf* both under photoautotrophic and mixotrophic growth conditions (fig. 14 D). This strongly suggests that glucose-6-phosphate dehydrogenase (ZWF) is the only metabolic route to generate-6-phosphogluconate and, thus, that no complete GDH/GK bypass is operating in *Synechocystis*.

Taken together, these results show that the existence of a complete GDH/GK bypass is very unlikely to exist in *Synechocystis*. However, it might still be possible that a GDH exists without involvement of a GK. The lack of detectable GDH activity in the enzyme activity measurements could be explained by a periplasmic quinone-dependent enzyme, which was lost during extract preparation. Such an enzyme could have the function to support the cell with additional reducing equivalents during chemoheterotrophic or mixotrophic conditions, similar as has been observed in the cyanobacterium *Nostoc*. A phosphate-solubilizing function of excreted gluconate, as it is observed in *Pseudomonas* or other phosphate-solubilizing bacteria, is unlikely, as *Synechocystis* is an aquatic cyanobacterium. In order to test whether a GDH without GK exists, further experiments, where extracellular gluconate concentrations are measured, would have to be conducted.

Finally, according to the results presented, it can be said that the Entner-Doudoroff pathway is very likely branching off the oxidative pentose phosphate pathway in *Synechocystis*. As a consequence, no GDH/GK bypass will be assumed in all further interpretations.

6.2 Physiological characterization of the KDPG aldolase deletion mutant *Δeda*

In order to elucidate the physiological role of the Entner-Doudoroff (ED) pathway in *Synechocystis*, growth behavior of a KDPG aldolase (Δ*eda*) deletion mutant was investigated under photoautotrophic, mixotrophic and chemoheterotrophic (LAHG) growth conditions prior to this dissertation. The results showed no growth phenotype under chemoheterotrophic (LAHG) and photoautotrophic conditions but an impaired growth under mixotrophic conditions (Chen *et al.*, 2016; Schreiber, 2016, unpublished). This led to the assumption that the ED pathway is important to mediate glucose catabolism during photosynthetic metabolism. As a continuation of these studies, various physiological parameters were determined in Δ*eda* under photoautotrophic and mixotrophic conditions during the course of this dissertation. The most prominent observable Δ*eda* phenotypes under continuous cultivation conditions were an impaired growth rate, an increased glycogen content and a reduced amount of photosynthetic pigments. Interestingly, these phenotypes were similarly present both under photoautotrophic and mixotrophic growth conditions, thus leading to the conclusion that the ED pathway is similarly important under both conditions. A physiological function of a glycolytic route during photoautotrophic conditions stands in contradiction to text book knowledge. A possible explanation for this has been proposed in the beginning of this dissertation in form of the glycolytic shunt model (chapter 2). However, the implications of the experimental results on the glycolytic shunt model will be discussed later (chapter 6.4). The following chapters will attempt a general assessment of the observable phenotypes of Δ*eda*.

6.2.1 Glycogen has an inflation effect on the OD

The increased glycogen contents, both under photoautotrophic and mixotrophic conditions, are among the strongest observable phenotypes of Δ*eda* (fig. 15 D and fig. 20 D). A plausible explanation for the increased glycogen contents is a redirection of carbon flux due to a blocking of the ED pathway. It can be argued that the redirection of carbon flux towards glycogen is the reason for the impaired growth of Δ*eda* since the redirected carbon can no longer be used for biomass synthesis. However, a correlation analysis between the OD and the carbon balance (as an equivalent of biomass) under mixotrophic conditions revealed that the cellular carbon balance correlated better with OD if the carbon that was stored as glycogen was also taken into account (fig. 18 E+F). This led to the conclusion that the cellular glycogen content has an influence on the measured OD. It follows, that the measured growth impairment of Δ*eda* (as it is measured by OD 750) could not have been due to a redirection of carbon flux towards glycogen but rather an impaired carbon uptake (glucose + CO_2). What is more, the actual growth rate of Δ*eda* is presumably even lower than OD measurements suggest, due to a masking effect of the increased glycogen content. In fact, this is not only true for growth rate measurements but for all physiologic parameters that were calibrated to the OD volume. The contribution of glycogen to

biomass (in terms of carbon) was on average 23.7 % in WT and 31.3 % in Δ*eda* under mixotrophic conditions and 2.3 % in WT and 6.2 % in Δ*eda* under photoautotrophic conditions (for calculations see chapter 5.4.2). Using these values, the relative contribution of non-glycogen biomass can be calculated, which were 76.3 % in WT and 68.7 % in Δ*eda* under mixotrophic and 97.7 % in WT and 93.8 % in Δ*eda* under photoautotrophic conditions. It follows, that the non-glycogen biomass (in terms of carbon) is 4 % higher in WT than in Δ*eda* under photoautotrophic and 11 % higher in WT than in Δ*eda* under mixotrophic conditions. If glycogen has the same influence on the measured OD than non-glycogen biomass, these numbers represent the correction factors to convert OD values to values that only represent non-glycogen biomass. A comparison between photoautotrophic and mixotrophic OD is especially problematic in this regard, since the relative difference between non-glycogen biomass is even higher between those conditions, namely 28 % between mixotrophically and photoautotrophically cultivated WT and 37 % between mixotrophically and photoautotrophically cultivated Δ*eda*. These calculations demonstrate that glycogen can have a significant inflation effect on the OD measurement, which not only affects the OD itself but also all parameters that are calibrated on OD. This effect can also be seen by the decline of OD in the experiment where glycogen is degraded during darkness (fig. 33 J). An inflation effect of glycogen on the OD can possibly also explain why cultures were not able to increase their growth rate when glycogen was degraded during light in comparison to normal autotrophic growth (fig. 32).

6.2.2 The Δ*eda* phenotype

As has already been pointed out in the previous chapter, it has been shown that the OD of mixotrophically growing cells correlated well with the cumulative sum of glucose and CO_2 uptake. This not only demonstrates that the observable growth impairment (as measured by OD) of Δ*eda* was not due to the increased redirection of carbon towards glycogen, it also discards an increased carbon loss in form of organic fermentation products or carbon overflow products (pyruvate or 2-oxoglutarate; Gründel et al., 2012) as the reason for the growth impairment of Δ*eda*. A comparison between CO_2 assimilation and glucose uptake rates of Δ*eda* under mixotrophic conditions furthermore indicated that the CO_2 assimilation was stronger impaired than the glucose uptake, thus suggesting that a reduced CO_2 assimilation was causing the growth phenotype of Δ*eda* under mixotrophic conditions. This is in line with the observation that the Δ*eda* phenotypes were also present under photoautotrophic conditions, where CO_2 assimilation constitutes the only method of carbon acquisition. From a general perspective, a reduced net CO_2 assimilation can be due to either a reduction of CO_2 assimilation or an increase of CO_2 decarboxylating processes. Unfortunately, the CO_2 assimilation rate measurements that were conducted during this dissertation did not allow a distinction between those two processes.

The decreased contents of the photosynthetic pigments chlorophyll *a* and phycocyanin were among the most prominent and constant phenotypes of Δ*eda*. It is plausible that a reduced amount of photosynthetic pigments goes hand in hand with a reduced photosynthetic yield of ATP and NADPH (Buttery & Buzzell, 1977). A reduced supply of ATP and NADPH, due to a reduced photosynthetic electron transport, could in turn lead to a reduced CO_2 fixation by the CBB cycle or an activation of respiration. In the same way, a reduced CO_2 fixation or an increased respiration could have lead to a down-regulation of the photosynthetic electron transport and thus a degradation of pigments. The known activators of glycogen synthesis in *Synechocystis* are 3-phosphoglycerate and thioredoxin (Gründel *et al*., 2012; Díaz-Troya *et al.*, 2014). If deletion of EDA lead to a reduced flux inside the CBB cycle, 3-phosphoglycerate concentrations might have risen, which could have lead to a stimulation of glycogen synthesis. The increased glycogen content might furthermore be connected to the reduced amount of photosynthetic pigments if the cells suffer stress due to an excess of electrons. Electron excess can lead to a down-regulation of photosynthesis as well as a stimulation of glycogen production via thioredoxin signaling (Díaz-Troya *et al.*, 2014). A similar phenotype has been shown during mixotrophic growth conditions where arginine was the sole nitrogen source (electron excess conditions) (Burgstaller 2017, unpublished; own preliminary results). As a consequence, a connection between the three Δ*eda* phenotypes of a reduced net CO_2 assimilation, a degradation of photosynthetic pigments and an increased glycogen content is very possible.

6.2.3 Comparison between phenotypes of Δ*eda* and Δ*zwf*

An interesting comparison can be made between the phenotypes of Δ*eda* and Δ*zwf*, the latter being a deletion mutant of the glucose-6-phosphate dehydrogenase. This enzyme constitutes the shared entry of the ED and the OPP pathway/shunt and as a consequence, deletion of this enzyme results in the blocking of both pathways. While Δ*zwf* also exhibited a slightly reduced growth under photoautotrophic conditions (fig. 27), interestingly, no increased glycogen contents were observable in Δ*zwf* (fig. 31). What is more, many of Δ*eda's* other phenotypes, such as a decreased glycogen degradation rate during light (fig. 33), reduced amounts of photosynthetic pigments (data not shown, preliminary result) as well as a reduced growth rate under mixotrophic conditions (Chen *et al.*, 2016) were also missing. A possible explanation for this is that the phenotypes of Δ*eda* were (at least to a great part) not due to a missing flux through the ED pathway but rather to secondary effects. Two plausible secondary effects that are caused by a blocked metabolic pathway are the accumulation of metabolites or a redirection of flux through an alternative pathway.

6.2.4 Metabolite accumulation

An accumulation of the metabolite 6-phosphogluconate (6PG) has been shown to occur in the Δ*eda*Δ*gnd* double deletion mutant (disruption of both ED and OPP pathway/shunt) (fig. 29). The measured cellular 6PG contents in Δ*eda*Δ*gnd* reached levels of up to 4 µg/OD*mL, which, to give a reference, roughly corresponds to the amount of glycogen in WT under photoautotrophic conditions. These high concentrations were made possible by the exergonic preceding reaction 6-phosphogluconolactonase (ΔG_r' of -21 KJ/mol at pH7 and 1 mM substrate and product concentration; Flamholz *et al.,* 2012). While such an accumulation is arguably unfavorable due to the carbon loss in form of the accumulated metabolite alone, additional secondary effects are very likely. Accordingly, it could be shown that 6PG has a strong inhibitory effect on glucose-6-phosphate dehydrogenase in mammals (Gaitonde *et al.*, 1989) and a proposed inhibitory effect on RubisCO in cyanobacteria (Codd & Stewart, 1977). An inhibitory effect of 6PG on RubisCO would provide explanation not only for the impaired growth under photoautotrophic conditions, but also for the inability of Δ*eda*Δ*gnd* to enhance its growth under elevated CO_2 concentrations (fig. 29). Interestingly, Δ*eda*Δ*gnd* was unable to grow and assimilate CO_2 under mixotrophic conditions, even though the cellular 6PG levels were not significantly higher than under photoautotrophic conditions (fig. 29; fig. 30). A lethal effect of glucose has been reported for other deletion mutants, for example for a mutant that is incapable of glycogen synthesis (Gründel *et al.*, 2012). If 6PG inhibits RubisCO, this suggests that glucose in combination with a (partially) inhibited CBB cycle is harmful. This can possibly be explained by a flooding of glucose into glycolytic and CBB metabolite pools that themselves accumulate and cause inhibitory effects, which finally shuts down carbon metabolism completely. An inhibitory effect of 6PG on PGI, as it has been described in mammals (Gaitonde *et al.*, 1989), can also not be excluded and should be investigated in future experiments.

The observable 6PG accumulation in Δ*eda*Δ*gnd* likely implies the accumulation of another metabolite, namely 2-keto-3-deoxy-6-phosphogluconate (KDPG). KDPG's position in metabolism lies between EDA and 6PG and since deletion of EDA is necessary for the KDPG accumulation to occur in Δ*eda*Δ*gnd* (since no 6PG accumulation was observable in Δ*gnd*), it can be reasoned that KDPG needs to accumulate first in order for 6PG accumulation to happen. In fact, due to the reaction equilibrium of the 6-phosphogluconate dehydratase (EDD), which strongly favors generation of KDPG (ΔG_r' of -43 KJ/mol at pH7 and 1 mM substrate and product concentration; Flamholz *et al.,* 2012), the putative accumulated amount of KDPG can be expected to even exceed the amount of accumulated 6PG in Δ*eda*Δ*gnd*.

The strongly exergonic nature of EDD makes an accumulation of KDPG also likely to occur in the Δ*eda* single mutant. In fact, it was shown in a KDPG aldolase deletion mutant of *E. coli* that KDPG not only accumulated but also led to an inhibition of growth (Fuhrmann *et al.,* 1998). However, the exact mechanism of inhibition could not be revealed yet. In *Pseudomonas*, who also employ an

Entner-Doudoroff pathway, it was shown that KDPG is an important regulatory molecule of central carbon metabolism (Campilongo *et al.*, 2017). Since the Δ*eda* phenotype in *Synechocystis* was only present during photoautotrophic and mixotrophic, but not during chemoheterotrophic conditions, it can be argued that if an inhibitory effect of KDPG occurs in *Synechocystis*, it either only comes to an accumulation of KDPG during light (due to a down-regulation of EDD during darkness), or the inhibitory effect is different from those observed in *E. coli* and *Pseudomonas,* The postulated inhibitory effect of KDPG in *Synechocystis* would thus likely either target photosynthetic metabolism or appear only in combination with photosynthetic metabolism. A stimulating effect of KDPG on glycogen synthesis is also plausible, since high metabolite concentrations indicate a carbon excess situation, which is known to stimulate glycogen synthesis (Gründel *et al.*, 2012). An inhibitory effect due to KDPG accumulation in Δ*eda* would be in agreement with the absence of phenotype in Δ*zwf*, where no KDPG formation should be possible. Further investigations are required in order to test this assumption.

The double deletion mutant Δ*eda*Δ*zwf* showed a growth rate that was even lower than Δ*eda's and* Δ*zwf's* under photoautotrophic conditions. This was surprising since deletion of ZWF already disrupts both the ED and the OPP pathway/shunt and an additional deletion of EDA was expected to have no effect. Unfortunately, Δ*eda*Δ*zwf* was not further characterized so it remains unclear whether Δ*eda's* other phenotypes, such as the increased glycogen content and reduced amount of photosynthetic pigments, were present in this mutant. This makes an explanation of the Δ*eda*Δ*zwf* phenotype rather difficult. A speculative explanation can be made on basis of the assumption that KDPG functions as a regulative molecule in *Synechocystis*. In the ZWF single deletion mutant, generation of KDPG could be achieved, from a thermodynamic point of view, due to a reverse activity of EDA, which is a bidirectional enzyme (ΔG_r' of -1.6 KJ/mol at pH7 and 1 mM substrate and product concentration; Flamholz *et al.*, 2012). Additional deletion of EDA hinders this ability and, accordingly, the Δ*eda*Δ*zwf* mutant should completely lack KDPG, which might, in low concentrations, be an activator for cellular processes. However, due to the lack of physiological characterization of Δ*eda*Δ*zwf*, this explanation remains rather speculative. What is more, a plotting of the growth rates of Δ*eda*Δ*zwf* against the date of experiment revealed that the growth phenotype weakened over time and reached similar levels of growth impairment at the end of this dissertation as the Δ*eda* and Δ*zwf* single mutants. This shows, that the additional harmful effect of the Δ*eda*Δ*zwf* mutant was overcome by evolution, which points to a regulatory problem. Further physiological characterization of the Δ*eda*Δ*zwf* mutant needs to be done in order to fully understand the observed growth phenotype.

6.2.5 Redirection of carbon flux

A redirection of carbon flux due to a disruption of a metabolic pathway is a common desired effect during biotechnological approaches. For example, a *Synechocystis* mutant that is impaired in the purine synthesis pathway was shown to exhibit increased ethanol production (Sengupta *et al.*, 2013). However, such a redirection of flux through an alternative pathway can also emerge as an unwanted side effect during the characterization of a deletion mutant, either by compensating for an actual harmful effect and thereby eliminating a potential phenotype or by causing a harmful effect itself and thereby producing the observable phenotype.

In Δ*eda*, a redirection of carbon flux through the OPP pathway/shunt can be presumed. This assumption is supported by the observation that 6PG accumulated in the Δ*eda*Δ*gnd* mutant but not in the Δ*eda* or Δ*gnd* single deletion mutants. However, to which extent the carbon flux is redirected through the OPP shunt and whether this is the reason for the Δ*eda* phenotype remains speculative. The OPP pathway/shunt is characterized by a decarboxylation and a concomitant NADPH reduction. An increased flux through the OPP pathway/shunt could thus have lead to an overly reduced NADPH pool, which could have caused a down-regulation of the photosynthetic electron transport, which in turn could have manifested itself in the observable degradation of photosynthetic pigments in Δ*eda*. Electron excess has also been shown to promote glycogen synthesis in *Synechocystis* via thioredoxin signaling (Cano *et al.*, 2018). The hypothesis that an increased flux through the OPP pathway/shunt generates electron stress is supported by the observation that the 6-phosphogluconate dehydrogenase deletion mutant Δ*gnd* (disruption of OPP pathway/shunt) exhibited a strongly increased growth rate in comparison to WT under mixotrophic growth conditions with arginine as the sole nitrogen source (high electron stress conditions) (Wollstadt, 2018, unpublished). However, whether an increased flux through the OPP shunt could also cause electron stress during photoautotrophic conditions remains questionable. The observation that the growth impairment of Δ*eda* seemed to decrease with increasing light intensities under photoautotrophic conditions is contradicting this hypothesis, since higher light intensities should result in more electron stress. The hypothesis would be, however, in line with the observable reduced net CO_2 assimilation in Δ*eda* under photoautotrophic conditions (due to the decarboxylation step) as well as the absence of phenotype in Δ*zwf*, where no such flux is possible.

6.2.6 Interaction with other proteins

A third possibility of a potential secondary effect as the reason for the Δ*eda* phenotype is an interaction of EDA with other proteins, i.e. a lack of such interaction in the Δ*eda* mutant. The missing interaction could have lead to an impaired activity of the interaction partner, which then could have resulted in the Δ*eda* phenotype. Plausible interaction partners are either neighboring enzymes (to form

metabolons; Sweetlove & Fernie., 2018) or otherwise functionally connected enzymes (to form regulatory networks like the CP12-PRK-GAPDH2 complex; Tamoi *et al*., 2005). The first enzyme of the methyl-erythritol-4-phosphate (MEP) pathway, 1-deoxy-xylulose-5-phosphate synthase (DXS), uses GAP and pyruvate as a substrate, which are identical with the products of the EDA reaction (Lindberg *et al.*, 2010). An interaction between EDA and DXS could thus facilitate and/or regulate flow into the MEP pathway. The MEP pathway is conducting the synthesis of isoprenoids, which are, among others, the precursors of carotinoids and chlorophyll (Lindberg *et al.*, 2010). An impaired flow into the MEP pathway could thus provide a good explanation for the observable decreased amount of chlorophyll in Δ*eda*. Other enzymes that might be connected to EDA are the glyceraldehyde-3-phosphate dehydrogenases (1 and 2) or other pyruvate-metabolizing enzymes.

6.2.7 Conclusion

As a conclusion of this chapter, it can be said that the Δ*eda* phenotype might, to a great part, not be due to a missing flux through the ED pathway/shunt but rather to secondary effects. These secondary effects could be a redirection of flux through alternative pathways (most likely the OPP pathway/shunt), an accumulation of metabolites (most likely KDPG) or an impaired interaction with other proteins. Further studies need to be done in order to reveal which secondary effects might occur in the Δ*eda* mutant. As a consequence of these secondary effects, an assessment of the importance of the ED pathway in *Synechocystis* is extremely difficult. Other mutants that might be useful for an evaluation of the ED pathway/shunt are Δ*zwf* and Δ*gnd* or, more specifically, the difference between the phenotypes of those two, since the Δ*zwf* mutant also blocks the OPP pathway/shunt. However, it has to be kept in mind that secondary effects might also occur in these mutants. Theoretically, these secondary effects could not only cause an overestimation of the importance of the deleted pathways, but also, and even more likely, an underestimation, since cells could be able to compensate the deletion, for example by a redirection of flux. Thus, even a lack of phenotype of Δ*zwf* or Δ*gnd* would not allow the conclusion that both ED and OPP pathway/shunt are unimportant, it would rather show that they are not essential under the respective conditions.

In order for (most) secondary effects to occur, at least a minimal flux through the respective pathway must have existed in the first place. It can thus be argued that the existence of secondary effect in the Δ*eda* mutant is an argument in favor of an operating ED pathway/shunt. The observable secondary effect of an accumulation of 6PG in the Δ*eda*Δ*gnd* double deletion mutant (fig. 29) together with the lack of accumulation in the Δ*eda* and Δ*gnd* single mutants, for example, is only explainable if at least a minimal flux through the ED pathway/shunt was occurring in the first place.

6.3 Phosphofructokinase and transaldolase

Phosphofructokinase (PFK), the key enzyme of the EMP pathway, was repeatedly shown to only have a minor activity in *Synechocystis* under chemoheterotrophic (LAHG) conditions and no substantial activity under mixotrophic conditions (Pelroy *et al.*, 1972; Knowles & Plaxton, 2003; Chen *et al.*, 2016). This is consistent with the results from this work, which showed no phenotype of the phosphofructokinase deletion mutant Δ*pfk* (both isoforms were deleted) under any tested condition (fig. 12; fig. 27; fig. 30; fig. 31; fig. 33; fig. 35). Under mixotrophic conditions, a flux through PFK would proceed in parallel to a flux through fructose-1,6-bisphosphatase (FBP). These two enzymes catalyze the same reaction in reverse direction, however, with the exception that one ATP is hydrolyzed in the PFK reaction but no ATP is generated in the FBP reaction. A simultaneous flux through both reactions would thus result in a futile ATP-dissipating cycle. Such a futile cycling around PFK is well-known (Katz & Rognstad, 1976) and has also been suggested to occur in *Synechocystis* (Yang *et al.*, 2002). Since cyanobacteria often face energy excess conditions during light when photosynthesis is operating, a futile cycle around PFK could help to release energy and furthermore fine tune the carbon metabolism with the light reaction of photosynthesis (Cano *et al*., 2018). Such a function of PFK in *Synechocystis* is arguably possible, since it was shown that both PFK isoforms of *Synechocystis* are non-allosteric, which means that they are not inhibited by ATP like the allosteric counterpart, which is the common type in eukaryotes (Knowles & Plaxton, 2003). A potential stimulation of PFK by ATP or an inhibition by orthophosphate could hypothetically occur in addition, in order to activate this enzyme in times of energy excess.

A second hypothetical function of PFK could occur if the subsequent reaction, fructose-1,6-bisphosphate aldolase (FBA), shows a net flux in catabolic direction. The resulting pathway would then resemble the first half of the EMP pathway. Under mixotrophic conditions, as well as under photoautotrophic conditions with a net glycogen degradation, this pathway could then function to funnel glucose into the CBB cycle in form of GAP and DHAP, similar as it has been hypothesized for the other three glycolytic shunts. The resulting hypothetical pathway can be termed the ‘EMP shunt’. Mixotrophic and photoautotrophic flux analyses have, without exception, shown a net flux direction of FBA in anabolic (CBB cycle) direction, which would make the EMP shunt impossible. However, all of these flux analyses assumed a steady-state. Especially under changing environmental conditions when the CBB cycle is completely devoid of triose-phosphates, a flux through the EMP shunt might be possible since GAP concentrations are so low that FBA does not show a net flux in anabolic direction. These are the same conditions where the ED shunt might be beneficial.

Transaldolase (TAL) is the only enzyme of the non-oxidative pentose phosphate pathway that is not shared with the CBB cycle. In the CBB cycle, the TAL reaction is bypassed by a combined activity of sedoheptulose-1,7-bisphosphate aldolase and sedoheptulose-1,7-bisphosphatase. In *Synechocystis*, both of these enzymes are bifunctional and secondarily catalyze the fructose-1,6-bisphosphate aldolase

and fructose-1,6-bisphosphatase reactions, respectively. Because of this, they are abbreviated as FBA and FBP (fig. 6). In comparison to TAL, the FBA/FBP variant utilizes one extra ATP and does thus have a higher metabolic driving force, which might be beneficial in stabilizing CBB flux. TAL is usually described as inactive during photoautotrophic conditions, both in cyanobacteria and chloroplasts (Sharkey & Weise, 2016). In plants, it was shown that TAL is (at least partially) inhibited by thioredoxin during light (Anderson, 1981). Interestingly, a flux through TAL has been reported in cyanobacteria under mixotrophic conditions. The observable flux roughly equaled the flux through the FBA/FBP variant (Yang *et al*., 2002; You *et al*., 2014; Nakajima *et al*., 2017). However, none of the authors provided any explanation for this observation. In the flux analysis that has been conducted during this dissertation, activity of TAL under mixotrophic conditions was confirmed (tab. 12).

A flux through TAL would arguably be especially advantageous in combination with the PGI shunt, since the PGI shunt produces fructose-6-phosphate (F6P), which is the substrate of TAL. If TAL is active, only 0.5 GAP are needed for each F6P that enters the regenerative phase of the CBB cycle. Without TAL, 2 GAP are needed for every F6P. By having an active TAL next to the default FBA/FBP variant, cells might increase metabolic flexibility during situations when glucose is funneled into the CBB cycle. This might be especially advantageous during changing environmental conditions.

6.4 Glycolytic shunt hypothesis

6.4.1 Glycolytic shunts under mixotrophic conditions

The central carbon metabolism under mixotrophic growth conditions is characterized by a degradation of glucose in the presence of a running CBB cycle. In the beginning of this dissertation, the presence of three glycolytic shunts has been suggested. The three shunts, namely the PGI shunt, the OPP shunt and the ED shunt, can provide routes to funnel glucose into the CBB cycle and thus function as an anaplerotic network. While, theoretically, the presence of the PGI and OPP shunt was already demonstrated by the flux data of various mixotrophic flux analyses in *Synechocystis* in the past 17 years, no such interpretation has been made (Yang *et al.*, 2002; You *et al.*, 2014; Nakajima *et al.*, 2014; Nakajima *et al.*, 2017; Ueda *et al.*, 2018). In order to provide further experimental evidence for the glycolytic shunt model and to measure the flux distribution through the three shunts under the mixotrophic cultivation conditions that were used in this work, another flux analysis was performed (chapter 5.5). For this, WT and various glycolytic deletion strains were fed with either ^{13}C1 or ^{13}C3 glucose and the labeling pattern of acetate was determined by NMR spectroscopy. The resulting labeling patterns of acetate in WT were identical with the predicted labeling patterns during PGI shunt usage (tab. 12). What is more, the Δ*pfk*Δ*zwf*Δ*gnd* triple deletion mutant, which was unable to use the

EMP, ED and OPP pathway as well as the ED and OPP shunt showed the same labeling pattern (tab. 12). This demonstrates that in the triple mutant, and very likely also in WT, the observable labeling pattern was indeed caused by a usage of the PGI shunt and not, for example, a combined usage of other pathways, such as the EMP plus the OPP pathway, which theoretically could also have resulted in the observable labeling pattern. As a consequence, it can be assumed that the PGI shunt is used to feed glucose into the CBB cycle in *Synechocystis* under mixotrophic conditions. While a major flux through the ED and OPP shunt can be disregarded due to the lack of the respective labeling in the WT, a small flux can not be excluded due to the resolution limitation of the experiment. The experimental results are generally in agreement with previously performed flux analyses, which showed the strongest flux from glucose to go through the PGI reactions towards fructose-6-phosphate under mixotrophic growth conditions (Yang *et al.*, 2002; Ueda *et al.*, 2018). However, while the authors reasoned the observable flux through PGI as a flux through the EMP pathway, the results presented here could show that fructose-6-phosphate is not further metabolized in the EMP pathway but rather enters the CBB cycle as an anaplerotic reaction. The observable unsubstantial flux through the OPP and ED shunt is in line with the results of the physiological characterization of the Δ*zwf* deletion mutant, which showed no phenotype under mixotrophic conditions (Chen *et al.*, 2016). However, the cultivation conditions that were used in this dissertation might have favored usage of the PGI shunt while the ED and OPP shunt might conduct higher fluxes at different mixotrophic cultivation conditions, for example at different light or CO_2 conditions.

The amount of flux through the three glycolytic shunts under mixotrophic conditions is presumably dependent on light intensity and CO_2 availability. Ueda *et al.* (2018) have shown that under low light conditions, glucose is primarily metabolized via the oxidative PP reactions (OPP shunt), whereas under high light conditions, glucose is mainly metabolized by PGI to yield fructose-6-phosphate (PGI shunt) (Ueda *et al.*, 2018). While the exact regulatory mechanism behind this partitioning is unknown, it is likely that glucose-6-phosphate dehydrogenase (ZWF) plays an important role in this regard. Pelroy *et al.* stated in 1972 that ribulose-1,5-bisphosphate causes a complete inhibition of ZWF during light conditions. However, it was later shown that ZWF remains active both under photoautotrophic and mixotrophic conditions (Takahashi *et al.*, 2008; Knowles & Plaxton, 2003). Today, it is believed that cyanobacterial ZWF activity is mostly redox regulated, either by a direct modification of thiol groups (Ueda *et al.*, 2018) or by NADPH inhibition (Preiser *et al.*, 2018). The cellular reduction level of cyanobacteria is more reduced under high light when photosynthesis is very active (carbon limiting conditions) than during low light and darkness (light limiting conditions), as has been shown via measurements of $NA(D)^+$ and NAD(P)H pools (Tamoi *et al.*, 2005). A dependency of ZWF activity on light/carbon availability thus seems very possible. Another candidate enzyme to be responsible for the regulation of glucose flux under mixotrophic conditions is PGI. While kinetic information on cyanobacterial PGI is scarce, the enzyme is much better described in plants. It was shown that PGI from the stroma of *Arabidopsis thaliana* and spinach leaves has a much higher K_M value for glucose-6-

phosphate than for fructose-6-phosphate (Preiser *et al.*, 2018; Schnarrenberger & Oeser, 1974). If this applies to cyanobacteria too, flux through the PGI shunt is arguably unfavored as long as ZWF is active.

The Entner-Doudoroff pathway has not been subject to any flux analysis in cyanobacteria yet, which means that there is no information available to support hypotheses about regulation of the ED shunt. Since the ED shunt branches off the OPP shunt, a regulation of ZWF activity arguably affects the ED shunt in the same way as the OPP shunt. This implies that the ED shunt is active under the same conditions as the OPP shunt, which is, according to the hypothesized regulatory mechanism, under light-limited mixotrophic conditions. However, it is possible that additional unknown regulatory mechanisms are occurring to allow a separate regulation of the ED and the OPP shunt. Potential targets for this are the second enzyme of the OPP shunt (GND) or the two enzymes of the ED shunt (EDD and EDA). It can be presumed that NADPH has an inhibitory effect on GND, similar as it has on ZWF. During elevated NADPH levels, a residual flux through ZWF might exist, which might then preferably enter the ED shunt, as GND activity is inhibited. Another possibility is that flux distribution through the ED and OPP shunt is feedback regulated by triose-phosphate concentrations and/or ribulose-5-phosphate concentration. Biomass producing reactions might cause cellular triose-phosphate concentrations to drop, which would impair autocatalysis of the CBB cycle. The ED shunt could fill up triose-phosphates by producing GAP. If triose-phosphate concentration is sufficiently high, the ED shunt would then be inhibited by feedback regulation. Ribulose-5-phosphate could cause a similar inhibition for the OPP shunt. Considering the aforementioned points, it is likely that the ED shunt and the OPP shunt function as antagonists, so that an increased flux through one shunt will decrease flux through the other. This idea is supported by the observation that 6-phosphogluconate accumulated in the Δ*eda*Δ*gnd* double deletion mutant but not in the Δ*eda* and Δ*gnd* single deletion mutants.

Taking a look at the ATP and NADPH yields of the three shunts might be helpful for further considerations of regulatory mechanisms. The calculations from chapter 5.9 revealed that each molecule of glucose that enters the CBB cycle via the OPP shunt instead of the PGI shunt results in a dissipation of 0.67 ATP and a gain of 1.67 NADPH (tab. 14 III). An increased flux through the OPP shunt, as it was hypothesized to occur under light-limited mixotrophic conditions, could thus result in an increased NADPH yield. These extra NADPH could be used to sustain non-CBB cycle biosynthetic reactions, for example fatty acid or chlorophyll synthesis. As has been mentioned earlier, the NADPH gain of the OPP shunt is due to the inherent decarboxylation step and a refixation of the decarboxylated CO_2 by RubisCO would diminish the additional NADPH yield. However, it can be presumed that a refixation of CO_2 is unlikely to occur during low light intensities, since cells are not CO_2 limited under this condition. The ED shunt was shown to have strong ATP dissipating properties, as each molecule of glucose that enters the CBB cycle via the ED shunt instead of the PGI shunt

results in a dissipation of 2 ATP. However, if the ED shunt is indeed functioning as an ATP dissipating mechanism, it is expected to be especially active under higher light intensities, which would challenge a hypothetical light-dependent down-regulation of ZWF.

As a summary of the previous, the following hypothetical explanation for the light dependency of glucose flux under mixotrophic conditions in cyanobacteria can be formulated: During darkness, the OPP pathway is operating. Due to the high cellular oxidation state, the redox-mediated molecule CP12 is oligomerized with the CBB cycle enzymes phosphoribulokinase (PRK) and glyceraldehyde-3-phosphate dehydrogenase (GAPDH), which results in an inhibition of their activity (Tamoi *et al.*, 2005). Upon illumination, the photosynthetic light reaction generates NADPH, which will reduce the cellular oxidation state and thus cause a dissipation of the CP12 complex and an activation of PRK and GAPDH2. The starting CO_2 fixation by RubisCO leads to a strong rise in the concentration of 3-phosphoglycerate, which will shift the reactions in the non-oxidative part of the PP pathway from a catabolic into an anabolic direction. Both ZWF and PGI are active, albeit the flux of glucose through ZWF is favored due to its exergonic nature (in combination with phosphogluconolactonase (PGL)) and the high K_M value of PGI for glucose-6-phosphate. Both the OPP and the ED are active under this condition. The OPP shunt generates extra NADPH, which helps to sustain biosynthetic reactions. The ED shunt presumably functions as a cross-valve in parallel to the OPP shunt and thereby controls flux through the OPP shunt and fine-tunes stoichiometry of the CBB cycle. With further increasing light intensities, ZWF activity is (partially) inhibited by rising NADPH levels and accumulating ribulose-1,5-bisphosphate. Reduction of ZWF activity causes glucose-6-phosphate concentrations to rise, which leads to an increased flux through the PGI shunt.

6.4.2 Glycolytic shunts funnel glycogen-derived glucose into the CBB cycle

As has been explained earlier (chapter 1.2.1), (uncompartmented) mixotrophic situations can also arise during photoautotrophic conditions, when glycogen (or starch in case of plants) is being degraded. A net glycogen degradation in cyanobacteria has been reported under various conditions, such as after awakening from dormancy (Doello *et al.*, 2018), after transfer from high light to low light (Liu *et al.*, 2013; Ueda *et al.*, 2018) or after transfer from high CO_2 to low CO_2 conditions (Eisenhut *et al.*, 2008). In this dissertation, another condition was found where glycogen was degraded during light: after transfer from mixotrophic to photoautotrophic growth conditions (fig. 32; fig. 33). The observable glycogen degradation rate during light was similarly fast as during darkness (fig. 33 F) and only slightly lower than the glucose uptake rate under mixotrophic conditions (fig. 17 G). What is more, the OPP shunt deletion mutants Δ*zwf* and Δ*gnd* exhibited the same glycogen degradation rate during light as the WT. These results strongly suggest that the glucose degradation mechanisms of glycogen-derived glucose and glucose that is taken up from the surrounding are identical. The addition of

glycogen-derived glucose to the CBB cycle arguably fulfills two purposes: 1. it can boost growth and return the glycogen levels back to normal, 2. it can fine-tune the CBB cycle during changing environmental conditions. While the first purpose is only relevant when excessive amounts of glycogen have been stored, the second purpose can also be achieved with normal photoautotrophic glycogen levels. In order to test the hypothesis that glycolytic shunts can funnel glycogen-derived glucose into the CBB cycle and thereby fine-tune the CBB cycle, an experiment was conducted where the electron flux into the CBB cycle was measured upon a darkness-light shift in various glycolytic deletion mutants. The results showed that not only deletion of Δ*eda*, but also of Δ*zwf* and Δ*gnd* lead to a delayed restart of the CBB cycle. As a consequence, a role of both the ED and the OPP shunt for an optimal restart of the CBB cycle can be deduced. However, it has been shown earlier that the Δ*eda* mutant presumably exhibits secondary effects that lead to the observable phenotypes under continuous cultivation conditions (see chapter 6.2). The same effects could also have lead to a delayed restart of the CBB cycle. Further characterization of secondary effects in Δ*eda* need to be done in order to exclude this.

The fact that the glycogen phosphorylase deletion mutant Δ*glgP*, which was incapable of glycogen degradation, exhibited a similarly impaired CBB restart as the glycolytic deletion mutants furthermore demonstrates that the glucose stem from the cellular glycogen pool and was not due to a cataplerotic flux out of the CBB cycle via a reverse PGI shunt. As a consequence of these results, it can be stated that S*ynechocystis* employs the OPP and likely also the ED shunt to mediate funneling of glycogen-derived glucose into the CBB cycle as a mean to facilitate restarting of the cycle.

The observable important role of the OPP shunt for an optimal restart of the CBB cycle seems surprising, considering that the OPP shunt was shown to not be essential under mixotrophic conditions as well as for glycogen degradation during light upon a shift from mixotrophic to photoautotrophic conditions. However, it does fit the hypothetical regulatory mechanism of shunt flux under mixotrophic conditions that has been postulated in the previous chapter. According to this model, flux through the PGI shunt could be constrained since glucose-6-phosphate concentrations are still too low in the first seconds upon initialization of glycogen degradation to enable a flux through PGI, which potentially has a high K_M value for glucose-6-phosphate. ZWF, on the other hand, should be very active due to the low cellular NADPH levels. A complete regeneration of ribulose-5-phosphate (Ru5P) via the OPP shunt is theoretically possible (fig. 36 G). Alternatively, a combination of PGI and ED shunt could also sustain regeneration of Ru5P by themselves (fig. 36 F).

In order to show that a flux of glucose into the CBB cycle can completely sustain regeneration of Ru5P, a glyceraldehyde-3-phosphate dehydrogenase 2 (CBB cycle isoform) deletion mutant (*Δgap2)* was tested for its mixotrophic growth capabilities. In agreement with previous results (Koksharova et al., 1998), Δ*gap2* was unable to grow under photoautotrophic conditions (fig. 26). Addition of glucose was able to rescue growth of Δ*gap2*, resulting in a growth rate that was lower than mixotrophically

grown WT but clearly exceeded chemoheterotrophic growth rates (fig. 26), thus showing that the observable growth behavior was not due to chemoheterotrophic metabolism. It can, however, not be excluded that heterotrophic metabolism was accomplished in combination with phototrophic metabolism, resulting in a photoheterotrophic metabolism, similar as it can be induced by addition of inhibitors of the photosynthetic electron chain, like DCMU or atrazine (Nakajima *et al.*, 2014). Addition of DCMU and glucose to photoautotrophically growing *Synechocystis* resulted in growth rates (data not shown) similar to what has been observed in the Δ*gap2* mutant upon addition of glucose. In order to test, whether Δ*gap2* exhibits mixotrophic or photoheterotrophic growth upon addition of glucose, CO_2 assimilation rates would have to be measured. If a CO_2 assimilation during light could be shown, this would indicate that the CBB cycle is active, which would prove the hypothesis that glucose can sustain regeneration of Ru5P in the CBB cycle by itself.

6.4.3 Glycolytic shunts under photoautotrophic conditions without glycogen participation

As has been mentioned previously, glycolytic shunts could also function under photoautotrophic conditions without involvement of glycogen. In this scenario, a cataplerotic flux out of the CBB cycle via PGI is required. Under this condition, only the OPP and the ED shunt could occur, since the PGI shunt is blocked by a flux through PGI in the reverse direction. In fact, a flux through the oxidative part of the pentose phosphate pathway under continuous photoautotrophic conditions has already been measured by various flux analyses (Young *et al.*, 2011; Knoop *et al.*, 2013; Nakajima *et al.*, 2017). The measured flux, which equaled to up to 13 % of fixed CO_2, was interpreted by the authors as either an incomplete suppression of OPP pathway flux (Young *et al.*, 2011) or as a ‘standby mode’ in anticipation of changing environmental conditions (Knoop *et al.*, 2013). A similar interpretation has been made by Sharkey & Weise, who suggested a flux through the oxidative part of the pentose phosphate pathway in plants and named it the ‘G6P shunt’ (Sharkey & Weise, 2016). They attributed a flux of 10-20 % of fixed CO_2 to the shunt and suggested that it functions as a futile cycle for ATP dissipation and furthermore refills the CBB cycle with triose phosphates (Sharkey & Weise, 2016). The flux analyses of *Synechocystis* showed that the flux through the OPP shunt was highest at low light intensities (Ueda *et al.*, 2018). This supports a hypothetical redox-mediated regulation of ZWF and implies that both the OPP and the ED shunt are especially important under low light intensities.

In the experiments that were conducted in this dissertation, the OPP shunt deletion mutant Δ*gnd* showed no growth impairment under continuous photoautotrophic cultivation conditions (fig. 27). This indicates that a flux through the OPP shunt is not essential under the cultivation conditions that were used during this dissertation. The ED shunt deletion mutant Δ*eda* did show a growth phenotype, however, as has been stated previously (chapter 6.2), the growth phenotype was likely due to secondary effects. The small observable growth impairment of the Δ*zwf* mutant, which is characterized

by a deletion of both the OPP and the ED shunt, indicates that a deletion of both shunts is slightly harmful (fig. 27). An experiment where the growth rates of WT and Δ*eda* were measured at different light intensities under photoautotrophic conditions showed that the growth impairment of Δ*eda* seemed to be stronger at low light than at high light (fig. 16). These results indicate a greater role of the ED shunt under low light and could also be considered as a support for the hypothetical down-regulation of ZWF at higher light intensities.

In order to acquire a tool to characterize the PGI shunt, the creation of a Δ*pgi* deletion mutant was attempted. Unfortunately, even several transformation attempts did not lead to a fully segregated mutant, which was demonstrated by the remaining PGI activity in the merodiploid mutants (fig. 25). The inability to delete glucose-6-phosphate isomerase (PGI) points to an essential role of this enzyme in *Synechocystis*. Segregation of the mutant was attempted during continuous photoautotrophic cultivation conditions. During these conditions, no flux through the PGI shunt is to be expected, as the main flux direction through PGI is supposedly anabolic to mediate either glycogen synthesis or a flux through the OPP or ED shunt. However, a lethal effect due to an inability to use the OPP/ED shunt can be excluded due to the ability of Δ*zwf* to grow (fig. 27) and, similarly, a lethal effect due to an inability to synthesize glycogen can also be excluded due to the ability of ADP-glucose pyrophosphorylase and glycogen synthase mutants to grow under photoautotrophic conditions (Gründel *et al.*, 2012; Cano *et al.*, 2018). As a consequence, the lethal effect of a deletion of PGI was most likely due to a missing regulatory function of PGI.

Calculations of the ATP and NADPH yields for usage of the ED and OPP shunt under photoautotrophic conditions without glycogen participation lead to the same results as under mixotrophic conditions, namely that both the OPP and especially the ED shunt can function as futile cycles for ATP dissipation (tab. 15). However, since ATP dissipation under low light conditions is not plausible since cells do not experience energy excess, ATP dissipation is presumably not the reason for glycolytic shunts to be used under this condition. The calculations furthermore showed that the OPP shunt can potentially be used to enable additional NADPH generation (tab. 15). As has been mentioned previously, the NADPH generation is caused by a decarboxylation and the cells could theoretically yield the same NADPH yield by simply reducing the amount of fixated carbon by RubisCO. However, this would reduce the flux rate in the CBB cycle. It can be hypothesized that a flux through the OPP shunt helps to maintain a higher flux rate in the CBB cycle, which might be beneficial during low light conditions when the CBB flux is relatively low.

Another interpretation for the importance of glycolytic shunts under photoautotrophic conditions without glycogen degradation can be made in regard to the suggestion made by Knoop *et al.* (2013), which was that a flux through the oxidative part of the oxidative pentose pathway is a ‘standby mode’ in anticipation of changing environmental conditions. The NADPH generation in the OPP shunt can be regulated much quicker than the NADPH generation in the photosynthetic electron transport. By

employing a constant flux through the OPP shunt, the cells thus have the option to both increase or decrease NADPH production on demand, by altering flux through the OPP shunt (tab. 15). In the same way, a constant small ATP dissipation by a flux through the ED shunt enables an alteration in both directions. A regulation of the flux through the OPP and ED shunt could thus constitute a mechanism to quickly alter the cellular NADPH and ATP pools and thereby improve synchronization with the photosynthetic light reaction. Theoretically, this only requires regulation of the activity of two enzymes of ZWF, GND or EDD/EDA. It is possible that the enzymes are directly regulated by NADPH and ATP concentrations in order to minimize response time. The OPP and ED shunts presumably occupy an antagonistic function, such that a decrease of flux through one shunt will lead to an increase of flux through the other. The cells can thus quickly regulate cellular NADPH and ATP levels just by altering the fluxes through the OPP and ED shunt.

6.4.4 The ED shunt can bypass the CBB cycle

It has been suggested earlier that the ED shunt can enable a cyclic process in combination with the gluconeogenetic part of the CB cycle and the PGI reaction (fig. 37 B). Interestingly, this combination of the CBB cycle with a cyclic ED shunt constitutes an alternative pyruvate generating mechanism that does not involve reactions of lower glycolysis. A similar mechanism has been observed in *Pseudomonas* species, who fuel a cyclic ED cycle with hexoses instead of CBB intermediates (Lessie & Phibbs, 1984). This constitutes a third way of pyruvate generation in *Synechocystis* next to the classical way employed by pyruvate dehydrogenase and a combination of phosphoenolpyruvate carboxylase (PEPC) and the malic enzyme (ME) (fig. 2). The three pathways differ in regard to their ATP yields: while classical pyruvate generation via PDH generates 2 ATP (one from the PDH reaction and one from the phosphoglycerate kinase reaction of lower glycolysis), pyruvate generation via the PEPC/ME bypass generates 1 ATP (from the phosphoglycerate kinase reaction of lower glycolysis) and the cyclic ED shunt generates no ATP at all (since it skips lower glycolysis completely). Having three different ways to synthesize pyruvate, thus, not only increases metabolic flexibility in regard to metabolite stoichiometry, but also in regard to the cellular energy level.

Pyruvate formation via a cyclic ED pathway/shunt could be especially relevant for plants that lack a plastidic phosphoglycerate mutase and enolase and can thus not accomplish lower glycolysis in their chloroplasts (Givan, 1999; Bar-Even, 2018). According to current knowledge, phosphoenolpyruvate and pyruvate needs of plastids are met by an import of phosphoenolpyruvate from the cytosol (Flügge *et al.*, 2011). A putative pyruvate generation via a cyclic ED pathway could provide an alternative method.

It is possible that the pyruvate that is generated by EDA is metabolically connected to another reaction via substrate channeling. Substrate channeling is commonly used to facilitate the regulation of metabolic pathways (Sweetlove & Fernie, 2018). However, substrate channeling has not been reported in cyanobacteria yet. As has been mentioned earlier (chapter 6.2.6), a connection between EDA and the first reaction of the MEP pathway would provide explanations for some of the observable secondary effects in the Δ*eda* mutant.

6.4.5 Conclusion

In summary, it can be said that the glycolytic shunt hypothesis could be experimentally confirmed. Experimental evidence was brought forward for the existence of all three glycolytic shunts. The results showed that glycolytic shunts can not only be used to funnel glucose into the CBB cycle under mixotrophic conditions, but also under photoautotrophic conditions when glycogen is degraded.

It was shown that the utilization of glycogen improves restarting the CBB cycle upon a darkness-light shift. The cellular glycogen pool can thus function as a metabolic buffer to improve flux in the CBB cycle upon demand, for example during changing environmental conditions.

By employing several shunts as an anaplerotic network around the CBB cycle, cells can arguably improve autocatalysis of the CBB cycle by controlling metabolite stoichiometry and compensating alterations that are made by draining biosynthetic reactions. Theoretical analyses have shown that usage of glycolytic shunts can furthermore influence cellular ATP and NADPH pools, which qualifies them as tools to improve synchronization with the photosynthetic light reaction. While the OPP shunt can be used as a means for quick NADPH generation, the ED shunt can constitute an ATP dissipating mechanism. An antagonistic function between the OPP and the ED shunt can furthermore be presumed.

Flux analyses suggest that even under continuous photoautotrophic conditions a background flux through the OPP (and ED) shunt occurs as a metabolic buffer in anticipation of environmental changes.

6.5 Outlook

It was shown that no glucose dehydrogenase/gluconate kinase bypass exists in *Synechocystis*. However, activity of a periplasmic glucose dehydrogenase that releases its product, gluconate, into the medium could not be excluded. In order to test for the existence of such an enzyme, extracellular gluconate concentrations could be measured. An overexpression and characterization of the candidate periplasmic glucose dehydrogenase (slr1608) might be worthwhile as well.

Further studies could also be made in order to identify secondary effects that could have lead to the observable phenotype of Δ*eda*. In order to test whether the Δ*eda* phenotype was due to an accumulation of KDPG, cellular KDPG concentrations could be measured in the Δ*eda* mutant as well as in the Δ*eda*Δ*gnd* double mutant. This could be done either enzymatically or via HPLC-MS. The Δ*eda*Δ*gnd*Δ*pfk*Δ*zwf* mutant could function as a control, since no KDPG accumulation can happen in this mutant. A putative inhibitory effect of KDPG on the activity of glycolytic key enzymes, such as Δ*zwf* or Δ*gnd*, could also be measured. In a similar study, the mechanism of an inhibitory effect of 6-phosphogluconate, which accumulated in Δ*eda*Δ*gnd*, could be further analyzed. Another secondary effect that could have caused the Δ*eda* phenotype was a redirection of flux through the OPP shunt. A suitable approach of investigation would be a metabolic flux analysis with HPLC-MS as the detection method. Whether the putative increased flux through the OPP shunt leads to electron stress can furthermore be investigated by measurements of the cellular NADPH/$NADP^+$ ratio.

An undistorted measurement of the flux through the glycolytic shunts can best be accomplished by metabolic flux analyses. This would constitute the first (published) flux analysis in *Synechocystis* that includes the ED pathway/shunt. All metabolic flux analyses that have been conducted in *Synechocystis* so far used continuous cultivation conditions. Since glycolytic shunts are presumably especially important during changing environmental conditions, a flux analysis during a noncontinuous cultivation, for example by alterations of light intensity, could be better suited to estimate the flux distributions through the glycolytic shunts. Another interesting approach would be a flux analysis that measures the labeling pattern upon degradation of a pre-labeled glycogen pool.

In order to complete the investigation whether addition of glucose can rescue mixotrophic growth of the Δ*gap2* deletion mutant, CO_2 assimilation rates could be measured in Δ*gap2* that is cultivated mixotrophically. This could prove that the observable growth type was indeed mixotrophic and not photoheterotrophic.

Finally, it might be worthwhile to investigate whether the experimental and theoretical results are also applicable to plastidic metabolism in plants.

7 References

Abed, R. M. M., Dobretsov, S. and Sudesh, K. (2009). "Applications of cyanobacteria in biotechnology." Journal of Applied Microbiology **106**(1): 1-12.

Alagesan, S., Gaudana, S. B., Sinha, A. and Wangikar, P. P. (2013). "Metabolic flux analysis of Cyanothece sp. ATCC 51142 under mixotrophic conditions." Photosynthesis Research **118**(1): 191-198.

Anderson, L. E. (1981). "Light inactivation of transaldolase in pea leaf chloroplasts." Biochemical and Biophysical Research Communications **99**(4): 1199-1202.

Anderson, S. L. and McIntosh, L. (1991). "Light-activated heterotrophic growth of the cyanobacterium Synechocystis sp strain PCC 6803 - a blue-light-requiring process." Journal of Bacteriology **173**(9): 2761-2767.

Antonovsky, N., Gleizer, S., Noor, E., Zohar, Y., Herz, E., Barenholz, U., Zelcbuch, L., Amram, S., Wides, A., Tepper, N., Davidi, D., Bar-On, Y., Bareia, T., Wernick, David G., Shani, I., Malitsky, S., Jona, G., Bar-Even, A. and Milo, R. (2016). "Sugar Synthesis from CO2 in Escherichia coli." Cell **166**(1): 115-125.

Asatsuma, S., Sawada, C., Itoh, K., Okito, M., Kitajima, A. and Mitsui, T. (2005). "Involvement of α-Amylase I-1 in Starch Degradation in Rice Chloroplasts." Plant and Cell Physiology **46**(6): 858-869.

Attwood, M. M., van Dijken, J. P. and Pronk, J. T. (1991). "Glucose metabolism and gluconic acid production by Acetobacter diazotrophicus." Journal of Fermentation and Bioengineering **72**(2): 101-105.

Bar-Even, A. (2018). "Daring metabolic designs for enhanced plant carbon fixation." Plant Science **273**: 71-83.

Bar-Even, A., Flamholz, A., Noor, E. and Milo, R. (2012 a). "Rethinking glycolysis: on the biochemical logic of metabolic pathways." Nature Chemical Biology **8**(6): 509-517.

Bar-Even, A., Flamholz, A., Noor, E. and Milo, R. (2012 b). "Thermodynamic constraints shape the structure of carbon fixation pathways." Biochimica et Biophysica Acta (BBA) - Bioenergetics **1817**(9): 1646-1659.

Bar-Even, A., Noor, E. and Milo, R. (2012 c). "A survey of carbon fixation pathways through a quantitative lens." Journal of Experimental Botany **63**(6): 2325-2342.

Belnap, J. (2003). "The world at your feet: desert biological soil crusts." Frontiers in Ecology and the Environment **1**(4): 181-189.

Bradford, M. M. (1976). "A rapid and sensitive method for the quantitation of microgram quantities of protein utilizing the principle of protein-dye binding." Analytical Biochemistry **72**(1-2): 248-254.

Buchanan, B. B. (1992). "Carbon dioxide assimilation in oxygenic and anoxygenic photosynthesis." Photosynthesis Research **33**(2): 147-162.

Buttery, B. and Buzzell, R. (1977). "The relationship between chlorophyll content and rate of photosynthesis in soybeans." Canadian Journal of Plant Science **57**(1): 1-5.

Campilongo, R., Fung, R. K., Little, R. H., Grenga, L., Trampari, E., Pepe, S., Chandra, G., Stevenson, C. E., Roncarati, D. and Malone, J. G. (2017). "One ligand, two regulators and three binding sites: How KDPG controls primary carbon metabolism in Pseudomonas." PLoS Genetics **13**(6): e1006839.

Cano, M., Holland, S. C., Artier, J., Burnap, R. L., Ghirardi, M., Morgan, J. A. and Yu, J. (2018). "Glycogen Synthesis and Metabolite Overflow Contribute to Energy Balancing in Cyanobacteria." Cell Reports **23**(3): 667-672.

Carrillo, N. and Ceccarelli, E. A. (2003). "Open questions in ferredoxin-NADP+ reductase catalytic mechanism." European Journal of Biochemistry **270**(9): 1900-1915.

Chen, X., Schreiber, K., Appel, J., Makowka, A., Fähnrich, B., Roettger, M., Hajirezaei, M. R., Sönnichsen, F. D., Schönheit, P., Martin, W. F. and Gutekunst, K. (2016). "The Entner–Doudoroff pathway is an overlooked glycolytic route in cyanobacteria and plants." Proceedings of the National Academy of Sciences **113**(19): 5441-5446.

Cheng, Y.-C. and Fleming, G. R. (2009). "Dynamics of Light Harvesting in Photosynthesis." Annual Review of Physical Chemistry **60**(1): 241-262.

Chojnacka, K. and Noworyta, A. (2004). "Evaluation of Spirulina sp. growth in photoautotrophic, heterotrophic and mixotrophic cultures." Enzyme and Microbial Technology **34**(5): 461-465.

Chomczynski, P. and Sacchi, N. (1987). "Single-step method of RNA isolation by acid guanidinium thiocyanate-phenol-chloroform extraction." Analytical Biochemistry **162**(1): 156-159.

Codd, G. A. and Stewart, W. D. P. (1977). "d-Ribulose 1,5-diphosphate carboxylase from the blue-green alga Aphanocapsa 6308." Archives of Microbiology **113**(1): 105-110.

Conway, T. (1992). "The Entner-Doudoroff pathway: history, physiology and molecular biology." Fems Microbiology Letters **103**(1): 1-28.

Cooley, J. W., Howitt, C. A. and Vermaas, W. F. J. (2000). "Succinate:Quinol Oxidoreductases in the Cyanobacterium Synechocystis sp. Strain PCC 6803: Presence and Function in Metabolism and Electron Transport." Journal of Bacteriology **182**(3): 714-722.

Cottrell, M. T. and Kirchman, D. L. (2009). "Photoheterotrophic Microbes in the Arctic Ocean in Summer and Winter." Applied and Environmental Microbiology **75**(15): 4958-4966.

De Los Ríos, A., Wierzchos, J. and Ascaso, C. (2014). "The lithic microbial ecosystems of Antarctica's McMurdo Dry Valleys." Antarctic Science **26**(5): 459-477.

Debnam, P. M., Shearer, G., Blackwood, L. and Kohl, D. H. (1997). "Evidence for channeling of intermediates in the oxidative pentose phosphate pathway by soybean and pea nodule extracts, yeast extracts, and purified yeast enzymes." European Journal of Biochemistry **246**(2): 283-290.

Díaz-Troya, S., López-Maury, L., Sánchez-Riego, A. M., Roldán, M. and Florencio, F. J. (2014). "Redox Regulation of Glycogen Biosynthesis in the Cyanobacterium Synechocystis sp. PCC 6803: Analysis of the AGP and Glycogen Synthases." Molecular Plant **7**(1): 87-100.

Doello, S., Klotz, A., Makowka, A., Gutekunst, K. and Forchhammer, K. (2018). "A Specific Glycogen Mobilization Strategy Enables Rapid Awakening of Dormant Cyanobacteria from Chlorosis." Plant Physiology **177**(2): 594-603.

Duhamel, S., Björkman, K. M. and Karl, D. M. (2012). "Light dependence of phosphorus uptake by microorganisms in the subtropical North and South Pacific Ocean." Aquatic Microbial Ecology **67**(3): 225-238.

Duhamel, S., Van Wambeke, F., Lefevre, D., Benavides, M. and Bonnet, S. (2018). "Mixotrophic metabolism by natural communities of unicellular cyanobacteria in the western tropical South Pacific Ocean." Environmental Microbiology **20**(8): 2743-2756.

Eiler, A. (2006). "Evidence for the ubiquity of mixotrophic bacteria in the upper ocean: implications and consequences." Applied and Environmental Microbiology **72**(12): 7431-7437.

Eisenhut, M., Huege, J., Schwarz, D., Bauwe, H., Kopka, J. and Hagemann, M. (2008). "Metabolome Phenotyping of Inorganic Carbon Limitation in Cells of the Wild Type and Photorespiratory Mutants of the Cyanobacterium Synechocystis sp. Strain PCC 6803." Plant Physiology **148**(4): 2109-2120.

Eitner, J. and Augustin, J. (2017). "Algae survive heat, cold and cosmic radiation." Fraunhofer Research News (2017): p. 1-4.

Fabris, M., Matthijs, M., Rombauts, S., Vyverman, W., Goossens, A. and Baart, G. J. E. (2012). "The metabolic blueprint of Phaeodactylum tricornutum reveals a eukaryotic Entner–Doudoroff glycolytic pathway." The Plant Journal **70**(6): 1004-1014.

Fernie, A. R., Zhang, Y. and Sweetlove, L. J. (2018). "Passing the Baton: Substrate Channelling in Respiratory Metabolism." Research **2018**: 16.

Flamholz, A., Noor, E., Bar-Even, A., Liebermeister, W. and Milo, R. (2013). "Glycolytic strategy as a tradeoff between energy yield and protein cost." Proceedings of the National Academy of Sciences **110**(24): 10039-10044.

Flamholz, A., Noor, E., Bar-Even, A. and Milo, R. (2012). "eQuilibrator-the biochemical thermodynamics calculator." Nucleic Acids Research **40**(Database issue): D770-D775.

Flügge, U.-I., Häusler, R. E., Ludewig, F. and Gierth, M. (2011). "The role of transporters in supplying energy to plant plastids." Journal of Experimental Botany **62**(7): 2381-2392.

Francisco, É. C., Franco, T. T., Wagner, R. and Jacob-Lopes, E. (2014). "Assessment of different carbohydrates as exogenous carbon source in cultivation of cyanobacteria." Bioprocess and Biosystems Engineering **37**(8): 1497-1505.

Fuhrman, L. K., Wanken, A., Nickerson, K. W. and Conway, T. (1998). "Rapid accumulation of intracellular 2-keto-3-deoxy-6-phosphogluconate in an Entner-Doudoroff aldolase mutant results in bacteriostasis." Fems Microbiology Letters **159**(2): 261-266.

Gaitonde, M. K., Murray, E. and Cunningham, V. J. (1989). "Effect of 6-Phosphogluconate on Phosphoglucose Isomerase in Rat Brain In Vitro and In Vivo." Journal of Neurochemistry **52**(5): 1348-1352.

Gibson, D. G., Young, L., Chuang, R.-Y., Venter, J. C., Hutchison III, C. A. and Smith, H. O. (2009). "Enzymatic assembly of DNA molecules up to several hundred kilobases." Nature Methods **6**(5): 343.

Givan, C. V. (1999). "Evolving concepts in plant glycolysis: two centuries of progress." Biological Reviews **74**(3): 277-309.

Gottschalk, G. (2012). “Bacterial Metabolism”, Springer Science & Business Media.

Graham, J. W., Williams, T. C., Morgan, M., Fernie, A. R., Ratcliffe, R. G. and Sweetlove, L. J. (2007). "Glycolytic enzymes associate dynamically with mitochondria in response to respiratory demand and support substrate channeling." The Plant Cell **19**(11): 3723-3738.

Grigorieva, G. and Shestakov, S. (1982). "Transformation in the cyanobacterium Synechocystis sp. 6803." Fems Microbiology Letters **13**(4): 367-370.

Grossman, A. R., Schaefer, M. R., Chiang, G. G. and Collier, J. L. (1993). "The phycobilisome, a light-harvesting complex responsive to environmental conditions." Microbiological Reviews **57**(3): 725-749.

Gründel, M., Scheunemann, R., Lockau, W. and Zilliges, Y. (2012). "Impaired glycogen synthesis causes metabolic overflow reactions and affects stress responses in the cyanobacterium Synechocystis sp. PCC 6803." Microbiology **158**(Pt 12): 3032-3043.

Gutekunst, K. (2018). "Hypothesis on the Synchronistic Evolution of Autotrophy and Heterotrophy." Trends in Biochemical Sciences **43**(6): 402-411.

Ikeuchi. M. and Tabata, S. (2001). "Synechocystis sp. PCC 6803—a useful tool in the study of the genetics of cyanobacteria." Photosynthesis Research **70**(1): 73-83

Juniper, B. E., Robins, R. J., Joel, D. M. (1989). "The carnivorous plants." London, UK: Academic Press

Kämäräinen, J., Huokko, T., Kreula, S., Jones, P. R., Aro, E. M. and Kallio, P. (2017). "Pyridine nucleotide transhydrogenase PntAB is essential for optimal growth and photosynthetic integrity under low-light mixotrophic conditions in Synechocystis sp. PCC 6803." New Phytologist **214**(1): 194-204.

Kaneko, T., Sato, S., Kotani, H., Tanaka, A., Asamizu, E., Nakamura, Y., Miyajima, N., Hirosawa, M., Sugiura, M., Sasamoto, S., Kimura, T., Hosouchi, T., Matsuno, A., Muraki, A., Nakazaki, N., Naruo, K., Okumura, S., Shimpo, S., Takeuchi, C., Wada, T., Watanabe, A., Yamada, M., Yasuda, M. and Tabata, S. (1996). "Sequence Analysis of the Genome of the Unicellular Cyanobacterium Synechocystis sp. Strain PCC6803. II. Sequence Determination of the Entire Genome and Assignment of Potential Protein-coding Regions." DNA Research **3**(3): 109-136.

Katz, J. and Rognstad, R. (1976). Futile Cycles in the Metabolism of Glucose. Current Topics in Cellular Regulation. B. L. Horecker and E. R. Stadtman, Academic Press. **10:** 237-289.

Klotz, A., Georg, J., Bučinská, L., Watanabe, S., Reimann, V., Januszewski, W., Sobotka, R., Jendrossek, D., Hess, Wolfgang, R. and Forchhammer, K. (2016). "Awakening of a Dormant Cyanobacterium from Nitrogen Chlorosis Reveals a Genetically Determined Program." Current Biology **26**(21): 2862-2872.

Knoop, H., Grundel, M., Zilliges, Y., Lehmann, R., Hoffmann, S., Lockau, W. and Steuer, R. (2013). "Flux Balance Analysis of Cyanobacterial Metabolism: The Metabolic Network of Synechocystis sp PCC 6803." Plos Computational Biology **9**(6).

Knoop, H., Zilliges, Y., Lockau, W. and Steuer, R. (2010). "The Metabolic Network of Synechocystis sp. PCC 6803: Systemic Properties of Autotrophic Growth." Plant Physiology **154**(1): 410-422.

Knoot, C. J., Ungerer, J., Wangikar, P. P. and Pakrasi, H. B. (2018). "Cyanobacteria: promising biocatalysts for sustainable chemical production." Journal of Biological Chemistry **293**(14): 5044-5052.

Knowles, V. L. and Plaxton, W. C. (2003). "From genome to enzyme: Analysis of key glycolytic and oxidative pentose-phosphate pathway enzymes in the cyanobacterium Synechocystis sp PCC 6803." Plant and Cell Physiology **44**(7): 758-763.

Koksharova, O., Schubert, M., Shestakov, S. and Cerff, R. (1998). "Genetic and biochemical evidence for distinct key functions of two highly divergent GAPDH genes in catabolic and anabolic carbon flow of the cyanobacterium Synechocystis sp. PCC 6803." Plant Molecular Biology **36**(1): 183-194.

Kresge, N., Simoni, R. D. and Hill, R. L. (2005). "Otto Fritz Meyerhof and the elucidation of the glycolytic pathway." Journal of Biological Chemistry **280**(4): e3-e3.

Kruger, N., Bulpin, P. and Ap Rees, T. (1983). "The extent of starch degradation in the light in pea leaves." Planta **157**(3): 271-273.

Kruger, N. J. and von Schaewen, A. (2003). "The oxidative pentose phosphate pathway: structure and organisation." Current Opinion in Plant Biology **6**(3): 236-246.

Kulasooriya, S. (2011). "Cyanobacteria: pioneers of planet earth." Ceylon Journal of Science (Bio. Sci.) **40**(2): 71-88.

Labarre, J., Thuriaux, P. and Chauvat, F. (1987). "Genetic analysis of amino acid transport in the facultatively heterotrophic cyanobacterium Synechocystis sp. strain 6803." Journal of Bacteriology **169**(10): 4668-4673.

Lessie, T. and Phibbs Jr, P. (1984). "Alternative pathways of carbohydrate utilization in pseudomonads." Annual Reviews in Microbiology **38**(1): 359-388.

Li, Y.-R., Tsai, W.-T., Hsu, Y.-C., Xie, M.-Z. and Chen, J.-J. (2014). "Comparison of Autotrophic and Mixotrophic Cultivation of Green Microalgal for Biodiesel Production." Energy Procedia **52**: 371-376.

Liang, Y., Sarkany, N. and Cui, Y. (2009). "Biomass and lipid productivities of Chlorella vulgaris under autotrophic, heterotrophic and mixotrophic growth conditions." Biotechnology Letters **31**(7): 1043-1049.

Lichtenthaler, H. K. (1987). Chlorophylls and carotenoids: pigments of photosynthetic biomembranes. Methods in Enzymology, Elsevier. **148:** 350-382.

Lindberg, P., Park, S. and Melis, A. (2010). "Engineering a platform for photosynthetic isoprene production in cyanobacteria, using Synechocystis as the model organism." Metabolic Engineering **12**(1): 70-79.

Liu, L., Hu, H., Gao, H. and Xu, X. (2013). "Role of two phosphohexomutase genes in glycogen synthesis in Synechocystis sp. PCC6803." Chinese Science Bulletin **58**(36): 4616-4621.

López-Calcagno, P. E., Howard, T. P. and Raines, C. A. (2014). "The CP12 protein family: a thioredoxin-mediated metabolic switch?" Frontiers in Plant Science **5**: 9.

Lopo, M., Montagud, A., Navarro, E., Cunha, I., Zille, A., de Córdoba, P. F., Moradas-Ferreira, P., Tamagnini, P. and Urchueguía, J. F. (2012). "Experimental and Modeling Analysis of Synechocystis sp. PCC 6803 Growth." Journal of Molecular Microbiology and Biotechnology **22**(2): 71-82.

Madigan, M. T., Martinko, J. M. and Parker, J. (1997). “Brock Biology of Microorganisms”, Prentice hall, Upper Saddle River, New Jersey.

Michelou, V. K., Cottrell, M. T. and Kirchman, D. L. (2007). "Light-Stimulated Bacterial Production and Amino Acid Assimilation by Cyanobacteria and Other Microbes in the North Atlantic Ocean." Applied and Environmental Microbiology **73**(17): 5539-5546.

Moore, L. R. (2013). "More mixotrophy in the marine microbial mix." Proceedings of the National Academy of Sciences **110**(21): 8323-8324.

Moriyama, T., Tajima, N., Sekine, K. and Sato, N. (2015). "Characterization of three putative xylulose 5-phosphate/fructose 6-phosphate phosphoketolases in the cyanobacterium Anabaena sp. PCC 7120." Bioscience, Biotechnology, and Biochemistry **79**(5): 767-774.

Mullineaux, C. W. (2014). "Co-existence of photosynthetic and respiratory activities in cyanobacterial thylakoid membranes." Biochimica et Biophysica Acta (BBA) - Bioenergetics **1837**(4): 503-511.

Mullineaux, C. W. and Emlyn-Jones, D. (2004). "State transitions: an example of acclimation to low-light stress." Journal of Experimental Botany **56**(411): 389-393.

Mullis, K., Faloona, F., Scharf, S., Saiki, R., Horn, G. and Erlich, H. (1986). “Specific enzymatic amplification of DNA in vitro: the polymerase chain reaction”. Cold Spring Harbor Symposia on Quantitative Biology **51**(1)**:** 263-273,

Munoz-Marin M. DC., Luque, I., Zubkov, M. V., Hill, P. G., Diez, J. and Garcia-Fernandez, J. M. (2013). "Prochlorococcus can use the Pro1404 transporter to take up glucose at nanomolar concentrations in the Atlantic Ocean." Proceedings of the National Academy of Sciences **110**(21): 8597-8602.

Myung, S., Wang, Y. and Zhang, Y.-H. P. (2010). "Fructose-1, 6-bisphosphatase from a hyper-thermophilic bacterium Thermotoga maritima: Characterization, metabolite stability, and its implications." Process Biochemistry **45**(12): 1882-1887.

Nakajima, T., Kajihata, S., Yoshikawa, K., Matsuda, F., Furusawa, C., Hirasawa, T. and Shimizu, H. (2014). "Integrated Metabolic Flux and Omics Analysis of Synechocystis sp. PCC 6803 under Mixotrophic and Photoheterotrophic Conditions." Plant and Cell Physiology **55**(9): 1605-1612.

Nakajima, T., Yoshikawa, K., Toya, Y., Matsuda, F. and Shimizu, H. (2017). "Metabolic Flux Analysis of the Synechocystis sp. PCC 6803 ΔnrtABCD Mutant Reveals a Mechanism for Metabolic Adaptation to Nitrogen-Limited Conditions." Plant and Cell Physiology **58**(3): 537-545.

Neuhaus, H. E. and Schulte, N. (1996). "Starch degradation in chloroplasts isolated from C3 or CAM (crassulacean acid metabolism)-induced Mesembryanthemum crystallinum L." Biochemical Journal **318**(3): 945-953.

Nogales, J., Gudmundsson, S., Knight, E. M., Palsson, B. O. and Thiele, I. (2012). "Detailing the optimality of photosynthesis in cyanobacteria through systems biology analysis." Proceedings of the National Academy of Sciences **109**(7): 2678-2683.

Nomura, T., Kono, Y. and Akazawa, T. (1969). "Enzymic mechanism of starch breakdown in germinating rice seeds II. Scutellum as the site of sucrose synthesis." Plant Physiology **44**(5): 765-769.

Novick, A. (1955). "Growth of bacteria." Annual Reviews in Microbiology **9**(1): 97-110.

Partensky, F., Hess, W. R. and Vaulot, D. (1999). "Prochlorococcus, a Marine Photosynthetic Prokaryote of Global Significance." Microbiology and Molecular Biology Reviews **63**(1): 106-127.

Peekhaus, N. and Conway, T. (1998). "What's for dinner?: Entner-Doudoroff metabolism in Escherichia coli." Journal of Bacteriology **180**(14): 3495-3502.

Pelroy, R. A., Stanier, R. Y. and Rippka, R. (1972). "Metabolism of glucose by unicellular blue-green-algae." Archiv Für Mikrobiologie **87**(4): 303-&.

Peltier, G., Aro, E.-M. and Shikanai, T. (2016). "NDH-1 and NDH-2 Plastoquinone Reductases in Oxygenic Photosynthesis." Annual Review of Plant Biology **67**(1): 55-80.

Plotkin, M., Hod, I., Zaban, A., Boden, S. A., Bagnall, D. M., Galushko, D. and Bergman, D. J. (2010). "Solar energy harvesting in the epicuticle of the oriental hornet (Vespa orientalis)." Naturwissenschaften **97**(12): 1067-1076.

Preiser, A. L., Banerjee, A., Fisher, N. and Sharkey, T. D. (2018). "Supply and consumption of glucose 6-phosphate in the chloroplast stroma." bioRxiv: 442434.

Price, G. D., Badger, M. R., Woodger, F. J. and Long, B. M. (2007). "Advances in understanding the cyanobacterial CO2-concentrating-mechanism (CCM): functional components, Ci transporters, diversity, genetic regulation and prospects for engineering into plants." Journal of Experimental Botany **59**(7): 1441-1461.

Pronk, J. T., Levering, P. R., Olijve, W. and van Dijken, J. P. (1989). "Role of NADP-dependent and quinoprotein glucose dehydrogenases in gluconic acid production by Gluconobacter oxydans." Enzyme and Microbial Technology **11**(3): 160-164.

Pulich, W. M. and Van Baalen, C. (1973). "Pyridine nucleotide-dependent glucose dehydrogenase activity in blue-green algae." Journal of Bacteriology **114**(1): 28-33.

Quick, W. P., Scheibe, R. and Neuhaus, H. E. (1995). "Induction of Hexose-Phosphate Translocator Activity in Spinach Chloroplasts." Plant Physiology **109**(1): 113-121.

Sambrook, J. and Russell, D. W. (2001). Molecular cloning: a laboratory manual (3-volume set), Cold spring harbor laboratory press New York.

Sanger, F., Nicklen, S. and Coulson, A. R. (1977). "DNA sequencing with chain-terminating inhibitors." Proceedings of the National Academy of Sciences **74**(12): 5463-5467.

Schirrmeister, B. E., Gugger, M. and Donoghue, P. C. J. (2015). "Cyanobacteria and the Great Oxidation Event: evidence from genes and fossils." Palaeontology **58**(5): 769-785.

Schlegel, H. G. (2007). "Allgemeine Mikrobiologie", Georg Thieme Verlag.

Schlesinger, W. H. and Bernhardt, E. S. (2013). “Biogeochemistry: an analysis of global change”, Academic Press

Schmidt, S., Raven, J. A. and Paungfoo-Lonhienne, C. (2013). "The mixotrophic nature of photosynthetic plants." Functional Plant Biology **40**(5): 425-438.

Schnarrenberger, C. and Oeser, A. (1974). "Two isoenzymes of glucosephosphate isomerase from spinach leaves and their intracellular compartmentation." European Journal of Biochemistry **45**(1): 77-82.

Schuller, J. M., Birrell, J. A., Tanaka, H., Konuma, T., Wulfhorst, H., Cox, N., Schuller, S. K., Thiemann, J., Lubitz, W., Sétif, P., Ikegami, T., Engel, B. D., Kurisu, G. and Nowaczyk, M. M. (2019). "Structural

adaptations of photosynthetic complex I enable ferredoxin-dependent electron transfer." Science **363**(6424): 257-260.

Selig, M., Xavier, K. B., Santos, H. and Schönheit, P. (1997). "Comparative analysis of Embden-Meyerhof and Entner-Doudoroff glycolytic pathways in hyperthermophilic archaea and the bacterium Thermotoga." Archives of Microbiology **167**(4): 217-232.

Selosse, M.-A. and Roy, M. (2009). "Green plants that feed on fungi: facts and questions about mixotrophy." Trends in Plant Science **14**(2): 64-70.

Sengupta, T., Bhushan, M. and Wangikar, P. P. (2013). "Metabolic modeling for multi-objective optimization of ethanol production in a Synechocystis mutant." Photosynthesis Research **118**(1-2): 155-165.

Sharkey, T. D. and Weise, S. E. (2016). "The glucose 6-phosphate shunt around the Calvin–Benson cycle." Journal of Experimental Botany **67**(14): 4067-4077.

Shen, G., Boussiba, S. and Vermaas, W. (1993). "Synechocystis sp PCC 6803 strains lacking photosystem I and phycobilisome function." The Plant Cell **5**(12): 1853-1863.

Shih, P. M. (2015). "Photosynthesis and early Earth." Current Biology **25**(19): R855-R859.

Shih, P. M. and Matzke, N. J. (2013). "Primary endosymbiosis events date to the later Proterozoic with cross-calibrated phylogenetic dating of duplicated ATPase proteins." Proceedings of the National Academy of Sciences **110**(30): 12355-12360.

Stal, L. J. and Moezelaar, R. (1997). "Fermentation in cyanobacteria." Fems Microbiology Reviews **21**(2): 179-211

Stanier, R. Y., Kunisawa, R., Mandel, M. and Cohen-Bazire, G. (1971). "Purification and properties of unicellular blue-green algae (order Chroococcales)." Bacteriological Reviews **35**(2): 171-205.

Stitt, M. and Heldt, H. W. (1981). "Simultaneous synthesis and degradation of starch in spinach chloroplasts in the light." Biochimica et Biophysica Acta (BBA) - Bioenergetics **638**(1): 1-11.

Stitt, M. and Zeeman, S. C. (2012). "Starch turnover: pathways, regulation and role in growth." Current Opinion in Plant Biology **15**(3): 282-292.

Strunecky, O., Kopejtka, K., Goecke, F., Tomasch, J., Lukavsky, J., Neori, A., Kahl, S., Pieper, D. H., Pilarski, P., Kaftan, D. and Koblizek, M. (2019). "High diversity of thermophilic cyanobacteria in Rupite hot spring identified by microscopy, cultivation, single-cell PCR and amplicon sequencing." Extremophiles **23**(1): 35-48.

Sweetlove, L. J. and Fernie, A. R. (2018). "The role of dynamic enzyme assemblies and substrate channelling in metabolic regulation." Nature Communications **9**(1): 2136.

Takahashi, H., Uchimiya, H. and Hihara, Y. (2008). "Difference in metabolite levels between photoautotrophic and photomixotrophic cultures of Synechocystis sp. PCC 6803 examined by capillary electrophoresis electrospray ionization mass spectrometry." Journal of Experimental Botany **59**(11): 3009-3018.

Tamoi, M., Miyazaki, T., Fukamizo, T. and Shigeoka, S. (2005). "The Calvin cycle in cyanobacteria is regulated by CP12 via the NAD(H)/NADP(H) ratio under light/dark conditions." The Plant Journal **42**(4): 504-513.

Ueda, K., Nakajima, T., Yoshikawa, K., Toya, Y., Matsuda, F. and Shimizu, H. (2018). "Metabolic flux of the oxidative pentose phosphate pathway under low light conditions in Synechocystis sp. PCC 6803." Journal of Bioscience and Bioengineering **126**(1): 38-43.

Valmalette, J. C., Dombrovsky, A., Brat, P., Mertz, C., Capovilla, M. and Robichon, A. (2012). "Light-induced electron transfer and ATP synthesis in a carotene synthesizing insect." Scientific Reports **2**: 579.

Vermaas, W. F. J. (2001). “Photosynthesis and Respiration in Cyanobacteria”. Encyclopedia of Life Sciences

Wan, N., DeLorenzo, D. M., He, L., You, L., Immethun, C. M., Wang, G., Baidoo, E. E. K., Hollinshead, W., Keasling, J. D., Moon, T. S. and Tang, Y. J. (2017). "Cyanobacterial carbon metabolism: Fluxome plasticity and oxygen dependence." Biotechnology and Bioengineering **114**(7): 1593-1602.

Wedel, N. and Soll, J. (1998). "Evolutionary conserved light regulation of Calvin cycle activity by NADPH-mediated reversible phosphoribulokinase/CP12/ glyceraldehyde-3-phosphate dehydrogenase complex dissociation." Proceedings of the National Academy of Sciences **95**(16): 9699-9704.

Whitton, B. A. (2012). “Ecology of cyanobacteria II: their diversity in space and time”, Springer Science & Business Media.

Wilson, A., Ajlani, G., Verbavatz, J.-M., Vass, I., Kerfeld, C. A. and Kirilovsky, D. (2006). "A Soluble Carotenoid Protein Involved in Phycobilisome-Related Energy Dissipation in Cyanobacteria." The Plant Cell **18**(4): 992-1007.

Xiong, W., Lee, T. C., Rommelfanger, S., Gjersing, E., Cano, M., Maness, P. C., Ghirardi, M. and Yu, J. (2015). "Phosphoketolase pathway contributes to carbon metabolism in cyanobacteria." Nat Plants **2**(15187): 187.

Yang, C., Hua, Q., Shimizu, K. (2002). "Metabolic Flux Analysis in Synechocystis Using Isotope Distribution from 13C-Labeled Glucose." Metabolic Engineering **4**(3): 202-216.

Yelton, A. P., Acinas, S. G., Sunagawa, S., Bork, P., Pedrós-Alió, C. and Chisholm, S. W. (2016). "Global genetic capacity for mixotrophy in marine picocyanobacteria." The Isme Journal **10**: 2946.

You, L., Berla, B., He, L., Pakrasi, H. B. and Tang, Y. J. (2014). "13C-MFA delineates the photomixotrophic metabolism of Synechocystis sp. PCC 6803 under light- and carbon-sufficient conditions." Biotechnology Journal **9**(5): 684-692.

Young, J. D., Shastri, A. A., Stephanopoulos, G. and Morgan, J. A. (2011). "Mapping photoautotrophic metabolism with isotopically nonstationary (13)C flux analysis." Metabolic Engineering **13**(6): 656-665.

Yu, H., Jia, S. and Dai, Y. (2008). "Growth characteristics of the cyanobacterium Nostoc flagelliforme in photoautotrophic, mixotrophic and heterotrophic cultivation." Journal of Applied Phycology **21**(1): 127.

Zavřel, T., Očenášová, P. and Červený, J. (2017). "Phenotypic characterization of Synechocystis sp. PCC 6803 substrains reveals differences in sensitivity to abiotic stress." Plos One **12**(12): e0189130.

Zerulla, K., Ludt, K. and Soppa, J. (2016). "The ploidy level of Synechocystis sp. PCC 6803 is highly variable and is influenced by growth phase and by chemical and physical external parameters." Microbiology **162**(5): 730-739.

Zhang, S. and Bryant, D. A. (2011). "The Tricarboxylic Acid Cycle in Cyanobacteria." Science **334**(6062): 1551-1553.

Zhang, Y., Beard, K. F. M., Swart, C., Bergmann, S., Krahnert, I., Nikoloski, Z., Graf, A., Ratcliffe, R. G., Sweetlove, L. J., Fernie, A. R. and Obata, T. (2017). "Protein-protein interactions and metabolite channelling in the plant tricarboxylic acid cycle." Nature Communications **8**: 15212.

Zhou, J., Zhang, H., Meng, H., Zhu, Y., Bao, G., Zhang, Y., Li, Y., Ma, Y. (2014). "Discovery of a super-strong promoter enables efficient production of heterologous proteins in cyanobacteria." Scientific Reports **4**: 4500

8 Appendix

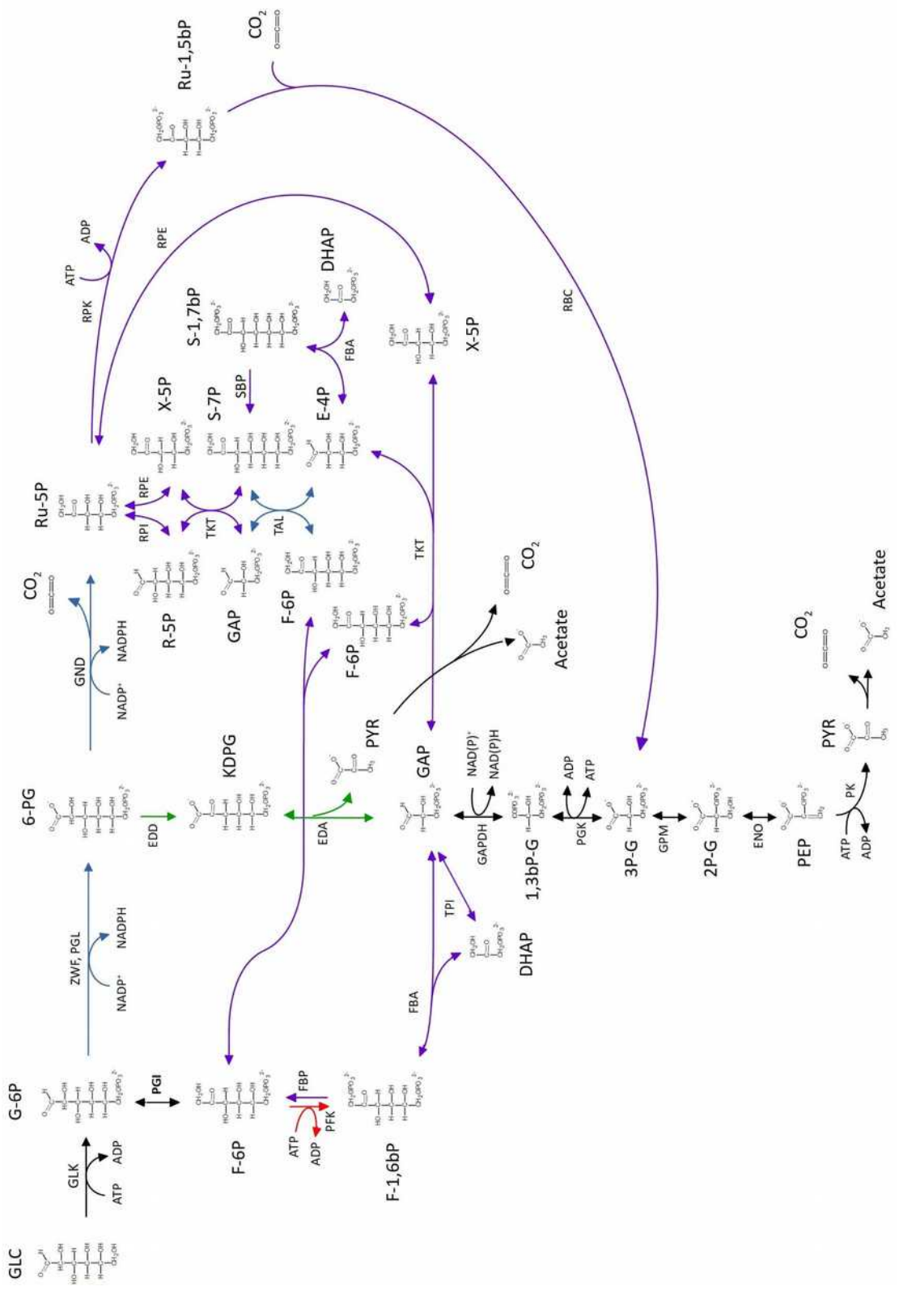

Figure S1: Structural formulas of intermediates of the three glycolytic routes and the Calvin-Benson-Bassham cycle in cyanobacteria

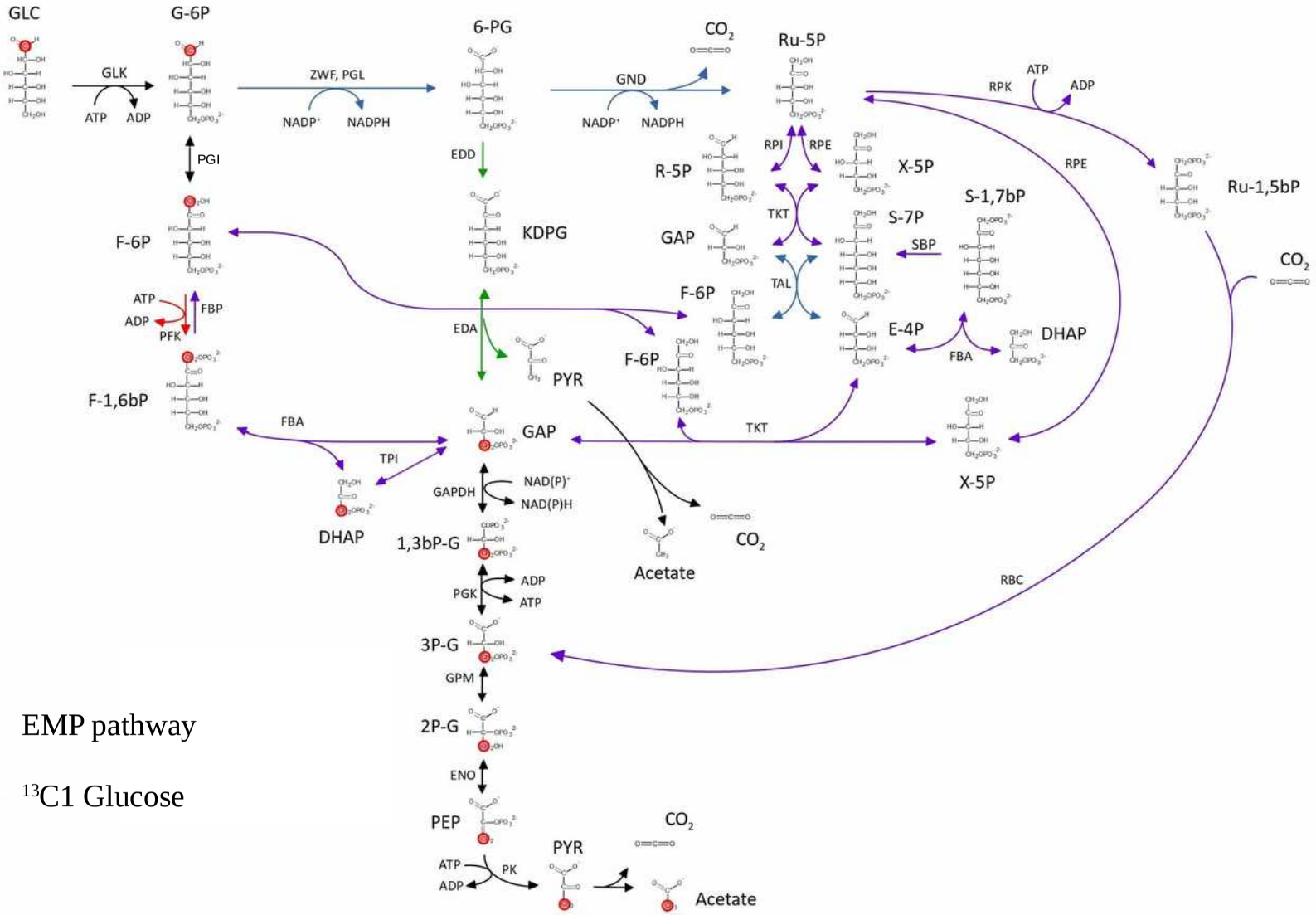

Figure S2: Expected labeling pattern during usage of the EMP pathway for metabolization of ^{13}C1 labeled glucose. Red circles indicate labeled carbon after first round and orange circles indicate labeled carbon after indefinite rounds.

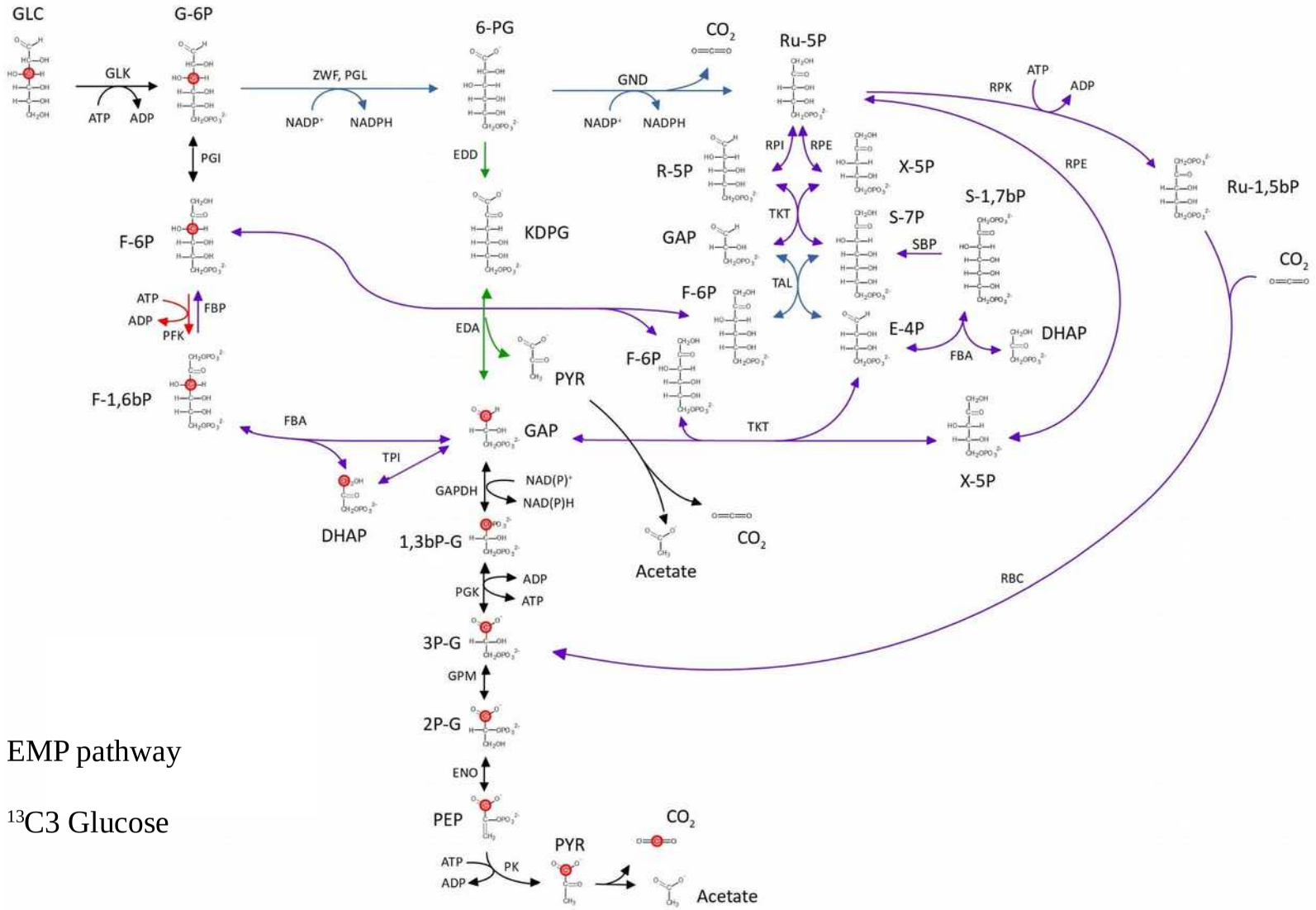

EMP pathway

^{13}C3 Glucose

Figure S3: Expected labeling pattern during usage of the EMP pathway for metabolization of ^{13}C3 labeled glucose. Red circles indicate labeled carbon after first round and orange circles indicate labeled carbon after indefinite rounds.

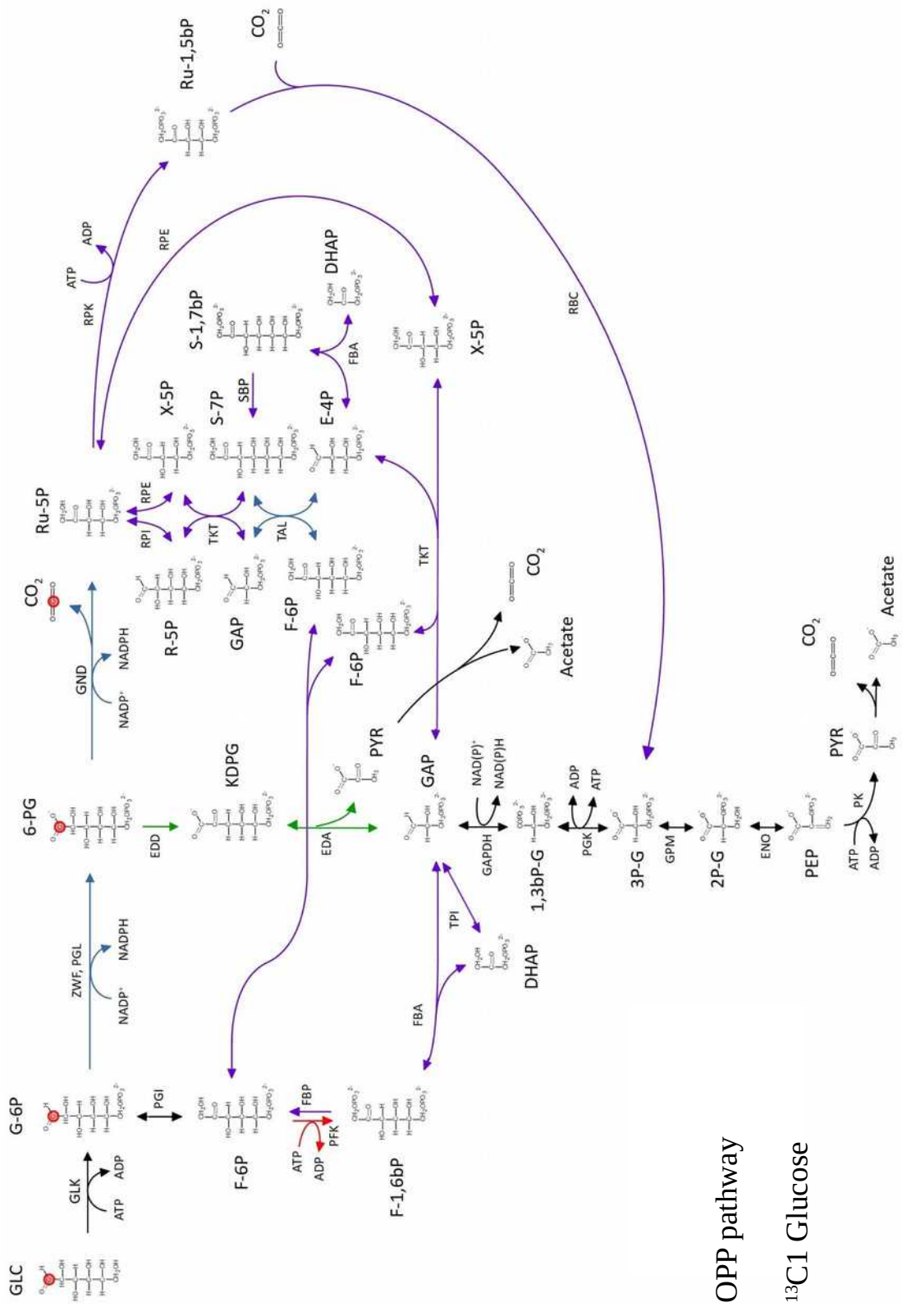

Figure S4: Expected labeling pattern during usage of the OPP pathway for metabolization of ^{13}C1 labeled glucose. Red circles indicate labeled carbon after first round and orange circles indicate labeled carbon after indefinite rounds.

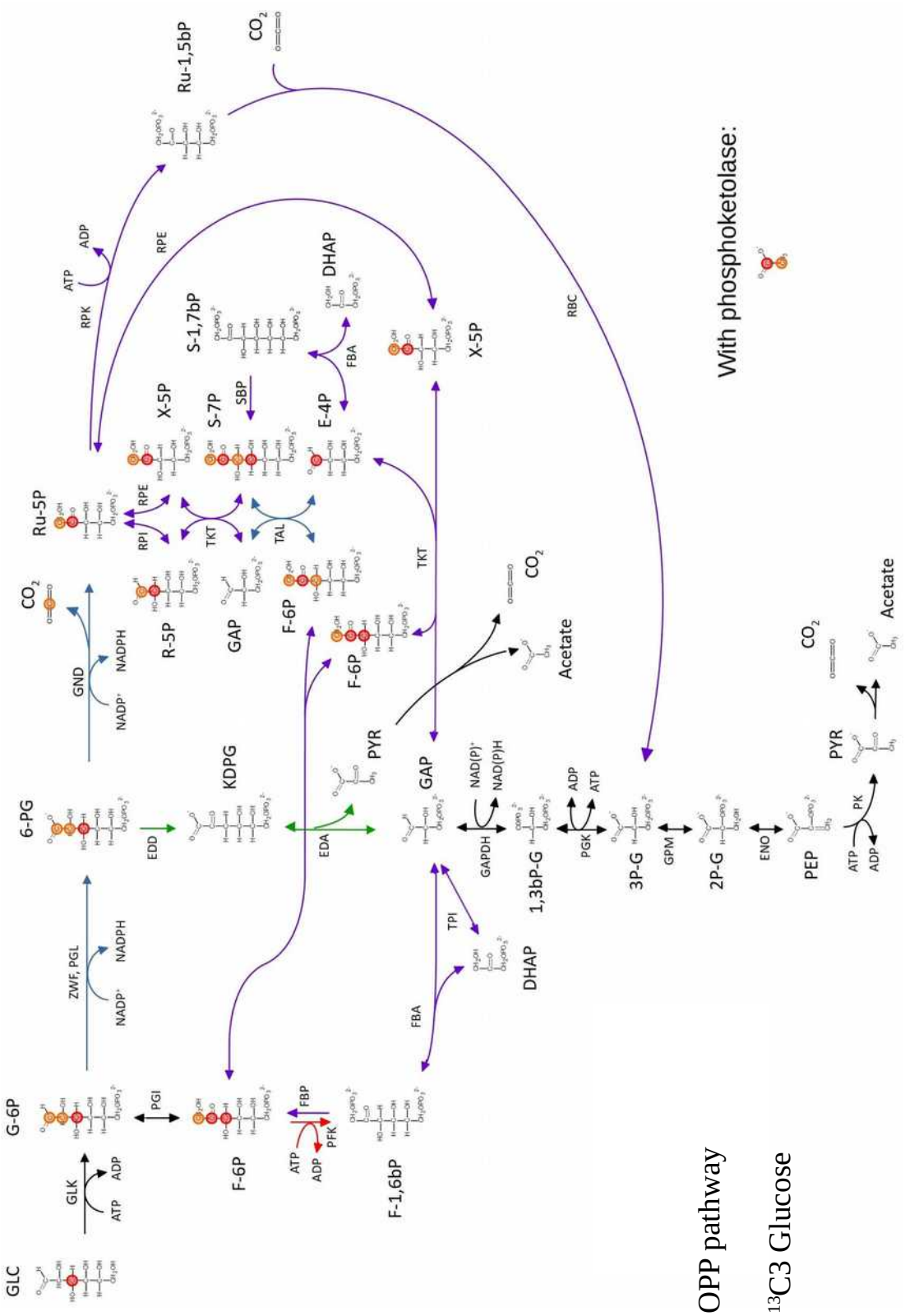

Figure S5: Expected labeling pattern during usage of the OPP pathway for metabolization of ^{13}C3 labeled glucose. Red circles indicate labeled carbon after first round and orange circles indicate labeled carbon after indefinite rounds.

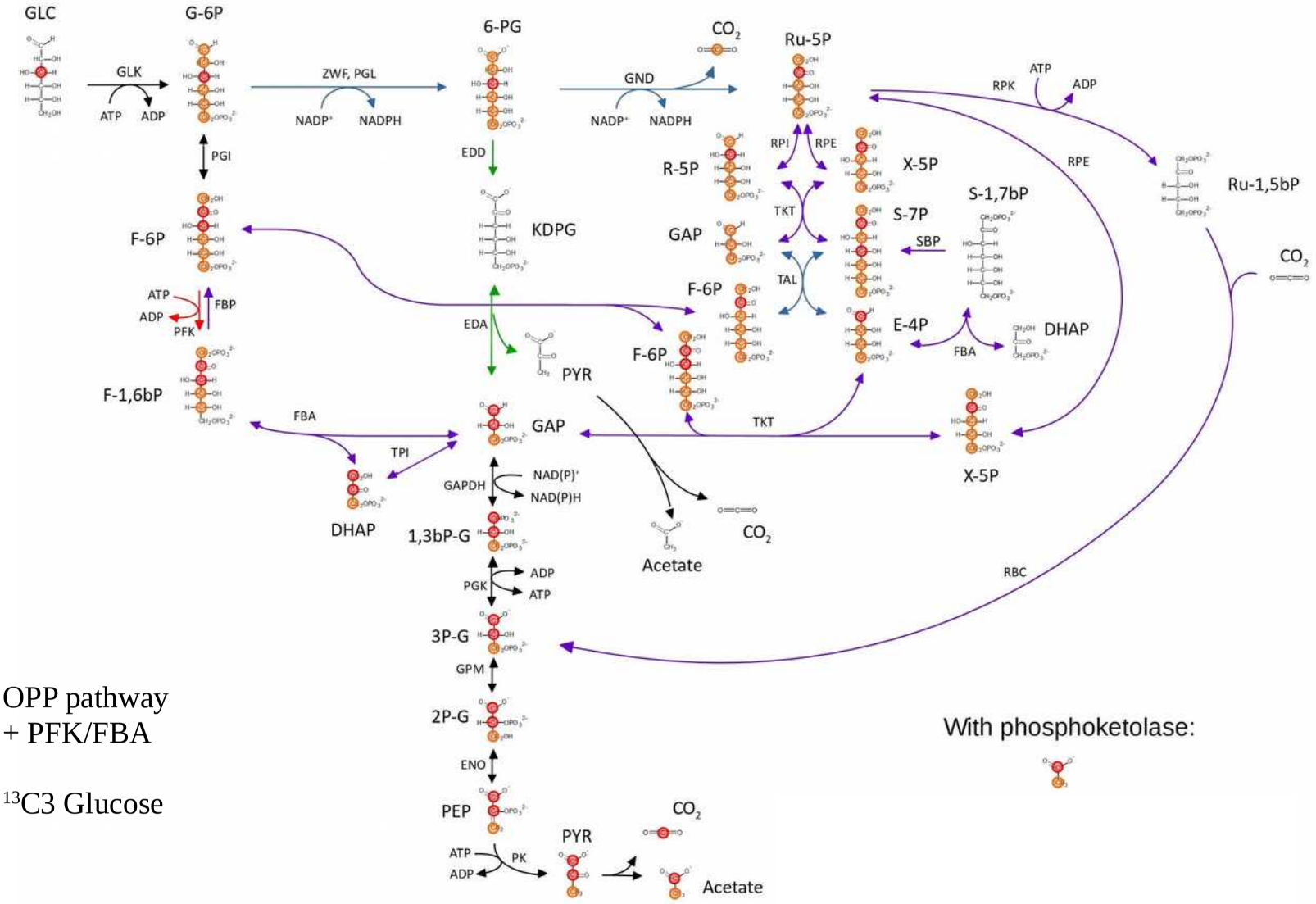

OPP pathway
+ PFK/FBA

^{13}C3 Glucose

Figure S6: Expected labeling pattern during usage of the OPP pathway plus PFK and FBA of the EMP pathway for metabolization of ^{13}C3 labeled glucose.
Red circles indicate labeled carbon after first round and orange circles indicate labeled carbon after indefinite rounds.

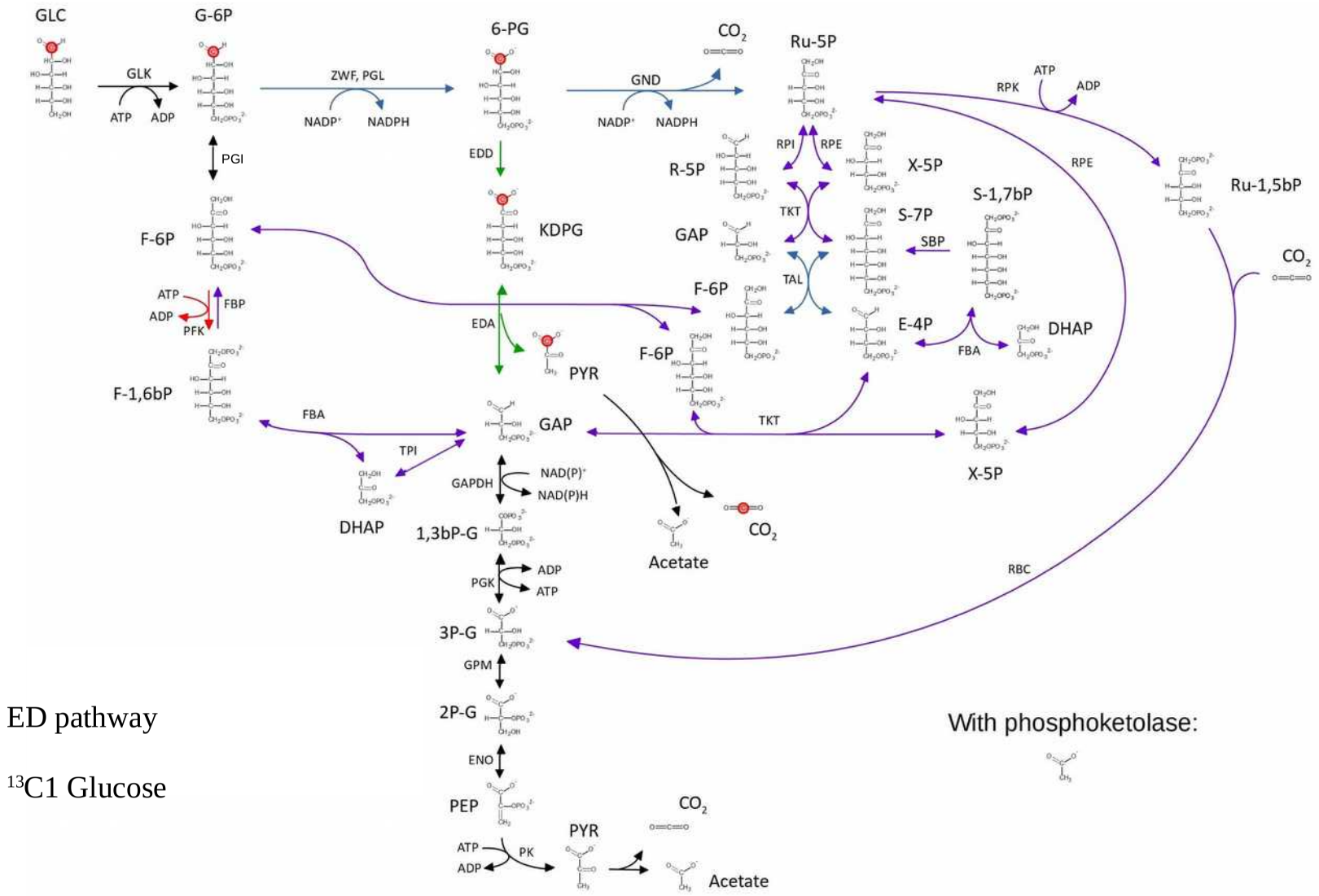

ED pathway

^{13}C1 Glucose

Figure S7: Expected labeling pattern during usage of the ED pathway for metabolization of ^{13}C1 labeled glucose. Red circles indicate labeled carbon after first round and orange circles indicate labeled carbon after indefinite rounds.

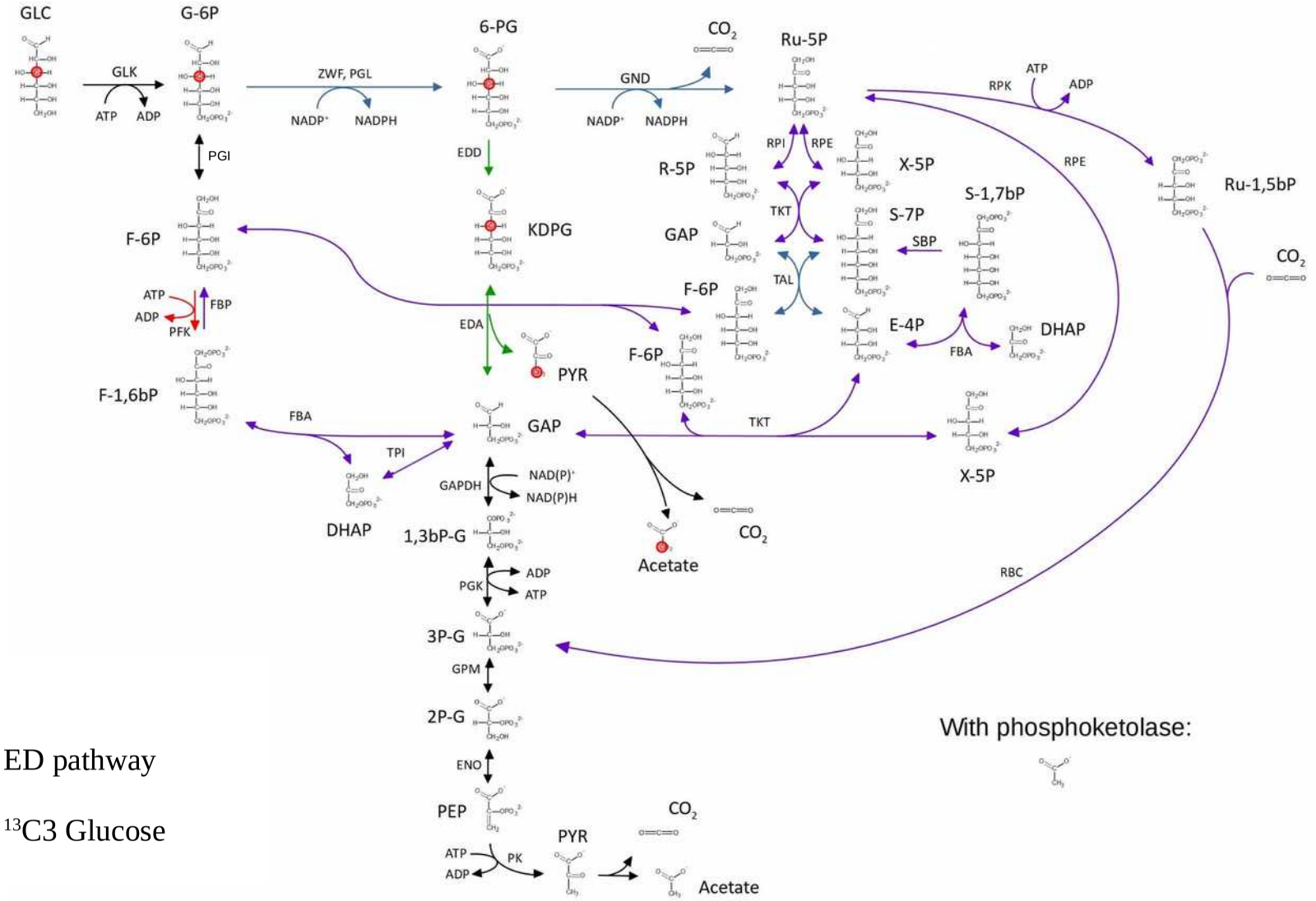

ED pathway

^{13}C3 Glucose

Figure S8: Expected labeling pattern during usage of the ED pathway for metabolization of ^{13}C3 labeled glucose. Red circles indicate labeled carbon after first round and orange circles indicate labeled carbon after indefinite rounds.

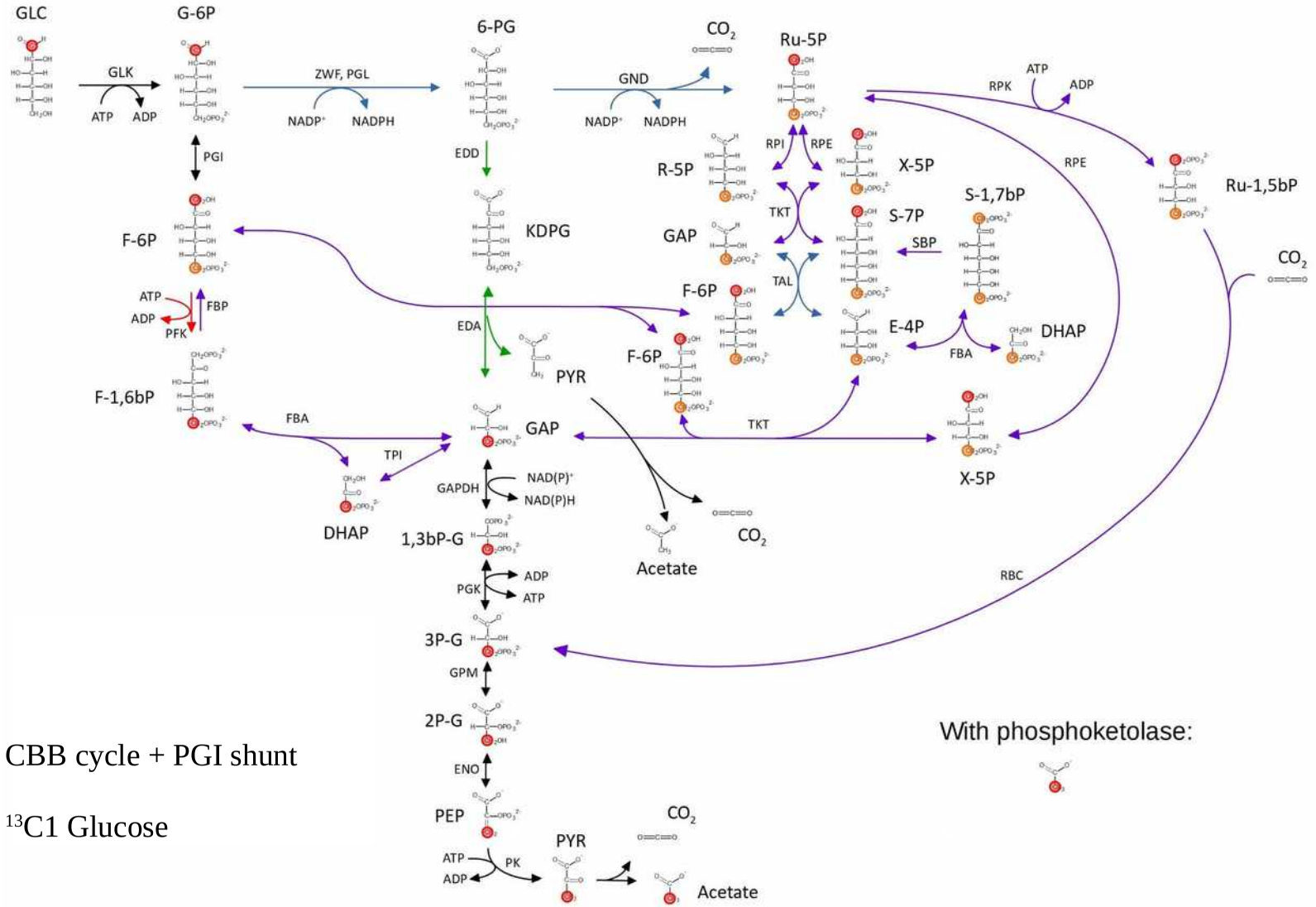

CBB cycle + PGI shunt

^{13}C1 Glucose

Figure S9: Expected labeling pattern during usage of the PGI shunt for metabolization of ^{13}C1 labeled glucose. Red circles indicate labeled carbon after first round and orange circles indicate labeled carbon after indefinite rounds.

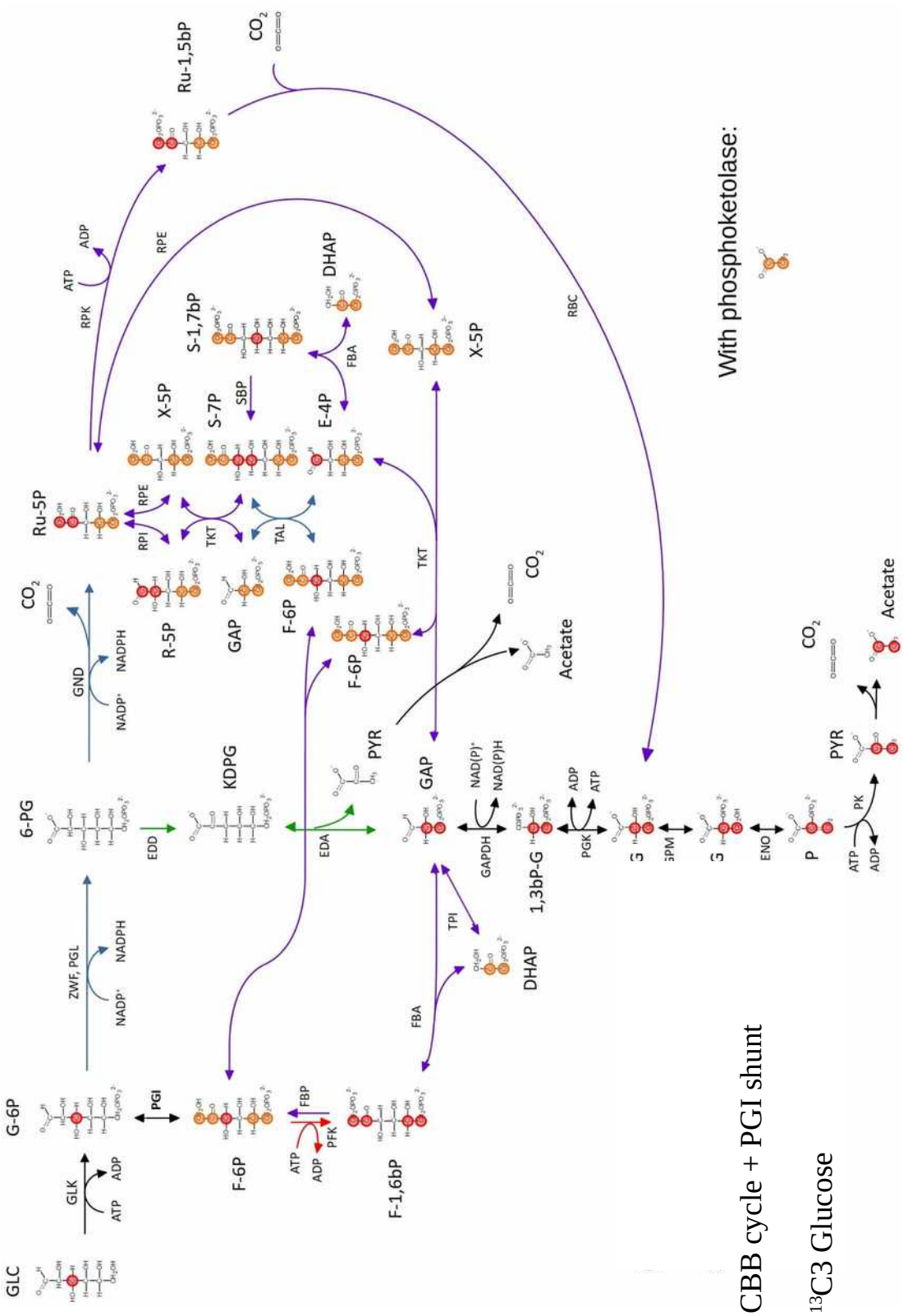

Figure S10: Expected labeling pattern during usage of the PGI shunt for metabolization of ^{13}C3 labeled glucose. Red circles indicate labeled carbon after first round and orange circles indicate labeled carbon after indefinite rounds.

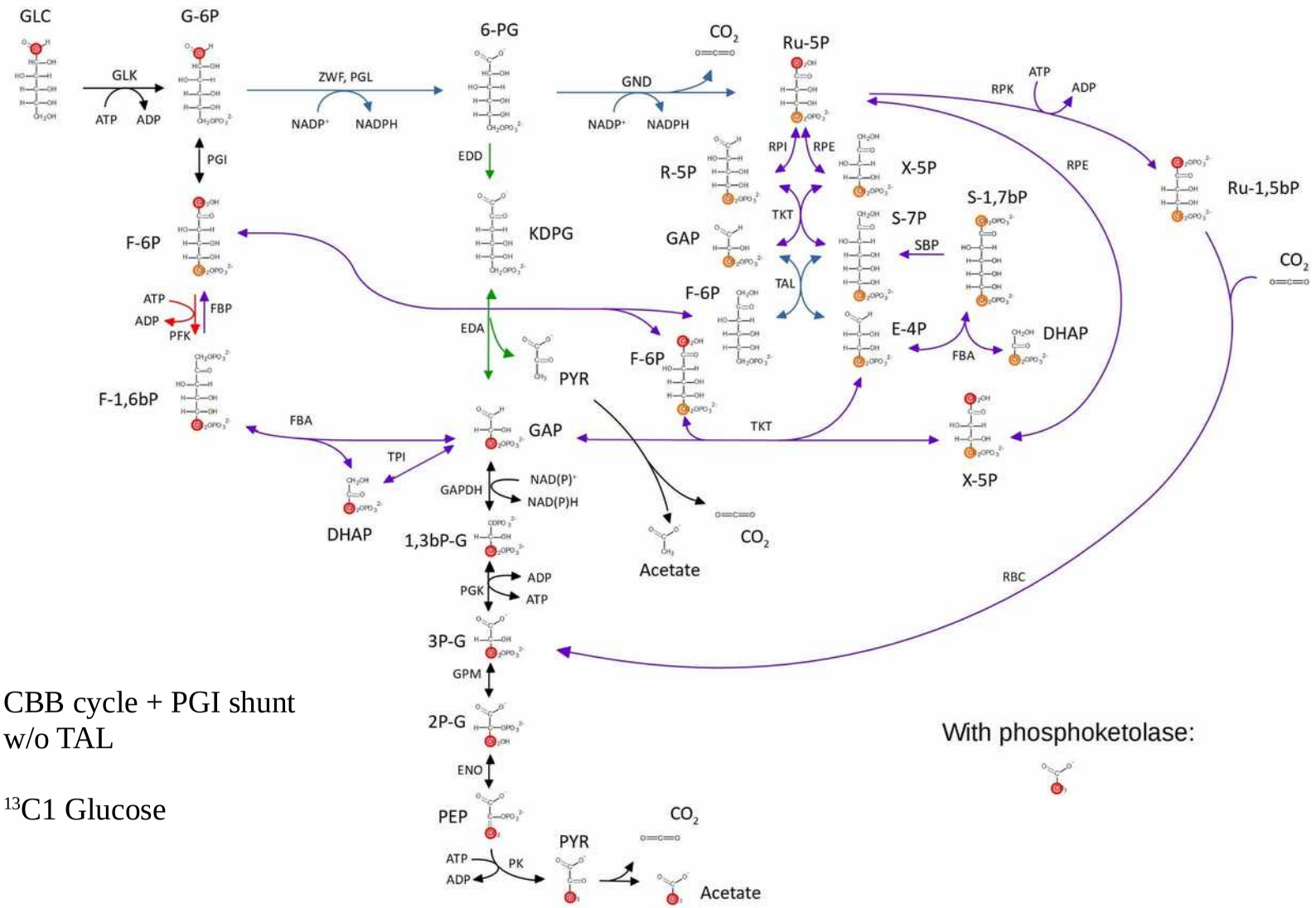

Figure S11: Expected labeling pattern during usage of the PGI shunt without participation of transaldolase (TAL) for metabolization of ^{13}C1 labeled glucose. Red circles indicate labeled carbon after first round and orange circles indicate labeled carbon after indefinite rounds.

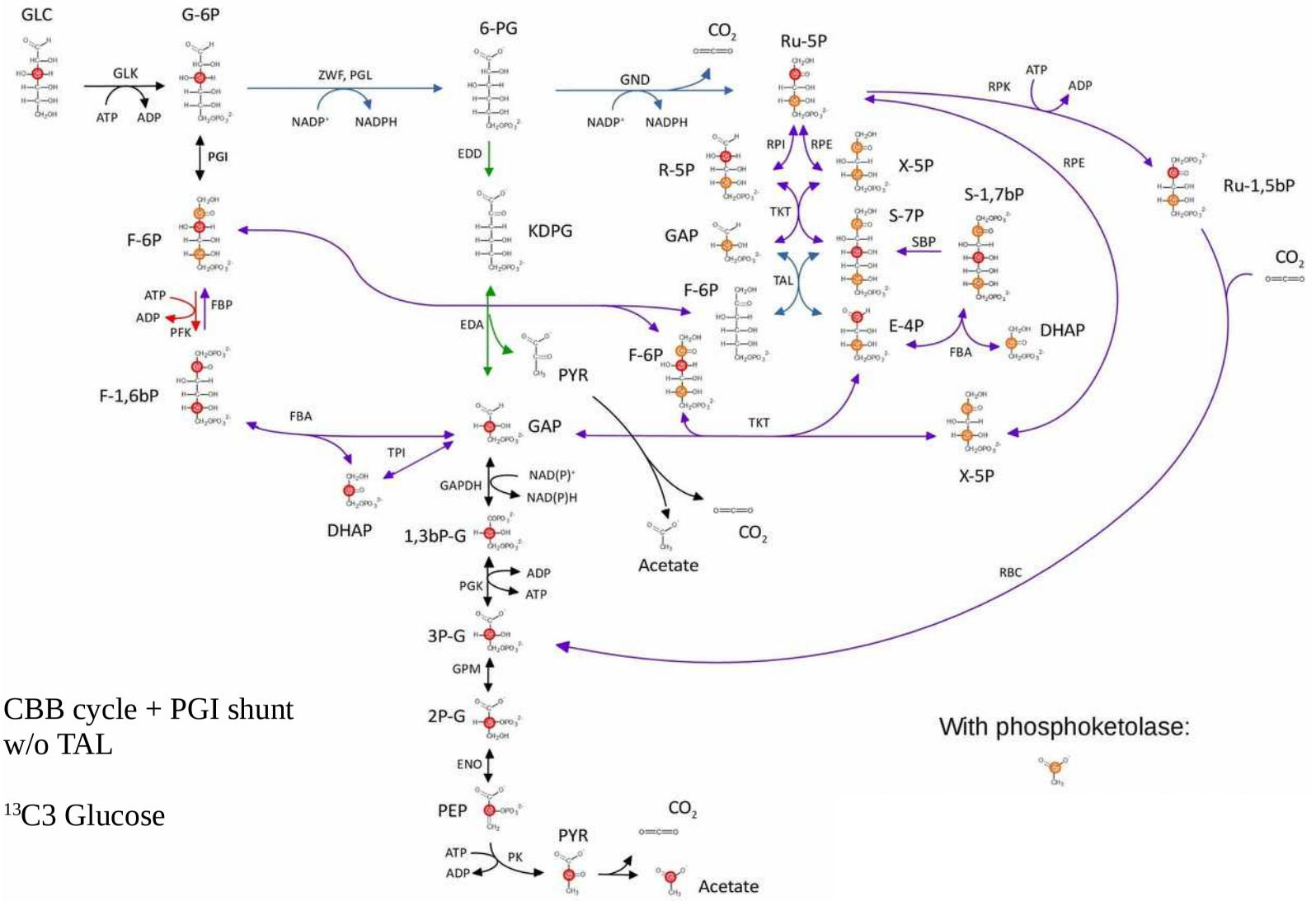

CBB cycle + PGI shunt
w/o TAL

^{13}C3 Glucose

Figure S12: Expected labeling pattern during usage of the PGI shunt without participation of transaldolase (TAL) for metabolization of ^{13}C3 labeled glucose. Red circles indicate labeled carbon after first round and orange circles indicate labeled carbon after indefinite rounds.

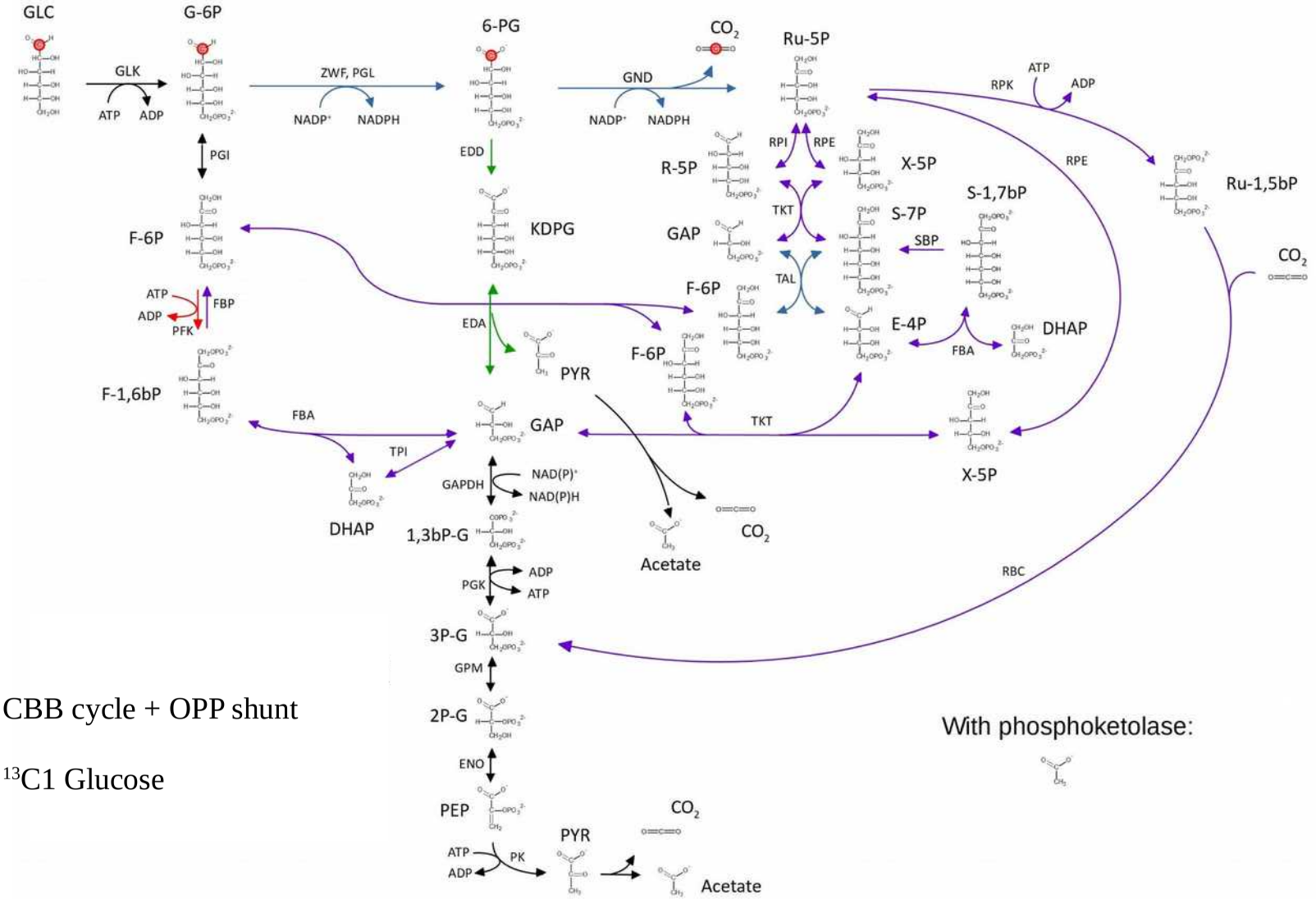

Figure S13: Expected labeling pattern during usage of the OPP shunt for metabolization of ^{13}C1 labeled glucose. Red circles indicate labeled carbon after first round and orange circles indicate labeled carbon after indefinite rounds.

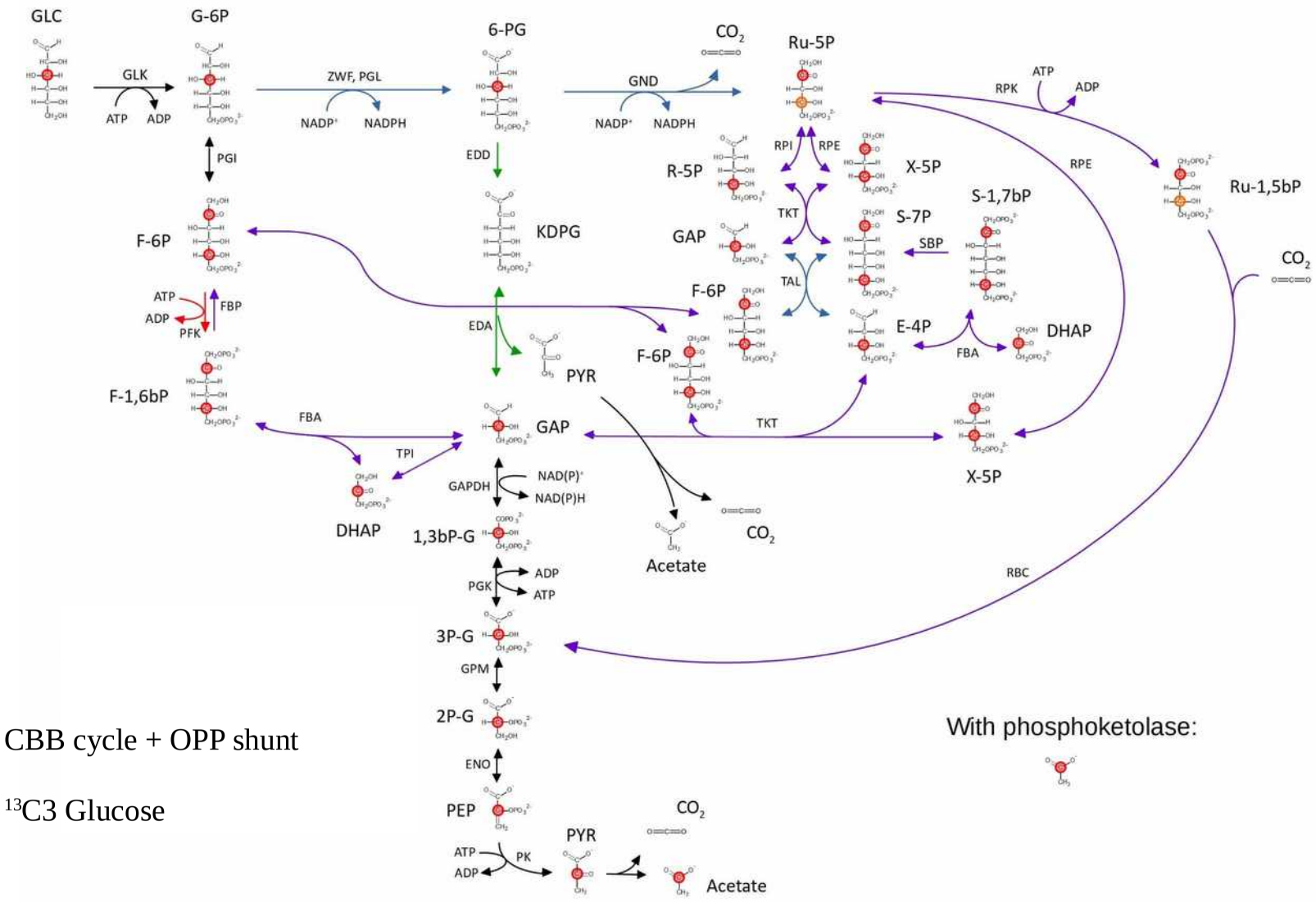

CBB cycle + OPP shunt

^{13}C3 Glucose

Figure S14: Expected labeling pattern during usage of the OPP shunt for metabolization of ^{13}C3 labeled glucose. Red circles indicate labeled carbon after first round and orange circles indicate labeled carbon after indefinite rounds.

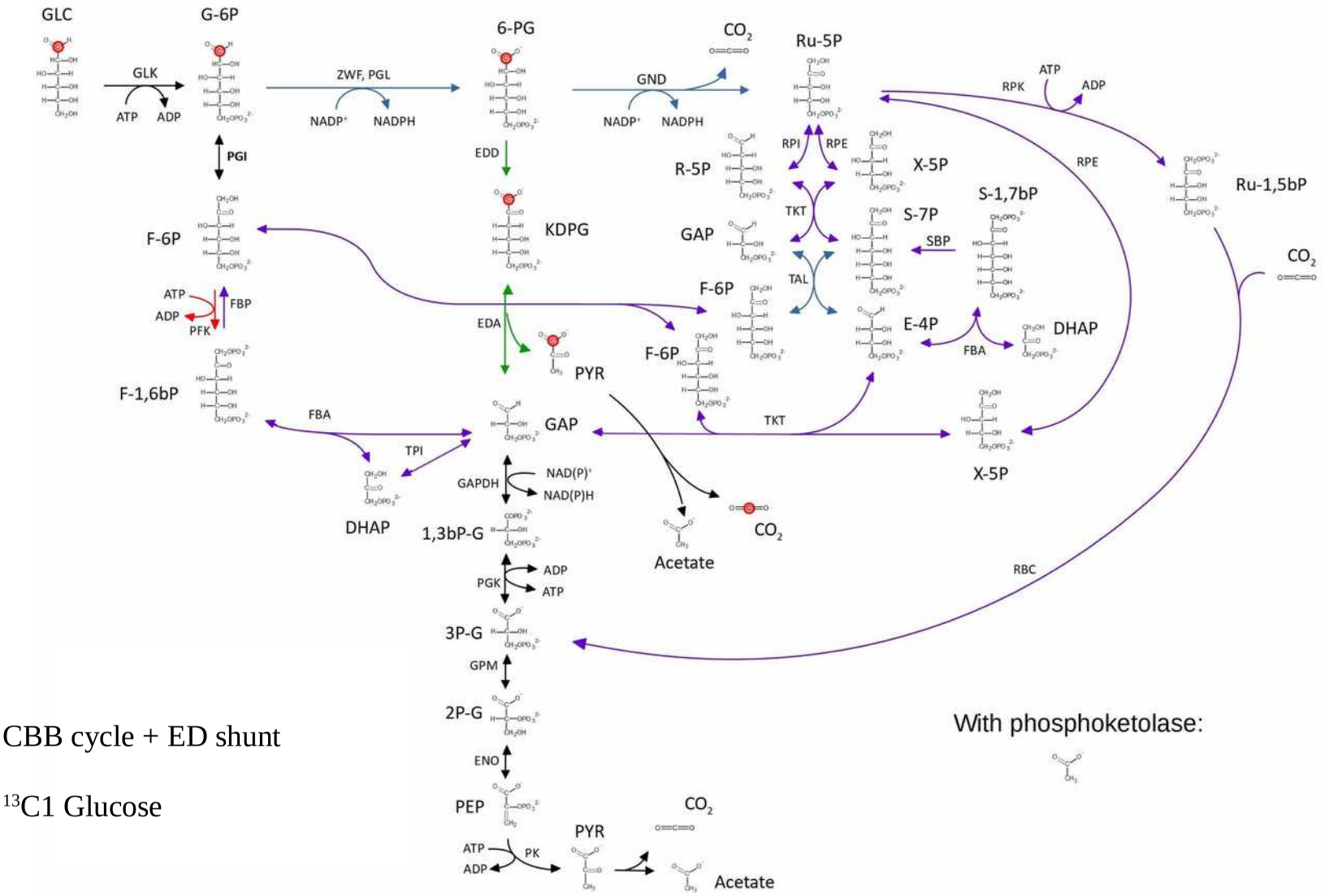

Figure S15: Expected labeling pattern during usage of the ED shunt for metabolization of ^{13}C1 labeled glucose. Red circles indicate labeled carbon after first round and orange circles indicate labeled carbon after indefinite rounds.

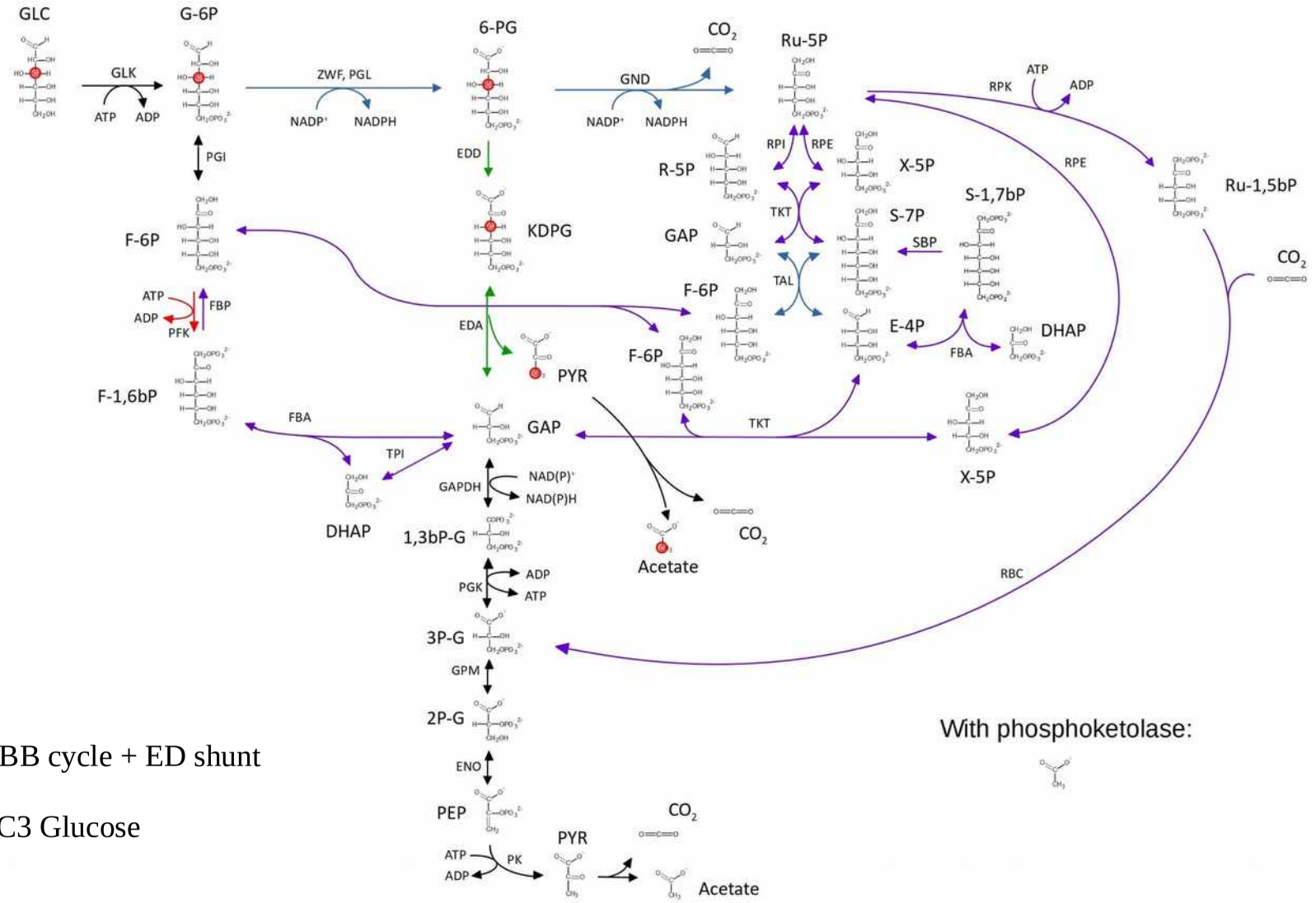

CBB cycle + ED shunt

^{13}C3 Glucose

Figure S16: Expected labeling pattern during usage of the ED shunt for metabolization of ^{13}C3 labeled glucose. Red circles indicate labeled carbon after first round and orange circles indicate labeled carbon after indefinite rounds.

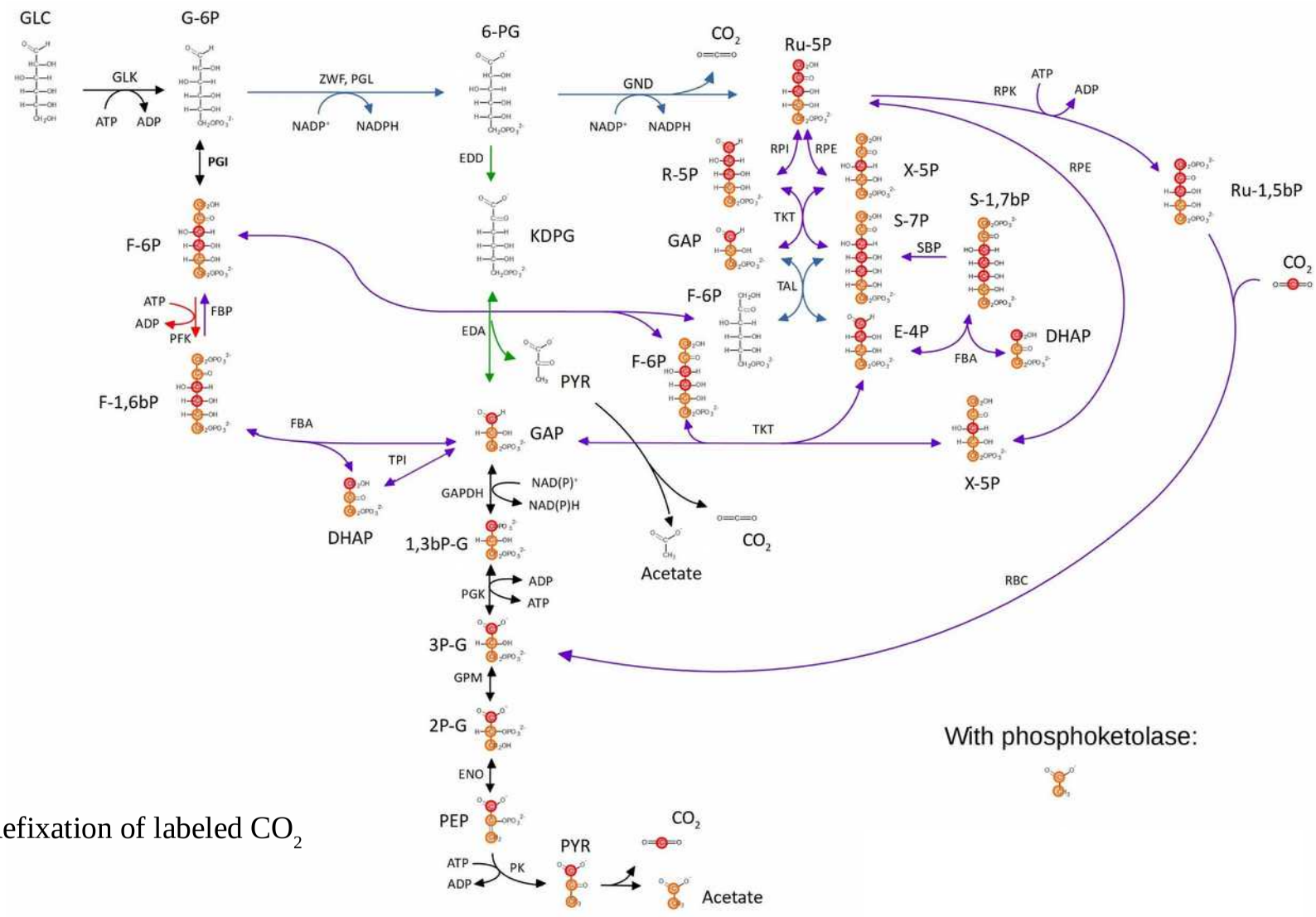

Figure S17: Expected labeling pattern during a refixation of labeled CO_2 by RubisCO. Red circles indicate labeled carbon after first round and orange circles indicate labeled carbon after indefinite rounds.

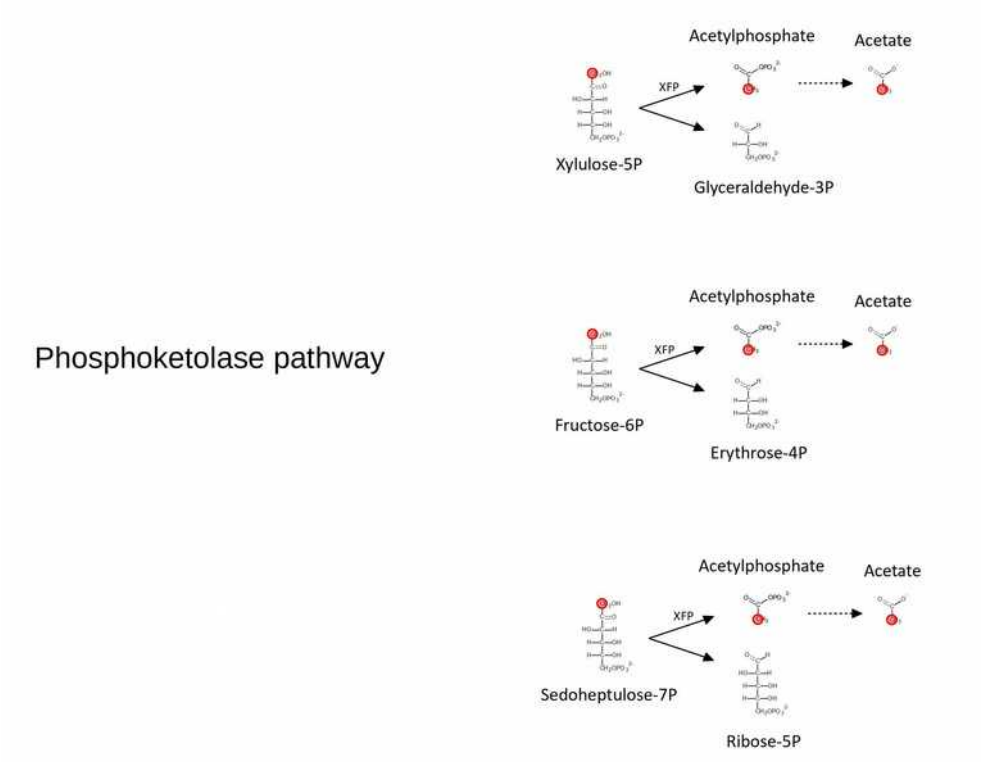

Figure S18: Expected labeling pattern during usage of the phosphoketolase pathway

9 Abbreviations

SI units and chemical formulas are not listed

6PG	6-phosphogluconate
6PGDH	6-phosphogluconate dehydrogenase
AB	antibiotic
ADP	adenosine diphosphate
AGP	ADP-glucose pyrophosphorylase
ATP	adenosine triphosphate
bp	basepairs
BSA	bovine serum albumine
CBB	Calvin-Benson-Bassham
CCM	carbon concentrating mechanism
Cm	chloramphenicol
CoA	coenzyme A
Cyt c	cytochrome c
DCMU	3-(3,4-dichlorophenyl)-1,1-dimethylurea
DHAP	dihydroxyacetonephosphate
DMB	2,3-dimethoxy-5-methyl-1,4-benzoquinone
DNA	deoxyribonucleic acid
dNTP	deoxynucleotide
DQ	duroquinone
DXS	1-deoxy-xylulose-5-phosphate synthase
E	Einstein (µmol photons*m^{-2}*s^{-1})
ED	Entner-Doudoroff
EDD	6-phosphogluconate dehydratase
EDA	2-keto-3-deoxy-6-phosphogluconate aldolase
ENO	enolase
Em	erythromycin
EMP	Embden-Meyerhof-Parnas
F6P	fructose-6-phosphate
Fd	ferredoxin
FAD	oxidized Flavin adenine dinucleotide
$FADH_2$	reduced Flavin adenine dinucleotide
FBA	fructose/seduheptulose-bisphosphate aldolase
FBP	fructose/seduheptulose bisphosphatase
FNR	ferredoxin-NADPH reductase
G6P	glucose-6-phosphate
G6PDH	glucose-6-phosphate dehydrogenase
GA	glycolaldehyde
GAP	glyceraldehyde-3-phosphate
GAPDH	glyceraldehyde-3-phosphate dehydrogenase
GDH	glucose dehydrogenase
GK	gluconate kinase
GLGP	glycogen phosphorylase
Glc	glucose
GLK	glucokinase
Gm	gentamicin

GND	6-phosphogluconate dehydrogenase
GP	glycogen phosphorylase
GS	glycogen synthase
h	hour(s)
HK	hexokinase
HPLC	high performance liquid chromatography
KDPG	2-keto-3-deoxy-6-phosphogluconate
kb	kilo basepair
Km	kanamycin
L	liter
LAHG	light activated heterotrophic growth
LED	light-emitting diode
min	minutes
ME	malic enzyme
MEP	methyl-erythritol-4-phosphate
MS	mass spectrometry
NAD(P)	oxidized nicotinamide adenine dinucleotide (phosphate)
NAD(P)H	reduced nicotinamide adenine dinucleotide (phosphate)
NDH	NADH:quinone oxidoreductase
NMR	nuclear magnetic resonance
OD	optical density
OPP	oxidative pentose phosphate
Ox	oxidase
PAM	pulse amplitude modulation
PC	plastocyanin
PCR	polymerase chain reaction
PETC	photosynthetic electron transport chain
PEP	phosphoenolpyruvate
PEPC	phosphoenolpyruvate carboxylase
PFK	phosphofructokinase
PGI	glucose-6-phosphate isomerase
PGK	phosphoglycerate kinase
PGAM	phosphoglycerate mutase
PGL	phosphogluconolactonase
PGM	phosphoglucomutase
PK	pyruvate kinase
PP	pentose phosphate
PPFD	photosynthetically active photon flux density
ppm	parts per million
PQ	plastoquinone
PS I	photosystem 1
PS II	photosystem 2
PRK	phosphoribulokinase
qP	photochemical quenching
RBC	ribulose-1,5-bisphosphate carboxylase/oxygenase
RPE	ribose-5-phosphate epimerase
RPI	ribose-5-phosphate isomerase
rpm	rotations per minute
RT	room temperature

Ru5P	ribulose-5-phosphate
RubisCO	ribulose-1,5-bisphosphate carboxylase/oxygenase
SDH	succinate dehydrogenase
Sp	spectinomycin
TAL	transaldolase
TCA	tricarboxylic acid cycle
TKT	transketolase
TPI	triosephosphate isomerase
Tris	tris(hydroxymethyl)aminomethane
U	unit (µmol substrate/s)
UV	ultraviolet
v	volume
w	weight
WT	wildtype
ZWF	glucose-6-phosphate dehydrogenase

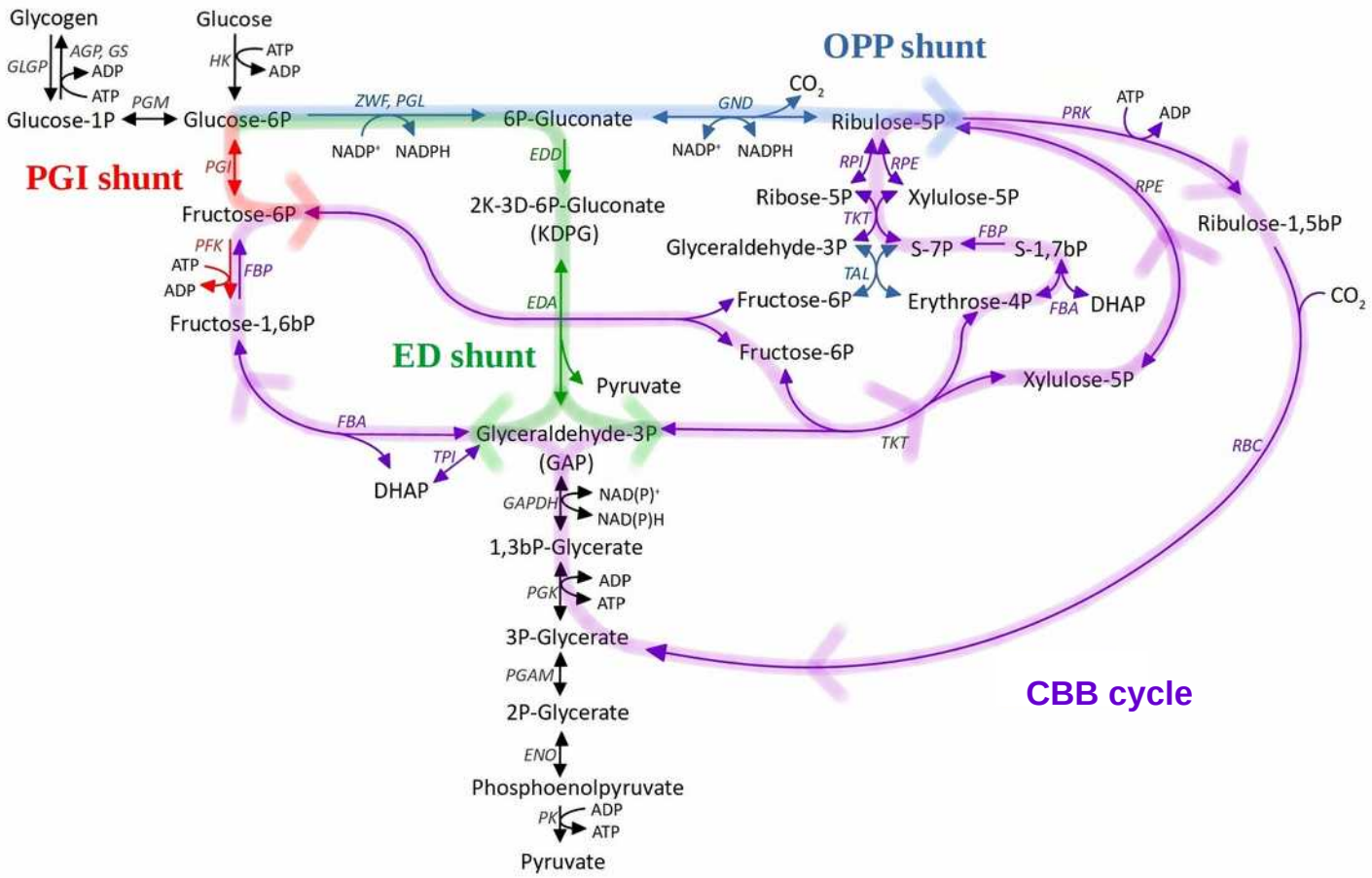
Glycogen
Glucose
GLGP
AGP, GS
ATP
ADP
HK
ATP
ADP
Glucose-1P
PGM
Glucose-6P
PGI shunt
PGI
Fructose-6P
PFK
ATP
ADP
FBP
Fructose-1,6bP
ZWF, PGL
NADP+
NADPH
6P-Gluconate
EDD
2K-3D-6P-Gluconate
(KDPG)
EDA
ED shunt
Pyruvate
FBA
TPI
DHAP
Glyceraldehyde-3P
(GAP)
GAPDH
NAD(P)+
NAD(P)H
1,3bP-Glycerate
PGK
ADP
ATP
3P-Glycerate
PGAM
2P-Glycerate
ENO
Phosphoenolpyruvate
PK
ADP
ATP
Pyruvate
OPP shunt
CO2
GND
NADP+
NADPH
Ribulose-5P
PRK
ATP
ADP
RPI
RPE
Ribose-5P
Xylulose-5P
TKT
Glyceraldehyde-3P
S-7P
FBP
S-1,7bP
TAL
Fructose-6P
Erythrose-4P
FBA
DHAP
Fructose-6P
Xylulose-5P
TKT
RPE
Ribulose-1,5bP
CO2
RBC
CBB cycle